Dissecting the cell type-specific role of FKBP51 in the stress response and whole-body metabolism

- The WHEN and WHERE matters –

Dissertation zur Erlangung des Doktorgrades der Naturwissenschaften

Doctor rerum naturalium (Dr. rer. nat.)

an der Fakultät für Biologie

der Ludwigs-Maximilians-Universität München

Lea Maria Brix

Munich, Germany
June 2022

Table of Contents

Abstract

Our world is facing a pandemic of stress-related disorders, ranging from mental health to cardiovascular and metabolic diseases, and there is an urgent need for effective and selective treatments. Despite enormous efforts and decades of research, we are still far from finding targeted interventions for most psychiatric but also metabolic diseases. The identification of genetic risk factors and subsequently deciphering their tissue- and cell type-specific role in physiology is an indispensable step towards a more comprehensive understanding of the molecular mechanisms underlying these disorders. One prominent example is the co-chaperone FKBP51, which has been linked to the development of psychiatric and metabolic disorders in humans. It has been shown to be involved in a plethora of cellular signaling pathways that modulate our hormonal stress response system, the hypothalamic-pituitary-adrenal (HPA axis), and whole-body metabolism. To dissect the tissue-specific role of FKBP51 in the HPA axis, we selectively manipulated FKBP51 expression in mouse paraventricular nucleus (PVN), the master regulator of the central stress response, and assessed the behavioral and endocrine phenotypes of these animals. We were further interested in whether loss of FKBP51 in corticotrope pro-opiomelanocortin (POMC) cells in the pituitary gland (PIT) affects negative feedback control of the HPA axis and age-related dysregulation of the stress response. Both cell type-specific studies on the involvement of FKBP51 in HPA axis (re)activity revealed a beneficial effect of attenuating *Fkbp5* expression, which is consistent with systemic endogenous knockout (KO) studies in rodents. To expand the existing knowledge on the role of FKBP51 in autophagy signaling, we knocked out and overexpressed (OE) the gene in the mediobasal hypothalamus (MBH), which is known for its key role in energy homeostasis and feeding behavior. Our study identified a novel group of molecular players called phosphoinositide protein family (WIPI proteins) that interact with FKBP51 to control autophagy signaling in the rodent MBH. Since the MBH is a heterogeneous structure with multiple neuronal subpopulations that all individually and synergistically contribute to shaping homeostasis, we set out to investigate the cell type-specific role of FKBP51 in steroidogenic factor 1 (*Sf1*) expressing neurons of the ventromedial hypothalamus (VMH) and *Pomc*-expressing cells of the arcuate nucleus (ARC). Intriguingly, KO of FKBP51 in these two MBH subnuclei had opposite effects on high-fat diet (HFD) induced body weight (BW) gain: KO of FKBP51 in VMH-SF1 neurons adversely affects whole-body metabolism, corresponding

to an MBH-wide KO of this co-chaperone. However, attenuation of *Fkbp5* expression in POMC neurons had positive effects on BW regulation under a HFD challenge. Thus, the collective results of this work highlight the importance of cell type-specific studies on the role of FKBP51 in homeostatic control and pave the way for future pharmacological intervention studies.

Zusammenfassung

Auf unsere Welt rollt eine Pandemie stressbedingter Störungen zu, die von psychischen Erkrankungen bis hin zu Herz-Kreislauf- und Stoffwechselerkrankungen reichen und es besteht ein dringender Bedarf an wirksamen Behandlungen. Trotz enormer Anstrengungen und jahrzehntelanger Forschung sind wir noch weit davon entfernt, gezielte Interventionen für die meisten psychiatrischen, aber auch metabolischen Erkrankungen zu finden. Die Identifizierung genetischer Risikofaktoren und die anschließende Entschlüsselung ihrer gewebs- und zelltypspezifischen Rolle in der Physiologie ist ein unerlässlicher Schritt zu einem umfassenderen Verständnis der molekularen Mechanismen, die diesen Erkrankungen zugrunde liegen. Ein bekanntes Beispiel ist das Co-Chaperon FKBP51, das mit der Entstehung von psychiatrischen und metabolischen Erkrankungen bei Menschen und Nagern in Verbindung gebracht wird. Es hat sich gezeigt, dass es an einer Vielzahl von zellulären Signalwegen beteiligt ist, die unser hormonelles Stressreaktionssystem, die Hypothalamus-Hypophysen-Nebennieren-Achse (HPA-Achse) und den Ganzkörperstoffwechsel modulieren. Um die gewebespezifische Rolle von FKBP51 in der HPA-Achse zu untersuchen, haben wir die FKBP51-Expression im paraventrikulären Nukleus (PVN) der Maus, der Steuerzentrale der hormonellen Stressreaktion, selektiv manipuliert und die Verhaltens- und endokrinen Phänotypen dieser Tiere untersucht. Des Weiteren waren wir daran interessiert, inwiefern der Verlust von FKBP51 in kortikotropen Proopiomelanocortin-Zellen (POMC) in der Hypophyse die negative Rückkopplung der HPA-Achse und die altersbedingte Dysregulation der Stressreaktion beeinflusst. Diese zelltypspezifischen Manipulationen der *Fkbp5* Expression ergaben einen positiven Effekt des Knockouts (KO) auf die (Re-)Aktivität der HPA-Achse, was mit systemischen endogenen KO-Studien in Nagern übereinstimmt. Um unser Wissen über die bereits etablierte Rolle von FKBP51 bei der Autophagie-Signalgebung zu erweitern, haben wir das Gen im mediobasalen Hypothalamus (MBH), der für seine Schlüsselrolle bei der Energiehomöostase und Fressverhalten bekannt ist, ausgeschaltet und überexprimiert (OE). In dieser Studie identifizierten wir eine neue Gruppe von molekularen Akteuren der Phosphoinositid Protein Familie (WIPI-Proteine), die mit FKBP51 interagieren und die Autophagie-Signalgebung im MBH der Nager steuern. Da der MBH eine heterogene Struktur mit mehreren neuronalen Subpopulationen ist, die alle einzeln und synergetisch zur Gestaltung der Homöostase beitragen, haben wir die zelltypspezifische Rolle von FKBP51 in

Steroidogenic Factor 1 (*Sf1*) exprimierenden Neuronen des ventromedialen Hypothalamus (VMH) und *Pomc*-exprimierenden Zellen des Nucleus arcuatus (ARC) untersucht. Interessanterweise hatte der KO von FKBP51 in diesen beiden MBH-Subkernen gegensätzliche Auswirkungen auf die durch eine hochkalorische Diät hervorgerufene Zunahme des Körpergewichts: Der KO von FKBP51 in VMH-SF1-Neuronen wirkt sich negativ auf den Ganzkörperstoffwechsel aus, was einem MBH-weiten KO dieses Co-Chaperons entspricht. Die Abschwächung der *Fkbp5*-Expression in POMC-Neuronen hatte jedoch positive Auswirkungen auf die Regulierung des Körpergewichts unter hochkalorischer Diät. Zusammenfassend unterstreicht diese Arbeit die Wichtigkeit zelltypspezifischer Studien zur Rolle von FKBP51 bei der homöostatischen Kontrolle und ebnet den Weg für zukünftige pharmakologische Interventionsstudien.

Abbreviations

51 KO	*Fkbp5* knockout
51 OE	*Fkbp5* overexpression
AAV	Adeno-associated virus
ACTH	Adrenocorticotropin hormone
AgRP	Agouti-related peptide
AKT	Protein kinase B
AMP	Adenosine monophosphate
AMPK	AMP-activated protein kinase
AP	Area postrema/Anterior pituitary gland
APA	American Psychological Association
ARC	Arcuate nucleus
AS160	AKT substrate 160
Atgs	Autophagy related genes
AV1BR	Arginine-vasopressin receptor 1 B
AUC	Area under the curve
AVP	Arginine-vasopressin
Atg7	Autophagy related gene 7
BAT	Brown adipose tissue
BDNF	Brain-derived neurotrophic factor
BNST	Bed nucleus of the stria terminalis
BW	Body weight
CART	Amphetamine-related transcript
CCK	Cholecystokinin
CORT	Corticosterone
CRH	Corticotropin-releasing hormone
CRHR1	Corticotropin-releasing hormone receptor 1
CSDS	Chronic social defeat stress
DEX	Dexamethasone
DMH	Dorsomedial hypothalamus

FKBP51	FK507-binding protein 51
FKBP52	FK506-binding protein 52
GABA	γ-aminobutyric acid
GC	Glucocorticoid
GLUT4	Glucose transporter 4
GLP1	Glucagon-like peptide 1
GR	Glucocorticoid receptor
GRE	Glucocorticoid response element
HFD	High-fat diet
HIP	Hippocampus
HOP	Hsp90-organizing-protein
HPA	Hypothalamic-pituitary-adrenal
HSP70	Heat shock protein 70
HSP90	Heat shock protein 90
IMM	Immunophilins
IR	Insulin receptor
IRS-1	Insulin receptor substrate 1
KO	Knockout
LC	Locus coeroleus
LepR	Leptin receptor
LH	Lateral hypothalamus
MC3R	Melanocortin 3 receptor
MC4R	Melanocortin 4 receptor
MBH	Mediobasal hypothalamus
MEE	Median eminence
MR	Mineralocorticoid receptor
mTOR	Mammalian target of rapamycin
NPY	Neuropeptide Y
NTS	Nucleus tractus solitarii
OE	Overexpression
OXT	Oxytocin

PHLPP	PH domain and leucine rich repeat protein phosphatase
PI3K	Phophoiosititde 3-kinase
PIT	Pituitary
POMC	Pro-opiomelanocortin
PP	Posterior pituitary
PPARγ	Peroxisome proliferator-activated receptor-γ
PTSD	Post-traumatic disorder
PVN	Paraventricular nucleus
RPA	Raphe pallidus
SAFit	Selective antagonist for FKBP51 by induced fit
SAM	Sympatho-adreno-medullary system
SF1	Steroidogenic factor 1
SIM1	Single-minded homologue 1
SKP2	S-phase kinase-associated protein 2
SNPs	Single nucleotide polymorphism
SNS	Sympathetic nervous system
SST	Somatostatin
SHR	Steroid hormone receptor
TPR	Tetratricopeptide repeat domain
TRH	Thyrotropin-releasing hormone
T2D	Type 2 diabetes
UCP1	Uncoupling-protein 1
VMH	Ventromedial hypothalamus
WAT	White adipose tissue
WD	Tryptophan-aspartic acid-repeat proteins
WIPI	WIPI
WT	Wildtype
ZF	Zona fasciculata
ZR	Zona reticularis
α-MSH	α-melanocyte-stimulating hormone

Publications

Chapter 2.1

Häusl, A.S.*, <u>Brix, L.M.*</u>, Hartmann, J., Pöhlmann, M.L., Lopez, J.P., Menegaz, D., Brivio, E., Engelhardt, C., Roeh, S., Bajaj, T., Rudolph, L., Stoffel, R., Hafner, K., Goss, H.M, Reul, J. M. H. M., Deussing, J.M., Eder, M., Ressler, K.J., Gassen, N.C., Chen, A. & Schmidt, M.V. (2021). The co-chaperone *Fkbp5* shapes the acute stress response in the paraventricular nucleus of the hypothalamus of male mice. *Molecular Psychiatry,* 26, 3060–3076. https://doi.org/10.1038/s41380-021-01044-x
*Shared first authorship with equal contribution

Chapter 2.2

<u>Brix, L.M.</u>, Häusl, A.S., Toksöz, I., Bordes, J., Doeselaar, L.V., Engelhardt, C., Narayan, S., Springer, M., Sterlemann, V., Deussing, J.M., Chen, A. & Schmidt, M.V. (2022). The co-chaperone FKBP51 modulates HPA axis activity and age-related maladaptation of the stress system in pituitary proopiomelanocortin cells. *Psychoneuroendocrinology*, 138, 105670. https://doi.org/10.1016/j.psyneuen.2022.105670

Chapter 2.3

Häusl, A.S., Bajaj, T., <u>Brix, L.M.</u>, Pöhlmann, M.L., Hafner, K., De Angelis, M., Nagler, J., Dethloff, F., Balsevich, G., Schramm, K.W., Giavalisco, P., Chen, A., Schmidt, M.V. & Gassen, N.C. (2022). Mediobasal hypothalamic FKBP51 acts as a molecular switch linking autophagy to whole-body metabolism. *Science Advances*, 8, 4797. https://doi.org/10.1126/SCIADV.ABI4797

Chapter 2.4

<u>Brix, L.M.</u>, Toksöz, I., Aman, L., Bordes, J., Doeselaar, L.V., Engelhardt, C., Häusl, A.S., Kovarova, V., Narayan, S., Springer, M., Sterlemann, Yang, H., Deussing, J.M. & Schmidt, M.V. (2022). Contribution of the co-chaperone FKBP51 in the ventromedial hypothalamus to metabolic homeostasis in male and female mice. *Molecular metabolism*. Manuscript under revision.

Chapter 2.5

Brix., L.M., Häusl, A.S., Toksöz, I., Aman, L., Bordes, J., Doeselaar, L.V., Engelhardt, Kovarova, V., Narayan, S., Springer, M., Sterlemann, Yang, H., Deussing, J.M. & Schmidt, M.V. (2022). Deletion of the co-chaperone FKBP51 in POMC- but not AGRP neurons of the arcuate nucleus improves whole-body metabolism in male and female mice. Manuscript in preparation.

Chapter 2.5

Additional Contributions

Doeselaar, L., Yang, H., Bordes, J., <u>Brix, L.M.</u>, Engelhardt, C., Tang, F., & Schmidt, M. V. (2020). Chronic social defeat stress in female mice leads to sex-specific behavioral and neuroendocrine effects. *Stress*, https://doi.org/10.1080/10253890.2020.1864319

Engelhardt, C., Tang, F., Elkhateib, R., Bordes, J., <u>Brix, L.M.</u>, Doeselaar, L., Häusl, A.S., Pöhlmann, M.L., Schraut, K.G., Yang, H., Chen, A., Deussing, J., & Schmidt, M.V. (2021). FKBP51 in the Oval Bed Nucleus of the Stria Terminalis Regulates Anxiety-Like Behavior. *eNeuro*, 8 (6). https://doi.org/10.1523/ENEURO.0425-21.2021

Declaration of Contribution

I hereby clarify that I contributed may own work to the current thesis, entitled *'Dissecting the cell type-specific role of FKBP51 in the stress response and whole-body metabolism - The WHEN and WHERE matters –'* in the following way:

Chapter 2.1

Designing and planning the study:

In collaboration with AH and MVS

Conducting the experiments:

In collaboration with AH, MP, DM, CE, TB

Analyzing the data:

Independently executed – Figure 6

Preparing the manuscript:

In collaboration with AH and MVS

Chapter 2.2

Designing and planning the study:

In collaboration with AH and MVS

Conducting the experiments:

In collaboration with AH, IT, JB, LvD, CE, SN, MS and VS

Analyzing the data:

Independently executed

Preparing the manuscript:

In collaboration with MVS

Chapter 2.3

Designing and planning the study:

In collaboration with AH, TB, NCG and MVS

Conducting the experiments:

In collaboration with AH, TB, MP, MH, MA, JN, FD, GB, GS and KG

Analyzing the data:

In collaboration with AH and TB

Preparing the manuscript:

In collaboration with AH, TB, NCG and MVS

Chapter 2.4

Designing and planning the study:

In collaboration with MVS

Conducting the experiments:

In collaboration with IT, LA, JB, LvD, CE, AH, VK, SN, MS, VS and HY

Analyzing the data:

Independently executed

Preparing the manuscript:

In collaboration with MVS

Chapter 2.5

Designing and planning the study:

In collaboration with AH and MVS

Conducting the experiments:

In collaboration with IT, LA, JB, LvD, CE, AH, VK, SN, MS, VS and HY

Analyzing the data:

Independently executed

Preparing the manuscript:

In collaboration with MVS

Munich, 1st of June, 2022

Lea Maria Brix

Hiermit bestätige ich die von Frau Lea Maria Brix angegebenen Beiträge zu den einzelnen Publikationen.

München, 1ˢᵗ of June, 2022

Mathias V. Schmidt

1. General Introduction

1.1 The pandemic of stress-related diseases

We live in a very stressful world: The COVID19 pandemic, climate change, Russia's invasion of Ukraine, and inflation are just some of the many stressors facing our modern society. As a result, these stressors can cause diminished productivity, accidents, absenteeism, and direct medical, legal, and insurance costs of $300 billion every year. National surveys conducted by the American Psychological Association (APA) show that 75% of adult Americans experienced moderate to high stress levels, with a trend towards increasing perceived stress levels throughout 2021. The combination of these stressors and the steady drumming of a crisis that shows no sign of stopping is causing the APA to sound the alarm: '*We are facing a national mental health crisis that could yield serious health and social consequences for years to come*.' (American Psychological Association, 2022). The idea that stress can determine a person's state of mind and negatively affect psychological health has been known for decades. Consistent with this view, there is ample scientific evidence that exposure to recent or chronic stressful events is associated with the occurrence of psychiatric diseases, such as depression, post-traumatic disorder (PTSD), and anxiety (De Kloet et al., 2005; Holsboer, 2000; McEwen, 2003; Selye, 1936).

While stress research has evolved around the consequences of stress on mental health, scientists have only recently connected ill-timed, chronic, and severe stressors with metabolic disturbances, such as cardiovascular disease, metabolic syndrome, type 2 diabetes (T2D), eating disorders, and obesity. Moreover, several chronic stress-related mental health disorders, such as depression, anxiety, and substance abuse, are often comorbid with metabolic abnormalities (Rabasa and Dickson, 2016; Russell and Lightman, 2019; Tomiyama, 2019; van der Kooij, 2020).

Even though there is a concise link between stress, metabolic diseases, and mental health, the question of how they are interwoven and whether they are mutually dependent remains unresolved. However, research suggests that the answer to this overarching question lies in our physiological stress response system, which has evolved to help us escape life-threatening situations by mobilizing the appropriate allocation of resources.

1.2 The stress response

1.2.1 History and concept of stress

Stress is a daily reality for most living organisms and the idea that stress matters for health and well-being is now widely accepted by the public and among many researchers and physicians. However, when it comes down to a concise definition of the term, it becomes clear that the perception of stress is highly subjective and variable across times and cultures, puzzling scientists for decades. The French physiologist Claude Bernard made the most fundamental contribution to stress research with his theory of the *milieu intérieur*: he stated that the maintenance of life depends crucially on keeping our internal milieu constant in the face of a changing environment (Bernard, 1872). Fifty years later, Walter Cannon expanded on Bernard's ideas of internal physiological mechanisms in response to toxic influences and introduced the term "homeostasis" (Cannon, 1915). However, it was not until 20 years later that Hans Selye coined the term 'stress response' to describe the non-specific pattern of physiological responses to stress (Selye, 1936). Today's classical concept of stress is based on Selye's theory that all living organisms strive towards a dynamic equilibrium (homeostasis) and that physical and psychological events, defined as 'stressors', threaten this equilibrium. As a result, behavior is directed towards appraising the stressor's destabilizing potential and reinstating homeostasis. Therefore, the stress response has evolved as an adaptive process, keeping us alert, motivated, and ready to avoid danger ('eustress'). However, if these stressors are of chronic or severe nature, or the stress response is inadequate ('distress'), the cost of reinstating this equilibrium becomes too high, a condition termed 'allostatic load' (McEwen, 2003). Such inappropriate responses and prolonged stressors can produce a vulnerable phenotype and serve as triggers for mechanisms that leave genetically predisposed individuals at increased risk for mental and metabolic illness.

1.2.2 The 'fight-or-flight' response

Our brain continuously integrates sensory information, identifies potential threats, and coordinates appropriate physiological responses to fine-tune homeostasis. The hypothalamic-pituitary-adrenal (HPA) axis and the sympatho-adreno-medullary system (SAM) are critical components of the stress response that integrate stress signals of actual or perceived threats. Shortly after a stressful event, activation of the SAM initiates the release of monoamines, including noradrenaline, dopamine, and serotonin, from sympathetic nerve

endings in the brainstem, such as the locus coeruleus (LC), which in turn triggers adrenalin and noradrenalin release from the adrenal medulla into the blood circulation (Valentino and Van Bockstaele, 2008). These catecholamines then cause immediate but short-lasting characteristic effects of the 'fight-or-flight' response in the periphery (e.g., increase in heart rate, respiration, pupil dilation, digestion), mobilizing the appropriate allocation of resources in a potentially threatening situation. Each monoamine contributes to specific behavioral aspects to collectively promote crucial behavioral strategies that help the individual overcome and survive the initial phase of a stressful event (Joëls and Baram, 2009; Ulrich-Lai and Herman, 2009). The second system, which response is slower but longer lasting compared to the 'fight or flight' response, is the HPA axis.

1.2.3 The HPA axis – Focus on the PVN

In the HPA axis, the paraventricular nucleus (PVN) in the hypothalamus stands out as the principal integrator of perceived stress signals. This nucleus contains three main functional neuronal types that act as central stress response regulators: parvocellular and magnocellular neurosecretory neurons and long-projecting neurons in the intermediocellular region. Parvocellular neurons send their projections to the median eminence (MEE) to regulate the release of corticotropin-releasing hormone (CRH) together with arginine-vasopressin (AVP), thyrotropin-releasing hormone (TRH), and somatostatin (SST) into the pituitary (PIT) to influence the synthesis and release of hormones from endocrine cells. Magnocellular neurons send their axons directly to the posterior lobe of the pituitary (PP) and secrete either oxytocin (OXT) or AVP directly into the general circulation. Long-projecting neurons in the intermediocellular component express mainly melanocortin 4 receptor (MC4R) and OXT, which project primarily to the hindbrain to regulate energy balance. Transcription factor single-minded homolog 1 (SIM1) is ubiquitously expressed in the PVN and acts as a critical regulatory gene of the PVN on AVP, TRH, CRH, and OXT expression (Qin et al., 2018) (see Figure 1).

Immediately after their release from the PVN, CRH and AVP act at their receptors (corticotropin-releasing hormone receptor 1 (CRHR1) and arginine-vasopressin receptor 1 B (AV1BR), respectively) to induce the transcription of pro-opiomelanocortin (POMC), and its downstream synthesis to adrenocorticotropin hormone (ACTH), which is released from corticotrope cells of the AP (Joëls and Baram, 2009; Rotondo et al., 2016). Peripheral ACTH

subsequently stimulates the release of glucocorticoids (GCs) (cortisol in humans and corticosterone (CORT) in rodents) from secretory cells of the zona fasciculata (ZF) and zona reticularis (ZR) of the adrenal cortex. This steroid hormone is considered the main hormonal end product of the HPA axis that ultimately acts on a plethora of peripheral organ systems and the brain to modulate downstream effects of the stress response by binding to glucocorticoid receptors (GR) and mineralocorticoid receptors (MR) (Sapolsky et al., 2000; Sheng et al., 2021; Sorrells et al., 2009). Further, GCs are involved in the negative feedback at several levels of the HPA axis, including the PIT, PVN, and hippocampus (HIP), to shut down the stress response and restore the homeostatic equilibrium (Myers et al., 2012) (see Figure 1). *Pomc*-expressing corticotropes in the AP gland are the key cell population of this GC-dependent negative feedback regulation of the HPA axis in the periphery. Consequently, they express high levels of GR receptors, and therefore GCs directly inhibit *Pomc* gene expression in pituitary corticotrope cells (Jenkins et al., 2013; Kageyama et al., 2021; Parvin et al., 2017).
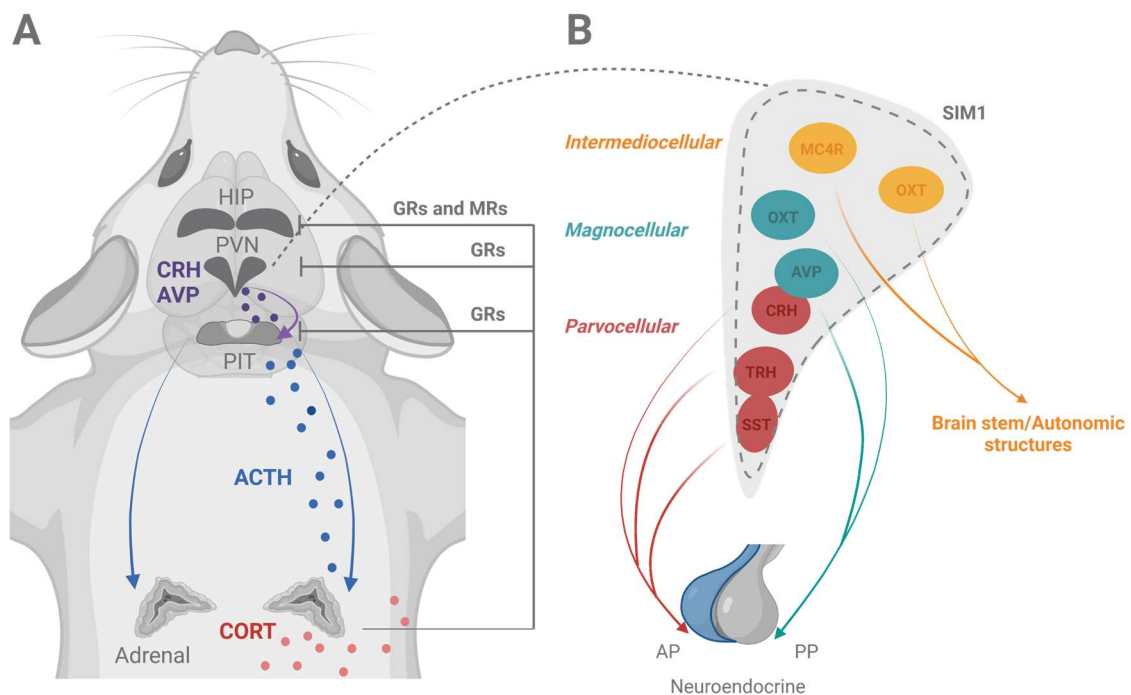
Created with BioRender.com

Figure 1: Hypothalamic-pituitary-adrenal (HPA) axis and cytoarchitecture of the paraventricular nucleus (PVN) of the hypothalamus

(A) Activation of the HPA axis by psychological or physiological stressors leads to the secretion of hypothalamic corticotropin-releasing hormone (CRH) and arginine-vasopressin (AVP) from the PVN. Subsequently, this triggers the secretion of adrenocorticotropin hormone (ACTH) from corticotrope

cells of the anterior pituitary (AP). ACTH stimulates the secretion of glucocorticoids (GCs) from the adrenal cortex (cortisol in humans and corticosterone (CORT) in rodents) that exert their function at the glucocorticoid (GR) and mineralocorticoid receptor (MR). Once perceived stressors have declined, GC-mediated negative feedback at several tissue targets along the HPA axis (pituitary (PIT), PVN, hippocampus (HIP)) shuts down the stress response and reinstates homeostasis. (**B)** Cytoarchitecture of the PVN highlighting relevant cellular subdivisions in the neuroendocrine stress response system. Parvocellular neurons (red), including somatostatin (SST), thyrotropin-releasing hormone (TRH), and corticotropin-releasing hormone (CRH), project to the median eminence (MEE) and are released into the anterior pituitary (AP) to initiate the HPA axis. The magnocellular neurons (green), including AVP and oxytocin (OXT) neurons, project to the posterior pituitary (PP). The long-projecting neurons in the intermediocellular compartment (yellow), including OXT and melanocortin 4 receptor (MC4R) neurons, project to autonomic structures in the brainstem, regulating energy balance. Transcription factor single-minded homolog 1 (SIM1) is ubiquitously expressed in the PVN and acts as a critical regulatory gene of the PVN on AVP, TRH, CRH, and OXT expression.

1.3 Corticosteroid hormones and their receptors

Independent of stress, GCs are secreted from the adrenal gland in about hourly pulses to synchronize and coordinate the mobilization of energy stores to meet the needs of an awake organism. This intrinsic rhythmicity introduces high inter-individual variation into the stress response and the fundamental processes underlying homeostasis (Young et al., 2004). The key to understanding stress-related and baseline HPA axis function lies within the receptor system that mediates the action of corticosteroids: the type II GR (encoded by the *Nr3c1*), selective for naturally occurring and synthetic GCs, and the type I MR (encoded by the *Nr3c2*), which binds CORT with a 10-fold higher affinity than the GR. Another steroid, aldosterone, can activate MR within the periphery in kidney and colon epithelial cells. Here, GCs are enzymatically converted by 11 β-hydroxysteroid dehydrogenase type II to inactivate CORT, thereby allowing the lower affinity ligand aldosterone to bin. Both receptors belong to the family of nuclear transcription factors and are ubiquitously expressed in the brain, where they exert distinct roles based on different locations and binding affinities (De Kloet et al., 2005). Besides their genomic actions, they are also involved in rapid, non-genomic effects at the cell membrane (Karst et al., 2022). The GR is expressed in neurons and glial cells in limbic areas that control the physiological and behavioral stress response, such as the amygdala, HIP, hypothalamus, and POMC cells within the AP. GR density is highest in parvocellular PVN-CRH

neurons. MR expression, on the other hand, is more restricted. It is abundant in the rodent and human HIP and other limbic brain areas such as the prefrontal cortex and amygdala, with a considerable co-expression of the two receptors in the hippocampal pyramidal cells of almost all species (Meijer et al., 2018). At baseline circulating GC levels, the MR is primarily activated, while the GR becomes activated only when GC levels are elevated during the circadian peak or under stressful conditions. With this, the GR is essential for negative feedback and terminating the stress response (de Kloet et al., 2019). To better understand the mechanistic basis of the negative feedback regulation of the HPA axis, it is crucial to decipher the underlying molecular mechanisms and identify vital players in the process.

1.4 Co-chaperone FKBP51 in HPA axis negative feedback

In the absence of GC binding, steroid hormone receptors (SHRs) such as the GR and MR remain in the cytoplasm in a heterodimeric protein complex with heat shock protein 90 (Hsp90), heat shock protein 70 (Hsp70), Hsp90-organizing- (Hop), and Hsp90-binding protein p23 (Cheung and Smith, 2000; Noddings et al., 2022). Upon activation (binding by GCs), the receptor undergoes conformational changes leading to dissociation from these cytoplasmic chaperones (see Figure 2). In brief, Hsp70 binds to and unfolds the GR in the cytosol. Hop recruits the GR:Hsp70 complex to Hsp90. Hop is dislodged from the complex upon binding of other co-chaperones via their tetratricopeptide repeat (TPR) domains to a universal TPR binding domain on Hsp90 during GR complex maturation. Among these are the mammalian FK506-binding proteins (FKBPs), FKBP51 (encoded by the *Fkbp5* gene), and FKBP52 (encoded by the *Fkbp4* gene). Upon release of Hop, p23 binds and stabilizes the GR:Hsp90:FKBP51/FKBP52 heterocomplex. Subsequently, the GR binds CORT, dimerizes and binds to its cognate DNA sequences, called glucocorticoid response elements (GRE), and induces transcription of downstream genes (Baker et al., 2019; Biddie and Hager, 2009; Cheung and Smith, 2000; Fries et al., 2017) (see Figure 2).

FKBP52 and FKBP51 both belong to the superfamily of immunophilins (IMM) that bind to immunosuppressant drugs, such as rapamycin and FK506 (Schreiber, 1991), and were identified as co-chaperones of Hsp90 regulating the responsiveness of SHRs (Smith et al., 1993). While FKBP51 and FKBP52 share more than 70 % sequence identity in mammals, they have opposing regulatory functions on GR signaling (Binder, 2009; Storer et al., 2011; Wochnik et al., 2005), where FKBP51 inhibits nuclear transactivation, while FKBP52 promotes

translocation to the nucleus. In an ultra-short negative feedback loop, FKBP51 is upregulated by active GR, which in turn decreases GR ligand-binding sensitivity and nuclear translocation efficiency. FKBP52, on the other hand, is considered to promote GR activity, which may be a combination of increased dynein binding as well as displacing the inhibitory effects of FKBP51 from the Hsp90-heterocomplex (Baker et al., 2019; Denny et al., 2000; Fries et al., 2017) (see Figure 2).
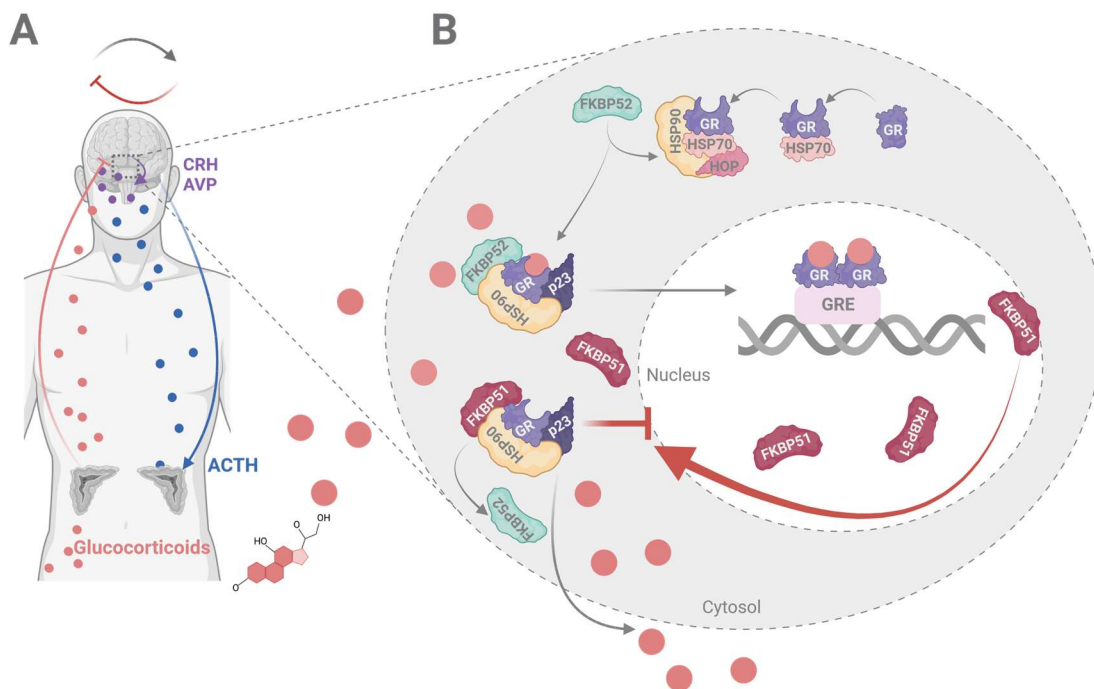
Created with BioRender.com

Figure 2: Schematic representation of key factors and chaperones involved in glucocorticoid receptor (GR) transactivation in response to glucocorticoids (GCs) and the FKBP51-mediated negative feedback loop

(A) Exemplary scheme of the negative feedback of the hypothalamic-pituitary-adrenal (HPA) axis by GCs in humans. (B) GCs secreted by the adrenal cortex after adrenocorticotropin releasing hormone (ACTH) binding cross the membrane and enter the cell. In the cytosol, the binding of heat shock protein 70 (HSP70) facilitates the folding of the GR into a conformation with low steroid affinity. Hsp90-organizing-protein (HOP) recruits GR:HSP70 to heat shock protein 90 (HSP90). Upon binding co-chaperones (FKBP51 and FKBP52), HOP is released from the complex, and p23 stabilizes the GR:HSP90 heterocomplex in a high-affinity state. The binding of FKBP51 to the complex decreases the affinity of GCs for GR and delays translocation to the nucleus. However, displacement of FKBP51 by FKBP52 increases ligand binding affinity, and nuclear translocation efficacy of the GR, allowing GCs to bind. The

GR dimerizes, migrates into the nucleus, and binds to GC response elements (GREs), activating transcription. The *Fkbp5* gene is one of the downstream target genes of the GR, resulting in an ultra-short negative feedback loop.

1.5 HPA-axis-related disease phenotypes – Focus on FKBP51

1.5.1   HPA axis in psychiatric diseases

Given its significant role in GR-mediated negative feedback control of the HPA axis, FKBP51 has been associated with diseases related to an imbalance of the stress hormone system. Most of those are related to acute or chronic exposure to stress, such as most neuropsychiatric disorders. Binder and colleagues could not only show that *Fkbp5* single nucleotide polymorphisms (SNPs) are connected to the antidepressant response and the recurrence of depressive episodes but also that increased *Fkbp5* expression following GR activation is associated with GR resistance and a higher risk for the onset of stress-related psychiatric diseases, such as depression and PTSD (see Figure 3 A) (Binder, 2009; Binder et al., 2008, 2004; Matosin et al., 2018; Zannas and Binder, 2014). The substantial involvement of FKBP51 in psychiatric disorders has encouraged preclinical research to investigate the mechanistic role of this co-chaperone in HPA axis (re)activity and disease using animal models. Endogenous overexpression of *Fkbp5* in squirrel monkeys, which have high circulating cortisol to compensate for low-affinity GRs, decreased hormone-binding affinity of the GR in these animals (see Figure 3 A) (Denny et al., 2000; Scammell et al., 2001; Westberry et al., 2006). Further, *Fkbp5* mRNA is ubiquitously expressed in the mouse brain and shows substantial overlap with the GR, e.g., in the HIP and hypothalamus (Scharf et al., 2011). Both in rats and mice, *Fkbp5* mRNA expression and FKBP51 protein level are inducible by the GC agonist dexamethasone (DEX), CORT, and by stress paradigms (Guidotti et al., 2012; Hartmann et al., 2012; Lee et al., 2011, 2010; Scharf et al., 2011; Yang et al., 2012). A knockout mouse line lacking FKBP51 (FKBP51$^{-/-}$/51KO) displays decreased HPA axis (re)activity and *Gr* expression changes in response to acute stressors, positively shaping the neuroendocrine profile of these animals (Hartmann et al., 2012; Touma et al., 2011).

1.5.2   HPA axis in aging

In addition to stressful acute or chronic living conditions and psychiatric disorders, aging leads to changes in the human's and rodent's hormonal stress responses. HPA axis function and

stress reactivity increase with age due to impaired negative feedback of the HPA axis (Belvederi Murri et al., 2014; Gupta and Morley, 2014; Sapolsky et al., 1986). In addition, various age-related morphological changes in the adrenal glands are associated with altered hormone secretion, leading to a gradual increase in GC secretion (Yiallouris et al., 2019). Therefore, the ability of the aging human to adequately terminate the stress response system is impaired. Consistent with these findings, the negative feedback regulation of the HPA system appears to be profoundly disrupted in aging rodents and non-human primates (Goncharova et al., 2002; Sapolsky, 1992). Interestingly, Sabbagh and colleagues showed that FKBP51 levels in rodents increase with aging, contributing to reduced resilience to depression-like behavior via impaired GC signaling, a phenotype absent in mice with complete *Fkbp5* knockout (O'Leary et al., 2011; Sabbagh et al., 2014). Furthermore, a clinical study by Zannas et al. confirmed a genome-wide epigenetic upregulation of FKBP51 by aging and stress in peripheral blood, promoting inflammation and cardiovascular risk in the elderly population (see Figure 3 B) (Zannas et al., 2019).

The stress- and age-induced pathophysiologies described all share an increase in FBKP51 levels and reduced GR-mediated negative feedback regulation of the HPA axis, which occurs at different hierarchical levels, including the HIP, PVN, and the PIT (Schmidt et al., 2009, 2005; Wagner et al., 2011). Intriguingly, all of these anatomical sites exhibit stress-induced expression changes of *Fkbp5* (Jenkins et al., 2013; Scharf et al., 2011). However, region- and cell type-specific functions of FKBP51 in stress system biology are still lacking.[1]

1.5.3   HPA axis in obesity

It has been well appreciated that chronic stress combined with a positive energy balance increases the risk for obesity, but the underlying mechanisms, molecular players, and circuits remain elusive (Bose et al., 2009). From an evolutionary point of view, it makes sense that stress affects metabolic processes: one of the primary goals of our stress response is to supply our body with energy in the form of glucose to escape life-threatening situations. However, the stressors of modern society often do not require a physical response as they are primarily psychosocial in nature. Consequently, excess cortisol (CORT in rodents) can eventually increase body fat accumulation in human and animal models resulting in weight gain (Björntorp, 2001; Björntorp and Rosmond, 2000). The pathways linking stress to obesity

---

[1] Adapted from Brix et al., 2022.

are diverse, ranging from cognition and behavior to eating and reward processing. One of the pathophysiological hallmarks of obesity is a hypersensitive HPA axis (Tomiyama, 2019). Clinical studies have shown that obese individuals have higher circulating levels of cortisol following pharmacological stimulation with ACTH or CRH, suggesting a hypersensitive HPA axis (Incollingo Rodriguez et al., 2015). Consistent with these findings in humans, diet-induced obese rats also have higher circulating CORT levels following physical stressors (Levin et al., 2000). One of the hallmarks of FKBP51 is its involvement in the negative feedback of the HPA axis, which fine-tunes our hormonal stress response system. Excess FKBP51 leads to hypersensitivity and impaired negative feedback of the HPA axis in *in vitro* and *in vivo*, resulting in elevated cortisol levels (see Figure 2). Besides a potential involvement of FKBP51 in metabolic phenotypes and obesity (see Figure 3 C, 1.6.1 and 1.6.2), this protein is involved in various metabolic signaling pathways that control homeostasis and energy metabolism (see Figure 4).
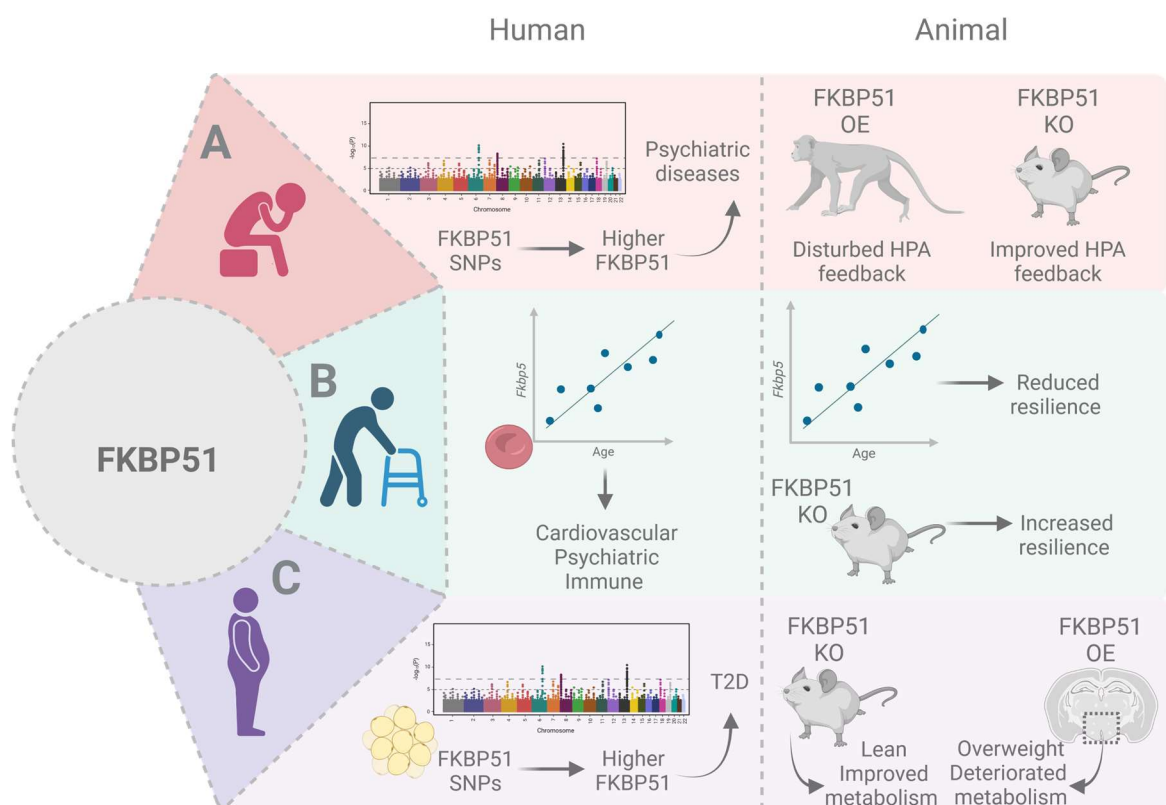
Created with BioRender.com

Figure 3: FKBP51 in clinical- and preclinical disease phenotypes

(A) *Psychiatric disorders:* In humans, *Fkbp5* single nucleotide polymorphisms (SNPs) are associated with a higher risk of developing stress-related psychiatric disorders such as depression and post-

traumatic stress disorder (PTSD). Endogenous FKBP51 overexpression (OE) decreases the hormone-binding affinity of the glucocorticoid receptor (GR) and disrupts negative feedback of the hypothalamic-pituitary-adrenal (HPA) axis. Knockout of FKBP51 (51KO) in mice improves (re)activity of the HPA axis and positively influences the neuroendocrine profile of these animals. **(B)** *Aging:* Clinical studies in human peripheral blood show a genome-wide epigenetic upregulation of FKBP51 and *Fkbp5* methylation by aging and stress, promoting inflammation, cardiovascular- and psychiatric risk in the elderly population. In mice, *Fkbp5* mRNA increases with age, which is positively correlated with lower resilience to age-related depression-like behaviors. 51KO increases resilience in aged animals and reverses age-related phenotypes. **(C)** *Obesity:* A study in human adipocytes identified various SNPs in the *Fkbp5* gene associated with type 2 diabetes (T2D), triglyceride accumulation, and altered cholesterol blood levels. Consistent with this, 51KO mice have a leaner body weight (BW) phenotype and improved metabolism. FKBP51 OE in the mediobasal hypothalamus (MBH) induces obesity and worsens metabolic outcomes under a high-fat diet (HFD) challenge.

1.6 FKBP51 and the molecular chaperoning of metabolism

Fkbp5 is abundantly expressed in metabolically relevant tissues in the periphery, such as adipocytes and skeletal muscle (Balsevich et al., 2017; Baughman et al., 1997; Pereira et al., 2014; Sidibeh et al., 2018) and brain regions, like the arcuate nucleus (ARC) and ventromedial hypothalamus (VMH), both well-established as neuronal hubs controlling energy balance (see 1.7) (Balsevich et al., 2014; Gautron et al., 2015; Scharf et al., 2011). Based on this expression profile, it is not surprising that animal and cell culture studies have uncovered new and potentially important roles for FKBP51 in metabolism.

1.6.1   FKBP51 in human metabolic phenotypes

The first clinical study by Pereira and colleagues on FKBP51 in 2014 investigated the effects of *Fkbp5* expression in adipose tissue on metabolic control. The authors could show that DEX has a direct regulatory role on FKBP51 level in subcutaneous and omental human adipose tissue. Higher *Fkbp5* gene expression in omental adipose tissue was associated with markers of insulin resistance. The same study identified 12 SNPs in the *Fkbp5* gene associated with T2D, triglyceride accumulation, and altered cholesterol blood levels in humans (see Figure 3 C) (Pereira et al., 2014). Four years later, Sidibeh et al. (2018) showed that in humans with T2D, the expression of *Fkbp5* was increased in subcutaneous adipose tissue and that the gene is associated with lipid metabolism and adipogenesis. They revealed that FKBP51 negatively correlates with genes involved in adipogenesis (Sidibeh et al., 2018). Supporting

the hypothesis that FKBP51 is a risk gene for insulin resistance and obesity (Fichna et al., 2018), two studies identified methylation of *Fkbp5* at introns 2 and 7 as a potential marker for GC resistance induced by FKBP51 (Ortiz et al., 2018; Resmini et al., 2016). Others have found that the SNP rs1360780 in the *Fkbp5* gene locus, which leads to increased FKBP51 level, is associated with reduced weight loss after bariatric surgery (Hartmann et al., 2016).

1.6.2   FKBP51 in preclinical metabolic phenotypes

The human studies on FKBP51 align with rodent preclinical studies showing that FKBP51 loss is beneficial for whole-body metabolism and energy homeostasis. In 2012 two studies reported that 51KO mice are leaner than their control littermates under a regular chow diet (Hartmann et al., 2012; Sanchez, 2012). Two years later, a study by Balsevich and colleagues revealed a positive correlation between chronic stress, *Fkbp5* mRNA, and BW gain, suggesting FKBP51 is a link between stress-related disorders and metabolic complications (Balsevich et al., 2014). Further, 51KO mice are resistant to a high-fat diet (HFD) induced weight gain; display improved glucose tolerance and increased energy expenditure (see Figure 3 C) (Balsevich et al., 2017; Stechschulte et al., 2016). A study by Soukas and colleagues revealed that leptin-deficient *ob/ob* mice have high expression levels of *Fkbp5* in white adipose tissue (WAT), which is reduced after several days of leptin treatment. This suggests that the co-chaperone is involved in leptin signaling pathways such as hunger and satiety (Soukas et al., 2000). Further, hypothalamic *Fkbp5* mRNA is induced by fasting, and viral overexpression of this gene in the hypothalamus results in increased vulnerability to a metabolic HFD challenge (see Figure 3 C) (Yang et al., 2012). Previous and ongoing molecular- and pathway analyses further decipher the mechanistic involvement of FKBP51 in homeostatic pathways such as protein kinase B (AKT)-signaling, adipogenesis, and autophagy.

1.6.3   FKBP51 in AKT-signaling

FKBP51 is known as a negative regulator of the cell growth regulator AKT. The AKT signaling pathway is a crucial player in cellular functions under healthy and pathological conditions. It could be shown that in cancer cells, FKBP51 acts as a scaffolding protein between AKT and PH domain leucine-rich repeat phosphatase (PHLPP) to facilitate the dephosphorylation and inactivation of AKT. In line with this regulatory role via AKT, loss of FKBP51 and AKT hyperactivation are implicated in several pancreatic and breast cancer cell lines (Pei et al., 2009). Interestingly, the AKT pathway is also involved in energy homeostasis as a nutrient

sensor (Kim et al., 2006). Further, it plays a vital role in the insulin-signaling cascade as it is involved in the peripheral control of hepatic glucose production (Schwartz et al., 2013) as well as insulin resistance (Samuel and Shulman, 2012). The first mechanistic *in vivo* study by Balsevich and colleagues demonstrated that FKBP51 plays a role in glucose homeostasis by regulating AKT2 signaling (see Figure 4 A). They identified a new link between FKBP51 and AKT substrate 160 (AS160), a substrate of AKT2 involved in glucose uptake in skeletal myotubes (Balsevich et al., 2017).

1.6.4   FKBP51 in adipocytes

Following the discovery that FKBP51 is one of the key proteins induced during WAT adipocyte differentiation (Toneatto et al., 2013; Yeh et al., 1995), Stechschulte and colleagues set out to investigate the underlying molecular mechanisms and pathways: *In vitro* studies in FKBP51-deficient mouse embryonic fibroblasts revealed that FKBP51 controls cellular adipogenesis via the AKT-p38 kinase-mediated phosphorylation of GRα and PPARγ (peroxisome proliferator-activated receptor-γ), the master regulator of adipocyte differentiation (see Figure 4 B). Loss of FKBP51 resulted in significantly reduced lipid accumulation, reduced fatty acid synthase activity, and expression of adipogenic genes (Stechschulte et al., 2014a, 2014b; Toneatto et al., 2015). Studies in FKBP51-deficient mice suggest that FKBP51 plays an essential role in WAT browning. 51KO mice show an upregulation of thermogenic genes, such as uncoupling-protein 1 (UCP1), associated with increased energy expenditure, which is a potential explanation for their lean phenotype (Balsevich et al., 2017; Stechschulte et al., 2016). Studies in human adipose tissue cultures confirm the results of preclinical studies in rodents: Pereira and colleagues were able to show that DEX exposure promotes *Fkbp5* expression in human adipose tissue and that increased levels of FKBP51 are associated with insulin resistance (Pereira et al., 2014). In human subcutaneous tissue, *Fkbp5* expression levels correlated positively with several indices of GC-induced-insulin resistance and were higher in individuals with T2D compared to controls (Sidibeh et al., 2018).

1.6.5   FKBP51 in autophagy

Autophagy is our body's way of cellular housekeeping: it is the natural, conserved degradation of cellular debris, such as misfolded proteins, damaged organelles, and pathogens. Cellular fragments are taken up by autophagosomes and degraded by fusion with lysosomes to form an autolysosome. These processes are orchestrated by a total of 30 autophagy-related genes

(Atgs) and regulatory hetero protein complexes, such as adenosine 5'-monophosphate (AMP)–activated protein kinase (AMPK), which are regulated via a complex pathway under the control of the mTOR kinase (mammalian target of rapamycin) signaling cascade (Dikic and Elazar, 2018). Hereby, autophagy is an adaptive process that responds to various stressors such as nutrient deprivation, high-calorie intake, infection, and inflammation and plays a vital role in regulating metabolic processes and obesity (Häusl et al., 2019; Zhang et al., 2018). Recent studies have added the tryptophan-aspartic acid (WD)-repeat proteins to the plethora of autophagy regulators. They interact with the phosphoinositide protein family (WIPI) and act as subordinate scaffold proteins linking autophagy signaling control and autophagosome formation (Bakula et al., 2017).

Studies by Gassen et al. (2019) have shown that FKBP51 plays a central role in autophagy and related mechanisms by binding to the essential autophagy regulators AKT and Beclin1. The binding of FKBP51 to Beclin1 alters its phosphorylation status and thus promotes the induction of autophagic processes. In addition, FKBP51 was shown to interact with PHLPP and AKT, favoring the dephosphorylation of AKT and promoting the recruitment of Beclin1 and its subsequent dephosphorylation (see Figure 4 C). Furthermore, the researchers showed that synthetic GCs, such as DEX and antidepressants, act synergistically with FKBP51 in the induction of autophagy (Gassen et al., 2015, 2014; Wang et al., 2012). Additionally, FKBP51 prevents Beclin1 from proteasomal degradation by reducing AKT-mediated phosphorylation of S-phase kinase-associated protein 2 (SKP2), thereby enhancing autophagy signaling (Gassen et al., 2019).

Data from human and preclinical studies suggest that FKBP51 plays a central role in whole-body metabolism and homeostasis, opening a new avenue of research for developing targeted therapeutic interventions to treat metabolic diseases and their comorbidities. However, to date, cell- and tissue-specific effects of FKBP51 on energy homeostasis *in vivo* are still lacking. A promising target to study the role of FKBP51 in energy homeostasis is the brain, particularly the mediobasal hypothalamus (MBH).
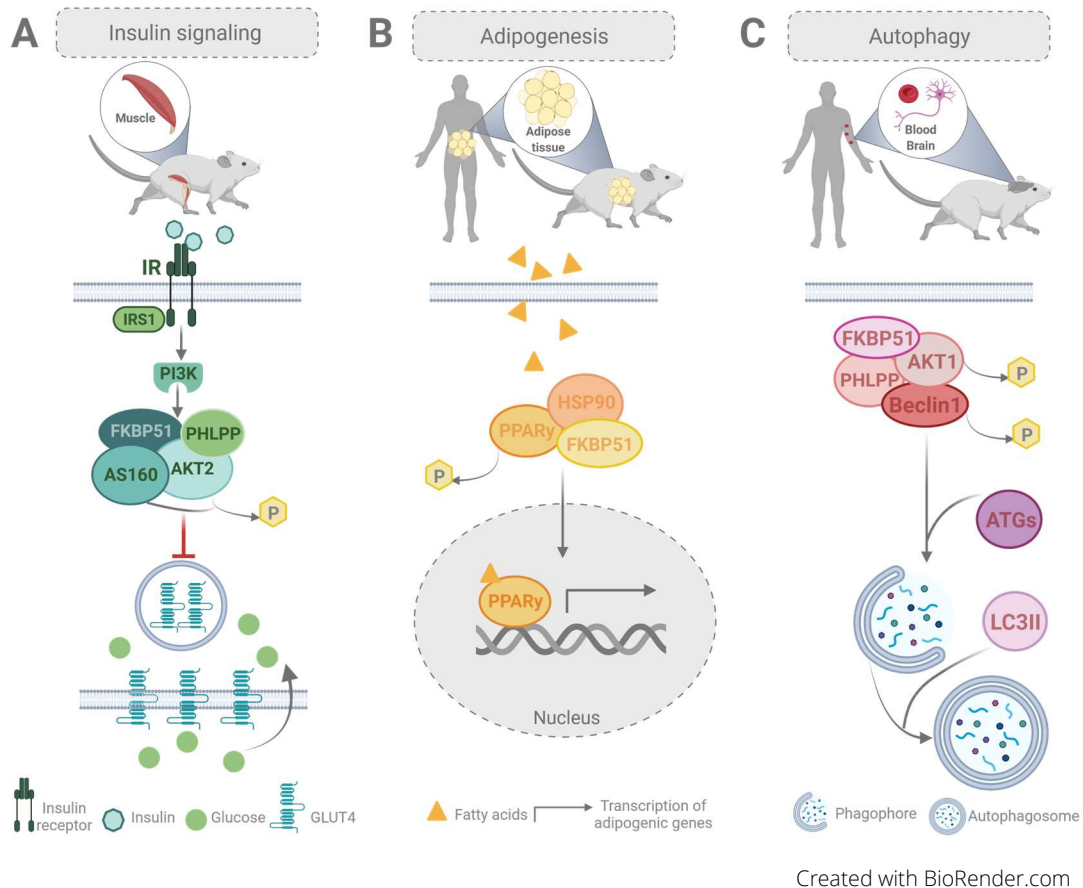
Created with BioRender.com

Figure 4: Molecular chaperoning of FKBP51 in cellular metabolic signaling cascades

(A) During insulin signaling in mouse skeletal muscle, FKBP51 scaffolds protein kinase B 2 (AKT2), PH domain leucine-rich repeat phosphatase 1 (PHLPP1), and AKT substrate 160 (AS160). In the presence of FKBP51, PHLPP-mediated inactivation of AKT2 and activation of AKT substrate 160 (AS160) are enhanced: PHLPP phosphatase activity is targeted towards AKT2 to inactivate it and decrease AS160 phosphorylation. Ultimately, this decreases glucose transporter 4 (GLUT4) recruitment to the cell surface and reduces glucose uptake. (B) FKBP51 increases the dephosphorylation of peroxisome proliferator-activated receptor-γ (PPARγ) (master regulator of adipogenesis) via the AKT-p38 signaling pathway to increase lipogenesis and decrease lipolysis in human and mouse adipose tissue. (C) In human peripheral blood and mouse brain cells, FKBP51 promotes the induction of autophagy signaling through dephosphorylation of Beclin1. Furthermore, FKBP51-mediated recruitment of PHLPP dephosphorylates the Beclin1-phosphorylating kinase AKT, which triggers downstream autophagy pathways.

1.7 Central control of energy homeostasis

The first scientist to describe the process of energy homeostasis was Kennedy in 1953, who discovered that food intake is controlled by a chemo-sensitive mechanism: His 'Lipostatic Model' assumes that signals proportional to the amount of fat in the body modulate the

amount of food consumed at each meal to maintain overall energy balance (Kennedy, 1953). Under physiological conditions, energy intake and expenditure are balanced by the biological process of 'energy homeostasis', which keeps body fat levels stable over time (Morton et al., 2014). This system is tightly regulated by complex processes in the peripheral and central nervous system involving thousands of genes, hormonal, and neuronal signaling networks that inform the central nervous system about the availability of stored nutrient resources (Lenard and Berthoud, 2008).

Despite the high efficacy of this system and its tight control in normal-weight individuals, the modern western world is confronted with a high prevalence of metabolic diseases, such as overweight, obesity, and T2D (Ryan et al., 2020), which highlights that the anatomy and functions of the neural systems involved in maintaining energy homeostasis are still poorly understood. This emphasizes that there is an urgent need for a deeper knowledge of the essential components driving and controlling this delicate system to tackle metabolic diseases.

1.7.1   Brain regions involved in energy homeostasis – Focus on the VMH

The hypothalamus is a dynamic brain region consisting of several distinct nuclei that contribute to neural circuits involved in energy homeostasis and food intake (see Figure 5 A, B). A long line of research dating back to the 1940s has uncovered a link between the brain and BW mediated by food intake, energy expenditure, body fat stores, and glucose signaling (Anand and Brobeck, 1951; Brobeck, 1946; Kennedy, 1950; Stellar, 1954). The identified regions of the hypothalamus constantly monitor metabolic signals that reflect the current energy status to adjust energy expenditure- and intake. Within this superordinate master regulator of whole-body metabolism, the ARC, located in the MBH has become one of the cornerstones of energy metabolism and food intake (Timper and Brüning, 2017). Located near the MEE, the ARC can sense peripheral nutrients and hormonal signals through two functionally distinct subpopulations (Myers and Olson, 2012): The orexigenic (appetite-stimulating) AgRP/NPY neurons expressing agouti-related peptide (AgRP) and neuropeptide Y (NPY), and the anorexigenic (appetite-suppressing) neurons that express POMC and amphetamine-related transcript (CART) (Balthasar et al., 2005). These first-order neurons, located in the ARC, gather information about the body's metabolic state and subsequently project to other intra- and extrahypothalamic brain areas (2nd order neurons) to maintain

energy homeostasis and to ensure nutrient demands are fulfilled (see 1.7.3) (Bellinger and Bernardis, 2002).

For a long time, the VMH and its importance for whole-body metabolism were underestimated and understudied. This is despite the fact that it was already described in the late 1940s as a potential neuronal center involved in energy homeostasis: A set of systematic lesions in rats in which several hypothalamic nuclei, including the VMH, PVN, and the dorsomedial hypothalamus (DMH), were destroyed, led to hyperphagia and obesity in these animals (Brobeck, 1946). Five years later, Brobeck and colleagues were able to show that lesions in the lateral hypothalamus (LH) lead to the opposite effect, namely hypophagia (Anand and Brobeck, 1951). These findings led to the postulation of the 'dual center model', which identified the VMH as the 'satiety center' with a high number of leptin receptors (LepR) and the LH as the 'hunger center' (Stellar, 1954). Today, we know that the VMH is a crucial target for insulin in the MBH as direct insulin infusions into this brain region decrease food intake and BW in rodents (Penicaud et al., 1989).

The heterogenous cytoarchitecture of the VMH is composed of different cell types with different gene expression patterns. The ubiquitously expressed *Nr5a1* gene, which encodes steroidogenic factor 1 (SF1), is specifically and exclusively expressed in the VMH within the brain. Here it acts as a transcription factor whose expression is essential for both the development and function of the VMH (Kurrasch et al., 2007; Parker et al., 2002). Studies using postnatal VMH-specific SF1 knockout mice mirrored the metabolic phenotype of VMH lesion in rats, highlighting the critical importance of SF1 in the VMH for healthy energy homeostasis; along with its role as a primary satiety center (Dhillon et al., 2006; Kim et al., 2011). Chemo- and optogenetic techniques that allow spatiotemporal neuronal manipulation showed that inactivation of *Sf1*-expressing neurons enhanced feeding behavior, decreased energy expenditure and thermogenesis, and blocked recovery from insulin-induced hypoglycemia via a variety of different hormone receptors, including LepR and insulin receptor (IR), nutrient sensors and sympathetic nervous system (SNS) activation (Fosch et al., 2021). Mice with specific deletion of the IR in SF1 neurons were protected from HFD-induced weight gain, which was associated with increased firing of POMC neurons. An effect that is likely driven by increased activity of glutamatergic projections from SF1 neurons (Klöckener et al., 2011).

1.7.2   The hypothalamic melanocortin pathway

The homeostatic regulatory neurocircuit underlying the interplay of these two subpopulations within the ARC is the central melanocortin pathway (see Figure 5) (Cone, 2005; Timper and Brüning, 2017). Both neuronal populations of the ARC (*Pomc*- and *AgRP/Npy*-expressing neurons, respectively) express receptors that can bind a wide variety of hormonal, neuronal, and metabolic signals such as leptin, ghrelin, insulin, glucose, serotonin, and leucine, which in turn act on these key neurons to regulate energy balance (Xu et al., 2011).

The two best characterized long-term adipostatic signaling molecules for the maintenance of whole-body energy homeostasis are leptin, secreted from adipose tissue, and insulin, secreted by the pancreas. Both humoral mediators circulate in proportion to body fat stores and have been shown to bind to AgRP/NPY and POMC neurons (Ellacott and Cone, 2006). AgRP/NPY neurons, which stimulate feeding behavior, food foraging, and locomotion when they are activated (Dietrich et al., 2015; Huang et al., 2013; Luquet et al., 2005), are inhibited by the binding of leptin (Cowley et al., 2001) and insulin (Spanswick et al., 2000). The effect of leptin as a humoral mediator on homeostasis was demonstrated in lep^{ob}/lep^{ob} mice lacking the leptin gene. These animals showed an increase in feeding behavior and developed severe obesity (Schwartz et al., 1996). Consistent with this phenotype, these mice showed elevated *Npy* mRNA expression (Thornton et al., 1997). Ghrelin, an acute hunger signal released from the gastrointestinal tract before meal onset, stimulates SST neurons in the tuberal region of the hypothalamus, facilitating energy intake (Cowley et al., 2003; Luo et al., 2018).

However, when leptin and insulin bind to POMC neurons, they activate this subpopulation in the ARC, promoting satiety, increased energy expenditure, and suppressed food intake (Hill et al., 2010; Schwartz et al., 1997; Timper and Brüning, 2017). This anorexigenic neuronal subpopulation of the MBH expresses the neuropeptide precursor POMC, which is cleaved to α-melanocyte-stimulating hormone (α-MSH). α-MSH mediates its effects via transmembrane melanocortin 3 and 4 receptors (MC3R/MC4R) on downstream targets, such as the PVN, VMH, and LH. Here, α-melanocyte acts as an agonist at these receptors (Millington, 2007), while AgRP is a high-affinity antagonist for both, promoting food intake and decreasing energy expenditure (Morton and Schwartz, 2001). Besides its antagonistic action on MC3R and MC4R receptors, preventing anorexigenic effects of α-MSH on 2nd order neurons (Morton and

Schwartz, 2001), AgRP/NPY neurons directly inhibit POMC neuron activity via inhibitory γ-aminobutyric acid (GABA) action at the level of the ARC (Cowley et al., 2001) (see Figure 5 D). Clinical and preclinical studies confirm their distinct roles, as patients with POMC deficiency (Krude et al., 1998) and POMC KO mice (Shen et al., 2017) develop severe metabolic complications such as obesity and hyperphagia. Mutations of the downstream α-MSH target MC4R are also strongly associated with obesity in humans (Farooqi and O'Rahilly, 2006; Yeo et al., 1998) and rodents, in which disruption of the MC4R results in hyperphagia, reduced energy expenditure, and impaired glucose homeostasis (Balthasar et al., 2005; Huszar et al., 1997). Preclinical AgRP/NPY ablation studies revealed that these neurons are critical for survival, as their loss leads to anorexia, rapid weight loss, and death by starvation (Krashes et al., 2011). Activation of AgRP/NPY neurons, on the other hand, produces a feeding response, decreases energy expenditure, and impairs glucose balance (Vohra et al., 2022). However, recent research has opened our eyes to a much more complex interplay between these two neuronal populations within the ARC that goes beyond this simplistic view of a 'ying and yang' interaction (Vohra et al., 2022). Most importantly, this sophisticated interplay does not function in isolation but in complex circuits involving intra- and extrahypothalamic connections to regulate complex behavior and homeostasis.

1.7.3 Intra- and extra-hypothalamic connections

Pomc- and *AgRP/Npy-*expressing neuronal subpopulations within the ARC project to 2nd order neurons in adjacent hypothalamic brain regions that express MC3R and MC4Rs, including the PVN, LH, VMH, and the DMH (Elmquist et al., 1998). These regions, in turn, project to other intra- and extrahypothalamic areas, resulting in an integrated response to energy intake- and expenditure. Here, the PVN has the highest and thus predominant MC4R population in the central nervous system, which regulates the inhibitory control of food intake (Krashes et al., 2016; Leibowitz et al., 1981). PVN neurons control sympathetic outflow to peripheral organs and secrete a variety of regulatory neuropeptides (Figure 5 E): brain-derived neurotrophic factor (BDNF), CRH, and TRH are downstream mediators that relay the effects MC4R activation on food intake and energy homeostasis via melanocortinergic neurons of the hypothalamus (Timper and Brüning, 2017). The energy expenditure that increases with MC4R activation is the result of increased sympathetic tone activating brown adipose tissue (BAT) (Voss-Andreae et al., 2007).

NPY/AgRP neurons, which send their inhibitory projections to the PVN and the LH, are stimulated by fasting to promote food intake and a positive energy balance (Betley et al., 2013). In addition, intrahypothalamic AgRP/NPY projections to the PVN and to the bed nucleus of the stria terminalis (BNST), which is involved in the control of feeding and reward behavior, were shown to decrease metabolic activity in BAT (Shi et al., 2013; Steculorum et al., 2016). POMC neurons innervate the PVN and the LH and send additional projections to the VMH and DMH, reducing feeding behavior via stimulation of MC3R/MC4R expressing neurons in these nuclei. Consequently, disruption of these projections by surgically removing the connections between the ARC and PVN results in obese phenotypes (Bell et al., 2000). In contrast to deletion studies in the PVN (Leibowitz et al., 1981), the DMH (Bellinger and Bernardis, 2002) and LH (Milam et al., 1980) revealed that these regions most likely involved in orexigenic signaling pathways, as their deletion produces a hypophagic, lean phenotype. Further, NPY/AgRP and POMC neurons receive excitatory glutamatergic input from the VMH and the PVN (Waterson and Horvath, 2015).

Despite the important role of the hypothalamus in maintaining energy homeostasis, the control of this highly complex process is not limited to this brain area alone. Hypothalamic nuclei have been shown to send their projections to several extrahypothalamic regions, such as the nucleus tractus solitarii (NTS), area postrema (AP), and raphe pallidus (RPA), all of which are located in the brainstem and influence satiety perception and food reward (see Figure 5 E) (Waterson and Horvath, 2015). The NTS plays a crucial role in suppressing food intake as this hindbrain nucleus expresses POMC neurons itself and is directly innervated by POMC terminals of the ARC to terminate meals and thereby maintain energy balance (Zheng et al., 2010). Besides its connection to the ARC, the NTS receives direct sensory information from the gastrointestinal tract via the afferent vagus nerve (Browning and Carson, 2021) and expresses a variety of receptors that can directly bind circulating nutrient satiety signals such as leptin, cholecystokinin (CCK), and glucagon-like peptide 1 (GLP1) and can thus act independently of hypothalamic neuronal circuits (Waterson and Horvath, 2015).
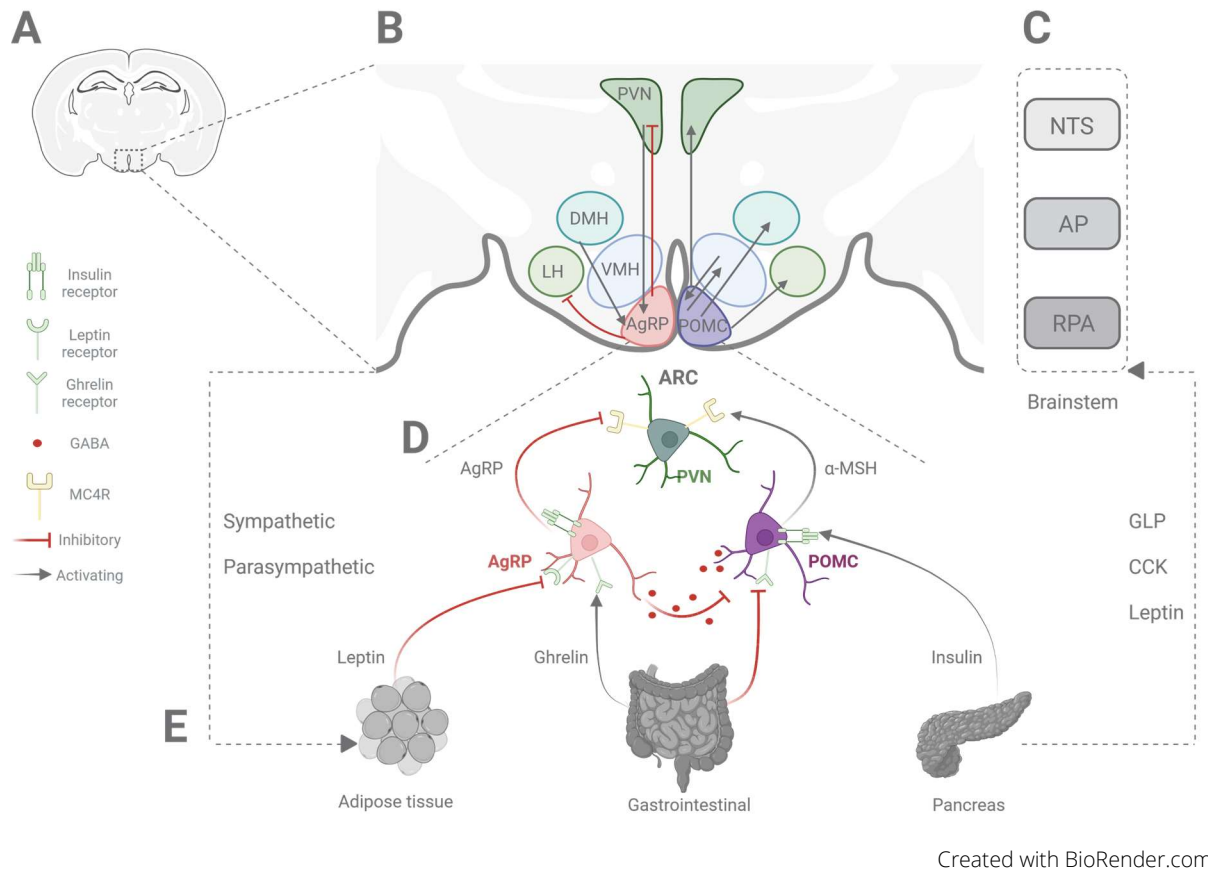
Created with BioRender.com

Figure 5: Hypothalamic and peripheral control of energy homeostasis

(A) Coronal section of a mouse brain highlighting the hypothalamus in the dashed square and figure legend. (B) Overview of selected hypothalamic brain areas and neuronal circuits controlling energy balance in the rodent brain. Neuropeptide Y (NPY)/agouti-related peptide (AgRP) neurons in the arcuate nucleus (ARC) (red) of the mediobasal hypothalamus (MBH) send their inhibitory projections to both the lateral hypothalamus (LH) and the paraventricular nucleus (PVN) to induce orexigenic pathways and promote feeding behavior. The dorsomedial hypothalamus (DMH) and PVN send their glutamatergic projections to NPY/AgRP neurons. Pro-opiomelanocortin (POMC) neurons (purple) innervate the PVN as well as the ventromedial hypothalamus (VMH), DMH, and LH and reduce feeding behavior via stimulation of melanocortin 4 receptor (MC4R)-expressing neurons in these nuclei. (C) Hypothalamic nuclei innervate extrahypothalamic nuclei in the brainstem, such as the nucleus tractus solitarii (NTS), area postrema (AP), and raphe nucleus (RPA), to control feeding behavior and energy homeostasis. (D) POMC and AgRP neurons in the ARC initiate the hypothalamic melanocortin pathway, which modulates the activity of post-synaptic MC4R neurons. The three primary hormonal mediators of feeding behavior, leptin, insulin, and ghrelin, act on POMC and NPY/AgRP neurons to modulate energy homeostasis. (E) The satiety signals leptin, cholecystokinin (CCK), and glucagon-like peptide 1 (GLP1) directly bind to their receptors in the brainstem, leading to meal termination. Adipose tissue is

abundantly innervated by hypothalamic sympathetic and parasympathetic fibers. Grey arrows represent activating and red, blunted arrows inhibitory neuronal inputs.

1.8 Rationale and thesis objectives

Clinical and preclinical studies position FKBP51 as a promising molecular target for the treatment of psychiatric and metabolic disorders and shed light on its potential overarching role in the underlying disease mechanisms. Research in rodents and humans has shown that this co-chaperone modulates biological signaling pathways central to homeostatic control, ranging from feedback mechanisms in our hormonal stress response system to autophagy and adipogenesis. An indispensable step towards targeted and effective pharmacological interventions for psychiatric and metabolic disorders is to decipher the tissue- and cell type-specific involvement of FKBP51 in these signaling pathways. So far, however, we lack knowledge about its exact role in specific brain regions, let alone in individual cell types. The present work, therefore responds to the urgent need for a more comprehensive, region- and cell type-specific understanding of the effects of FKBP51 to pave the way for future pharmacological intervention studies. To this end, I aimed to address the following research questions:

I.   What is the central role of FKBP51 in the PVN of the hypothalamus in modulating negative feedback control of the HPA axis? (Chapter 2.1)

II.   What is the peripheral role of FKBP51 in the pituitary gland in modulating negative feedback control of the HPA axis, and how does it affect aging-related dysregulation of the hormonal stress response system? (Chapter 2.2)

III.   In what way does modulation of *Fkbp5* expression in the rodent MBH influence autophagy signaling, and which molecular players are involved in the process? (Chapter 2.3)

IV.   How does FKBP51 in the rodent VMH (Chapter 2.4) and in *Pomc* expressing neurons of the ARC (Chapter 2.5) shape whole-body metabolism and energy homeostasis?

2. Research articles

2.1 The co-chaperone *Fkbp5* shapes the acute stress response in the paraventricular nucleus of the hypothalamus of male mice

Häusl, A.S.*, <u>Brix, L.M.</u>*, Hartmann, J., Pöhlmann, M.L., Lopez, J.P., Menegaz, D., Brivio, E., Engelhardt, C., Roeh, S., Bajaj, T., Rudolph, L., Stoffel, R., Hafner, K., Goss, H.M., Reul, J. M. H. M., Deussing, J.M., Eder, M., Ressler, K.J., Gassen, N.C., Chen, A. & Schmidt, M.V.

*Shared first authorship

ARTICLE

The co-chaperone Fkbp5 shapes the acute stress response in the paraventricular nucleus of the hypothalamus of male mice

Alexander S. Häusl[1] · Lea M. Brix[1,2] · Jakob Hartmann [3] · Max L. Pöhlmann[1] · Juan-Pablo Lopez[4] ·
Danusa Menegaz[5] · Elena Brivio [2,4] · Clara Engelhardt[1] · Simone Roeh[6] · Thomas Bajaj[7] · Lisa Rudolph[4] ·
Rainer Stoffel[4] · Kathrin Hafner[6] · Hannah M. Goss[8] · Johannes M. H. M. Reul [8] · Jan M. Deussing [9] ·
Matthias Eder[5] · Kerry J. Ressler [3] · Nils C. Gassen [6,7] · Alon Chen[4,10] · Mathias V. Schmidt [1]

Abstract

Disturbed activation or regulation of the stress response through the hypothalamic-pituitary-adrenal (HPA) axis is a fundamental component of multiple stress-related diseases, including psychiatric, metabolic, and immune disorders. The FK506 binding protein 51 (FKBP5) is a negative regulator of the glucocorticoid receptor (GR), the main driver of HPA axis regulation, and *FKBP5* polymorphisms have been repeatedly linked to stress-related disorders in humans. However, the specific role of *Fkbp5* in the paraventricular nucleus of the hypothalamus (PVN) in shaping HPA axis (re)activity remains to be elucidated. We here demonstrate that the deletion of *Fkbp5* in Sim1^{+} neurons dampens the acute stress response and increases GR sensitivity. In contrast, *Fkbp5* overexpression in the PVN results in a chronic HPA axis over-activation, and a PVN-specific rescue of *Fkbp5* expression in full *Fkbp5* KO mice normalizes the HPA axis phenotype. Single-cell RNA sequencing revealed the cell-type-specific expression pattern of *Fkbp5* in the PVN and showed that *Fkbp5* expression is specifically upregulated in *Crh*^{+} neurons after stress. Finally, *Crh*-specific *Fkbp5* overexpression alters *Crh* neuron activity, but only partially recapitulates the PVN-specific *Fkbp5* overexpression phenotype. Together, the data establish the central and cell-type-specific importance of *Fkbp5* in the PVN in shaping HPA axis regulation and the acute stress response.

Introduction

Life is full of challenges and appropriate coping with such events implies proper activation and termination of the stress response. The hypothalamic-pituitary-adrenal (HPA) axis is the central orchestrator of the stress response and its end product glucocorticoids (cortisol in humans, corticosterone (CORT) in rodents) mediates the adaptation to acute

These authors contributed equally: Alexander S. Häusl, Lea M. Brix

Supplementary information The online version contains supplementary material available at https://doi.org/10.1038/s41380-021-01044-x.

✉ Mathias V. Schmidt
    mschmidt@psych.mpg.de

1   Research Group Neurobiology of Stress Resilience, Max Planck Institute of Psychiatry, Munich, Germany

2   International Max Planck Research School for Translational Psychiatry (IMPRS-TP), Munich, Germany

3   Department of Psychiatry, Harvard Medical School, McLean Hospital, Belmont, MA, USA

4   Department of Stress Neurobiology and Neurogenetics, Max Planck Institute of Psychiatry, Munich, Germany

5   Electrophysiology Core Unit, Max Planck Institute of Psychiatry, Munich, Germany

6   Department of Translational Research in Psychiatry, Max Planck Institute of Psychiatry, Munich, Germany

7   Department of Psychiatry and Psychotherapy, Bonn Clinical Center, University of Bonn, Bonn, Germany

8   Neuro-Epigenetics Research Group, Bristol Medical School, University of Bristol, Bristol, United Kingdom

9   Research Group Molecular Neurogenetics, Max Planck Institute of Psychiatry, Munich, Germany

10 Department of Neurobiology, Weizmann Institute of Science, Rehovot, Israel

and chronic stressors in peripheral tissues as well as in the brain [1]. A hallmark of HPA axis regulation is the negative feedback on the secretion of stress hormones to terminate the stress response which is controlled by glucocorticoids via the glucocorticoid receptor (GR).

A critical regulator of GR and therefore key to a successful termination of the stress response is FK506 binding protein 51 (FKBP5), which is encoded by the *FKBP5* gene [2]. FKBP5 is an Hsp90-associated co-chaperone that restricts GR function by reducing ligand binding, delaying nuclear translocation, and decreasing GR-dependent transcriptional activity [3, 4]. Hence, higher levels of *FKBP5* mRNA are associated with higher levels of circulating cortisol and reduced negative feedback inhibition of the stress response [5–9]. Consequently, GR-induced *FKBP5* levels reflect the environmental stress condition, and as such, *FKBP5* expression has been used as a stress-responsive gene marker [10]. Importantly, *FKBP5* polymorphisms have been consistently associated with stress-related psychiatric disorders such as major depression and PTSD [11–13], where a demethylation-mediated increase in *FKBP5* expression was identified as causal in risk-allele carriers [14].

Despite the central importance of FKBP5 in stress system biology and stress-related disorders, detailed functional and mechanistic studies are still largely missing. Only a few human post-mortem studies focus on central tissue in order to dissect FKBP5 mechanisms [15, 16], while the majority of studies use peripheral blood mononuclear cells as a correlate of FKBP5 brain activity [17]. Most of the animal data were obtained from wild-type (WT) or conventional *Fkbp5* knockout mice, thereby lacking cell-type-specific insights of Fkbp5 function [8, 18]. To tackle this paucity of information, we here investigate the specific role of Fkbp5 in the paraventricular nucleus of the hypothalamus (PVN) the key brain region orchestrating the stress response [19]. Interestingly, previous data in rats suggested a potentially decisive role of Fkbp5 expression in the PVN to drive HPA axis hyperactivity achieved by a selective breeding approach [20]. Using site-specific manipulations of *Fkbp5*, single-cell RNA expression profiling, and functional downstream pathway analyzes, our data unravel a key role of PVN Fkbp5 in shaping the body's stress system (re) activity, with important implications for its contribution to stress-related disorders.

Material and methods

Animals and animal housing

All experiments were performed in accordance with the European Communities' Council Directive 2010/63/EU. The protocols were approved by the committee for the care and use of laboratory animals of the Government of Upper Bavaria, Germany. The mouse lines *Fkbp5*$^{lox/lox}$, *Fkbp5*$^{PVN-/-}$, *Fkbp5*$^{Frt/Frt}$, and CRH-ires-CRE/Ai9 were generated in house. Experiments were performed on male mice aged between 3 and 5 months unless stated otherwise in the results section. During the experimental time, animals were kept singly housed in individually ventilated cages (IVC; 30 cm × 16 cm × 16 cm; 501 cm^2), serviced by a central airflow system (Tecniplast, IVC Green Line—GM500). Animals were maintained on a 12:12 h light/dark cycle, with constant temperature (23 ± 2 °C) and humidity of 55% during all times. Experimental animals received *ad libitum* access to water and a standard research diet (Altromin 1318, Altromin GmbH, Germany) and IVCs had sufficient bedding and nesting material as well as a wooden tunnel for environmental enrichment. Animals were allocated to experimental groups in a semi-randomized fashion and data analysis was performed blinded to the group allocation.

Generation of Fkbp5 mice

Conditional *Fkbp5* knockout mice are derived from embryonic stem cell clone EPD0741_3_H03 which was targeted by the knockout mouse project (KOMP). Frozen sperm obtained from the KOMP repository at UC Davis was used to generate knockout mice (*Fkbp5*$^{tm1a(KOMP)Wtsi}$) by in vitro fertilization. These mice designated as *Fkbp5*$^{Frt/Frt}$ are capable to re-express functional Fkbp5 upon Flp recombinase-mediated excision of an frt-flanked reporter-selection cassette integrated into the *Fkbp5* gene. Mice with a floxed *Fkbp5* gene designated as *Fkbp5*$^{lox/lox}$ (*Fkbp5*$^{tm1c(KOMP)Wtsi}$) were obtained by breeding *Fkbp5*$^{Frt/Frt}$ mice to Deleter-Flpe mice [21]. Finally, mice lacking *Fkbp5* in PVN neurons (*Fkbp5*$^{PVN-/-}$) were obtained by breeding *Fkbp5*$^{lox/lox}$ mice to Sim1-Cre mice [22]. The CRH-ires-CRE/Ai9 mouse line was generated previously [23]. Genotyping details are available upon request.

Viral overexpression and rescue of *Fkbp5*

For overexpression and rescue experiments, stereotactic injections were performed as described previously [24]. In brief, mice aged between 10 and 12 weeks were anesthetized with isoflurane, and 0.2 µl of the below-mentioned viruses (titers: 1.6 × 10$^{12–13}$ genomic particles/ml) were bilaterally injected in the PVN at 0.05 µl/min by glass capillaries with tip resistance of 2–4 MΩ in a stereotactic apparatus. The following coordinates were used: −0.45 mm anterior to bregma, 0.3 mm lateral from midline, and 4.8 mm below the surface of the skull, targeting the PVN. After surgery, mice were treated for 3 days with Metacam via i.p. injections and were allowed to recover for 3–4 weeks before

the start of the testing. Successful overexpression or reinstatement of *Fkbp5* was verified by ISH and RNAscope. For in vivo experiments, we used adeno-associated bicistronic AAV1/2 vectors. In the overexpression experiments, the vector contained a CAG-HA-tagged-FKBP51-WPRE-BGH-polyA expression cassette (containing the coding sequence of human Fkbp51 NCBI CCDS ID CCDS4808.1). The same vector constructs without expression of *Fkbp5* (CAG-Null/Empty-WPRE-BGH-polyA) was used as a control. For the *Crh* specific overexpression of *Fkbp5*, we used a viral vector containing an AAV1/2-Cre-dept-HA-FKBP51 (pAAV-Cre-dependent-CAG-HA-human wildtype FKBP51 WPRE-BGH-polyA) and a control virus containing AAV1/2-Cre-dept-GFP (pAAV-Cre-dependent-CAG-GFP-WPRGE-BGH-polyA). Virus production, amplification, and purification were performed by GeneDetect. For the rescue experiment, a viral vector containing a flippase expressing cassette (AAV2-eSYN-eGFP-T2A-FLPo, Vector Biolabs; VB1093) was used to induce endogenous *Fkbp5* expression in *Fkbp5*[FRT/FRT] mice. Control animals were injected with a control virus (AAV2-eSYN-eGFP; Vector Biolabs; VB1107).

Acute stress paradigm

For acute stress exposure, the restraint stress paradigm was used, as it was shown to be a reliable and robust stressor in rodents [25]. One to 2 h after lights on each animal was placed in a restrainer (50 ml falcon tube with holes at the bottom and the lid to provide enough oxygen and space for tail movement) for 15 min in their individual home cage. After 15 min, animals were removed from the tube and the first blood sample was collected by tail cut. Until the following tail cuts at 30, 60, and 90 min after stress onset, the animals remained in their home cage to recover. Basal CORT levels (morning CORT) were collected one week prior to the acute stress paradigm at 8 a.m.

Combined Dex/CRH test

To investigate the HPA axis function we performed a combined Dex/CRH test as described previously [8]. On an experimental day, mice were injected with a low dose of dexamethasone (0.05 mg/kg, Dex-Ratiopharm, 7633932) via i.p injections at 9 a.m. in the morning. At this dose Dex does not cross the blood-brain barrier and acts predominantly in the periphery [26] Here, the most important site of action in relation to HPA axis function, especially when combined with a challenge with the neuropeptide CRH, is the pituitary. Thus, 6 h after Dex injection, a blood sample was collected via tail cut (after Dex value), followed by an injection of CRH (0.15 mg/kg, CRH Ferrin Amp). Thirty-minute after CRH injection, another blood sample

was obtained (after CRH value). All samples from the acute stress experiments and the Dex/CRH test were collected in 1.5 ml EDTA-coated microcentrifuge tubes (Sarstedt, Germany). All blood samples were kept on ice and were centrifuged for 15 min at 8000 rpm and 4 °C. Plasma was transferred to new, labeled microcentrifuge tubes and stored at −20 °C until further processing.

Sampling procedure

On the day of sacrifice, animals were deeply anesthetized with isoflurane and sacrificed by decapitation. Trunk blood was collected in labeled 1.5 ml EDTA-coated microcentrifuge tubes (Sarstedt, Germany) and kept on ice until centrifugation. After centrifugation (4 °C, 8000 rpm for 1 min) the plasma was removed and transferred to new, labeled tubes and stored at −20 °C until hormone quantification. For mRNA analysis, brains were removed, snap-frozen in isopentane at −40 °C, and stored at −80 °C for ISH. For protein analysis, brains were removed and placed inside a brain matrix with the hypothalamus facing upwards (spacing 1 mm, World Precision Instruments, Berlin, Germany). Starting from the middle of the chiasma opticum, a 1 mm thick brain slice was removed. The PVN was further isolated by cutting the slice on both sides of the PVN along the fornices (parallel to the 3rd ventricle) as a landmark and a horizontal cut between the reuniens and the thalamic nucleus. Finally, the slice containing the third ventricle was bisected, and the distal part discarded. The remaining part (containing the PVN) was immediately shocked frozen and stored at −80 °C until protein analysis [27]. The adrenals and thymus glands were dissected from fat and weighed.

Hormone assessment

CORT and ACTH concentrations were determined by radioimmunoassay using a corticosterone double-antibody ^{125}I RIA kit (sensitivity: 12.5 ng/ml, MP Biomedicals Inc.) and adrenocorticotropic double-antibody hormone ^{125}I RIA kit (sensitivity: 10 pg/ml, MP Biomedicals Inc.) and were used following the manufacturers' instructions. Radioactivity of the pellet was measured with a gamma counter (Packard Cobra II Auto Gamma; Perkin-Elmer). Fifteen-minute post-stress analysis of ACTH concentrations was analyzed by using ACTH ELISA (IBL international GmBH, RE53081) and the ELISA was performed as recommended by the manufacturer. Final CORT and ACTH levels were derived from the standard curve.

In situ hybridization (ISH)

ISH was used to analyze mRNA expression of the major stress markers, *Fkbp5*, *Gr*, *Crh*, and *Avp*. Therefore, frozen

brains were sectioned at −20 °C in a cryostat microtome at 20 μm, thaw mounted on Super Frost Plus slides, dried, and stored at −80 °C. The ISH using ^{35}S UTP labeled ribonucleotide probes was performed as described previously [28, 29]. All primer details are available upon request. Briefly, sections were fixed in 4% paraformaldehyde and acetylated in 0.25% acetic anhydride in 0.1 M triethanolamine/HCl. Subsequently, brain sections were dehydrated in increasing concentrations of ethanol. The antisense cRNA probes were transcribed from a linearized plasmid. Tissue sections were saturated with 100 μl of hybridization buffer containing approximately 1.5×10^6 cpm ^{35}S labeled riboprobe. Brain sections were coverslipped and incubated overnight at 55 °C. On the next day, the sections were rinsed in 2 × SSC (standard saline citrate), treated with RNAse A (20 mg/l). After several washing steps with SSC solutions at room temperature, the sections were washed in 0.1 × SSC for 1 h at 65 °C and dehydrated through increasing concentrations of ethanol. Finally, the slides were air-dried and exposed to Kodak Biomax MR films (Eastman Kodak Co., Rochester, NY) and developed. Autoradiographs were digitized, and expression was determined by optical densitometry utilizing the freely available NIH ImageJ software. The mean of four measurements of two different brain slices was calculated for each animal. The data were analyzed blindly, always subtracting the background signal of a nearby structure not expressing the gene of interest from the measurements. For *Fkbp5*, exemplary slides were dipped in Kodak NTB2 emulsion (Eastman Kodak Co., Rochester, NY) and exposed at 4 °C for representative pictures; exposure time was adjusted to average expression level. Slides were developed and examined with a light microscope with darkfield condensers to show mRNA expression.

RNAscope analysis and cell counting

For the RNAscope experiments, C57Bl/6 male mice were obtained from The Jackson Laboratory (Bar Harbor, ME, USA). All procedures conformed to National Institutes of Health guidelines and were approved by McLean Hospital Institutional Animal Care and Use Committee. Mice were housed in a temperature-controlled colony in the animal facilities of McLean Hospital in Belmont, MA, USA. All mice were group-housed and maintained on a 12:12 h light/dark cycle (lights on at 7 a.m.). Food and water were available ad libitum unless specified otherwise. Mice were 12 weeks at the time of tissue collection. Animals were allowed to acclimate to the room for 1 week before the beginning of the experiment. During the experiment, mice were either left undisturbed (ctrl) or subjected to 14 h (overnight) of food deprivation prior to sacrifice. During stress procedure, animals were kept in their home cages and

had free access to tap water. All mice were sacrificed by decapitation in the morning (08:00 to 08:30 a.m.) following quick anesthesia by isoflurane. Brains were removed, snap-frozen in isopentane at −40 °C, and stored at −80 °C. Frozen brains were sectioned in the coronal plane at −20 °C in a cryostat microtome at 18 μm, mounted on Super Frost Plus slides, and stored at −80 °C. The RNA Scope Fluorescent Multiplex Reagent kit (cat. no. 320850, Advanced Cell Diagnostics, Newark, CA, USA) was used for mRNA staining. Probes used for staining were; mm-Avp-C3, mm-Crh-C3, mm-Fkbp5-C2, mm-Oxt-C3, mm-Sst-C3, and mm-Trh-C3. The staining procedure was performed according to the manufacturer's specifications. Briefly, sections were fixed in 4% paraformaldehyde for 15 min at 4 °C. Subsequently, brain sections were dehydrated in increasing concentrations of ethanol. Next, tissue sections were incubated with protease IV for 30 min at room temperature. Probes (probe diluent (cat. no. 300041 used instead of C1-probe), Fkbp5-C2, and one of the above C3-probes) were hybridized for 2 h at 40 °C followed by four hybridization steps of the amplification reagents 1–4. Next, sections were counterstained with DAPI, cover-slipped, and stored at 4 °C until image acquisition. Images of the PVN (left and right side) were acquired by an experimenter blinded to the condition of the animals. Sixteen-bit images of each section were acquired on a Leica SP8 confocal microscope using a 40× objective ($n = 3$ animals per marker and condition). For every individual marker, all images were acquired using identical settings for laser power, detector gain, and amplifier offset. Images of both sides were acquired as a z-stack of 3 steps of 1.0 μm each. *Fkbp5* mRNA expression and co-expression were analyzed using ImageJ with the experimenter blinded to the condition of the animals. *Fkbp5* mRNA was counted manually and each cell containing 1 mRNA dot was counted as positive.

Single-cell sequencing. Tissue dissociation

Single-cell sequencing was performed on PVN tissue dissected from male C57Bl/6 mice aged between 8 and 12 weeks. Therefore, mice were anesthetized lethally using isoflurane and perfused with cold PBS. Brains were quickly dissected, transferred to ice-cold oxygenated artificial cerebral spinal fluid (aCSF), and kept in the same solution during dissection. Sectioning was performed using a 0.5 mm stainless steel adult mouse brain matrice (Kent Scientific) and a Personna double edge prep razor blade. A slide (approximately −0.58 mm Bregma to −1.22 mm Bregma) was obtained from each brain and the extended PVN was manually dissected under the microscope. The PVN from five different mice was pooled and dissociated using the Papain dissociation system (Worthington) following the manufacturer's instructions. All solutions were

oxygenated with a mixture of 5% CO_2 in O_2. After this, the cell suspension was filtered with a 30 μm filter (Partec) and kept in cold and oxygenated aCSF.

Cell capture, library preparation, and high-throughput sequencing

Cell suspensions of PVN with ~1,000,000 cells/μL were used. Cells were loaded onto two lanes of a 10X Genomics Chromium chip per factory recommendations. Reverse transcription and library preparation was performed using the 10X genomics single-cell v2.0 kit following the 10X genomics protocol. The library molar concentration and fragment length were quantified by qPCR using KAPA Library Quant (Kapa Biosystems) and Bioanalyzer (Agilent high sensitivity DNA kit), respectively. The library was sequenced on a single lane of an Illumina HiSeq4000 system generating 100 bp paired-end reads at a depth of ~340 million reads per sample.

Quality control and identification of cell clusters

Pre-processing of the data was done using the 10X genomics cell ranger software version 2.1.1 in default mode. The 10X genomics supplied reference data for the mm10 assembly and corresponding gene annotation was used for alignment and quantification. All further analysis was performed using SCANPY version 1.3.7 [30]. A total of 5.113 cells were included after filtering gene counts (<750 and >6.000), UMI counts (>25.000), and the fraction of mitochondrial counts (>0.2). Combat [31] was used to remove chromium channels as batch effects from normalized data. The 4.000 most variable genes were subsequently used as input for Louvain cluster detection. Cell types were determined using a combination of marker genes identified from the literature and gene ontology for cell types using the web-based tool: mousebrain.org (http://mousebrain.org/genesearch.html).

Western blot analysis

Protein extracts were obtained by lysing cells in RIPA buffer (150 mM NaCl, 1% IGEPAL CA-630, 0.5% Sodium deoxycholate, 0.1% SDS 50 mM Tris (pH8.0)) freshly supplemented with protease inhibitor (Merck Millipore, Darmstadt, Germany), benzonase (Merck Millipore), 5 mM DTT (Sigma Aldrich, Munich, Germany), and phosphatase inhibitor cocktail (Roche, Penzberg, Germany). Proteins were separated by SDS-PAGE and electro-transferred onto nitrocellulose membranes. Blots were placed in Tris-buffered saline, supplemented with 0.05% Tween (Sigma Aldrich) and 5% non-fat milk for 1 h at room temperature, and then incubated with primary antibody (diluted in TBS/0.05% Tween)

overnight at 4 °C. The following primary antibodies were used: Actin (1:5000, Santa Cruz Biotechnologies, sc-1616), GR (1:1000, Cell Signaling Technology, #3660), p-GR Ser211 (1:500, Sigma, SAB4503820), p-GR Ser226 (1:1000, Sigma, SAB4503874), p-GR 203 (1:500, Sigma, SAB4504585), FKBP51 (1:1000, Bethyl, A301-430A).

Subsequently, blots were washed and probed with the respective horseradish peroxidase or fluorophore-conjugated secondary antibody for 1 h at room temperature. The immuno-reactive bands were visualized either using ECL detection reagent (Millipore, Billerica, MA, USA) or directly by excitation of the respective fluorophore. Determination of the band intensities was performed with BioRad, ChemiDoc MP. For quantification of phosphorylated GR, the intensity of phosphor-GR was always referred to as the signal intensity of the corresponding total GR.

Chromatin preparation for chromatin immunoprecipitation (ChIP) analysis

The GR ChIP was performed as previously described [32]. We added 1 mM AEBSF or 0.1 mM PMSF, 5 mM Na^+-Butyrate (NaBut), and PhosSTOP phosphatase inhibitor cocktail tablets (1 per 10 ml; Roche, Burgess Hill, UK) to all solutions unless otherwise stated. Briefly, hypothalamus tissues from four mice were cross-linked for 10 min in 1% formaldehyde in PBS. Crosslinking was terminated by adding glycine (5 min, final concentration 200 μM) and centrifuged (5 min, 6000 g, 4 °C). Pellets were washed three times with ice-cold PBS. Next, the pellets were re-suspended in ice-cold Lysis Buffer [50 mM Tris-HCl pH 8, 150 mM NaCl, 5 mM EDTA pH 8.0, 0.5% v/v Igepal, 0.5% Na-deoxycholate, 1% SDS, 5 mM NaBut, 2 mM AEBSF, 1 mM Na3VO4, complete ultra EDTA-free protease inhibitor tablets and PhosSTOP phosphatase inhibitor cocktail tablet (both 1 per 10 ml, Roche, Burgess Hill, UK)] and rotated for 15 min at 4 °C. Samples were aliquoted, sonicated (high power; 2 × 10 cycles; 30 s ON, 60 s OFF) using a water-cooled (4 °C) Bioruptor Pico (Diagenode, Liège, Belgium) and centrifuged (10 min, 20,000 g, 4 °C). Supernatants (containing the sheared chromatin) were recombined and re-aliquoted into fresh tubes for subsequent ChIP analysis and for assessment of Input DNA (i.e., the starting material). Chromatin was sonicated to a length of ~500 base pairs.

For ChIP analysis

Aliquots of chromatin were diluted ten-times in ice-cold Dilution Buffer [50 mM Tris-HCl pH 8.0, 150 mM NaCl, 5 mM EDTA pH 8.0, 1% v/v Triton, 0.1% Na-deoxycholate 5 mM NaBut, 1 mM AEBSF, complete ultra EDTA-free protease inhibitor tablets and PhosSTOP phosphatase inhibitor

cocktail tablet (both 1 per 10 ml, Roche)]. 10 µl of GR antibody (ProteinTech, USA) was added to each sample, and tubes were rotated overnight at 4 °C. Protein A-coated Dynabeads® (Life Technologies) were washed once in ice-cold 0.5% BSA/PBS before blocking overnight at 4 °C. Pre-blocked beads were washed once in ice-cold Dilution buffer, re-suspended in the antibody:chromatin mix, and allowed to incubate for 3 h at 4 °C to allow binding of beads to anti-body:chromatin complexes. After 3 h, the samples were placed in a magnetic stand to allow the beads (with the Bound fraction bound) to separate from the liquid "Unbound" fraction. Beads carrying the Bound chromatin were washed three times with ice-cold RIPA buffer [10 mM Tris-HCl pH 7.5, 1 mM EDTA pH 7.5, 0.1% SDS, 0.5 mM EGTA, 1% Triton, 0.1% Na-Deoxycholate, 140 mM NaCl + inhibitors] and washed twice with ice-cold Tris-EDTA buffer. Bound DNA was eluted in two steps at room temperature; first with 200 µl Elution buffer 1 (10 mM Tris-HCl pH 7.4, 50 mM NaCl, 1.5% SDS) and second with 100 µl Elution buffer 2 (10 mM Tris-HCl pH 7.4, 50 mM NaCl, 0.5% SDS). Crosslinks were reversed by the addition of NaCl (final concentration 200 mM) and overnight incubation at 65 °C. The next day, samples were incubated first with RNase A (60 µg/ml, 37 °C, 1 h), followed by incubation with proteinase K (250 µg/ml, 37 °C, 3.5 h). DNA was purified using a QIAquick PCR purification kit (Qiagen) as per the manufacturer's instructions. Input samples were incubated overnight at 65 °C with 200 mM NaCl to reverse crosslinks, incubated with RNase A and proteinase K (overnight), and DNA was purified using a Qiagen PCR purification kit. All samples (bounds and inputs) were diluted to a standardized concentration with nuclease-free water and analyzed by qPCR as described below using primers/probes (forward: 5′–TGTCAATGGACAAGTCATAAGAAACC; reverse: 5′–GAATCTCACATCCAATTATATCAACAGAT; probe: 5′–TTCCATTTTCGGGCTCGTTGACGTC). The binding of GR was expressed as a percentage of input DNA, i.e., % Input, which is a measure of the enrichment of steroid receptor bound to specific genomic sequences.

qPCR analysis

Mastermix for qPCR was prepared to contain 900 nM forward and reverse primers, 200 nM probe, 1X TaqMan fast mastermix (Life Technologies, Paisley, UK), and nuclease-free water. Primers and dual-labeled probes with 6-FAM as the fluorescent dye and TAMRA are the quencher were designed using Primer Express software (Version 3.0.1, Life Technologies). Standard curves were performed for each primer pair and the qPCR efficiency was calculated using the equation: $E = ((10 − 1/\text{slope}) − 1) \times 100$ (where E is qPCR efficiency and the slope is the gradient of the standard curve). Only primer pairs with efficiencies greater than 90% were used. Quantitative PCR was performed using a StepOne Plus machine (Life Technologies, Paisley, UK). Taq enzymes were activated at 95 °C for 20 s, then 40 cycles of 95 °C (1 s) to 60 °C (20 s) were performed to amplify samples.

Electrophysiology

A separate cohort of CRH-ires-CRE/Ai9 mice (Fkbp5$^{\text{CRH OE}}$ $n = 4$, Control $n = 4$) was used for electrophysiology experiments. Mice underwent surgery as described above. After 3–4 weeks of recovery, mice were anesthetized with isoflurane and decapitated. The brain was rapidly removed from the cranial cavity and, using a vibratome (HM650V, Thermo Scientific), 350 µm-thick coronal slices containing the PVN were cut in an ice-cold carbonated gas (95% O_2/5% CO_2)-saturated solution consisting of (in mM): 87 NaCl, 2.5 KCl, 25 NaHCO$_3$, 1.25 NaH$_2$PO$_4$, 0.5 CaCl$_2$, 7 MgCl$_2$, 10 glucose, and 75 sucrose. Slices were incubated in carbonated physiological saline for 30 min at 34 °C and, afterward, for at least 30 min at room temperature (23–25 °C). The physiological saline contained (in mM): 125 NaCl, 2.5 KCl, 25 NaHCO$_3$, 1.25 NaH$_2$PO$_4$, 2 CaCl$_2$, 1 MgCl$_2$, and 10 glucose. Using infrared video microscopy, somatic whole-cell voltage-clamp recordings from control and FKBP51-overexpressing PVN neurons (identified by fluorescence imaging; seal resistance >1 GΩ; holding potential −70 mV, corrected for a liquid junction potential of 10 mV) were performed with an EPC 10 amplifier (HEKA) at room temperature in physiological saline (2–3 ml/min flow rate) containing picrotoxin (100 µM) and TTX (1 µM). Patch pipettes (3–4 MΩ open tip resistance) were filled with a solution consisting of (in mM): 125 CsCH$_3$SO$_3$, 8 NaCl, 10 HEPES, 0.5 EGTA, 4 Mg-ATP, 0.3 Na-GTP, and 20 Na$_2$-phosphocreatine (pH adjusted to 7.2 with CsOH). Five minutes after a break-in to the cell, AMPA receptor-mediated miniature excitatory postsynaptic currents (mEPSCs) were recorded for 5 min. Offline analysis of mEPSCs was conducted using the Mini Analysis Program (Synaptosoft). Recordings, where series resistance changed by more than 10%, were excluded from the analysis.

Statistical analysis

The data presented are shown as means ± SEM and sample sizes are indicated in the figure legends. All data were analyzed by the commercially available software SPSS 17.0 and GraphPad 8.0. When two groups were compared, the unpaired student's t-test was applied. If data were not normally distributed the non-parametric Mann–Whitney test (MW-test) was used. For four group comparisons, a two-way analysis of variance (ANOVA) was performed,
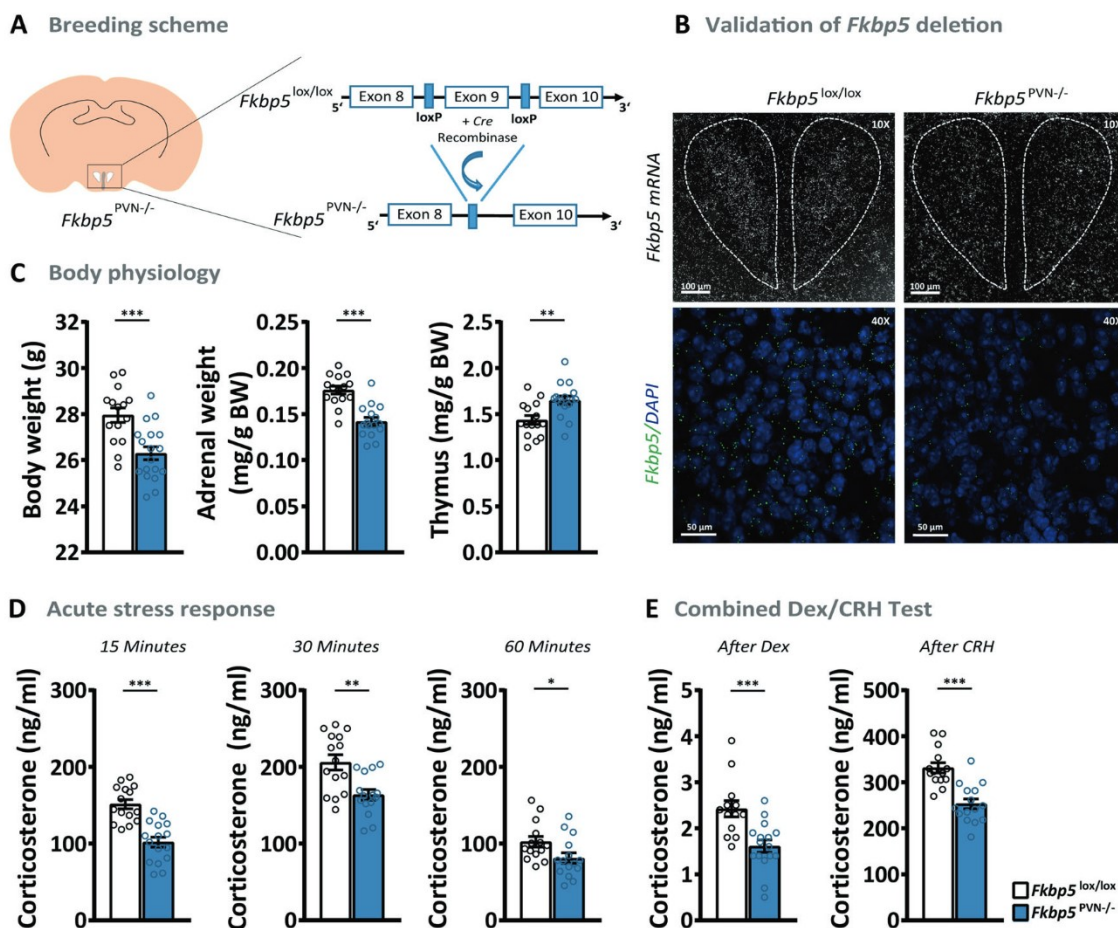
A Breeding scheme

B Validation of *Fkbp5* deletion

C Body physiology

D Acute stress response

E Combined Dex/CRH Test

Fig. 1 Loss of *Fkbp5* in the PVN alters HPA axis physiology. A Cre-LoxP based generation of the $Fkbp5^{PVN-/-}$ mouse line. **B** Validation of *Fkbp5* mRNA expression in the PVN via in situ hybridization (ISH) and RNAscope (for mRNA quantification see Supplementary Fig. 1A). **C** $Fkbp5^{PVN-/-}$ mice $(n = 16)$ presented reduced body weight, lowered adrenal weights, and increased thymus weights under non-stressed conditions compared to their WT littermates $(n = 15)$. **D** Corticosterone levels were significantly reduced following a 15 min restraint stress until at least 60 min after stress onset. **E** A combined Dex/CRH test showed a significantly pronounced response to a low dose of dexamethasone as well as a dampened response to CRH injection. Data are received from mice between 16 and 20 weeks of age and are presented as mean ± SEM. All data were analyzed with a student's *t*-test. $*p < 0.05$, $**p < 0.01$, and $***p < 0.001$.

followed by a posthoc test, as appropriate. *P* values of less than 0.05 were considered statistically significant. The sample size was chosen such that with a type 1 error of 0.05 and a type 2 error of 0.2 the effect size should be at least 1.2-fold of the pooled standard deviation. All data were tested for outliers using the Grubbs test.

Results

Loss of Fkbp5 in the PVN alters HPA axis physiology

To study the effects of Fkbp5 in the PVN, we first generated PVN-specific conditional *Fkbp5* knockout mice $(Fkbp5^{PVN-/-})$ by crossing $Fkbp5^{lox/lox}$ mice (generated in-house; for details see methods) with the Sim1-Cre mouse line, which expresses *Cre* recombinase in Sim1$^+$

neurons mostly concentrated within the PVN (Fig. 1A). The successful deletion of *Fkbp5* in the PVN was assessed by mRNA and protein analysis (Fig. 1B and Supplementary Fig. 1). Under basal conditions, adult mice (16–20 weeks of age) lacking Fkbp5 in the PVN showed significantly lower body-, and adrenal weights and higher thymus weights compared to their WT littermates (Fig. 1C). Interestingly, $Fkbp5^{PVN-/-}$ mice in young adolescence (8 weeks of age) showed no significant differences in body weight, adrenal, or thymus weights (Supplementary Fig. 2), indicating an age-dependent phenotype of Fkbp5 in the HPA-axis' response.

As PVN *Fkbp5* mRNA levels are highly responsive to an acute stressor [10], we hypothesized that $Fkbp5^{PVN-/-}$ mice have an altered stress response following an acute challenge. Under basal conditions during the circadian trough,

no differences in corticosterone secretion were detected in young and adult mice (Supplementary Figs. 1 and 2). However, already after 15 min of restraint stress adult and young $Fkbp5^{PVN-/-}$ mice displayed significantly reduced plasma corticosterone levels compared to the control group (Fig. 1D). The dampened stress response was persistent for 60 min in adult mice, while the effect has vanished in young mice already 30 min after stress onset (Fig. 1D and Supplementary Fig. 2). Levels of the adrenocorticotropic hormone (ACTH) were not altered under basal or acute stressed conditions (Supplementary Fig. 1).

To further investigate the effect of Fkbp5 on GR sensitivity, we performed combined dexamethasone (Dex, a synthetic GC)—corticotropin-releasing hormone (CRH) test on adults $Fkbp5^{PVN-/-}$ mice. The combined Dex/CRH test is a method to analyze HPA axis (dys)function in depressed individuals or animals, measuring the responsiveness of the body's stress response system through suppression (by Dex injection) and stimulation (by CRH injection) of the HPA axis [33]. The injection of a low dose of Dex (0.05 mg/kg) resulted in a reduction in blood corticosterone levels compared to the evening corticosterone levels in both groups. Interestingly, mice lacking Fkbp5 in the PVN showed 1.5-fold lower levels of corticosterone compared to their WT littermates. Following CRH stimulation (0.15 mg/kg) $Fkbp5^{PVN-/-}$ mice showed a significantly lower reaction to CRH than control mice (Fig. 1E). These data indicate that specific deletion of Fkbp5 in the PVN dampens HPA axis response and enhances GR sensitivity.

Overexpression of *Fkbp5* in the PVN induces a stress-like phenotype in C57Bl/6 mice under basal conditions

Chronic or acute stress upregulates Fkbp5 in distinct brain regions, such as the PVN [10]. Therefore, we were interested to explore whether selective overexpression of Fkbp5 in the PVN would be sufficient to affect body physiology and stress system regulation. To do so, we bilaterally injected 200 nl of an adeno-associated virus (AAV) containing an Fkbp5 overexpression vector into the PVN of 10–12 weeks old C57Bl/6 mice ($Fkbp5^{PVN OE}$, Fig. 2A, B). The AAV-mediated overexpression resulted in a (fourfold) increase in Fkbp5 mRNA and protein levels (Fkbp5) in the PVN (Supplementary Fig. 3).

Intriguingly, Fkbp5 overexpression altered the physiology of stress-responsive organs. $Fkbp5^{PVN OE}$ animals showed a significantly reduced thymus weight and increased adrenal weights compared to their littermates (Fig. 2C), the hallmark of chronically stressed animals [34, 35]. Furthermore, overexpression of Fkbp5 affected the circadian rhythm of corticosterone secretion, indicated by increased blood corticosterone levels in the morning as well

as the evening (Fig. 2D). Consequently, ACTH levels of $Fkbp5^{PVN OE}$ animals were also increased under non-stressed conditions (Supplementary Fig. 3). Next, we analyzed distinguished stress markers under basal conditions in order to determine whether consequences of PVN-specific Fkbp5 overexpression are also detectable at the molecular level. Nr1c3 and Crh mRNA expression in the PVN were increased in $Fkbp5^{PVN OE}$ animals under basal conditions; however, to a lesser extent than the increase of Fkbp5 mRNA due to viral overexpression. Avp mRNA levels were not altered (Supplementary Fig. 3). Together, these results are comparable to chronically stressed animals and demonstrate that local overexpression of Fkbp5 in the PVN is sufficient to mimic a stress-like phenotype without physically challenging the animals.

In accordance with the knock-out studies of the $Fkbp5^{PVN-/-}$ animals, we investigated the endocrinology of $Fkbp5^{PVN OE}$ animals after an acute challenge. As expected, we detected higher blood corticosterone levels in $Fkbp5^{PVN OE}$ mice 15 and 30 min after stress onset compared to the stressed controls (Fig. 2E). However, we could not detect any difference in ACTH release after stress (Supplementary Fig. 3). No differences between both groups were observed 60 and 90 min after restraint stress (Fig. 2E and Supplementary Fig. 3). These data show that $Fkbp5^{PVN OE}$ mice have a hyperactive HPA axis response and are more vulnerable to acute stress exposure.

To further assess GR sensitivity in Fkbp5 overexpressing animals, we again tested the response to a combined Dex/CRH test. While control animals showed a decline (<5 ng/ml) in blood corticosterone levels 6 h after Dex injection, $Fkbp5^{PVN OE}$ mice showed almost no response to Dex treatment (Fig. 2F). Interestingly, the subsequent CRH injection resulted in a higher corticosterone release in $Fkbp5^{PVN OE}$ mice compared to controls (Fig. 2F). These results suggest that excess levels of Fkbp5 in the PVN lead to a decreased GR sensitivity and thereby to an altered HPA axis response. Taken together, animals overexpressing Fkbp5 in the PVN show a hyperactive function of the HPA axis under basal and acute stress conditions, thereby mimicking the physiological hallmarks of chronic stress exposure and HPA axis hyperactivity, as observed in multiple stress-related diseases [36].

Reinstatement of endogenous *Fkbp5* in the PVN of global *Fkbp5* knock-out animals normalizes the body's stress response

Global loss of Fkbp5 results in a more sensitive GR and better-coping behavior of mice after stress [8, 17, 28, 34], and our results demonstrated that Fkbp5 in the PVN is necessary for an undisturbed stress system function. Thus, we were encouraged to test whether the reinstatement of
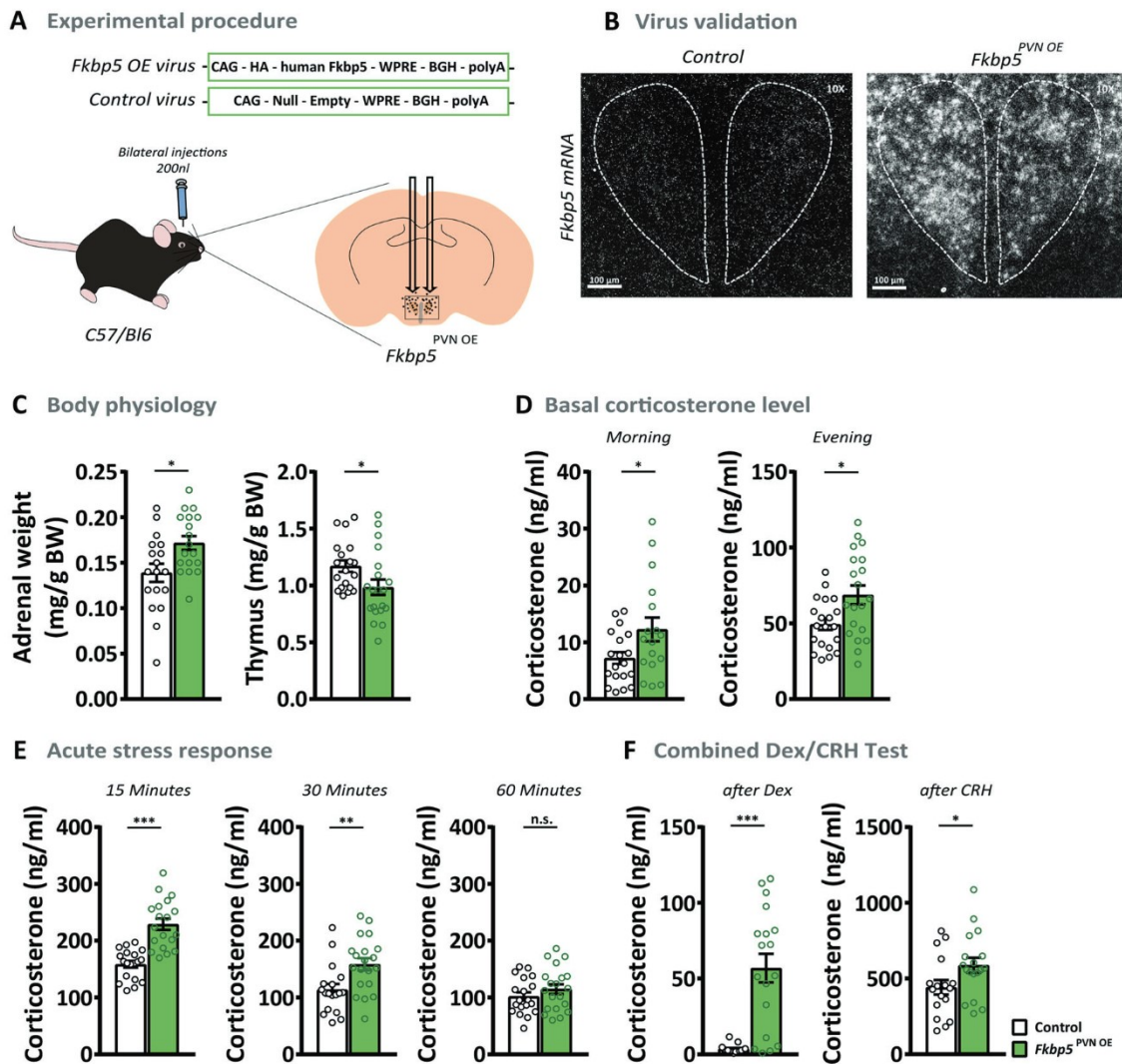
A Experimental procedure

B Virus validation

Fig. 2 The overexpression of *Fkbp5* in C57Bl/6 mice induces a stress-like phenotype under basal conditions. A Overexpression of *Fkbp5* in the PVN was achieved by bilateral viral injections. **B** Validation of *Fkbp5* mRNA overexpression in the PVN by ISH (see Supplementary Fig. 3A for mRNA quantification). **C** $Fkbp5^{PVN\ OE}$ mice ($n = 20$) showed significantly increased adrenal weights and a reduced thymus weight under non-stressed conditions compared to the controls ($n = 20$). **D** *Fkbp5* overexpression resulted in heightened corticosterone levels during the day. **E** Fifteen and 30 min after stress

onset, $Fkbp5^{PVN\ OE}$ mice displayed significantly higher corticosterone levels. **F** $Fkbp5^{PVN\ OE}$ mice showed significantly elevated corticosterone 6 h after dexamethasone treatment. The following CRH injection further significantly increased the corticosterone release compared to controls. Data are presented as mean ± SEM. All data were received from mice between 14 and 20 weeks of age and analyzed a with student's *t*-test. $*p < 0.05$, $**p < 0.01$, $***p < 0.001$, *n.s.* not significant.

native *Fkbp5* expression only in the PVN is sufficient to push the HPA axis activity of global *Fkbp5* knock-out animals to a wildtype level. Therefore, we injected an Flp recombinase expressing virus into 12–14 weeks old $Fkbp5^{Frt/Frt}$ mice. These mice carry an FRT flanked reporter selection (stop) cassette within the *Fkbp5* locus, leading to a disruption of the Fkbp5 function. We compared $Fkbp5^{Frt/Frt}$ mice to WT littermates and observed a similar HPA-axis phenotype to the well-established Fkbp5 full KO lines ([8] and Supplementary Fig. 4). An Flp removes the stop cassette from the *Fkbp5* locus, resulting in endogenous *Fkbp5* re-expression (Fig. 3A, B, Supplementary Fig. 5). In

parallel to the two previous mouse models, we assessed body physiology, basal corticosterone levels, and the acute stress response. Interestingly, mice with re-instated *Fkbp5* expression ($Fkbp5^{PVN\ Rescue}$) showed significantly higher adrenal weights as compared to their control littermates (Fig. 3C). Furthermore, we observed that the reinstatement of *Fkbp5* in the PVN resulted in significantly increased blood CORT levels in the morning under basal conditions (Fig. 3D), with no effect on thymus weights, evening CORT, and ACTH levels (Supplementary Fig. 5). ISH analysis revealed significantly higher levels of *Crh* mRNA, but no changes in *Nr1c3* and *Avp* mRNA expression in the
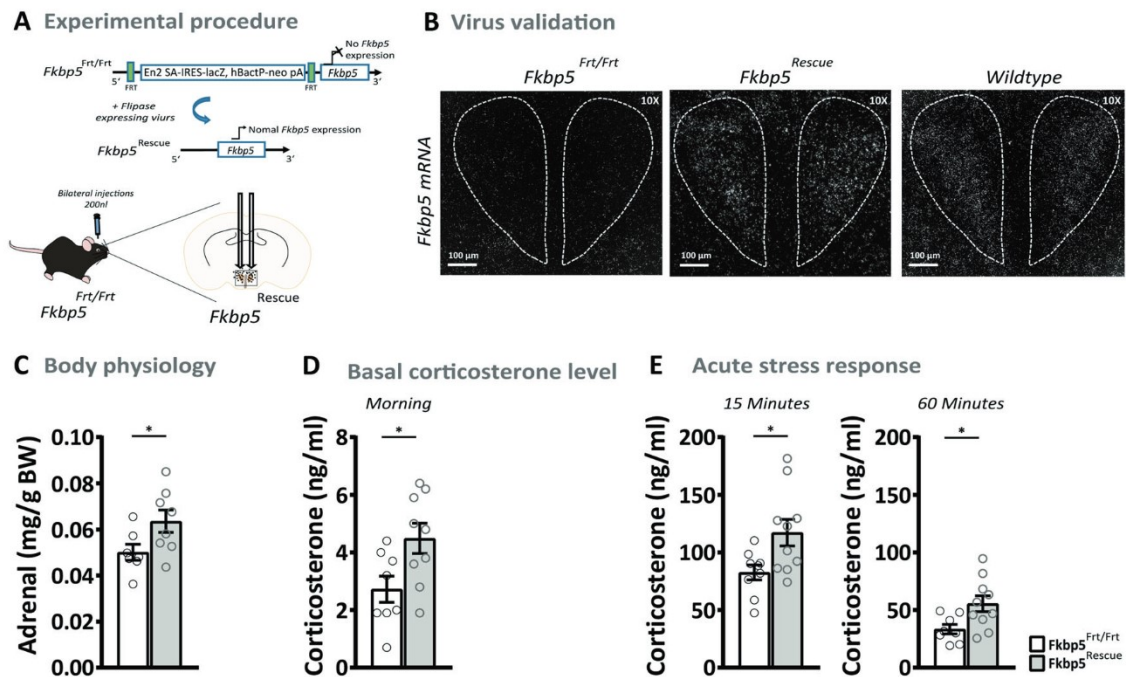
Fig. 3 The reinstatement of endogenous *Fkbp5* in the PVN of global *Fkbp5* knock-out animals. A Experimental procedure. **B** Validation of successful *Fkbp5* rescue by ISH (see Supplementary Fig. 5A for mRNA quantification) and comparable WT *Fkbp5* expression. **C** The reinstatement of *Fkbp5* in the PVN resulted in increased adrenal weights and elevated morning corticosterone levels under basal conditions **D**. Furthermore, *Fkbp5* re-instated animals displayed a significantly higher corticosterone response after restraint stress **E**. For comparison of Fkbp5^Frt/Frt and WT see control experiments in Supplementary Fig. 4. Data are presented as mean ± SEM. All data were received from mice between 16 and 20 weeks of age and analyzed a with student's *t*-test. $*p < 0.05$.

PVN under basal conditions (Supplementary Fig. 5). Next, we monitored blood corticosterone levels after 15 min of restraint stress. Here, we observed significantly higher corticosterone levels 15 and 60 min after stress onset (Fig. 3E). No differences were detected in the combined Dex/CRH test (Supplementary Fig. 5), which suggests that a PVN-driven over-activation of the HPA axis might be necessary for desensitization of GRs in the PVN and the pituitary. These rescue experiments underline the importance of Fkbp5 in the acute stress response and demonstrate that Fkbp5 in the PVN is necessary and sufficient to regulate HPA axis (re)activity.

Fkbp5 manipulation directly affects GR phosphorylation

It is well known that ligand-binding induced phosphorylation of GR plays an important role in response to hormone signaling [37]. The main phosphorylation sites involved in hormone signaling of GR are Serine(Ser)^{203} (mouse S^{212}), Ser^{211} (mouse Ser^{220}), and Ser^{226} (mouse Ser^{234}) and are associated with GR activity [37, 38]. Here, we tested the hypothesis that the co-chaperone Fkbp5 regulates phosphorylation of GR in *Fkbp5*$^{PVN-/-}$ and *Fkbp5*$^{PVN\ OE}$ mouse lines. To do so, we dissected the PVN of *Fkbp5*$^{PVN-/-}$ and

Fkbp5$^{PVN\ OE}$ mice and measured the phosphorylation levels of Ser^{203}, Ser^{211}, and Ser^{234} under basal and stress conditions.

Under basal conditions, animals lacking Fkbp5 in the PVN showed significantly less GR phosphorylation at Ser^{203} (Fig. 4A). Furthermore, *Fkbp5*$^{PVN-/-}$ animals displayed higher phosphorylation of GR at Ser^{234} and Ser^{211} in comparison to their WT littermates (Fig. 4B, C). Under stressed conditions, deletion of Fkbp5 had the same effects on pGR^{Ser211} and pGR^{Ser234} as we observed under basal conditions (Fig. 4B, C). Levels of pGR^{Ser203} were found to be unchanged in the *Fkbp5*$^{PVN-/-}$ after acute stress compared to the basal levels. However, pGR^{Ser203} levels of the control group increased after stress (Fig. 4A).

Intriguingly, *Fkbp5*$^{PVN\ OE}$ animals showed exactly the opposing phenotype at all three phosphorylation sites with less pGr^{Ser234} and pGr^{Ser211} and higher phosphorylation at Ser^{203} under basal conditions (Fig. 4E–G). In parallel to the unstressed condition, the overexpression of *Fkbp5* resulted in less GR phosphorylation at Ser^{211} and higher levels of pGR^{Ser203} compared to their control group after stress (Fig. 4E, F). Interestingly, levels of pGR^{Ser234} were unchanged after stress (Fig. 4G). Notably, total GR levels were not significantly altered in both experimental groups and conditions (Fig. 4D, H). Despite the altered GR phosphorylation, we could not detect any significant changes in
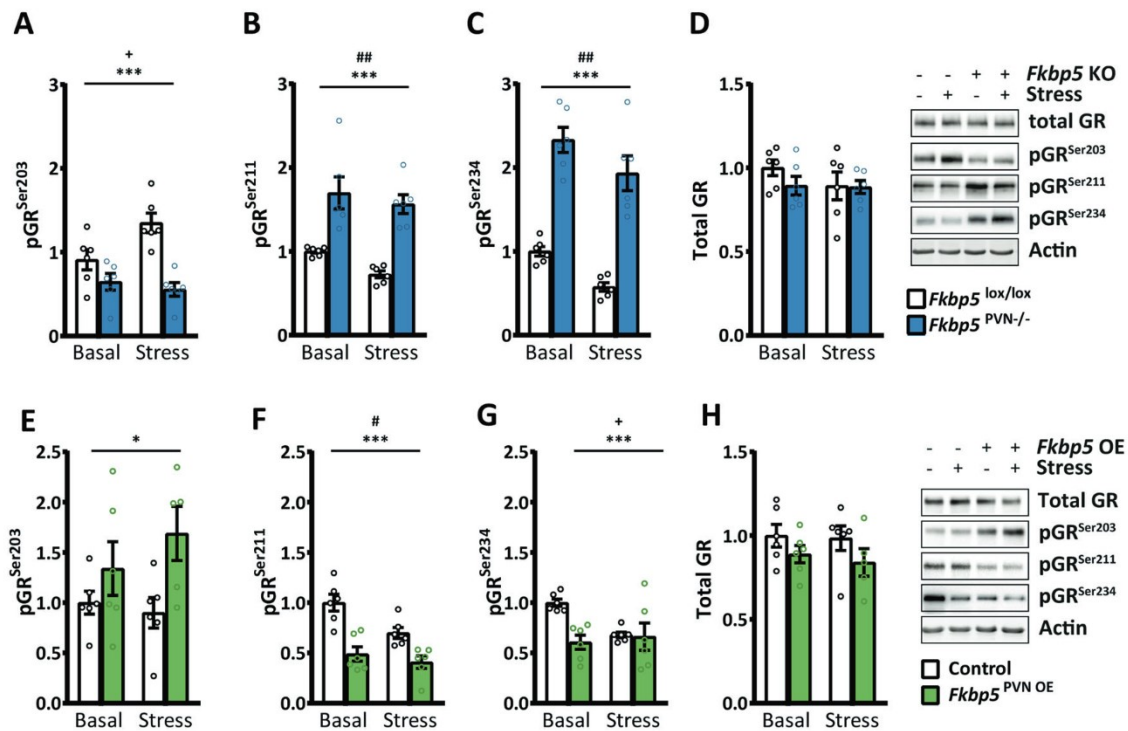
Fig. 4 Fkbp5 manipulation affects phosphorylation of the glucocorticoid receptor (GR). **A** Animals lacking Fkbp5 in the PVN showed significantly lower phosphorylation at pGR^{Ser203} and higher levels of (**B**) pGR^{Ser211} and (**C**) pGR^{Ser234} compared to the control animals. **D** Fkbp5$^{PVN-/-}$ mice showed no differences in total GR. **E** Fkbp5$^{PVN OE}$ animals showed the opposite effect on GR phosphorylation with higher phosphorylation on pGr^{Ser203}. **F** In addition, we observed significantly lower phosphorylation at the GR sites Ser^{211} and (**G**) Ser^{234}. **H** Fkbp5 overexpression had no effect on total GR protein level. Representative blots are shown in (**D**) and (**H**). Group size for (**A**)–(**H**): 6 vs. 6. Data were received from animals between 16 and 20 weeks of age and are presented as relative fold change to control condition, mean ± SEM, and were analyzed with a two-way ANOVA. *significant genotype effect, (*$p < 0.05$, **$p < 0.01$, ***$p < 0.001$). +significant genotype × stress interaction (+$p < 0.05$), #significant stress effect (#$p < 0.05$, ##$p < 0.01$).

GR enrichment at the glucocorticoid response element (GRE) in the *Crh* gene after acute stress (Supplementary Fig. 6), which may be due to the use of an antibody that recognizes all GR molecules irrespective of its phosphorylation state.

Overall, our data demonstrate that *Fkbp5* manipulation in the PVN affects GR phosphorylation at all three major phosphorylation sites and thereby affects GR activity.

Fkbp5 in the PVN acts in a complex cellular context

To further unravel the expression profile of Fkbp5 in the PVN and to detect cellular populations that might be mediating the effects of Fkbp5 on HPA axis control, we used a single-cell RNA sequencing dataset consisting of 5113 single cells isolated from the PVN of C57Bl/6 male mice [39]. The single-cell expression data reveal a complex cellular composition, with the majority of cells identified as neurons (38%), ependymal cells (25%), and astrocytes (14%) (Fig. 5A–C). *Fkbp5* was found to be differentially and cell-type specifically expressed, with the biggest *Fkbp5*⁺ cell population found in GABAergic neurons (42%). A significant expression of *Fkbp5* was also detected

in neuronal populations known to be directly involved in HPA axis regulation, most prominently in *Crh* positive neurons (Fig. 5D). However, it is important to point out that the expression levels of *Fkbp5* are relatively low. Unfortunately, lowly expressed genes may not be detected using this technique [40] and therefore many *Fkbp5* positive cells may have remained undetected in this dataset. To circumvent this problem, we next performed a targeted co-expression study of *Fkbp5* with five major markers that are characteristic of the stress response oxytocin (*Oxt*), somatostatin (*Sst*), vasopressin (*Avp*), thyrotropin-releasing hormone (*Trh*), and *Crh* under basal and stress conditions (Fig. 5E, Supplementary Fig. 7). We observed a strong but not complete co-localization of *Fkbp5* expression with these neuropeptide-expressing cellular populations in the PVN under basal conditions. Interestingly, a detailed quantification of the change in co-expression following stress revealed that there was a significant increase in *Crh-Fkbp5* co-localization only in the *Crh*-expressing neurons (Fig. 5E, F and Supplementary Fig. 8).

These data reveal the complex cell-type-specific expression pattern of *Fkbp5* under stress and basal conditions in the PVN. The significant increase of FKBP51 in
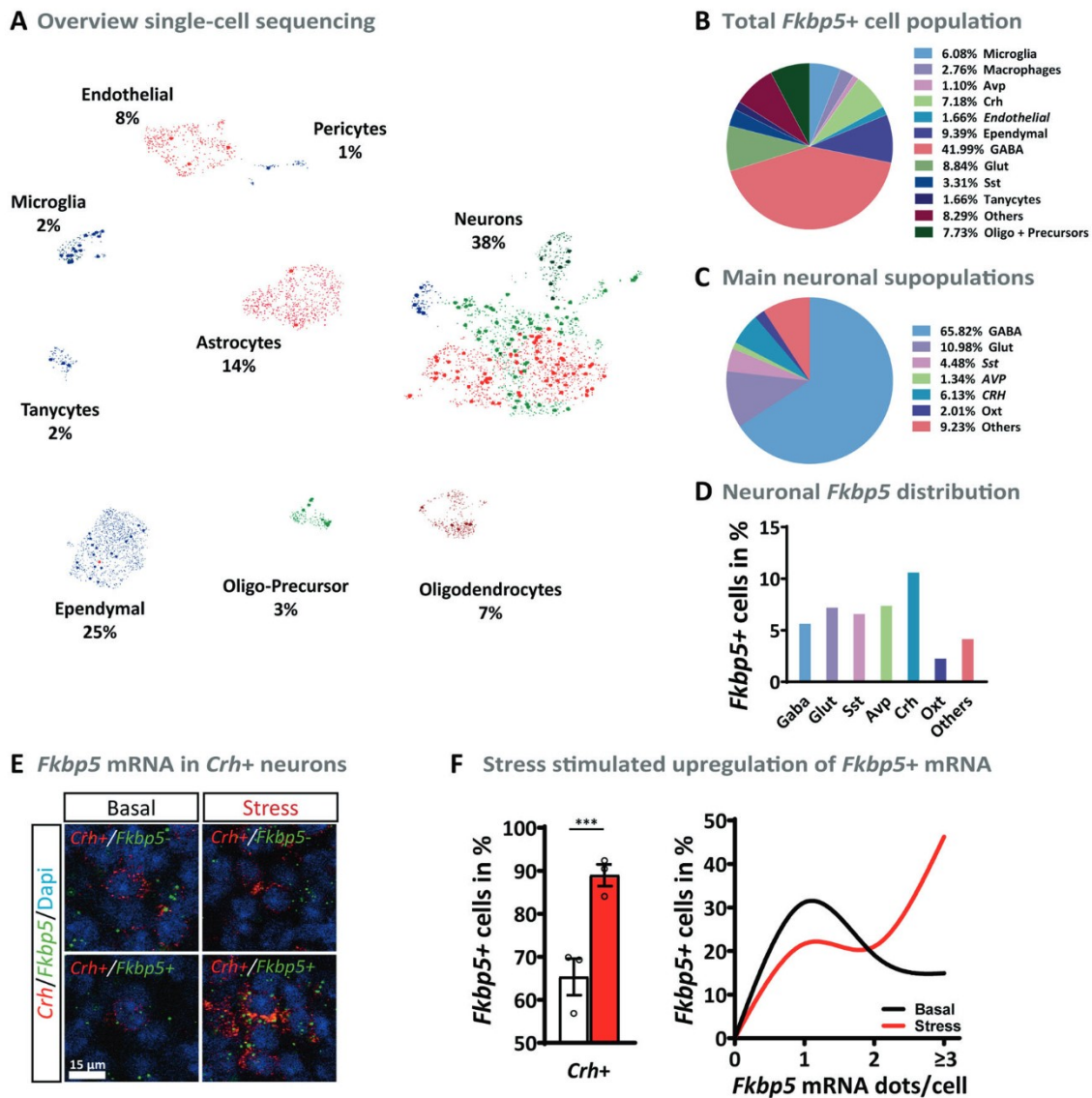
Fig. 5 Single-cell RNA sequencing of cells in the PVN of C57Bl/6 male mice under non-stressed conditions. A Single-cell sequencing depicted several different cell types. With the majority being neurons (38%), ependymal cells (25%), and astrocytes (14%). $Fkbp5^+$ cells are highlighted. **B** Diversity of $Fkbp5^+$ cell population. **C** Neurons could be divided mostly into GABAergic (66%) and glutamatergic (Glut, 11%) cells. Furthermore, the well-known stress markers corticotropin-releasing hormone (*Crh*, 6%), somatostatin (*Sst*, 5%), oxytocin (*Oxt*,

2%), and vasopressin (*Avp*, 1%) could be detected under basal conditions. **D** Fkbp5$^+$ cells of selected neuronal subpopulations under basal conditions. **E** RNAscope validation of *Fkbp5* mRNA expression in *Crh* + neurons. **F** Quantity of $Fkbp5^+$ cells, as well as Fkbp5 mRNA levels, are significantly increased after stress. Data are were received from animals between 8 and 12 weeks of age and are presented as mean ± SEM. For (**E**): data were analyzed with student's *t*-test. ***$p < 0.001$.

Crh positive neurons after an acute stress challenge encouraged us to specifically manipulated FKBP51 in Crh positive neurons.

Crh-specific overexpression of Fkbp5 in the PVN alters HPA axis physiology and CRH neuronal activity

Based on the observed increase in *Crh-Fkbp5* co-localization post-stress (Fig. 5E, F and Supplementary

Fig. 8), we were interested whether a *Crh*-specific *Fkbp5* overexpression in the PVN could drive the stress-like phenotype observed in the unspecific PVN overexpression (Fig. 2) and whether this neuron-specific manipulation alters CRH neuronal activity. Therefore, we bilaterally injected 200 nl of an AAV containing a Cre-dependent *Fkpb5* overexpression vector into the PVN of adult (26 weeks) CRH-ires-CRE/Ai9 mice expressing tdTomato specifically in CRH neurons (*Fkbp5*$^{CRH OE}$) (Fig. 6A). Cre-dependent AAV mediated overexpression resulted in a

A Experimental procedure

B Virus validation

C Body physiology

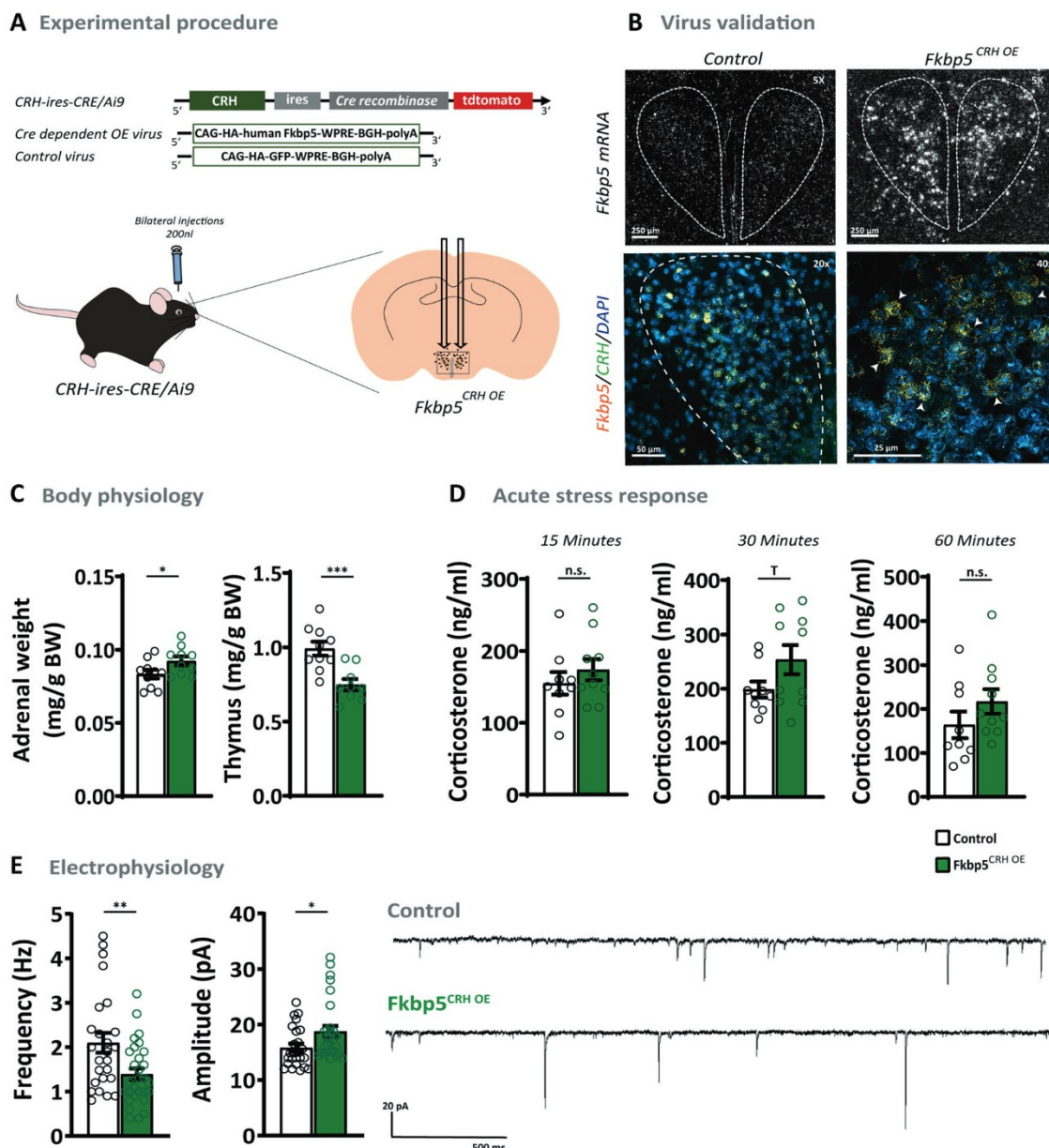
D Acute stress response

E Electrophysiology

Fig. 6 The *Crh*-specific overexpression of *Fkbp5* in the PVN. A *Crh*-specific overexpression of *Fkbp5* in the PVN was achieved by bilateral injections of a Cre-dependent *Fkbp5* overexpression virus in the PVN of CRH-ires-CRE/Ai9 mice. **B** Validation of *Crh*-specific *Fkbp5* mRNA overexpression in the PVN by ISH and RNAscope. Arrowheads pointing at viral *Fkbp5* expressing *Crh*⁺ neurons (For mRNA quantification see Supplementary Fig. 9D). **C** *Fkbp5*^CRH OE mice showed significantly increased adrenal weights ($n = 10$) and reduced thymus weights ($n = 9$) under non-stressed conditions compared to the controls ($n = 10$). **D** Corticosterone levels were mildly, but not significantly increased in *Fkbp5*^CRH OE at 15, 30, and 60 min post-stress (*Fkbp5*^CRH OE $n = 10$; Control $n = 9$). **E** *Fkbp5*^CRH OE mice displayed a decrease in CRH neuronal mEPSC frequency accompanied by an increased amplitude (*Fkbp5*^CRH OE $n_{mouse} = 4$; $n_{neuron} = 29$; Control $n_{mouse} = 4$; $n_{neuron} = 25$), which is reflected in two representative recording traces. Data are presented as mean ± SEM. All data were received from animals between 30 and 34 weeks of age and analyzed with the student's *t*-test. *$p < 0.05$, **$p < 0.01$, ***$p < 0.001$, $T = 0.05 < p < 0.1$, *n.s.* not significant.

fourfold increase of *Fkbp5* mRNA level in the PVN and *Crh* specificity of *Fkbp5* overexpression was successfully confirmed by RNAscope (Fig. 6B and Supplementary Fig. 9E). Under basal conditions, *Fkbp5*^CRH OE mice displayed significantly increased adrenal weights and reduced thymus weights compared to the control group (Fig. 6C),

indicative of chronic hyperactivity of the HPA axis. Surprisingly, the circadian rhythm of corticosterone secretion (Supplementary Fig. 9A), as well as stress-induced corticosterone level (Fig. 6D), were unaffected by the *Crh*-specific *Fkbp5* overexpression. Further, basal and 15 min post-stress ACTH level and DEX/CRH corticosterone level

remained unaffected in $Fkbp5^{CRH\ OE}$ mice (Supplementary Fig. 9B–D). To further assess the impact of $Fkbp5$ overexpression on neuronal activity in Crh positive (Crh^+) neurons in the PVN, we recorded AMPA receptor-mediated mEPSCs in these cells using cell patch-clamp recordings in a separate cohort. $Fkbp5$ overexpression decreased the frequency of mEPSC frequency while increasing amplitude (Fig. 6E). This data shows that the $Fkbp5$ expression level in Crh^+ neurons can steer CRH neuronal activity within the PVN, whereas the baseline- and stress phenotype of $Fkbp5^{CRH\ OE}$ mice is mostly unaffected by the manipulation, identifying Crh^+ neurons as one important but not the only driver of the observed stress-like $Fkbp5^{PVN\ OE}$ phenotype.

Discussion

FKBP5 was first associated with stress-related disorders in 2004 [13] and has been studied extensively over the past 15 years with regard to stress regulation and sensitivity. However, detailed cell-type and region-specific manipulations of Fkbp5 in the brain are still lacking. In this study, we highlight the importance of this co-chaperone in the regulation of the acute stress response through the combined analysis of deletion, overexpression, and rescue of $Fkbp5$ exclusively in the PVN.

$Fkbp5$ is a stress-responsive gene and past research has shown that its main effects occur after chronic or acute stress [8, 18, 28, 32, 41]. Given that deletion of $Fkbp5$ in the PVN mimics the previously described phenotype of $Fkbp5$ KO mice [28, 41], with regard to their basal neuroendocrine profile and HPA axis function, our data illustrate that the functional contribution of $Fkbp5$ to HPA axis activity is centered in the PVN. In addition, reinstatement of native basal $Fkbp5$ expression in the PVN of $Fkbp5$ KO mice was sufficient to normalize HPA axis function. Interestingly, the phenotype of intensified HPA axis suppression due to the loss of $Fkbp5$ in the PVN emerges only in adult animals, excluding developmental effects and underlining the previously reported importance of Fkbp5 in aging [42, 43].

Further, our results highlight the essential role of Fkbp5 in stress adaptation, as PVN-specific Fkbp5 excess is sufficient to reproduce all physiological and endocrinological hallmarks of a chronic stress situation [29, 44]. Interestingly, the results of our $Fkbp5^{PVN\ OE}$ cohort are comparable to the neuroendocrine effect of GR deletion in the PVN [45] and are in line with the high PVN-specific FKBP5 expression in rats with a hyperactive HPA axis [20]. The consequence of a heightened $Fkbp5$ expression in the PVN is twofold. Firstly, it leads to direct changes in GR sensitivity and downstream GR signaling directly in the PVN. Secondly, PVN $Fkbp5$ overexpression dramatically affects GR sensitivity and feedback at the level of the pituitary, as

demonstrated by the inability of a low Dex dose (that does not cross the blood-brain barrier and acts predominantly at the level of the pituitary [26]) to suppress corticosterone secretion. This secondary effect is likely due to the constant overproduction of CRH in the PVN and very similar to the effects of HPA hyperactivity observed in many depressed patients [33, 46].

Mechanistically, we explored the role of Fkbp5 in modulating GR phosphorylation. The status of GR phosphorylation at Ser^{211}, Ser^{203}, and Ser^{234} is associated with transcriptional activity, nuclear localization, and ability to associate with GRE containing promoters [37]. Whereas higher levels of phosphorylation at Ser^{211} are associated with full transcriptional activity and localization in the nucleus, increased phosphorylation of Ser^{203} is linked to a transcriptionally inactive form of GR within the cytoplasm and thereby less active GR [38, 47, 48]. In our experiments, overexpression of Fkbp5 resulted in dephosphorylation at Ser^{211} and higher phosphorylation at Ser^{203}, suggesting that the GR is mostly located in the cytoplasm and less active. Deletion of Fkbp5 showed the opposing effect, indicating a more active GR in $Fkbp5^{PVN-/-}$ animals. Unfortunately, we were not able to analyze the GR phosphorylation in our $Fkbp5^{PVN\ Rescue}$ animals due to technical and breeding issues and therefore can only speculate that FKBP5$^{PVN\ Rescue}$ animals might have elevated levels of pGRSer203 and decreased levels of pGRSer211 and pGRSer234. It has previously been reported that GR phosphorylation is regulated by several kinases, including CDK5 and ERK [37, 49], and Fkbp5 has also been shown to be associated with CDK5 in the brain [50]. Therefore, we hypothesize that Fkbp5 also interacts with CDK5 to phosphorylate GR at multiple phosphorylation sites, thereby directly affecting ligand-dependent GR activity.

Given the complexity of the different cell types with highly specialized functions in the brain, it is essential to gain a deeper understanding of the cellular architecture of the PVN and the specific function of Fkbp5 in this context. Previously, it was assumed that Fkbp5 is quite widely expressed in most cell types of the nervous system [51]. However, our current data suggest that while $Fkbp5$ is indeed expressed in the PVN, it is enriched in specific subpopulations, including for example GABAergic neurons, Crh^+ neurons, and microglia, but largely absent in others, such as astrocytes and endothelial cells. Interestingly, when quantifying Fkbp5 regulation, we identified a highly selective regulation of $Fkbp5$ in Crh^+ neurons, further supporting the central role of Fkbp5-controlled GR feedback in this neuronal subpopulation.

To further disentangle the role of $Fkbp5$ within Crh positive neurons in the acute stress response and HPA-axis feedback regulation, we selectively overexpressed $Fkbp5$ in Crh^+ cells within the PVN and assessed baseline- and

stress-induced phenotypes paralleled by selective patch-clamp recordings from Crh^+ neurons. *Fkbp5* overexpression enhanced the amplitude of mEPSCs in Crh^+ cells indicating a postsynaptic and, thus, the direct effect of our *Fkbp5* manipulation on excitatory neurotransmission onto these neurons. This effect, which was accompanied by a diminished rate of mEPSC, potentially arises from accelerated recycling of internalized AMPA receptors to the postsynaptic density [52] and suggests an increased activity of Crh^+-cells. However, *Fkbp5* overexpression only partially recapitulating the HPA-axis phenotype observed in the $Fkbp5^{PVN\ OE}$ mice. The unselective *Fkbp5* overexpression in $Fkbp5^{PVN\ OE}$ animals targeted a broad range of *Fkbp5* expressing cell populations within the PVN, amongst which are oxytocin and vasopressin. Their essential contribution to the initiation and termination of the HPA-axis is well established, with vasopressin (together with CRH) inducing ACTH release from the pituitary [53] and oxytocin enhancing the negative feedback helping to dampen the stress response [54]. Hence, our data suggest that Fkbp5 might play an essential role in at least one further neuronal subpopulation of the PVN driving the observed stress-like phenotype of $Fkbp5^{PVN\ OE}$ mice in concert with CRH neurons.

The current study also comes with a number of limitations. Importantly, only male animals were used and the conclusions should therefore only be drawn with respect to male HPA axis regulation. Furthermore, given the fact that we did not observe differences in ACTH levels after stress, we cannot exclude that *Fkbp5* manipulations in the PVN also drive changes in adrenal sensitivity, e.g., via alterations of sympathetic adrenal innervation [55]. Furthermore, the time course of CRH and ACTH release is quite different from the CORT response, so our measures may have missed a differential regulation. In fact, a modest increase in circulating ACTH at certain times of the circadian rhythm can indeed lead to adrenal hypertrophy and increased sensitivity, thereby contributing to increased CORT secretion even following comparable ACTH levels. Finally, the lack of ACTH data in the Dex/CRH test was technically unavoidable but also limits the conclusions with regard to the involved mechanism.

In summary, this study is the first to specifically manipulate Fkbp5 in the PVN and underlines its central importance in shaping HPA axis regulation and the acute stress response. The results have far-reaching implications for our understanding of stress physiology and stress-related disorders.

Compliance with ethical standards

References

1. De Kloet ER, Joëls M, Holsboer F. Stress and the brain: from adaptation to disease. Nat Rev Neurosci. 2005;6:463–75.
2. Sinars CR, Cheung-Flynn J, Rimerman RA, Scammell JG, Smith DF, Clardy J. Structure of the large FK506-binding protein FKBP51, an Hsp90-binding protein and a component of steroid receptor complexes. Proc Natl Acad Sci USA. 2003;100:868–73.
3. Wochnik GM, Rüegg J, Abel GA, Schmidt U, Holsboer F, Rein T. FK506-binding proteins 51 and 52 differentially regulate dynein interaction and nuclear translocation of the glucocorticoid receptor in mammalian cells. J Biol Chem. 2005;280:4609–16.
4. Scammell JG, Denny WB, Valentine DL, Smiths DF. Overexpression of the FK506-binding immunophilin FKBP51 is the

common cause of glucocorticoid resistance in three new world primates. Gen Comp Endocrinol. 2001;124:152–65.

5. Binder EB, Bradley RG, Liu W, Epstein MP, Deveau TC, Mercer KB. et al. Association of FKBP5 polymorphisms and childhood abuse with risk of posttraumatic stress disorder symptoms in adults. JAMA. 2008;299:1291–305.

6. Denny WB, Valentine DL, Reynolds PD, Smith DF, Scammell JG. Squirrel monkey immunophilin FKBP51 is a potent inhibitor of glucocorticoid receptor binding. Endocrinology. 2000;141: 4107–13.

7. Ising M, Depping AM, Siebertz A, Lucae S, Unschuld PG, Kloiber S, et al. Polymorphisms in the FKBP5 gene region modulate recovery from psychosocial stress in healthy controls. Eur J Neurosci. 2008;28:389–98.

8. Touma C, Gassen NC, Herrmann L, Cheung-Flynn J, Bll DR, Ionescu IA. et al. FK506 binding protein 5 shapes stress responsiveness: modulation of neuroendocrine reactivity and coping behavior. Biol Psychiatry. 2011;70:928–36.

9. Westberry JM, Sadosky PW, Hubler TR, Gross KL, Scammell JG. Glucocorticoid resistance in squirrel monkeys results from a combination of a transcriptionally incompetent glucocorticoid receptor and overexpression of the glucocorticoid receptor co-chaperone FKBP51. J Steroid Biochem Mol Biol. 2006;100:34–41.

10. Scharf SH, Liebl C, Binder EB, Schmidt MV, Müller MB. Expression and regulation of the Fkbp5 gene in the adult mouse brain. PLoS ONE. 2011;6:1–10.

11. Zannas AS, Binder EB. Gene-environment interactions at the FKBP5 locus: sensitive periods, mechanisms and pleiotropism. Genes Brain Behav. 2014;13:25–37.

12. Matosin N, Halldorsdottir T, Binder EB. Understanding the molecular mechanisms underpinning gene by environment interactions in psychiatric disorders: the FKBP5 model. 2018. https://doi.org/10.1016/j.biopsych.2018.01.021.

13. Binder EB, Salyakina D, Lichtner P, Wochnik GM, Ising M, Pütz B, et al. Polymorphisms in FKBP5 are associated with increased recurrence of depressive episodes and rapid response to anti-depressant treatment. Nat Genet. 2004;36:1319–25.

14. Klengel T, Mehta D, Anacker C, Rex-Haffner M, Pruessner JC, Pariante CM, et al. Allele-specific FKBP5 DNA demethylation mediates gene-childhood trauma interactions. Nat Neurosci. 2013;16:33–41.

15. Young KA, Thompson PM, Cruz DA, Williamson DE, Selemon LD. BA11 FKBP5 expression levels correlate with dendritic spine density in postmortem PTSD and controls. Neurobiol Stress. 2015;2:67–72.

16. Sinclair D, Fillman SG, Webster MJ, Weickert CS. Dysregulation of glucocorticoid receptor co-factors FKBP5, BAG1 and PTGES3 in prefrontal cortex in psychotic illness. Sci Rep. 2013;3:1–10.

17. Gassen NC, Hartmann J, Zschocke J, Stepan J, Hafner K, Zellner A, et al. Association of FKBP51 with priming of autophagy pathways and mediation of antidepressant treatment response: evidence in cells, mice, and humans. PLoS Med. 2014;11: e1001755.

18. Hartmann J, Wagner KV, Gaali S, Kirschner A, Kozany C, Ruhter G, et al. Pharmacological inhibition of the psychiatric risk factor FKBP51 has anxiolytic properties. J Neurosci. 2015;35:9007–16.

19. Herman JP, McKlveen JM, Ghosal S, Kopp B, Wulsin A, Makinson R, et al. Regulation of the hypothalamic-pituitary-adrenocortical stress response. Compr Physiol. 2016;6:603–21.

20. Walker SE, Zanoletti O, Guillot de Suduiraut I, Sandi C. Constitutive differences in glucocorticoid responsiveness to stress are related to variation in aggression and anxiety-related behaviors. Psychoneuroendocrinology. 2017. https://doi.org/10.1016/j.psyneuen.2017.06.011.

21. Rodríguez CI, Buchholz F, Galloway J, Sequerra R, Kasper J, Ayala R, et al. High-efficiency deleter mice show that FLPe is an alternative to Cre- loxP. Nat Genet. 2000;25:139–40.

22. Balthasar N, Dalgaard LT, Lee CE, Yu J, Funahashi H, Williams T, et al. Divergence of melanocortin pathways in the control of food intake and energy expenditure. Cell. 2005;123:493–505.

23. Dedic N, Kühne C, Jakovcevski M, Hartmann J, Genewsky AJ, Gomes KS, et al. Chronic CRH depletion from GABAergic, long-range projection neurons in the extended amygdala reduces dopamine release and increases anxiety. Nat Neurosci. 2018;21:803–7.

24. Schmidt MV, Schulke J-P, Liebl C, Stiess M, Avrabos C, Bock J, et al. Tumor suppressor down-regulated in renal cell carcinoma 1 (DRR1) is a stress-induced actin bundling factor that modulates synaptic efficacy and cognition. Proc Natl Acad Sci USA. 2011;108:17213–8.

25. Paré WP, Glavin GB. Restraint stress in biomedical research: a review. Neurosci Biobehav Rev. 1986;10:339–70.

26. Karssen AM, Meijer OC, Berry A, Sanjuan Piñol R, De Kloet ER. Low doses of dexamethasone can produce a hypocorticosteroid state in the brain. Endocrinology. 2005;146:5587–95.

27. Jakovcevski M, Schachner M, Morellini F. Susceptibility to the long-term anxiogenic effects of an acute stressor is mediated by the activation of the glucocorticoid receptors. Neuropharmacology. 2011;61:1297–305.

28. Hartmann J, Wagner KV, Liebl C, Scharf SH, Wang XD, Wolf M, et al. The involvement of FK506-binding protein 51 (FKBP5) in the behavioral and neuroendocrine effects of chronic social defeat stress. Neuropharmacology. 2012;62:332–9.

29. Schmidt MV, Sterlemann V, Ganea K, Liebl C, Alam S, Harbich D, et al. Persistent neuroendocrine and behavioral effects of a novel, etiologically relevant mouse paradigm for chronic social stress during adolescence. Psychoneuroendocrinology. 2007;32:417–29.

30. Alexander Wolf F. PA and FJT. SCANPY: large-scale single cell data analysis. Genome Biol. 2017;19:2926–34.

31. Johnson WE, Li C, Rabinovic A. Adjusting batch effects in microarray expression data using empirical Bayes methods. Biostatistics. 2007;8:118–27.

32. Mifsud KR, Reul JMHM. Acute stress enhances heterodimerization and binding of corticosteroid receptors at glucocorticoid target genes in the hippocampus. Proc Natl Acad Sci USA. 2016;113:11336–41.

33. Ising M, Holsboer F. Genetics of stress response and stress-related disorders. Dialogues Clin Neurosci. 2006;8:433–44.

34. Wagner KV, Marinescu D, Hartmann J, Wang XD, Labermaier C, Scharf SH, et al. Differences in FKBP51 regulation following chronic social defeat stress correlate with individual stress sensitivity: influence of paroxetine treatment. Neuropsychopharmacology. 2012;37:2797–808.

35. Nestler EJ, Barrot M, DiLeone RJ, Eisch AJ, Gold SJ, Monteggia LM. Neurobiology of depression. Neuron. 2002;34:13–25.

36. Tsigos C, Chrousos GP. Hypothalamic-pituitary-adrenal axis, neuroendocrine factors and stress. J Psychosom Res. 2002;53:865–71.

37. Galliher-Beckley AJ, Cidlowski JA. Emerging roles of glucocorticoid receptor phosphorylation in modulating glucocorticoid hormone action in health and disease. IUBMB Life. 2009;61:979–86.

38. Wang Z, Frederick J, Garabedian MJ. Deciphering the phosphorylation 'code' of the glucocorticoid receptor in vivo. J Biol Chem. 2002;277:26573–80.

39. Dournes C, Dine J, Lopez J-P, Brivio E, Anderzhanova E, Roeh S, et al. Hypothalamic glucocorticoid receptor in CRF neurons is essential for HPA axis habituation to repeated stressor. BioRxiv. 2020:2020.11.30.402024.

40. Luecken MD, Theis FJ. Current best practices in single-cell RNA-seq analysis: a tutorial. Mol Syst Biol. 2019;15:e8746.

41. Hoeijmakers L, Harbich D, Schmid B, Lucassen PJ, Wagner KV, Schmidt MV, et al. Depletion of FKBP51 in female mice shapes HPA axis activity. PLoS ONE. 2014. https://doi.org/10.1371/journal.pone.0095796.

42. Sabbagh JJ, O'Leary JC, Blair LJ, Klengel T, Nordhues BA, Fontaine SN, et al. Age-associated epigenetic upregulation of the FKBP5 gene selectively impairs stress resiliency. PLoS ONE. 2014;9:e107241.

43. O'Leary JC, Dharia S, Blair LJ, Brady S, Johnson AG, Peters M, et al. A new anti-depressive strategy for the elderly: ablation of FKBP5/FKBP51. PLoS ONE. 2011;6:e24840.

44. Klein F, Lemaire V, Sandi C, Vitiello S, Van der Logt J, Laurent PE. et al. Prolonged increase of corticosterone secretion by chronic social stress does not necessarily impair immune functions. Life Sci. 1992;50:723–31.

45. Laryea G, Arnett M, Muglia LJ. Ontogeny of hypothalamic glucocorticoid receptor-mediated inhibition of the hypothalamic-pituitary-adrenal axis in mice. Stress. 2015. https://doi.org/10.3109/10253890.2015.1046832.

46. De Kloet ER. Hormones and the stressed brain. Ann N Y Acad Sci. 2004;1018:1–15.

47. Blind RD, Garabedian MJ. Differential recruitment of glucocorticoid receptor phospho-isoforms to glucocorticoid-induced genes. J Steroid Biochem Mol Biol. 2008;109:150–7.

48. Krstic MD, Rogatsky I, Yamamoto KR, Garabedian MJ. Mitogen-activated and cyclin-dependent protein kinases selectively and differentially modulate transcriptional enhancement by the glucocorticoid receptor. Mol Cell Biol. 1997;17:3947–54.

49. Kino T, Ichijo T, Amin ND, Kesavapany S, Wang Y, Kim N, et al. Cyclin-dependent kinase 5 differentially regulates the transcriptional activity of the glucocorticoid receptor through phosphorylation: clinical implications for the nervous system response to glucocorticoids and stress. Mol Endocrinol. 2007;21:1552–68.

50. Gassen NC, Hartmann J, Zannas AS, Kretzschmar A, Zschocke J, Maccarrone G, et al. FKBP51 inhibits GSK3β and augments the effects of distinct psychotropic medications. Mol Psychiatry. 2016;21:277–89.

51. Scharf SH, Schmidt MV. Animal models of stress vulnerability and resilience in translational research. Curr Psychiatry Rep. 2012;14:159–65.

52. Blair LJ, Criado-Marrero M, Zheng D, Wang X, Kamath S, Nordhues BA, et al. The disease-associated chaperone FKBP51 impairs cognitive function by accelerating AMPA receptor recycling. ENeuro. 2019;6:ENEURO.0242–18.

53. Sapolsky RM, Romero LM, Munck AU. How do glucocorticoids influence stress responses? Integrating permissive, suppressive, stimulatory, and preparative actions. Endocr Rev. 2000;21:55–89.

54. Winter J, Jurek B. The interplay between oxytocin and the CRF system: regulation of the stress response. Cell Tissue Res. 2019.

55. Leon-Mercado L, Chao DHM, Basualdo M del C, Kawata M, Escobar C, et al. The arcuate nucleus: a site of fast negative feedback for corticosterone secretion in male rats. ENeuro. 2017. https://doi.org/10.1523/ENEURO.0350-16.2017.

Supplementary figures.
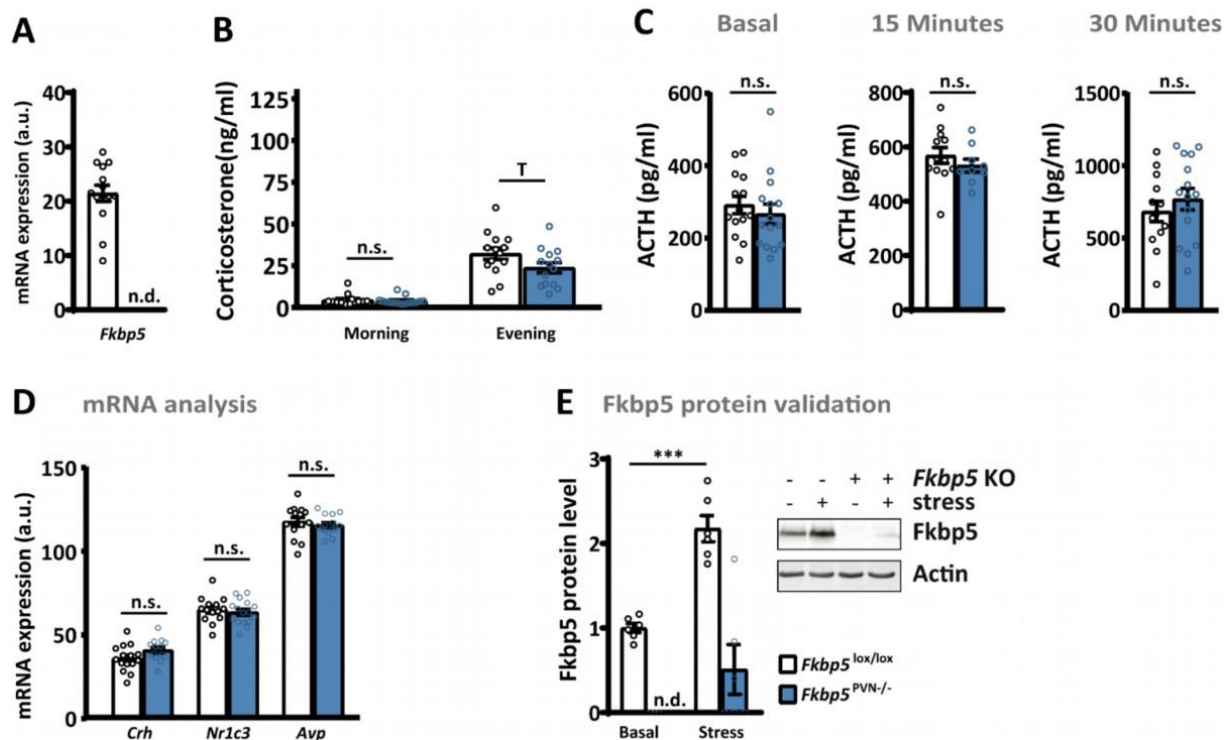
Supplementary Figure 1: Corticosterone and ACTH levels of *Fkbp5*[PVN-/-] mice (16-20 weeks of age).

(A) Validation of the *Fkbp5* deletion in *Fkbp5*[PVN-/-] *animals* (*Fkbp5*[PVN-/-] n = 16; *Fkbp5*[lox/lox] n =15)*.* **(B)** *Fkbp5* deletion in the PVN has no effect on basal CORT levels (*Fkbp5*[PVN-/-] n = 16; *Fkbp5*[lox/lox] n =15). **(C)** ACTH levels under basal,15 and 30 minutes after stress onset were unaltered (*Fkbp5*[PVN-/-] n = 9-16; *Fkbp5*[lox/lox] n =12-15). **(D)** mRNA changes of stress responsive genes within the PVN under basal conditions (*Fkbp5*[PVN-/-] n = 16; *Fkbp5*[lox/lox] n =15). **(E)** Fkbp5 protein levels under basal and stress conditions (*Fkbp5*[PVN-/-] n = 6; *Fkbp5*[lox/lox] n = 6 for stressed and non-stressed group). All data were received from mice between 16 and 20 weeks of age and are presented as mean ± SEM and were analyzed with a student's t-test (A-D) or with a two way ANOVA (E). n.d. = not detectable; n.s. = not significant; T = $0.05 < p < 0.1$; *** = $p < 0.001$.
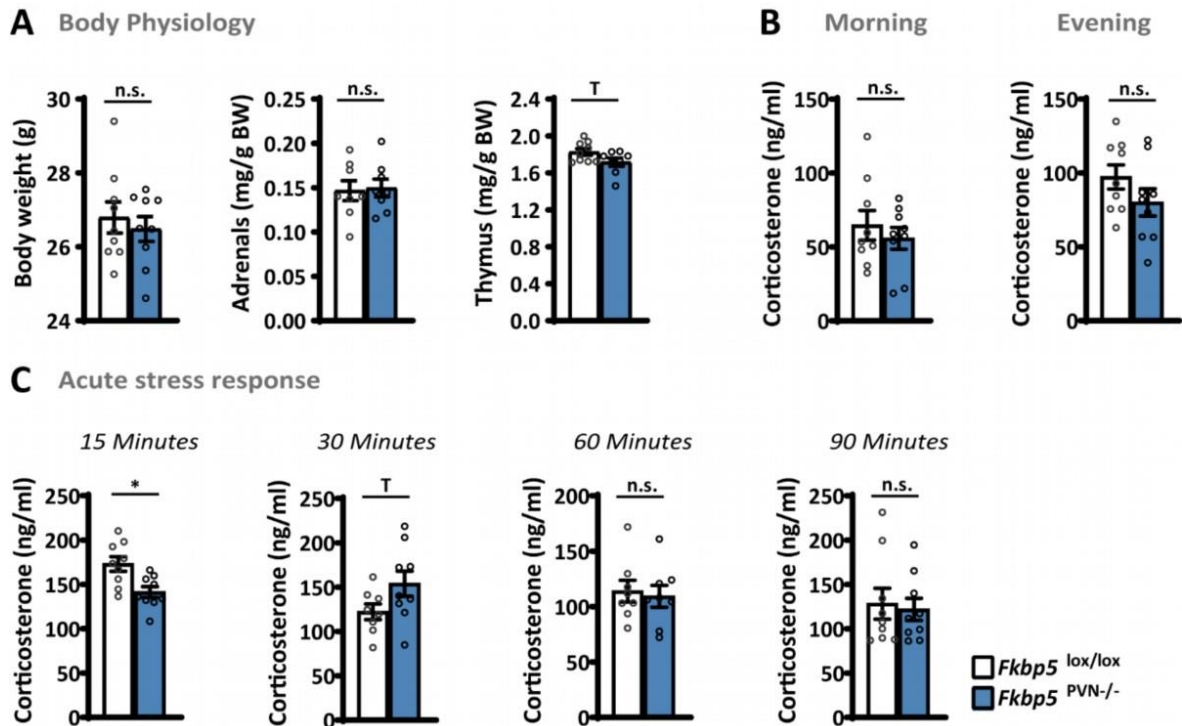
Supplementary Figure 2: Young mice with *Fkbp5* deletion in the PVN. **(A)** Animals with an age of 8-10 weeks had no alterations in body physiology. **(B)** Morning and evening corticosterone levels were unchanged. **(C)** FKBP51$^{PVN-/-}$ animals had significantly lower corticosterone levels 15 minutes after stress onset compared to the control group (group size for A-C: *Fkbp5*$^{PVN-/-}$ n = 9; *Fkbp5*$^{lox/lox}$ n =9). All data were received from mice between 8 and 10 weeks of age and are presented as mean ± SEM. Data were analyzed with a student's t-test. n.s. = not significant; T = $0.05 < p < 0.1$; * = $p < 0.05$.
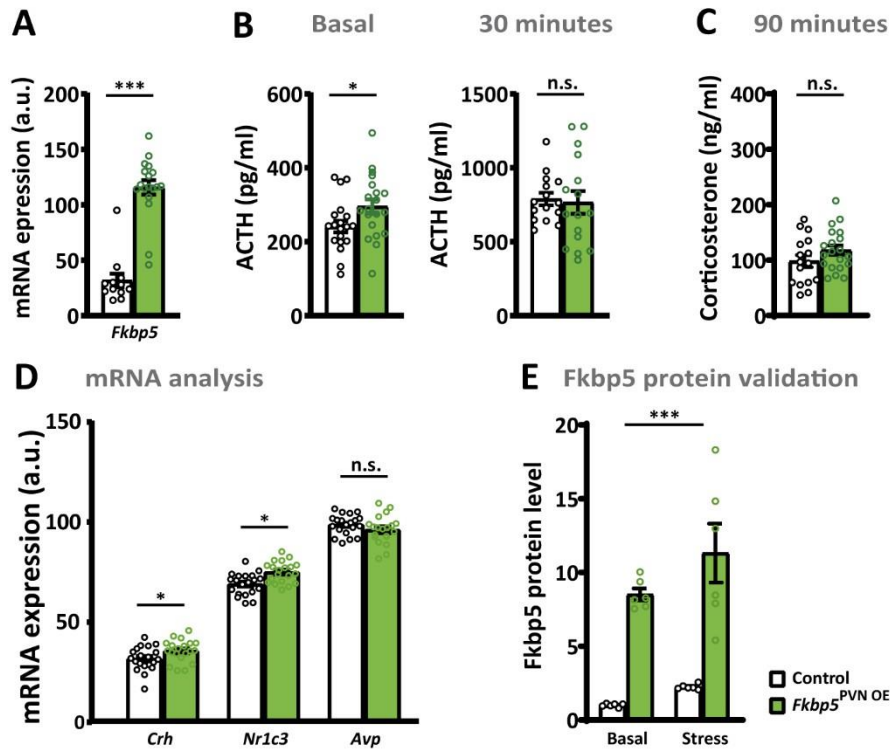
Supplementary Figure 3: Overexpression of *Fkbp5* in the PVN affected ACTH and mRNA levels. (A) *Fkbp5* overexpression resulted in a significant increase of *Fkbp5* mRNA (n (control) = 12 vs n (*Fkbp5*PVN OE) = 18). **(B)** ACTH levels were significantly higher in *Fkbp5*PVN OE mice under basal conditions (n = 20 vs. 20) and unchanged 30 minutes after stress onset (n = 12 vs. 12) compared to their controls. **(C)** We did not detect any differences in corticosterone levels 60 minutes after stress onset (n = 20 vs. 20). **(D)** mRNA levels of *N1c3* and *Crh* and *Avp* under basal conditions (n = 20 vs. 20). **(E)** Viral overexpression resulted in a 4-fold Fkbp5 protein upregulation (n = 6 vs. 6 for stress and non-stressed groups). All data were received from mice between 14-20 weeks of age and are presented as mean ± SEM and were analyzed with a student's t-test (A-D) or with a two way ANOVA (E). n.s. = not significant; * = p < 0.05, *** = p < 0.001.
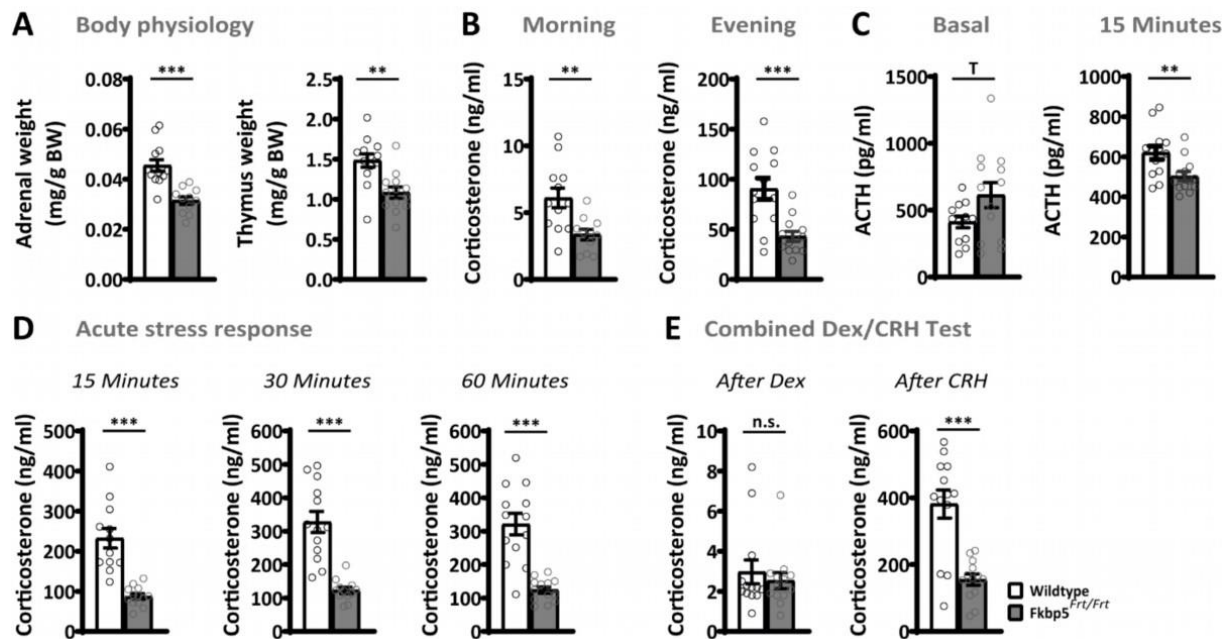
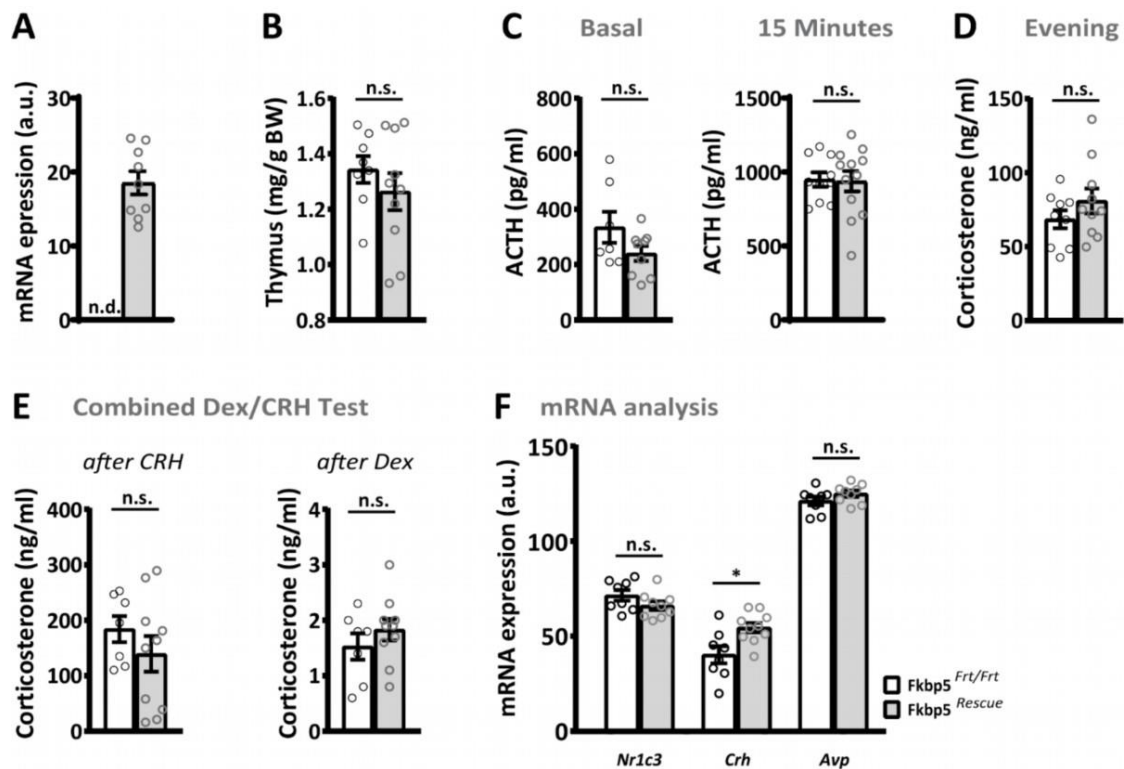**Supplementary Figure 4: Validation of the *Fkbp5*Frt/Frt mouse line in comparison to wildtype littermates. (A)** Adrenal and thymus weights on sacrifice day. **(B)** Morning and evening corticosterone levels. **(C)** ACTH under basal conditions and 15 minutes after stress onset**. (D)** Corticosterone after 15 minutes of restrain stress. **(E)** Combined Dex/CRH test. For all groups, n (wildtype) = 12 vs. n (*Fkbp5*Frt/Frt) = 11). All data were received from mice of 16-24 weeks of age and are presented as mean ± SEM and were analyzed with a student's t-test. n.s. = not significant; T = 0.05 < p < 0.1; ** = p < 0.01, *** = p < 0.001.

Supplementary Figure 5: Corticosterone and ACTH levels of *Fkbp5*^{Rescue} mice. (A) Validation of *Fkbp5* mRNA expression compared to *Fkbp5*^{Frt/Frt}. **(B)** *Fkbp5* reinstatement had no effect on thymus weights. **(C)** ACTH hormone levels were unaltered under basal and 15 minutes after stress. **(D)** Evening corticosterone. **(E)** Rescue of endogenous *Fkbp5* in global knock-out animals had no significant effect on the Dex/CRH test. **(F)** mRNA levels of stress responsive genes under basal conditions. Group sizes for A-F: *Fkbp5*^{Rescue} n = 10; *Fkbp5*^{Frt/Frt} n =9). All data were received from mice between 16 and 20 weeks of age and are presented as mean ± SEM and were analyzed with a student's t-test. n.s. = not significant; n.d. = not detectable; * = p < 0.05.
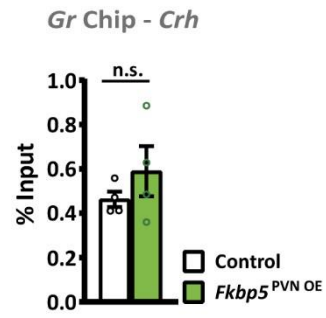
Supplementary Figure 6: GR to GRE binding within the *Crh* gene after stress. Mice were sacrificed 30 minutes after stress onset. Every n consists of a pool of 4 individual hypothalami. All data were received from mice aged between 12-16 weeks and are indicated as mean ± SEM and were analyzed with a student's t-test; (n = 4 vs. 4); n.s. = not significant.
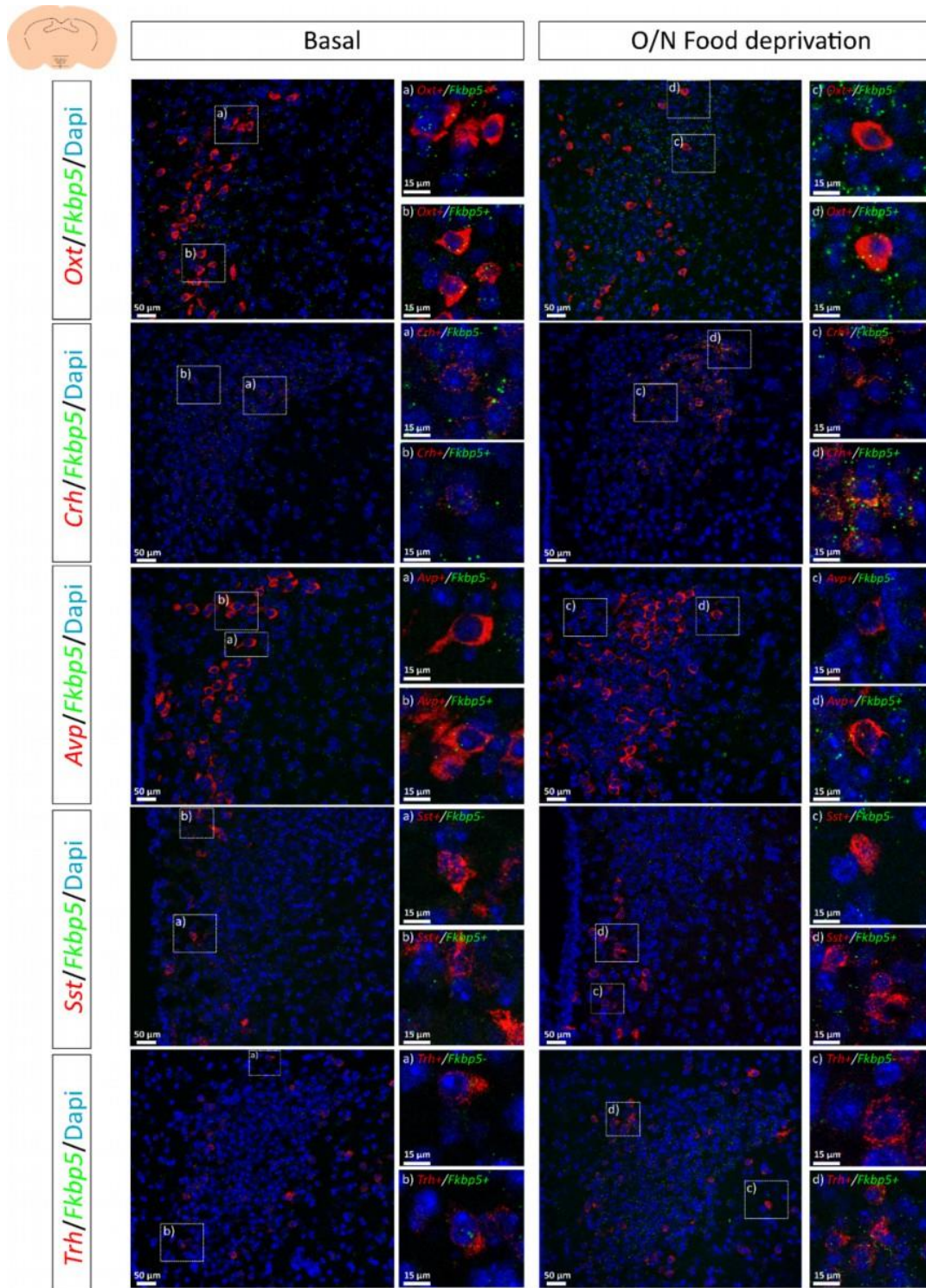
Supplementary Figure 7: RNAscope analysis of *Fkbp5* expression in stress response neuronal cell populations of C57Bl/6 under basal and stressed conditions. In comparison to single-cell sequencing, RNAscope revealed a significant higher co-localization ratio of *Fkbp5* in oxytocin (*Oxt*), corticotropin-releasing hormone (*Crh*), vasopressin (*Avp*), somatostatin (*Sst*) and thyronine releasing hormone (*Trh*) neurons. Overnight food deprivation increased *Fkbp5* mRNA in all cell populations.
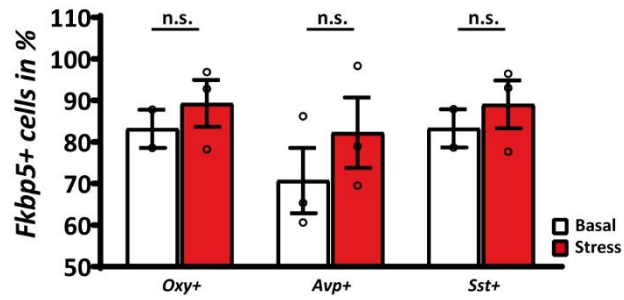
Supplementary Figure 8: Quantification of *Fkbp5* co-localization in stress response markers under basal and stress conditions. Under basal conditions *Fkbp5* mRNA signal was detected in 83% of *Oxt*+ neurons, 68% in *Avp*+ and 84% of *Sst*+ neurons. We monitored a non-significant increase in *Fkbp5* mRNA expression in all neuronal populations. Each n represents an average of the detected *Fkbp5*+ cells within six z-stacks of 1um each (3 per PVN side). Data are were received from animals between 8-12 weeks of age and are presented as mean ± SEM and were analyzed with a student's t-test. n.s. = not significant.
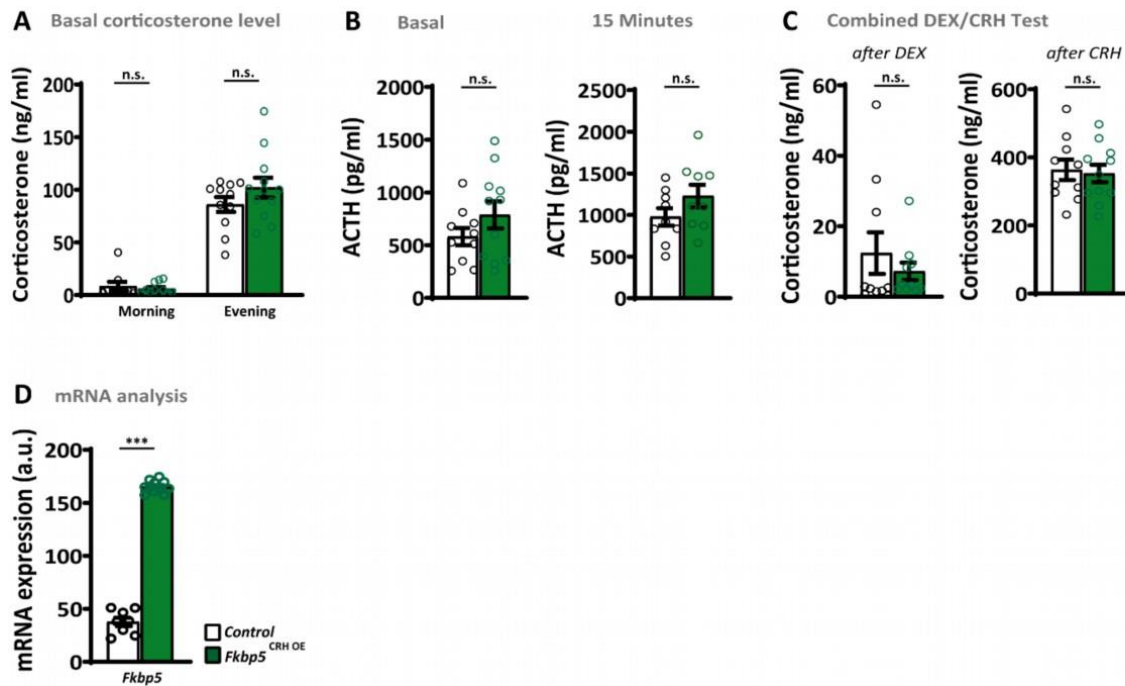
Supplementary Figure 9: Corticosterone and ACTH levels of *Fkbp5*CRH OE mice. (A) *Fkbp5* overexpression in CRH neurons within the PVN had no effect on basal morning (*Fkbp5*CRH OE n = 11; *Control* n = 9) and evening (*Fkbp5*CRH OE n = 12; Control n = 11) CORT level. **(B)** ACTH level were unaltered at baseline (*Fkbp5*CRH OE n = 11; Control n = 10) and 15 minutes post stress (*Fkbp5*CRH OE n = 9; Control n = 9). **(C)** In the combined Dex/CRH test CORT level were unaltered in *Fkbp5*CRH OE ($n_{after\ DEX}$ = 10; $n_{after\ CRH}$ = 11) compared to controls (n = 10) **(D)** *Fkbp5* mRNA expression level. All data are presented as mean ± SEM and were analyzed with a student's t-test. n.s. = not significant; *** = p < 0.001.

2.2 The co-chaperone FKBP51 modulates HPA axis activity and age-related maladaptation of the stress system in pituitary proopiomelanocortin cells

Brix, L.M., Häusl, A.S., Toksöz, I., Bordes, J., Doeselaar, L.V., Engelhardt, C., Narayan, S., Springer, M., Sterlemann, V., Deussing, J.M., Chen, A. & Schmidt, M.V.

Originally published in:

Psychoneuroendocrinology, 2022, 138, 105670.

The co-chaperone FKBP51 modulates HPA axis activity and age-related maladaptation of the stress system in pituitary proopiomelanocortin cells

Lea M. Brix [a,b,*], Alexander S. Häusl [a], Irmak Toksöz [a], Joeri Bordes [a], Lotte van Doeselaar [a,b], Clara Engelhardt [a], Sowmya Narayan [a,b], Margherita Springer [a], Vera Sterlemann [a], Jan M. Deussing [c], Alon Chen [d,e], Mathias V. Schmidt [a,**]

[a] Research Group Neurobiology of Stress Resilience, Max Planck Institute of Psychiatry, 80804 Munich, Germany
[b] International Max Planck Research School for Translational Psychiatry (IMPRS-TP), 80804 Munich, Germany
[c] Research Group Molecular Neurogenetics, Max Planck Institute of Psychiatry, 80804 Munich, Germany
[d] Department of Stress Neurobiology and Neurogenetics, Max Planck Institute of Psychiatry, 80804 Munich, Germany
[e] Weizmann Institute of Science, Department of Neurobiology, 7610001 Rehovot, Israel

ARTICLE INFO

ABSTRACT

Glucocorticoid (GC)-mediated negative feedback of the hypothalamic-pituitary-adrenal (HPA) axis, the body's physiological stress response system, is tightly regulated and essential for appropriate termination of this hormonal cascade. Disturbed regulation and maladaptive response of this axis are fundamental components of multiple stress-induced psychiatric and metabolic diseases and aging. The co-chaperone FK506 binding protein 51 (FKBP51) is a negative regulator of the GC receptor (GR), is highly stress responsive, and its polymorphisms have been repeatedly associated with stress-related disorders and dysfunctions in humans and rodents. Proopiomelanocortin (*Pomc*)-expressing corticotropes in the anterior pituitary gland are one of the key cell populations of this closed-loop GC-dependent negative feedback regulation of the HPA axis in the periphery. However, the cell type-specific role of FKBP51 in anterior pituitary corticotrope POMC cells and its impact on age-related HPA axis disturbances are yet to be elucidated. Here, using a combination of endogenous knockout and viral rescue, we show that male mice lacking FKBP51 in *Pomc*-expressing cells exhibit enhanced GR-mediated negative feedback and are protected from age-related disruption of their diurnal corticosterone (CORT) rhythm. Our study highlights the complexity of tissue- and cell type-specific, but also cross-tissue effects of FKBP51 in the rodent stress response at different ages and extends our understanding of potential targets for pharmacological intervention in stress- and age-related disorders.

1. Introduction

Our world is facing an unprecedented number of mental health diseases, with major depressive disorder (MDD) being the most common in different age groups (James et al., 2018). Hence, studying the mechanisms and biomarkers underlying increased stress vulnerability at different age periods throughout an individual's lifetime is crucial for the prevention and treatment of stress-induced disorders that are widespread in the aging population (Belvederi Murri et al., 2014).

MDD is a multifactorial and polygenic disorder, which results from a complex interplay of genetic risk factors together with environmental factors that cumulatively act throughout an individual's life to shape disease susceptibility (Uher, 2008; Wray et al., 2018). One interesting candidate identified in this context is the FK506 binding protein 51 (FKBP51; encoded by the *FKBP5* gene), a co-chaperone of heat-shock protein 90 (Hsp90) (Sinars et al., 2003), which has been reliably associated with the occurrence of stress-related psychiatric disorders (Binder et al., 2008, 2004; Matosin et al., 2018; Zannas and Binder, 2014). This genetic risk factor is a key player in glucocorticoid receptor (GR)-mediated negative feedback regulation of the HPA axis; the stress-induced hormonal signaling cascade that results in the release of glucocorticoids (GCs; cortisol in humans, and CORT in rodents) from the adrenal glands (De Kloet et al., 2005). As a complex with Hsp90, FKBP51 negatively regulates GR sensitivity by lowering the receptor's affinity to CORT and

reducing its nuclear translocation efficacy (Wochnik et al., 2005). In turn, *FKBP5* expression is induced via active GR and thereby provides an ultra-short, negative feedback loop for GR-sensitivity (Denny et al., 2000). Demethylation-mediated increase of *FKBP5* expression in risk-allele carriers was shown to reduce GR-mediated negative feedback and prolong activation of the hormonal stress response and is therefore considered a major genetic risk factor of stress-related disorders, such as MDD and post-traumatic stress disorder (Binder, 2009).

Besides stressful acute or chronic life conditions and psychiatric disorders, aging is well known to cause alterations in the hormonal stress response system in humans and rodents. HPA axis function and stress responsiveness are increased with age as a result of disturbed HPA axis negative feedback regulation (Belvederi Murri et al., 2014; Gupta and Morley, 2014; Sapolsky et al., 1986). Further, various aging-induced morphological changes of the adrenal glands are associated with alterations in hormonal output, resulting in a gradual increase in GC secretion (Yiallouris et al., 2019). Hence, the ability to adequately terminate the stress response system is impaired in the aging human population. In line with these findings, appropriate negative feedback regulation of the HPA system appeared to be profoundly dysregulated in aging rodents and non-human primates (Goncharova et al., 2019; Sapolsky, 1992). Interestingly, Sabbagh and colleagues showed that FKBP51 levels in rodents increase with aging, which contributes to impaired resiliency to depressive-like behaviors via disrupted GC signaling, a phenotype that is absent in full *Fkbp5* knockout mice (O'Leary et al., 2011; Sabbagh et al., 2014). Further, a human population study by Zannas et al. confirmed genome-wide epigenetic upregulation of FKBP51 by aging and stress in peripheral blood, thereby driving inflammation and cardiovascular risk in the elderly population (Zannas et al., 2019).

Described stress- and age-induced pathophysiologies share an increase in FBKP51 levels and reduced GR-mediated negative feedback regulation of the HPA axis, which has been shown to occur at different hierarchical levels, including the hippocampus, paraventricular nucleus of the hypothalamus (PVN) and the pituitary gland (Schmidt et al., 2009, 2005; Wagner et al., 2011), with all of these anatomical sites displaying stress-induced expression changes of *FKBP5* (Jenkins et al., 2013; Scharf et al., 2011). Despite its well-established role as a genetic risk factor, region- and cell type-specific functions of FKBP51 in the context of stress system biology are rare. A study recently published by our lab found that FKBP51 in the PVN shapes HPA axis negative feedback and (re)activity (Häusl et al., 2021). PVN specific knockout of *Fkbp5* in male C57/Bl6n mice improved GR-mediated negative feedback sensitivity and dampened the acute stress response whereas an overexpression reversed the effects, causing greater endocrine stress vulnerability.

To further disentangle the site- and cell type-specific contributions of FKBP51 to stress- and age-related HPA axis imbalance, we here investigated its functional role within the pituitary gland, the central endocrine hub of the HPA axis, which plays a key role in GR-mediated negative feedback control (Schmidt et al., 2009; Wagner et al., 2011). We profiled stress-related behavior and neuroendocrine phenotypes in young and aging male mice of a conditional knockout lineage lacking FKBP51 in all proopiomelanocortin (*Pomc*)-expressing cells (*Pomc*^Fkbp5-/-^). This mainly involves the pituitary gland in the periphery, but also some neuronal structures such as the arcuate nucleus (ARC) as the primary central site of expression and a smaller population in the brainstem nucleus of the solitary tract (NTS) (Balthasar et al., 2004; Quarta et al., 2021; Toda et al., 2017). In line with their described function in the HPA axis, we here demonstrate that FKBP51 in POMC cells of the pituitary is the main driver of improved HPA axis negative feedback regulation and prevents an aging-induced increase in diurnal CORT release.

2. Material and methods

2.1. Animals and animal housing

All experiments and protocols were approved by the committee for the Care and Use of Laboratory animals of the Government of Upper Bavaria and were performed in accordance with the European Communities' Council Directive 2010/63/EU. Throughout the experiments, all effort was made to minimize any suffering of the animals. The mouse lines *Fkbp5*^lox/lox^ and *Pomc*^Fkbp5-/-^ were obtained from the in-house breeding facility of the Max Planck Institute of Psychiatry and are all bred on C57/BL6n background. Young *Fkbp5*^lox/lox^ and *Pomc*^Fkbp5-/-^ males were aged 3–4 months and aging animals were 7–8 months old at the onset of the experiments. All animals were kept single housed in individually ventilated cages (IVC; 30 cm $\times$ 16 cm $\times$ 16 cm; 501 cm^2) serviced by a central airflow system (Tecniplast, IVC Green Line – GM500). Animals had ad libitum access to water (tap water) and food (standard research diet by Altromin 1318, Altromin GmbH, Germany) and were maintained under constant environmental conditions (12:12 hr light/dark cycle, 23 $\pm$ 2 °C and humidity of 55%). All IVCs had sufficient bedding and nesting material as well as a wooden tunnel for environmental enrichment. Animals were allocated to experimental groups in a semi-randomized fashion, data analysis and execution of experiments were performed blinded to group allocation.

2.2. Generation of Fkbp5^lox/lox^ and Pomc^Fkbp5-/-^ lines

Mice with a floxed *Fkbp5* gene designated as *Fkbp5*^lox/lox^ (*Fkbp5*^tm1c (KOMP)Wtsi^) were obtained by breeding *Fkbp5*^Frt/Frt^ full knockout mice to Deleter-Flpe mice (Rodríguez et al., 2000). The conditional *Fkbp5*^Frt/Frt^ knockout mice are derived from embryonic stem cell clone EPD0741_3_H03 which was targeted by the knockout mouse project (KOMP). Frozen sperm obtained from the KOMP repository at UC Davis was used to generate knockout mice (*Fkbp5*^tm1a(KOMP)Wtsi^) by in vitro fertilization. Finally, mice lacking *Fkbp5* in POMC neurons of the arcuate nucleus and POMC cells in the pituitary (POMC^Fkbp5-/-^) were obtained by breeding *Fkbp5*^lox/lox^ mice to POMC-Cre mice (Balthasar et al., 2004). Genotyping details are available upon request.

2.3. Viral rescue of FKBP51 in the ARC

POMC-specific rescue of *Fkbp5* expression (Fkbp5^Rescue^) was achieved by bilateral injections of a *Cre*-dependent *Fkbp5* overexpression virus (pAAV-Cre-dependent-CAG-HA-human wildtype FKBP51 WPRE-BGH-polyA, titer: 1.3 $\times 10^{12}$ genomic particles/ml, Gene Detect GD1001-RV) into the ARC of *Pomc*^Fkbp5-/-^ knockout mice. For knockout- and wildtype controls, *Pomc*^Fkbp5-/-^ and *Fkbp5*^lox/lox^ (referred to after virus injection as Control^KO^ and Control^lox/lox^, respectively) were injected with an AAV2-eSyn-GFP control virus (titer: 1.3 $\times 10^9$ genomic particles/ml, Vector Biolabs VB1107). Stereotactic surgeries were performed as described previously (Häusl et al., 2021). In brief, male mice between 3 and 5 months of age were anesthetized with isoflurane and fixated in a stereotactic apparatus. Then, 0.5 μl of above-mentioned viruses were bilaterally injected into the ARC at a 0.05 μl/min flow rate with glass capillaries with a tip resistance of 2 – 4 MΩ. To target the ARC the following coordinates were used: - 1.5 mm anterior to bregma, 0.35 mm lateral from midline, and 5.8 mm below the surface of the skull. After surgery, animals were treated with Metacam i.p. for three days and were allowed to recover for four weeks before initiating the experimental phase.

2.4. Combined DEX/CRH test

To investigate the negative feedback sensitivity of the HPA axis, we performed a combined dexamethasone (DEX)/corticotropin-releasing hormone (CRH) test as described previously (Touma et al., 2011). In the

morning (8:00 AM) of the experimental day, mice were injected i.p. with a low dose of the synthetic adrenal corticosteroid DEX (0.05 mg/kg, Dex-Ratiopharm, 7633932), which was shown not to cross the blood brain barrier (BBB) but predominantly act in the periphery (Karssen et al., 2005). Here, the pituitary is the most important site of action in relation to HPA axis function, especially in combination with a subsequent CRH challenge. Six hours after DEX injection, blood was collected via tail cut immediately followed by an i.p. injection of CRH (0.15 mg/kg, CRH Ferrin Amp). A second blood sample was obtained 30 min after CRH injection. All experimental blood samples were collected in 1.5 ml EDTA-coated microcentrifuge tubes (Kabe Labortechnik, Germany), immediately stored on ice and centrifuged for 15 min at 8000 rpm at 4 °C. 10 µl of plasma were transferred to new, labeled 2 ml microcentrifuge tubes and stored at − 80 °C until further processing.

2.5. Acute restraint stress paradigm

The acute restraint stress paradigm is perceived as a severe stressor robustly inducing the entire spectrum of known allostatic responses in rodents and was therefore the stress paradigm of choice. At 8:00 AM, one hour after the lights were switched on, each animal was placed in a custom-made restrainer (50 ml falcon tube with holes at the bottom and the lid to provide enough oxygen and space for tail movement) for 15 min in their home cage. After 15 min, animals were removed from the tube and the first blood sample was collected by tail cut. Subsequent blood samples at 30, 60, and 90 min post stress were collected in the home cage via tail cut and animals were left undisturbed in between sampling procedures.

2.6. Tissue sampling procedure

On the day of sacrifice, animals were weighed, deeply anesthetized with isoflurane and sacrificed by decapitation. Trunk blood (basal morning CORT and basal adrenocorticotropin hormone (ACTH)) was collected in labeled 1.5 ml EDTA-coated microcentrifuge tubes (Kabe Labortechnik, Germany) and kept on ice until centrifugation. After centrifugation (4 °C, 8000 rpm for 15 min) plasma was removed and transferred to new, labeled 2 ml tubes and stored at − 80 °C until hormone quantification. For mRNA analyses, brains were removed, and the pituitary was dissected from the skull and manually attached to the brain. Brains were snap-frozen in isopentane at − 40 °C and stored at − 80 °C until further processing. The adrenals were dissected from fat and weighed.

Evening CORT blood samples were collected between 5:00 and 7:00 PM via tail poking. Therefore, animals were poked in the tail tip with a needle and blood drops were collected with 1.5 ml EDTA-coated microcentrifuge tubes (Kabe Labortechnik, Germany). This sampling technique is less invasive while still providing sufficient blood volumes for further analysis.

2.7. Hormone assessment

Baseline and post stress plasma CORT (ng/ml) and baseline ACTH (pg/ml) concentrations were determined by radioimmunoassay using CORT ^{125}I RIA kit (sensitivity: 12.5 ng/ml, MP Biomedicals Inc) and ACTH ^{125}I RIA kit (sensitivity: 10 pg/ml, MP Biomedicals Inc) following the manufacturers' instructions. Radioactivity of the pellet was measured with a gamma counter (Packard Cobra II Auto Gamma; Perkin-Elmer). ACTH and CORT were assessed 15 min post stress using an ACTH ELISA (IBL international GmbH, RE53081) according to the manufacturer's instructions. Final CORT and ACTH levels were derived from the standard curve.

2.8. Double in-situ hybridization – Co-expression analysis

To initially check co-expression of *Fkbp5* mRNA with *Pomc*$^+$ cells, we performed a double in-situ hybridization (DISH) using ^{35}S UTP labeled *Fkbp5* and DIG labelled *Pomc* riboprobes in 3 – 4 months old C57/Bl6n males. Frozen brains were sectioned at 20 µm in the coronal plane through the level of the hypothalamic PVN, dorsal and ventral hippocampus and pituitary at − 20 °C in a cryostat microtome. Sections were thaw mounted on Super Frost Plus slides, dried and stored at − 80 °C. The antisense cRNA probes were transcribed from a linearized plasmid for *Fkbp5* and *Pomc*. All primer details are available upon request. Radioactive labeling of the ^{35}S UTP labeled *Fkbp5* ribonucleotide probe was performed as described previously (Häusl et al., 2021; Schmidt et al., 2007). Digoxigenin (DIG) labeling of the nonradioactive *Pomc* probe using the 10 × DIG RNA labeling mix (Roche, Switzerland) was performed according to the manufacturer's protocol. Concentration of DIG *Pomc* riboprobe was assessed in a serial dilution of the probe compared to a control RNA riboprobe with a known concentration. DISH was performed as previously described (Refojo et al., 2011).

2.9. In-situ hybridization – post DEX/CRH

To analyze post DEX/CRH mRNA expression of *Gr* and *Pomc* cell population within the pituitary, we performed in-situ hybridization (ISH). Therefore, frozen brains were processed as described for the DISH and ISH using ^{35}S UTP labeled ribonucleotide probes (*Gr* and *Pomc*) was performed as described previously (Häusl et al., 2021; Schmidt et al., 2007). All primer details are available upon request. For signal detection, the slides were exposed to Kodak Biomax MR films (Eastman Kodak Co., Rochester, NY) and developed. Exposure times varied according to the radioactive properties of each riboprobe. Autoradiographs were digitized, and expression was determined by optical densitometry utilizing the freely available NIH ImageJ software (NIH, Bethesda, MD, USA). The grey value of left and right side of the anterior pituitary was measured within a circular template (16 width × 16 height) in every slice analyzed (1 slice per animal). The data were analyzed blindly, always subtracting the background signal of a nearby structure not expressing the gene of interest from the measurements.

2.10. RNA scope – Validation of knockout and quantification of off-target effects

To validate successful knockout of *Fkbp5* mRNA in *Pomc*$^+$ cells in the ARC and pituitary, we performed a RNAScope experiment on brain sections of the *Pomc*$^{Fkbp5-/-}$ mouse line under basal conditions (3 – 4 months of age). Brains were processed as described above for ISH. The RNA Scope Fluorescent Multiplex Reagent kit (cat. no. 320850, Advanced Cell Diagnostics, Newark, CA, USA) was used for mRNA staining. Probes used for staining were; *Fkbp5* (Mm-Fkbp5-C1) and *Pomc* (Mm-Pomc-C3). The *Fkpb5* probe spans Exon 9, which is deleted in our model, but also targets neighboring exons. Consequently, the probe may still bind to truncated mRNA leading to a residual Fkbp5 mRNA signal in knock-out cells, even though no functional FKBP51 protein can be expressed. The staining procedure was performed according to manufacturer's specifications and as performed previously (Häusl et al., 2021). Images of the arcuate nucleus (left and right side) and the pituitary were acquired by an experimenter blinded to the condition of the animals. Sixteen-bit images of each section were acquired on a Zeiss confocal microscope using a 20x and 40x objective (n = 3 animals per marker and condition). For every section, all images were acquired using identical settings for laser power, detector gain, and amplifier offset. *Fkbp5* mRNA expression was analyzed using ImageJ with the experimenter blinded to the genotype of the animals and was counted manually. Each *Pomc*$^+$ cell containing one or more *Fkbp5* mRNA puncta was counted as positive and calculated as percentage of *Fkbp5* positive cells from total number of *Pomc*- expressing cells. For cell-type unspecific quantification of potential off-target effects of the knockout, *Fkbp5* mRNA puncta were manually counted in 30 *DAPI*$^+$ and *Pomc*$^-$ cells per image analyzed (same images as used for knockout quantification) and

average number of puncta per *Pomc*⁻ cell was calculated.

2.11. Behavioral stress phenotyping

All behavioral tests were performed between 8:00 AM and 12:00 PM in a room adjacent to the animal housing room and were recorded and tracked using the automated video-tracking system Anymaze 6.3 (Stoelting, Dublin, IE).

2.11.1. Open field test

The first behavioral task of the test battery was the open field test (OF) to assess locomotor activity and anxiety-like behavior. The empty OF arenas (50 ×50 × 50 cm) were made of gray polyvinyl chloride (PVC) which were evenly illuminated (~ 20 lux) throughout the course of the experiment. All animals were placed in the lower left corner of the arena right before recording and tracking was started manually. During a total of 15 min, distance travelled, entries to – and time spent in inner zone were analyzed.

2.11.2. Elevated plus maze

To further assess anxiety-like behavior, animals were tested in the elevated plus maze (EPM) on day two of the behavioral testing period. The elevated maze (50 cm above ground) consisted of two opposing open arms (30 ×5 × 0.5 cm) and two opposing enclosed arms (30 ×5 × 0.5 cm) of grey PVC, which were connected by a central platform (5 ×5 cm) shaping a plus sign. Lighting conditions were set to 20 lux in the closed arms and remained unchanged during the experiment. At the beginning of the test, animals were placed in the center zone, facing an enclosed arm before recording and tracking was started manually. Mice were allowed to explore the maze for a total of 10 min during which the time spent in the open arms and entries and total distance were analyzed.

2.11.3. Dark-light box test

Finally, we assessed anxiety in the dark-light box test (DALI) at the third day of behavioral testing. The DALI apparatus has two compartments: One light compartment (30 ×20 × 25 cm) evenly illuminated at ~700 lux and a dark and protected compartment (15 ×20 × 25 cm) which was dimly lit with a maximum illumination of ~15 lux in the transition area. A door and a covered acrylic-glass tunnel of 4 cm in width connected the two areas of the apparatus allowing the animal to transit freely from one to the other compartment. Mice were placed in the lower left corner of the dark compartment, facing the center before manually starting the test and were recorded for a total of 5 min. To assess anxiety, time spent- and number of entries to the light compartment were measured.

2.12. Statistical analysis

The data presented are shown as means ± SEM and samples sizes are indicated in the figure legends and in the main text. All data were analyzed by the commercially available GraphPad Prism 9.0 software (GraphPad Software, San Diego, California, USA). When two groups were compared, the unpaired *student's t test* was applied. If data were not normally distributed the non-parametric *Mann-Whitney test* (*MW test*) was used. Data with more than two groups were tested by the appropriate analysis of variance (ANOVA) model followed by *Bonferroni* post-hoc analysis to determine statistical significance between individual groups. *P* values of less than 0.05 were considered statistically significant. The sample size was chosen such that with a type 1 error of 0.05 and a type 2 error of 0.2 the effect size should be at least 1.2-fold of the pooled standard deviation. Outliers were assessed with the online available Graph Pad outlier calculator performing the two-sided *Grubb's* outlier test.

3. Results

3.1. Co-expression of Fkbp5 with Pomc and validation of successful Fkbp5 knockout

To validate co-expression of *Fkbp5* with *Pomc*⁺ cells we performed a DISH in 3 – 4 months old C57/Bl6n males under baseline conditions. Besides a high expression level of *Pomc* mRNA within the pituitary, *Pomc* is also abundantly expressed within the ARC and further in a small fraction of POMC neurons in the brainstem NTS (Quarta et al., 2021; Toda et al., 2017). In this study, co-expression was investigated solely in *Pomc*-expressing cells within the ARC and pituitary. Qualitative analysis of DISH radiographs successfully revealed co-expression of *Pomc* mRNA (pink DIG labeling) and *Fkbp5* mRNA (black ³⁵S UTP labeling) in neurons of the ARC and cells in the pituitary gland (Fig. 1A).

To study the site-specific effects of FKBP51 in *Pomc*-expressing cells on stress physiology, we generated POMC-specific conditional *Fkbp5* knockout mice (*Pomc*$^{Fkbp5-/-}$) by crossing the *Fkbp5*$^{lox/lox}$ with the POMC-*Cre* line, which expresses *Cre*-recombinase under the *Pomc* promoter (Fig. 1B). Successful reduction of *Fkbp5* expression within *Pomc*⁺ cells in the pituitary and ARC was assessed by semi-quantitative analysis of RNAScope fluorescent mRNA staining (Fig. 1C, D). The number of *Pomc*⁺ cells expressing *Fkbp5* within the pituitary and ARC is significantly reduced in *Pomc*$^{Fkbp5-/-}$ mice compared to control *Fkbp5*$^{lox/lox}$ mice (ARC: $U = 0$, $p < 0.001$, PIT: $t_8 = 2.35$, $p = 0.047$) (Fig. 1D). Quantification of off-target effects of our knockout revealed unchanged expression of *Fkbp5* mRNA in *Dapi*⁺ and *Pomc*⁻ cells both in ARC ($t_{11} = 0.92$, $p = 0.38$) and pituitary ($t_9 = 0.38$, $p = 0.71$) of Pomc$^{Fkbp5-/-}$ compared to controls (Supplementary Fig. 1).

3.2. GR-mediated negative feedback sensitivity is improved in young Pomc$^{Fkbp5-/-}$ at the level of the pituitary

To investigate the impact of our *Fkbp5* disruption on stress system biology, cohorts of young (3–4 months) *Pomc*$^{Fkbp5-/-}$ and control male mice underwent stress-related endocrine and behavioral phenotyping.

Bodyweight ($t_{39} = 0.56$, $p = 0.58$) and adrenal weight ($t_{30} = 0.86$, $p = 0.4$) at the day of sacrifice were not different in the first cohort tested ($n_{Pomc}$$^{Fkbp5-/-}$ =21, $n_{Fkbp5}$$^{lox/lox}$ = 20) (Fig. 2A). Further, baseline morning (8:00 AM) and evening (6:00 PM) CORT were unaltered in young *Pomc*$^{Fkbp5-/-}$ mice (morning: $U = 92.5$, $p = 0.42$; evening: $t_{30} = 0.37$, $p = 0.72$) (Fig. 2B). Morning and 15 min post stress ACTH (Fig. 2B and C) were assessed in a second cohort ($n_{Pomc}$$^{Fkbp5-/-}$ = 8, $n_{Fkbp5}$$^{lox/lox}$ = 12) for reasons of experimental practicability. Morning baseline ACTH measures were significantly reduced in knockout animals and post stress ACTH values showed a trend towards reduced levels in young *Pomc*$^{Fkbp5-/-}$ mice (morning: $U = 18$, $p = 0.02$, post stress: $t_{18} = 1.77$, $p = 0.09$). We further assessed the animal's CORT response 15 and 60 min after an acute restraint stress in the first cohort, which revealed a genotype-specific difference in the recovery phase at T60 (T15: $t_{30} = 0.23$, $p = 0.83$; T60: $U = 66$, $p = 0.03$) (Fig. 2C).

With the pituitary being a central endocrine hub of the HPA axis and one of the main anatomical sites of GR-mediated negative feedback regulation (Toda et al., 2017), we hypothesized that a knockout of *Fkbp5* in cells of the pituitary would alter HPA axis (re)activity. To test this hypothesis, we investigated GR-mediated feedback sensitivity in a combined DEX/CRH test in the first cohort of young *Pomc*$^{Fkbp5-/-}$ mice. This endocrine function test is one of the diagnostic hallmarks of MDD and one of the most sensitive measures of subtle changes in HPA system regulation. Hence, it has been applied extensively in human and rodent HPA axis function studies and is widely used as a state dependent marker to monitor HPA axis abnormalities (Ising et al., 2005; Mokhtari et al., 2013). By injecting a low dose of DEX (0.05 mg/kg), the synthetic GC does not cross the BBB, thereby acting predominantly in the periphery (for details see 2.4). Here, the pituitary is the most important site of action in relation to HPA axis function, especially in combination with a
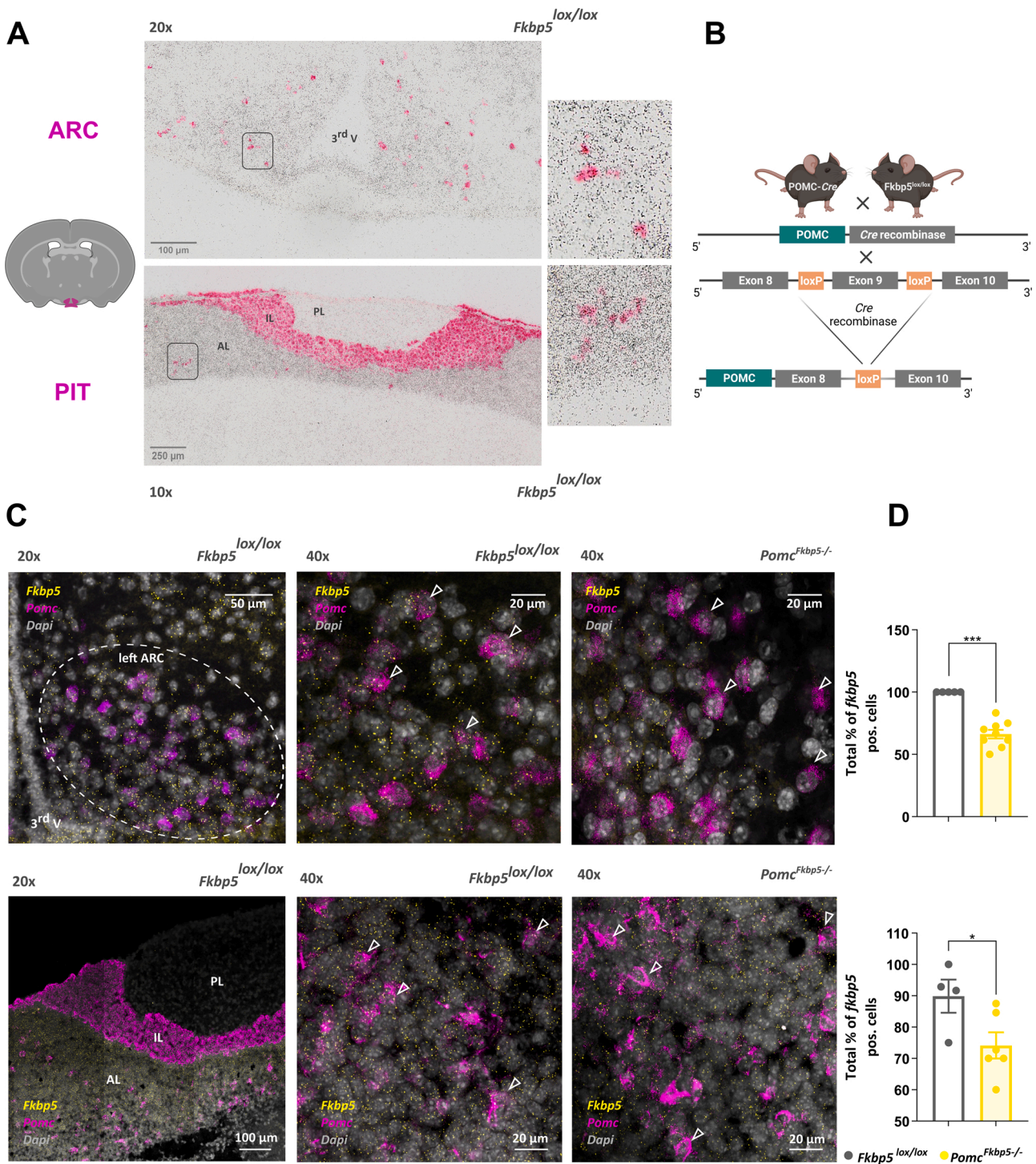
Fig. 1. Validation of *Fkbp5* knockout in *Pomc*-expressing neurons in the ARC and pituitary. A Qualitative co-expression analysis of *Fkbp5* (black 35 S UTP labeling) and *Pomc* mRNA (pink DIG labeling) via double-in situ hybridization in neurons of the ARC and cells of the pituitary. Grey squares highlight double-positive cells that are zoomed in on in the panels on the right. B *Cre*-LoxP based generation of the conditional POMC-specific *Fkbp5* knockout mouse line (*Pomc^Fkbp5-/-*). C Representative confocal images of RNAScope of *Fkbp5* mRNA expression in *Pomc^+* cells in the ARC (upper panels) and pituitary (lower panels) of *Fkbp5^lox/lox* controls vs. *Pomc^Fkbp5-/-* knockout. D Quantification of the total percentage of *Fkbp5* positive cells that co-express *Pomc* mRNA revealed significant reduction of *Fkbp5* expression in the *Pomc^Fkbp5-/-* knockout line (n = number of analyzed 40x confocal images of either left or right ARC or pituitary, ARC: $n_{KO} = 9$, $n_{Control} = 5$; pituitary: $n_{KO} = 6$, $n_{Control} = 4$). Data are received from mice between 16 and 20 weeks of age and are presented as mean ± SEM. * p < 0.05, * ** p < 0.001.

subsequent CRH challenge. This allowed us to specifically investigate the effects of FKBP51 action on HPA axis (re)activity within the pituitary gland and separate observed effects from FKBP51 in POMC neurons within the ARC. The injection of a low dose of DEX resulted in a drastic reduction in blood CORT in both groups to the same extend. Following

CRH stimulation, *Pomc^Fkbp5-/-* mice showed a significantly attenuated reaction to CRH compared to control mice (after DEX: $U = 41$, $p = 0.34$; after CRH: $t_{29} = 4.24$, $p = 0.0002$) (Fig. 2D). Interestingly, *ISH* analysis of the pituitary 30 min after CRH injection revealed significantly lower *Pomc* mRNA expression level in *Pomc^Fkbp5-/-* compared to WT littermates
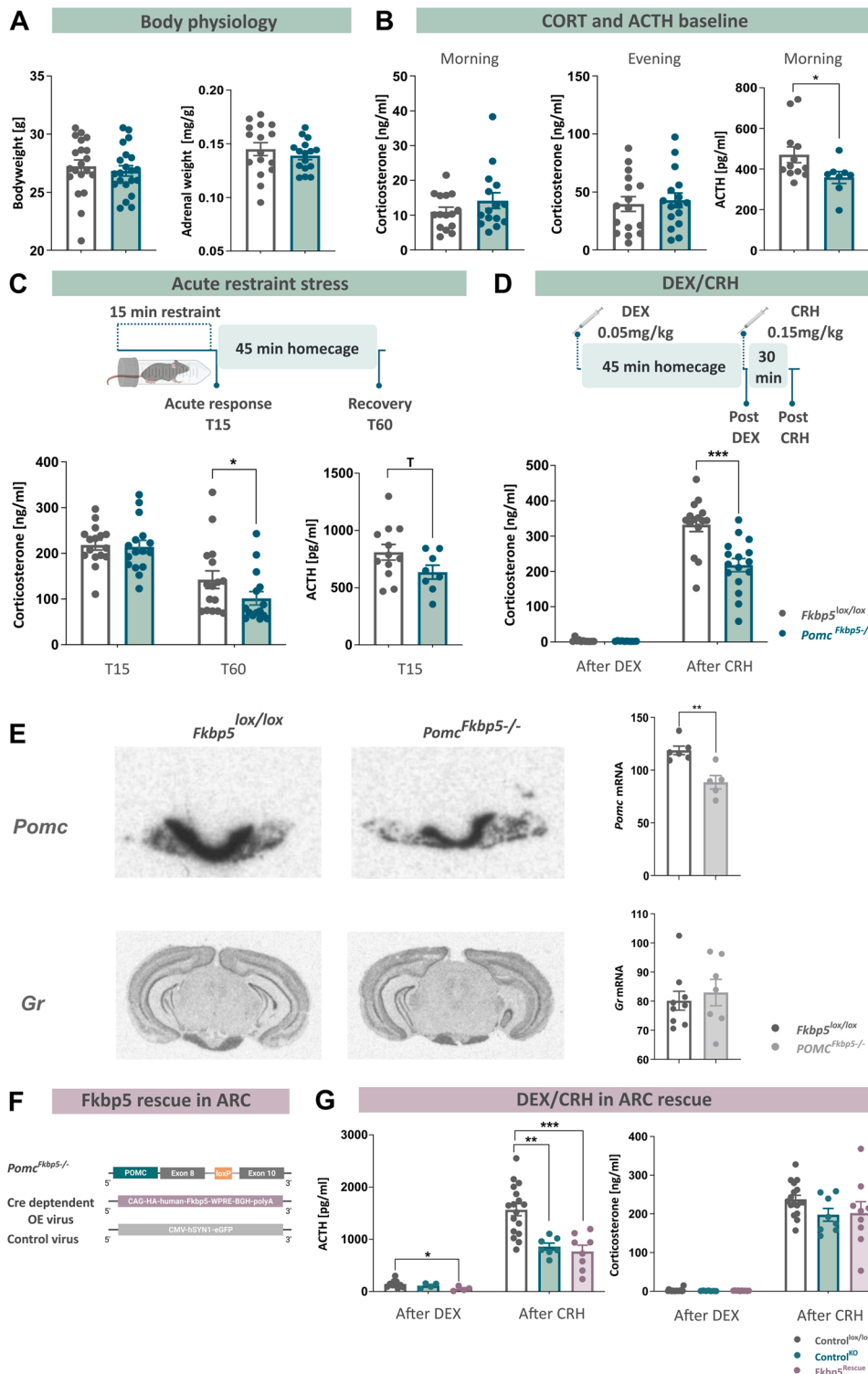
Fig. 2. Inactivation of *Fkbp5* in POMC cells of young animals affects GR-mediated feedback sensitivity of the HPA axis at the level of the pituitary. A Bodyweight and relative adrenal weights were unaltered in a first cohort of young (3 – 4 months) *Pomc^Fkbp5-/-* (n = 20) compared to controls (*Fkbp5^lox/lox* = 21). B Baseline morning and evening CORT levels were unaltered in these knockout animals. Morning baseline ACTH measures were significantly decreased in a second cohort of *Pomc^Fkbp5-/-* (n_*Fkbp5*^lox/lox = 12; n_*Pomc*^Fkbp5-/- = 8). C 60 min after an acute restraint stress, *Pomc^Fkbp5-/-* mice in the first cohort displayed significantly reduced CORT levels. Further, there was a trend towards reduced ACTH levels fifteen minutes post stress in the knockout line. D In the DEX/CRH test *Pomc^Fkbp5-/-* animals displayed a significant decrease in CRH-mediated CORT overshoot. E ISH analysis of the pituitary 30 min after CRH injection revealed significantly lower *Pomc* mRNA expression level in *Pomc^Fkbp5-/-* (n_pomc = 5) compared to WT littermates (n_pomc = 6) and unaltered *gr* mRNA (n_*Pomc*^Fkbp5-/- = 7; n_*Fkbp5*^lox/lox = 9). F Rescue of *Fkbp5* expression was achieved by bilateral viral injections of a *Cre*-dependent *Fkbp5* overexpression virus into the ARC of the *Pomc^Fkbp5-/-* knockout line (Fkbp5^Rescue, n = 10). *Fkbp5^lox/lox* (n = 20) and *Pomc^Fkbp5-/-* knockout animals (n = 10) received an eGFP control virus (referred to as Control^lox/lox and Control^KO). G CORT and ACTH levels post CRH injection confirmed reduced overshoot in the knockout line (Control^KO) compared to Control^lox/lox. FKBP51-reinstated animals (Fkbp5^Rescue) displayed CORT levels comparable to the knockout line and significantly reduced ACTH levels post DEX and CRH injection in comparison to Control^lox/lox. Data are represented as mean ± SEM. All data were received from mice between 3 and 4 months of age. * p < 0.05, ** p < 0.01, *** p < 0.001, T < 0.1.

(t_9 = 4.1, *p* = 0.003), while *Gr* mRNA expression was unaltered (t_{14} = 0.52, *p* = 0.62) (Fig. 2E). These data indicate that deletion of FKBP51 in POMC cells suppresses HPA axis (re)activity and improves negative feedback potentially by downregulation of *Pomc* mRNA expression within corticotrope cells of the anterior pituitary.

To pin down the observed DEX/CRH phenotype to *Pomc*-expressing cells within the pituitary and to further rule out a contribution of the ARC, we restored native *Fkbp5* expression exclusively within the ARC via *Cre*-dependent viral *Fkbp5* overexpression in *Pomc^Fkbp5-/-* knockout

animals (Fkbp5^Rescue, n = 10). *Pomc^Fkbp5-/-* mice injected with an eGFP control virus served as the knockout control group (Control^KO, n = 10) and *Fkbp5^lox/lox* injected with the same control construct that belonged to the Control^lox/lox (n = 19) group (Fig. 2F). A one-way ANOVA of ACTH values post CRH revealed significant differences between all three groups ($F_{2,29}$ = 14.21, *p* < 0.0001). *Bonferroni* post-hoc analysis revealed significantly blunted ACTH levels in the viral knockout and rescue group compared to controls (Control^KO: *p* = 0.002, Fkbp5^Rescue: *p* = 0.0002). ACTH levels after DEX were reduced in rescue animals

compared to controls ($F_{2,15} = 3.2$, $p = 0.07$; *Bonferroni* post-hoc: $p = 0.047$). CORT measures after CRH failed to reach significance when comparing all three groups in the ANOVA but showed the expected trend towards lower CORT levels in Control^{KO} and Fkbp5^{Rescue} compared to controls ($F_{2,31} = 1.78$, $p = 0.18$). CORT after DEX was not different between groups, confirming DEX/CRH findings from the previous cohort ($F_{2,32} = 0.85$, $p = 0.44$) (Fig. 2G). This rescue experiment demonstrates that reinstatement of *Fkbp5* expression within the ARC fails to restore control ACTH and CORT levels in the DEX/CRH, indicating an exclusive role of the pituitary in generating endocrine phenotypes observed in the previous experiment.

To further deepen our understanding of a potential behavioral effect of the *Fkbp5* inactivation in POMC cells, we assessed stress related behavioral parameters in the second cohort of young *Pomc*$^{Fkbp5-/-}$ (n = 8) and controls (n = 12) in an OF, EPM, and DALI (Supplementary Fig. 2). In the OF, young *Pomc*$^{Fkbp5-/-}$ animals entered the inner zone significantly more often than controls ($t_{18} = 2.11$, $p = 0.049$), spent less time immobile ($t_{18} = 2.42$, $p = 0.03$), covered a higher total distance ($t_{18} = 3.31$, $p = 0.004$) with significantly greater mean speed ($t_{18} = 3.29$, $p = 0.004$) and more line crossings ($t_{18} = 3.82$, $p = 0.0013$) (Supplementary Fig. 2A). In line with this behavioral phenotype, time immobile ($t_{18} = 2.83$, $p = 0.01$), total distance ($U = 13$, $p = 0.006$), mean speed ($U = 14.5$, $p = 0.007$) and line crossings ($U = 11.5$, $p = 0.003$) were all significantly increased in the EPM. However, entries into the open arm were not different between genotypes in this test ($t_{18} = 0.25$, $p = 0.81$) (Supplementary Fig. 2B). In the DALI, animals with a knockout of *Fkbp5* spent significantly more time in the lit compartment than controls ($t_{18} = 2.29$, $p = 0.04$). Further, this group covered a greater total distance

within the lit zone ($t_{18} = 2.3$, $p = 0.04$) and spent more time mobile ($t_{18} = 2.02$, $p = 0.06$). However, in contrast to the OF and EPM, the mean speed was not significantly increased in *Pomc*$^{Fkbp5-/-}$ ($U = 38$, $p = 0.46$) (Supplementary Fig. 2C). While this test battery in young animals did not yield a clear behavioral phenotype, well-established anxiety measures in the DALI (lit zone time) and OF (inner zone entries) alluded to the idea that the inactivation of *Fkbp5* drives a mild anxiolytic phenotype in young *Pomc*$^{Fkbp5-/-}$. However, these results need to be interpreted with caution due to the robust hyperlocomotion observed in the *Pomc*$^{Fkbp5-/-}$ mice, which can also have a direct effect on these measures independent of an anxiety phenotype.

3.3. Loss of FKBP51 in POMC cells reverses aging-induced increase in baseline CORT levels

As aging was shown to induce disturbed negative feedback regulation of the HPA axis together with upregulated levels of circulating GCs and increased *Fkbp5* expression in rodents and humans, we hypothesized that age-induced upregulation of FKBP51 could drive a stress-related endocrine and behavioral phenotype in aging *Pomc*$^{Fkbp5-/-}$ mice. In a first cohort of aging (7 – 8 months) *Pomc*$^{Fkbp5-/-}$ (n = 15) and controls (n = 13) bodyweight ($t_{26} = 0.1$, $p = 0.92$) and adrenal weight ($t_{26} = 0.79$, $p = 0.44$) did not differ between genotypes (Fig. 3A). Intriguingly, the lack of FKBP51 affected levels of circadian CORT secretion, indicated by decreased blood CORT levels in the morning ($U = 47$, $p = 0.02$) and in the evening ($t_{24} = 2.18$, $p = 0.04$), which prevented *Pomc*$^{Fkbp5-/-}$ from age-induced increases in CORT observed in controls. Baseline morning ACTH levels measured in the second cohort of aging animals (7
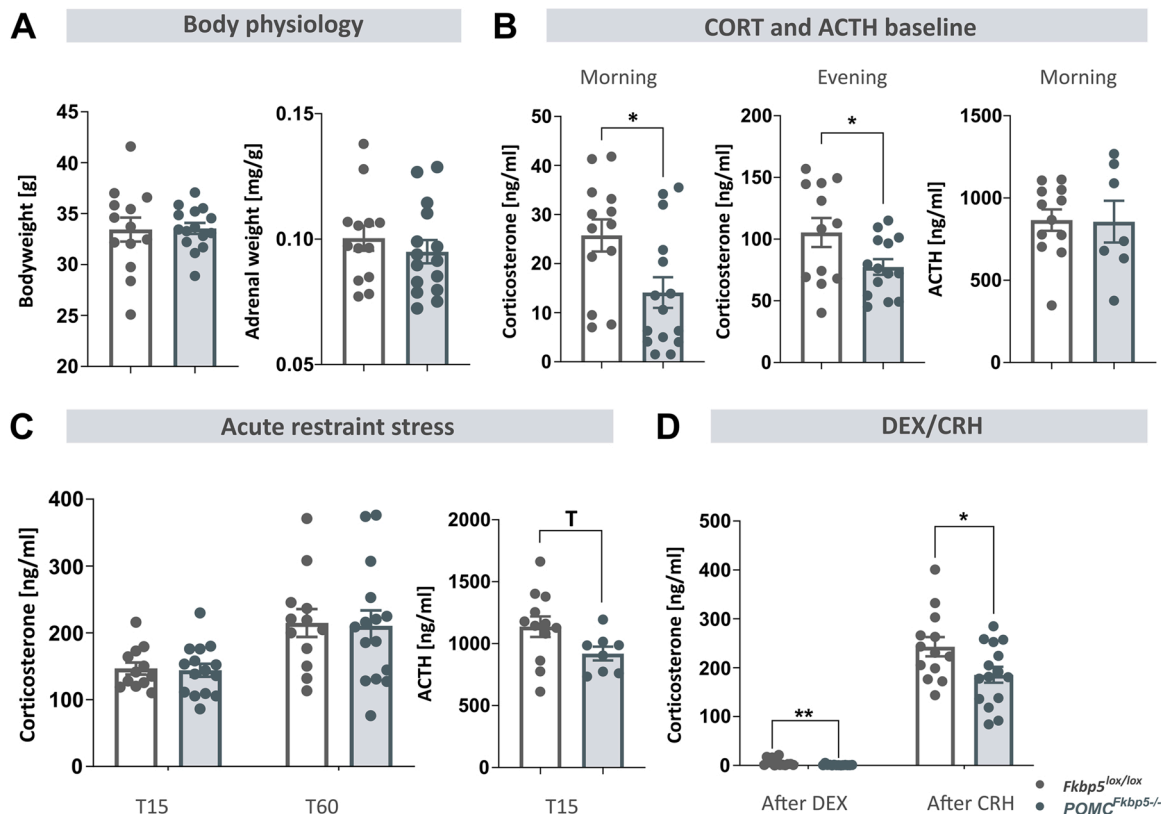
Fig. 3. Knockout of *Fkbp5* in POMC cells of aging animals confirms improved GR-mediated feedback sensitivity of the HPA axis and altered baseline CORT levels. A Bodyweight and relative adrenal weights were unaltered in a first cohort of aging (7 – 8 months) *Pomc*$^{Fkbp5-/-}$ (n = 15) compared to control *Fkbp5*$^{lox/lox}$ (n = 13). B Baseline morning and evening CORT levels were significantly reduced in knockout animals with no differences in morning baseline ACTH levels in the second cohort of *Pomc*$^{Fkbp5-/-}$ (n$_{Fkbp5}$$^{lox/lox}$ = 12; n$_{Pomc}$$^{Fkbp5-/-}$ = 8). C Fifteen and 60 min after an acute restraint stress, *Pomc*$^{Fkbp5-/-}$ mice displayed unaltered CORT. Further, ACTH levels were reduced fifteen minutes post stress in the second aging knockout cohort. D In the DEX/CRH test aging *Pomc*$^{Fkbp5-/-}$ animals displayed a significantly enhanced decrease of CORT after DEX and blunted CRH-mediated CORT overshoot. Data are represented as mean ± SEM. All data were from mice between 7 and 8 months of age. *p < 0.05, * * p < 0.01, T < 0.1.

– 8 months, $n_{PomcFkbp5-/-} = 8$, $n_{Fkbp5lox/lox} = 12$) remained unchanged ($t_{17} = 0.08$, $p = 0.94$), indicative of a counter-regulatory effect (Fig. 3B). The acute stress challenge confirmed reported prolongation of the HPA axis response in aging rodents, which was unaffected by the lack of FKBP51 in POMC cells (T15: $t_{25} = 0.2$, $p = 0.84$; T60: $t_{25} = 0.13$, $p = 0.9$). ACTH measurements taken 15 min post stress in aging animals (2nd cohort) confirmed findings in young animals with a trend towards reduced levels of this stress hormone ($t_{18} = 1.94$, $p = 0.07$) (Fig. 3C). In the DEX/CRH, aging knockout animals display significantly lower CORT values post DEX ($U = 38.5$, $p = 0.009$) and CRH ($t_{26} = 2.28$, $p = 0.03$), further indicating an aggravation of the endocrine phenotype observed in young *Pomc^{Fkbp5-/-}* mice (Fig. 3D). Behavioral data in aging animals confirmed the OF hyperlocomotion phenotype observed in young *Pomc^{Fkbp5-/-}* (OF$_{time immobile}$: $t_{18} = 3.0$, $p = 0.008$; OF$_{total distance}$: $t_{18} = 2.74$, $p = 0.01$; OF$_{mean speed}$: $t_{18} = 2.78$, $p = 0.01$; OF$_{line crossings}$: $t_{18} = 2.63$, $p = 0.02$) (Supplementary Fig. 3A). However, the potential anxiolytic phenotypes identified in the OF and DALI that were seen in the young mice were abolished in aging animals (OF$_{inner zone entries}$: $t_{18} = 1.33$, $p = 0.2$; EPM$_{open arm entries}$: $t_{18} = 0.22$, $p = 0.83$; EPM$_{time immobile}$: $t_{18} = 0.27$, $p = 0.8$; EPM$_{total distance}$: $t_{18} = 0.48$, $p = 0.64$; EPM$_{mean speed}$: $t_{18} = 0.44$, $p = 0.67$; EPM$_{line crossings}$: $t_{18} = 0.27$, $p = 0.8$; DALI$_{lit zone time}$: $U = 47$, $p = 0.97$; DALI$_{time mobile}$: $t_{18} = 1.16$, $p = 0.26$; DALI$_{total distance}$: $t_{18} = 0.94$, $p = 0.36$; DALI$_{mean speed}$: $t_{18} = 0.1$, $p = 0.92$) (Supplementary Fig. 3B, C). These data emphasize the role of FKBP51 in aging-induced HPA axis dysfunction and indicate a beneficial effect of FKBP51 reduction in *Pomc*-expressing cells of the pituitary and neurons within the ARC.

4. Discussion

Over the past few years, the literature on the central role of FKBP51 in stress system biology has grown steadily, vastly improving our understanding of the genetic and molecular basis of physiological and maladaptive processes in the field of stress research. However, most of these studies investigated FKBP51 through systemic rather than region- or cell type-specific manipulation of its gene expression. This study is the first to investigate cell type-specific effects of this co-chaperone in-vivo on stress regulation and sensitivity, as well as the age-related maladaptation of this system. We demonstrate that FKBP51 in POMC cells of the pituitary is the main driver of improved HPA axis negative feedback regulation in the DEX/CRH test and prevents an aging-induced increase in diurnal CORT release, while no other physiological or behavioral alterations besides the ones reported in this study were observed.

Pomc-expressing corticotropes in the anterior pituitary gland (adenohypophysis) are the key cell population of the closed-loop GC-dependent negative feedback regulation of the HPA axis in the periphery. Consequently, they express high levels of GR receptors and GCs were shown to directly inhibit *Pomc* gene expression in pituitary corticotrope cells (Jenkins et al., 2013; Kageyama et al., 2021; Parvin et al., 2017). Further, the POMC protein is a precursor of ACTH and thereby essential in the hormonal signaling cascade initiated by stress (Harno et al., 2018). POMC cells in the ARC of the MBH have emerged as important in the melanocortin circuit controlling homeostatic functions by decreasing food intake and increasing energy dissipation (Quarta et al., 2021).

While FKBP51 is known to be expressed and upregulated by GCs in the pituitary (Jenkins et al., 2013) and in the ARC (Wray et al., 2019), we are the first to demonstrate distinct co-expression of *Pomc* and *Fkbp5* mRNA and to successfully knock out FKBP51 at these sites in-vivo. Assessment of peripheral GR-mediated HPA axis negative feedback regulation and (re)activation in the DEX/CRH test with a low dose of DEX (that does not cross the BBB and acts predominantly at GRs at the level of the pituitary (Karssen et al., 2005)) revealed an attenuated CORT shift after CRH administration in young *Pomc^{Fkbp5-/-}* animals whereas DEX-induced CORT suppression remained unchanged in this cohort. Furthermore, young *Pomc^{Fkbp5-/-}* mice showed improved

recovery-CORT levels 60 min after an acute stress exposure. Reduced morning ACTH level together with unchanged morning and evening CORT in these young *Pomc^{Fkbp5-/-}* animals suggest that there are compensatory mechanisms responsible for this discrepancy, e.g., increased ACTH sensitivity at the level of the adrenal. Taken together, our results in this young cohort of FKBP51 knockout animals suggests improved negative feedback regulation and attenuated HPA axis (re) activity. Since our knockout of *Fkbp5* partially resembles the opposite endocrine phenotype of a *Gr* knockout in pituitary POMC cells (Schmidt et al., 2009), FKBP51 in this specific pituitary cell type directly affects negative feedback sensitivity at the GR, thus controlling HPA axis (re) activity in-vivo (Denny et al., 2000; Wochnik et al., 2005). A recent in-vitro study by Kageyama et al. on DEX treated mouse corticotrope POMC cells revealed counterregulatory roles of FKBP51 and DEX in mediating *Pomc* and *Gr* mRNA expression (Kageyama et al., 2021). They could show that DEX suppressed *Pomc*, Gr and *Fkbp4* gene expression (encoding for the FKBP52 protein) while increasing *Fkbp5* mRNA (Jenkins et al., 2013). Interestingly, a knockdown of *Fkbp4* counteracted DEX-mediated *Pomc* mRNA downregulation while *Fkbp5* knockdown further decreased *Pomc* mRNA expression. Therefore, they concluded that FKBP52 directly contributes to the negative feedback of GCs while FKBP51 itself reduces the efficiency of GCs on POMC downregulation (Kageyama et al., 2021), an effect of FKBP51 on *Pomc* mRNA expression that we could confirm in-vivo. This proposed mechanism could further explain why we do not observe differences in negative feedback regulation post DEX in the young cohort but a dampened (re)activation of the HPA axis after CRH in our *Fkbp5* knockout animals.

There is a growing body of research investigating a potential role of the ARC in the regulation of the HPA axis and diurnal CORT cycle, with most studies concluding that neuropeptide-Y (NPY)/agouti-related protein (AgRP) neurons, the second set of players in the melanocortin pathway, are involved in this process (Fang et al., 2021; Leon-Mercado et al., 2017; Shimizu et al., 2008; Xin-Yun et al., 2002). However, there is increasing evidence that also POMC ARC neurons respond to stress and that they are involved in stress-related behaviors and endocrine changes, particularly via melanocyte-stimulating hormone alpha (α-MSH; POMC cleavage product) and the melanocortin pathway (Liu et al., 2007; Qu et al., 2020). As we cannot rule out an impact of FKBP51 in POMC neurons of the ARC without an appropriate control experiment to attribute observed changes in HPA axis (re)activity to a disruption of *Fkbp5* in the pituitary alone, we reinstated *Fkbp5* expression exclusively in the ARC by *Cre*-specific viral *Fkbp5* rescue in *Pomc^{Fkbp5-/-}*. Supporting our hypothesis of a pituitary-driven DEX/CRH phenotype, Fkbp5^{Rescue} animals resembled dampened HPA axis (re)activation (CORT and ACTH post-CRH), which was observed in Control^{KO} and the *Pomc^{Fkbp5-/-}* line. Further, the absence of alterations in circadian CORT levels in young knockout animals are in line with a pituitary-driven HPA axis phenotype as these functions are predominantly steered centrally by the PVN (acute stress response) (Häusl et al., 2021) and the suprachiasmatic nucleus (SCN) (circadian rhythm) (Kalsbeek et al., 2012). However, the precise contribution of specifically the PVN in relation to the pituitary for negative feedback control of the HPA axis still warrants further studies, potentially also by using inducible knockouts that avoid developmental compensations. Taken together, this study is the first to confirm a GR-mediated role of FKBP51 on *Pomc* mRNA expression in cells of the anterior pituitary in-vivo, dampening HPA axis (re)activity and improving negative feedback sensitivity after a challenge in young male mice.

As negative feedback suppression by GR agonists is known to be less effective in old age (Veldhuis, 2013), to alter circadian GC hormone rhythms (Van Cauter et al., 1996) and to increase the expression of *Fkbp5* (O'Leary et al., 2011; Sabbagh et al., 2014; Zannas et al., 2019), we hypothesized that age-related HPA axis dysfunction is positively influenced by inactivation of *Fkbp5* in POMC cells of the pituitary gland. Indeed, under basal conditions during the circadian trough, we observed significantly lower baseline morning and evening CORT levels in aging

knockout animals, suggesting that $Pomc^{Fkbp5-/-}$ are protected from the known age-related increase in diurnal CORT levels (Sapolsky, 1992; Sapolsky et al., 1986; Van Cauter et al., 1996). Further, older knockout animals show an enhanced improvement of their endocrine phenotype in the DEX/CRH assay with lower CORT levels not only after CRH as in young mice, but already after DEX. Interestingly, a study by Givalois et al. has shown that *Pomc* mRNA expression in corticotrope cells of the adenohypophysis decreased significantly with age, leading to a decline in HPA axis activity (Givalois and Pelletier, 1999). This age-related decrease of POMC, in conjunction with an increase of FKBP51 in the elderly, could amplify the negative effects of FKBP51 on the GC-mediated downregulation of *Pomc* mRNA expression in the pituitary that we and Kageyama et al. have observed (Kageyama et al., 2021). The potentiation of negative FKBP51 action on *Pomc* mRNA expression in aging animals could explain why we only observe the beneficial effects of a *Fkbp5* knockout on diurnal CORT rhythm (and after DEX) in older $Pomc^{Fkbp5-/-}$. Furthermore, aging animals were hyporesponsive to the acute stress 15 min post stress (Buechel et al., 2014) and showed a delayed but prolonged elevation of CORT levels (Sapolsky et al., 1983, 1986). However, there was no difference between aging knockout and control animals in the recovery phase as seen in young animals. This could be explained by observed shift in the stress response in the older animals, which may have caused us to miss the right time to capture potential differences. In addition to the novel role of FKBP51 on *Pomc* mRNA expression in pituitary corticotropes, this study is the first to describe cell type-specific effects of this gene on age-related HPA axis dysfunction.

In the behavioral test battery, young $Pomc^{Fkbp5-/-}$ animals displayed a potential anxiolytic phenotype in standard behavioral stress tests comparable to that of the full *Fkbp5* knockout line (Hartmann et al., 2012; Touma et al., 2011), which is most likely a secondary effect of their endocrine phenotype. Aging $Pomc^{Fkbp5-/-}$ showed less pronounced anxiolytic effects in stressful test situations than young knockout mice, which is in line with their hyporesponsive phenotype in the acute stress response.

Considering that the disruption of *Fkbp5* in the pituitary partially resembles not only the HPA axis (re)activity of mice with complete *Fkbp5* knockout (Hartmann et al., 2012; Touma et al., 2011), but also a PVN-specific knockout of *Fkbp5* (Häusl et al., 2021) and that it fails to fully induce the aging phenotype of full *Fkbp5* knockout described by O'Leary et al. (O'Leary et al., 2011), this study emphasizes the complexity of tissue- and cell type-specific, but also cross-tissue effects of FKBP51 in the stress response.

This study also comes with some limitations: Importantly, only male animals were used and the conclusions should therefore only be drawn with respect to male HPA axis regulation. Further, the rescue experiment targets the ARC only, therefore we cannot fully rule out a contribution of the NTS to observed endocrine phenotypes, as this small neuronal subpopulation innervates other stress-responsive brain regions, such as the locus coeruleus (Reyes et al., 2006). However, the NTS is protected by the BBB just like the ARC (Wang et al., 2008), and therefore we are convinced that improved HPA axis (re)activation in the DEX/CRH test in aging and young $Pomc^{Fkbp5-/-}$ animals is exclusively driven by POMC cells in the pituitary. Finally, it is important to clarify that eight-month-old mice are not aged in the sense of senescence, but are an appropriate model to capture a time window in the aging process that adequately reflects incipient changes in HPA axis function (Sabbagh et al., 2014).

In conclusion, we demonstrate that male mice with a knockout of FKBP51 in corticotrope cells of the anterior pituitary display improved negative feedback and attenuated HPA axis (re)activity. Furthermore, animals lacking FKBP51 in POMC cells in the adenohypophysis are protected from age-induced disturbances in diurnal CORT rhythm, emphasizing a key role of this stress-related protein in the aging process. Remarkably, these beneficial effects are mediated via pituitary FKBP51 in the periphery, further enhancing our understanding of potential

target tissues for pharmacological intervention in stress- and age-related disorders.

Author contributions

L.M.B, A.S.H and M.V.S.: Conceived the project and designed the experiments. **J.M.D.:** Provided scientific expertise for establishing the $Pomc^{Fkbp5-/-}$ mouse line. **L.M.B.** managed the mouse lines. **L.M.B and I. T.** designed and performed RNAscope experiments and manual counting of cells. **L.M.B** performed experiments, surgeries and analysis of data. **I. T., J.B., L.v.D., C.E., S.N., M.S. and V.S.** assisted with the experiments. **L.M.B.:** Wrote the initial version of the manuscript. **M.V.S.:** Supervised the research and all authors revised the manuscript.

Declaration of Competing Interest

None.

Acknowledgments

Appendix A. Supporting information

Supplementary data associated with this article can be found in the online version at doi:10.1016/j.psyneuen.2022.105670.
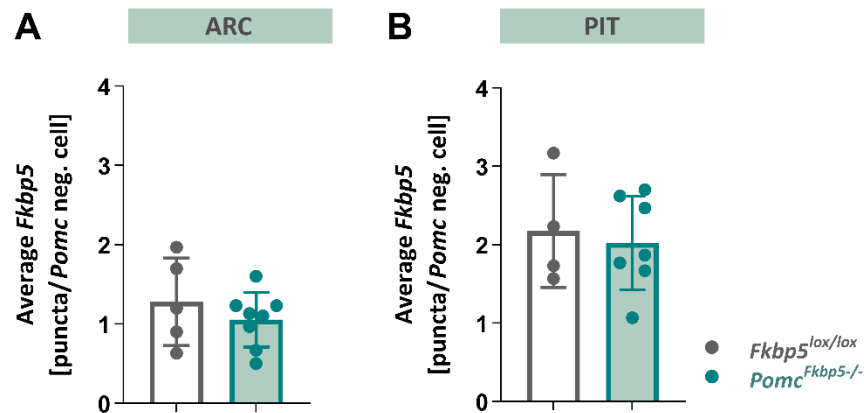
References

Balthasar, N., Coppari, R., McMinn, J., Liu, S.M., Lee, C.E., Tang, V., Kenny, C.D., McGovern, R.A., Chua, S.C., Elmquist, J.K., Lowell, B.B., 2004. Leptin receptor signaling in POMC neurons is required for normal body weight homeostasis. Neuron 42, 983–991. https://doi.org/10.1016/j.neuron.2004.06.004.

Belvederi Murri, M., Pariante, C., Mondelli, V., Masotti, M., Atti, A.R., Mellacqua, Z., Antonioli, M., Ghio, L., Menchetti, M., Zanetidou, S., Innamorati, M., Amore, M., 2014. HPA axis and aging in depression: systematic review and meta-analysis. Psychoneuroendocrinology 41, 46–62. https://doi.org/10.1016/j.psyneuen.2013.12.004.

Binder, E.B., 2009. The role of FKBP5, a co-chaperone of the glucocorticoid receptor in the pathogenesis and therapy of affective and anxiety disorders. Psychoneuroendocrinology 34, 186–195. https://doi.org/10.1016/j.psyneuen.2009.05.021.

Binder, E.B., Salyakina, D., Lichtner, P., Wochnik, G.M., Ising, M., Pütz, B., Papiol, S., Seaman, S., Lucae, S., Kohli, M.A., Nickel, T., Künzel, H.E., Fuchs, B., Majer, M., Pfennig, A., Kern, N., Brunner, J., Modell, S., Baghai, T., Deiml, T., Zill, P., Bondy, B., Rupprecht, R., Messer, T., Köhnlein, O., Dabitz, H., Brückl, T., Müller, N., Pfister, H., Lieb, R., Mueller, J.C., Löhmussaar, E., Strom, T.M., Bettecken, T., Meitinger, T., Uhr, M., Rein, T., Holsboer, F., Muller-Myhsok, B., 2004. Polymorphisms in FKBP5 are associated with increased recurrence of depressive episodes and rapid response to antidepressant treatment. Nat. Genet. 36, 1319–1325. https://doi.org/10.1038/ng1479.

Binder, E.B., Bradley, R.G., Liu, W., Epstein, M.P., Deveau, T.C., Mercer, K.B., Tang, Y., Gillespie, C.F., Heim, C.M., Nemeroff, C.B., Schwartz, A.C., Cubells, J.F., Ressler, K. J., 2008. Association of FKBP5 polymorphisms and childhood abuse with risk of posttraumatic stress disorder symptoms in adults. JAMA - J. Am. Med. Assoc. 299, 1291–1305. https://doi.org/10.1001/jama.299.11.1291.

Buechel, H.M., Popovic, J., Staggs, K.H., Anderson, K.L., Thibault, O., Blalock, E., 2014. Aged rats are hypo-responsive to acute restraint: implications for psychosocial stress in aging. Front. Aging Neurosci. 6, 13. https://doi.org/10.3389/FNAGI.2014.00013.

De Kloet, E.R., Joëls, M., Holsboer, F., 2005. Stress and the brain: from adaptation to disease. Nat. Rev. Neurosci. 6, 463–475. https://doi.org/10.1038/nrn1683.

Denny, W.B., Valentine, D.L., Reynolds, P.D., Smith, D.F., Scammell, J.G., 2000. Squirrel monkey immunophilin FKBP51 is a potent inhibitor of glucocorticoid receptor

binding. Endocrinology 141, 4107–4113. https://doi.org/10.1210/endo.141.11.7785.

Fang, X., Jiang, S., Wang, J., Bai, Y., Kim, C.S., Blake, D., Weintraub, N.L., Lei, Y., Lu, X. Y., 2021. Chronic unpredictable stress induces depression-related behaviors by suppressing AgRP neuron activity. Mol. Psychiatry 26, 2299–2315. https://doi.org/10.1038/s41380-020-01004-x.

Givalois, Li, Pelletier, 1999. Effects of ageing and dehydroepiandrosterone administration on pro-opiomelanocortin mRNA expression in the anterior and intermediate lobes of the rat pituitary. J. Neuroendocrinol. 11, 737–742. https://doi.org/10.1046/J.1365-2826.1999.00392.X.

Goncharova, N.D., Chigarova, O., Rudenko, N., Oganyan, T., 2019. Glucocorticoid negative feedback in regulation of the hypothalamic-pituitary-adrenal axis in rhesus monkeys with various types of adaptive behavior: individual and age-related differences. Front. Endocrinol. (Lausanne) 10, 24. https://doi.org/10.3389/fendo.2019.00024.

Gupta, D., Morley, J.E., 2014. Hypothalamic-Pituitary-Adrenal (HPA) Axis and Aging. In: Comprehensive Physiology. John Wiley & Sons, Inc, Hoboken, NJ, USA, pp. 1495–1510. https://doi.org/10.1002/cphy.c130049.

Harno, E., Ramamoorthy, T.G., Coll, A.P., White, A., 2018. POMC: the physiological power of hormone processing. Physiol. Rev. 98, 2381–2430. https://doi.org/10.1152/PHYSREV.00024.2017.

Hartmann, J., Wagner, K., Liebl, C., Scharf, S., Wang, X., Wolf, M., Hausch, F., Rein, T., Schmidt, U., Touma, C., Cheung-Flynn, J., Cox, M., Smith, D., Holsboer, F., Müller, M., Schmidt, M., 2012. The involvement of FK506-binding protein 51 (FKBP5) in the behavioral and neuroendocrine effects of chronic social defeat stress. Neuropharmacology 62, 332–339. https://doi.org/10.1016/J.NEUROPHARM.2011.07.041.

Häusl, A.S., Brix, L.M., Hartmann, J., Pöhlmann, M.L., Lopez, J.-P., Menegaz, D., Brivio, E., Engelhardt, C., Roeh, S., Bajaj, T., Rudolph, L., Stoffel, R., Hafner, K., Goss, H.M., Reul, J.M.H.M., Deussing, J.M., Eder, M., Ressler, K.J., Gassen, N.C., Chen, A., Schmidt, M.V., 2021. The co-chaperone Fkbp5 shapes the acute stress response in the paraventricular nucleus of the hypothalamus of male mice. Mol. Psychiatry 2021, 1–17. https://doi.org/10.1038/s41380-021-01044-x.

Ising, M., Künzel, H.E., Binder, E.B., Nickel, T., Modell, S., Holsboer, F., 2005. The combined dexamethasone/CRH test as a potential surrogate marker in depression. Prog. Neuropsychopharmacol. Biol. Psychiatry 29, 1085–1093. https://doi.org/10.1016/j.pnpbp.2005.03.014.

James, S.L., Abate, D., Abate, K.H., Abay, S.M., Abbafati, C., Abbasi, N., et al., 2018. Global, regional, and national incidence, prevalence, and years lived with disability for 354 Diseases and Injuries for 195 countries and territories, 1990-2017: a systematic analysis for the Global Burden of Disease Study 2017. Lancet 392, 1789–1858. https://doi.org/10.1016/S0140-6736(18)32279-7.

Jenkins, S.A., Ellestad, L.E., Mukherjee, M., Narayana, J., Cogburn, L.A., Porter, T.E., 2013. Glucocorticoid-induced changes in gene expression in embryonic anterior pituitary cells. Physiol. Genom. 45, 422–433. https://doi.org/10.1152/physiolgenomics.00154.2012.

Kageyama, K., Iwasaki, Y., Watanuki, Y., Niioka, K., Daimon, M., 2021. Differential effects of fkbp4 and fkbp5 on regulation of the proopiomelanocortin gene in murine AtT-20 corticotroph cells. Int. J. Mol. Sci. 22, 5724. https://doi.org/10.3390/IJMS22115724.

Kalsbeek, A., van der Spek, R., Lei, J., Endert, E., Buijs, R.M., Fliers, E., 2012. Circadian rhythms in the hypothalamo–pituitary–adrenal (HPA) axis. Mol. Cell. Endocrinol. 349, 20–29. https://doi.org/10.1016/J.MCE.2011.06.042.

Karssen, A.M., Meijer, O.C., Berry, A., Sanjuan Piñol, R., de Kloet, E.R., 2005. Low doses of dexamethasone can produce a hypocorticosteroid state in the brain. Endocrinology 146, 5587–5595. https://doi.org/10.1210/en.2005-0501.

Leon-Mercado, L., Chao, D.H.M., Basualdo, M., del, C., Kawata, M., Escobar, C., Buijs, R. M., 2017. The arcuate nucleus: a site of fast negative feedback for corticosterone secretion in male rats. eNeuro 4, 350–366. https://doi.org/10.1523/ENEURO.0350-16.2017.

Liu, J., Garza, J.C., Truong, H.V., Henschel, J., Zhang, W., Lu, X.Y., 2007. The melanocortinergic pathway is rapidly recruited by emotional stress and contributes to stress-induced anorexia and anxiety-like behavior. Endocrinology 148 (11), 5531–5540. https://doi.org/10.1210/en.2007-0745.

Matosin, N., Halldorsdottir, T., Binder, E.B., 2018. Understanding the molecular mechanisms underpinning gene by environment interactions in psychiatric disorders: the FKBP5 model. Biol. Psychiatry 83, 821–830. https://doi.org/10.1016/j.biopsych.2018.01.021.

Mokhtari, M., Arfken, C., Boutros, N., 2013. The DEX/CRH test for major depression: a potentially useful diagnostic test. Psychiatry Res 208, 131–139. https://doi.org/10.1016/j.psychres.2012.09.032.

O'Leary, J.C., Dharia, S., Blair, L.J., Brady, S., Johnson, A.G., Peters, M., Cheung-Flynn, J., Cox, M.B., Erausquin, G., de, Weeber, E.J., Jinwal, U.K., Dickey, C.A., 2011. A new anti-depressive strategy for the elderly: ablation of FKBP5/FKBP51. PLoS One 6, e24840. https://doi.org/10.1371/JOURNAL.PONE.0024840.

Parvin, R., Saito-Hakoda, A., Shimada, H., Shimizu, K., Noro, E., Iwasaki, Y., Fujiwara, K., Yokoyama, A., Sugawara, A., 2017. Role of NeuroD1 on the negative regulation of Pomc expression by glucocorticoid. PLoS One 12, e0175435. https://doi.org/10.1371/JOURNAL.PONE.0175435.

Qu, N., He, Y., Wang, C., Xu, P., Yang, Y., Cai, X., Liu, H., Yu, K., Pei, Z., Hyseni, I., Sun, Z., Fukuda, M., Li, Y., Tian, Q., Xu, Y., 2020. A POMC-originated circuit regulates stress-induced hypophagia, depression, and anhedonia. Mol. Psychiatry 25 (5), 1006–1021. https://doi.org/10.1038/s41380-019-0506-1.

Quarta, C., Claret, M., Zeltser, L.M., Williams, K.W., Yeo, G.S.H., Tschöp, M.H., Diano, S., Brüning, J.C., Cota, D., 2021. POMC neuronal heterogeneity in energy balance and

beyond: an integrated view. Nat. Metab. 3, 299–308. https://doi.org/10.1038/s42255-021-00345-3.

Refojo, D., Schweizer, M., Kuehne, C., Ehrenberg, S., Thoeringer, C., Vogl, A.M., Dedic, N., Schumacher, M., Von Wolff, G., Avrabos, C., Touma, C., Engblom, D., Schütz, G., Nave, K.A., Eder, M., Wotjak, C.T., Sillaber, I., Holsboer, F., Wurst, W., Deussing, J.M., 2011. Glutamatergic and dopaminergic neurons mediate anxiogenic and anxiolytic effects of CRHR1. Science 80 (333), 1903–1907. https://doi.org/10.1126/SCIENCE.1202107.

Reyes, B.A.S., Glaser, J.D., Magtoto, R., Van Bockstaele, E.J., 2006. Pro-opiomelanocortin colocalizes with corticotropin- releasing factor in axon terminals of the noradrenergic nucleus locus coeruleus. Eur. J. Neurosci. 23 (8), 2067–2077. https://doi.org/10.1111/j.1460-9568.2006.04744.x.

Rodríguez, C., Buchholz, F., Galloway, J., Sequerra, R., Kasper, J., Ayala, R., Stewart, A., Dymecki, S., 2000. High-efficiency deleter mice show that FLPe is an alternative to Cre- loxP. Nat. Genet 25, 139–140. https://doi.org/10.1038/75973.

Sabbagh, J.J., O'Leary, J.C., Blair, L.J., Klengel, T., Nordhues, B.A., Fontaine, S.N., Binder, E.B., Dickey, C.A., 2014. Age-associated epigenetic upregulation of the FKBP5 gene selectively impairs stress resiliency. PLoS One 9, 107241. https://doi.org/10.1371/journal.pone.0107241.

Sapolsky, R.M., 1992. Do glucocorticoid concentrations rise with age in the rat? Neurobiol. Aging 13, 171–174. https://doi.org/10.1016/0197-4580(92)90025-S.

Sapolsky, R.M., Krey, L.C., McEwen, B.S., 1983. The adrenocortical stress-response in the aged male rat: impairment of recovery from stress. Exp. Gerontol. 18, 55–64. https://doi.org/10.1016/0531-5565(83)90051-7.

Sapolsky, R.M., Krey, L.C., McEwen, B.S., 1986. The neuroendocrinology of stress and aging: the glucocorticoid cascade hypothesis*. Endocr. Rev. 7, 284–301. https://doi.org/10.1210/edrv-7-3-284.

Scharf, S.H., Liebl, C., Binder, E.B., Schmidt, M.V., Müller, M.B., 2011. Expression and regulation of the Fkbp5 gene in the adult mouse brain. PLoS One 6. https://doi.org/10.1371/journal.pone.0016883.

Schmidt, M.V., Levine, S., Oitzl, M.S., Van Der Mark, M., Müller, M.B., Holsboer, F., De Kloet, E.R., 2005. Glucocorticoid receptor blockade disinhibits pituitary-adrenal activity during the stress hyporesponsive period of the mouse. Endocrinology 146, 1458–1464. https://doi.org/10.1210/en.2004-1042.

Schmidt, M.V., Sterlemann, V., Ganea, K., Liebl, C., Alam, S., Harbich, D., Greetfeld, M., Uhr, M., Holsboer, F., Müller, M.B., 2007. Persistent neuroendocrine and behavioral effects of a novel, etiologically relevant mouse paradigm for chronic social stress during adolescence. Psychoneuroendocrinology 32, 417–429. https://doi.org/10.1016/j.psyneuen.2007.02.011.

Schmidt, M.V., Sterlemann, V., Wagner, K., Niederleitner, B., Ganea, K., Liebl, C., Deussing, J.M., Berger, S., Schütz, G., Holsboer, F., Müller, M.B., 2009. Postnatal glucocorticoid excess due to pituitary glucocorticoid receptor deficiency: differential short- and long-term consequences. Endocrinology 150, 2709–2716. https://doi.org/10.1210/en.2008-1211.

Shimizu, H., Arima, H., Watanabe, M., Goto, M., Banno, R., Sato, I., Ozaki, N., Nagasaki, H., Oiso, Y., 2008. Glucocorticoids increase neuropeptide Y and agouti-related peptide gene expression via adenosine monophosphate-activated protein kinase signaling in the arcuate nucleus of rats. Endocrinology 149, 4544–4553. https://doi.org/10.1210/EN.2008-0229.

Sinars, C.R., Cheung-Flynn, J., Rimerman, R.A., Scammell, J.G., Smith, D.F., Clardy, J., 2003. Structure of the large FK506-binding protein FKBP51, an Hsp90-binding protein and a component of steroid receptor complexes. Proc. Natl. Acad. Sci. U. S. A 100, 868–873. https://doi.org/10.1073/pnas.0231020100.

Toda, C., Santoro, A., Kim, J.D., Diano, S., 2017. POMC neurons: from birth to death. Annu. Rev. Physiol. 79, 209–236. https://doi.org/10.1146/annurev-physiol-022516-034110.

Touma, C., Gassen, N.C., Herrmann, L., Cheung-Flynn, J., Bll, D.R., Ionescu, I.A., Heinzmann, J.M., Knapman, A., Siebertz, A., Depping, A.M., Hartmann, J., Hausch, F., Schmidt, M.V., Holsboer, F., Ising, M., Cox, M.B., Schmidt, U., Rein, T., 2011. FK506 binding protein 5 shapes stress responsiveness: modulation of neuroendocrine reactivity and coping behavior. Biol. Psychiatry 70, 928–936. https://doi.org/10.1016/j.biopsych.2011.07.023.

Uher, R., 2008. The implications of gene-environment interactions in depression: will cause inform cure? Mol. Psychiatry 13, 1070–1078. https://doi.org/10.1038/mp.2008.92.

Van Cauter, E., Leproult, R., Kupfer, D.J., 1996. Effects of gender and age on the levels and circadian rhythmicity of plasma cortisol. J. Clin. Endocrinol. Metab. 81, 2468–2473. https://doi.org/10.1210/JCEM.81.7.8675562.

Veldhuis, J.D., 2013. Changes in pituitary function with aging and implications for patient care. Nat. Rev. Endocrinol. 9, 205. https://doi.org/10.1038/NRENDO.2013.38.

Wagner, K.V., Wang, X.D., Liebl, C., Scharf, S.H., Müller, M.B., Schmidt, M.V., 2011. Pituitary glucocorticoid receptor deletion reduces vulnerability to chronic stress. Psychoneuroendocrinology 36, 579–587. https://doi.org/10.1016/j.psyneuen.2010.09.007.

Wang, Q.P., Guan, J.L., Pan, W., Kastin, A.J., Shioda, S., 2008. A diffusion barrier between the area postrema and nucleus tractus solitarius. Neurochem. Res. 33 (10), 2035–2043. https://doi.org/10.1007/s11064-008-9676-y.

Wochnik, G.M., Rüegg, J., Abel, G.A., Schmidt, U., Holsboer, F., Rein, T., 2005. FK506-binding proteins 51 and 52 differentially regulate dynein interaction and nuclear translocation of the glucocorticoid receptor in mammalian cells. J. Biol. Chem. 280, 4609–4616. https://doi.org/10.1074/jbc.M407498200.

Wray, J.R., Davies, A., Sefton, C., Allen, T.J., Adamson, A., Chapman, P., Lam, B.Y.H., Yeo, G.S.H., Coll, A.P., Harno, E., White, A., 2019. Global transcriptomic analysis of the arcuate nucleus following chronic glucocorticoid treatment. Mol. Metab. 26, 5–17. https://doi.org/10.1016/J.MOLMET.2019.05.008.

Wray, N.R., Ripke, S., Mattheisen, M., Trzaskowski, M., Byrne, E.M., Abdellaoui, A., et al., 2018. Genome-wide association analyses identify 44 risk variants and refine the genetic architecture of major depression. Nat. Genet. 50, 668–681. https://doi.org/10.1038/s41588-018-0090-3.

Xin-Yun, L., Shieh, K., Kabbaj, M., Barsh, G., Akil, H., Watson, S., 2002. Diurnal rhythm of agouti-related protein and its relation to corticosterone and food intake. Endocrinology 143, 3905–3915. https://doi.org/10.1210/EN.2002-220150.

Yiallouris, A., Tsioutis, C., Agapidaki, E., Zafeiri, M., Agouridis, A.P., Ntourakis, D., Johnson, E.O., 2019. Adrenal aging and its implications on stress responsiveness in humans. Front. Endocrinol. (Lausanne). 10, 54. https://doi.org/10.3389/fendo.2019.00054.

Zannas, A.S., Binder, E.B., 2014. Gene-environment interactions at the FKBP5 locus: sensitive periods, mechanisms and pleiotropism. Genes, Brain Behav. 13, 25–37. https://doi.org/10.1111/gbb.12104.

Zannas, A.S., Jia, M., Hafner, K., Baumert, J., Wiechmann, T., Pape, J.C., Arloth, J., Ködel, M., Martinelli, S., Roitman, M., Röh, S., Haehle, A., Emeny, R.T., Iurato, S., Carrillo-Roa, T., Lahti, J., Räikkönen, K., Eriksson, J.G., Drake, A.J., Waldenberger, M., Wahl, S., Kunze, S., Lucae, S., Bradley, B., Gieger, C., Hausch, F., Smith, A.K., Ressler, K.J., Müller-Myhsok, B., Ladwig, K.H., Rein, T., Gassen, N.C., Binder, E.B., 2019. Epigenetic upregulation of FKBP5 by aging and stress contributes to NF-κB-driven inflammation and cardiovascular risk. Proc. Natl. Acad. Sci. U. S. A 166, 11370–11379. https://doi.org/10.1073/pnas.1816847116.

Supplementary Figures

Suppl Figure 1: Quantification of cell-type unspecific off-target effects in *Pomc*^{Fkbp5-/-} and *Fkbp5*^{lox/lox}.

Quantification of the average number of *Fkbp5* mRNA puncta per *Pomc* negative (*Pomc* neg.) and *DAPI* positive cell in RNAScope images of arcuate nucleus (ARC; **A**) and pituitary (PIT; **B**) revealed that there are no off-target effects of the knockout. *Fkbp5* mRNA puncta were counted manually in 30 cells per image and the average number of puncta per cell was calculated. n = number of analyzed 40x confocal images of either left or right ARC or pituitary, ARC: nKO = 8, nControl = 5; pituitary: nKO = 7, nControl = 4). Data are received from mice between 16 to 20 weeks of age and are presented as mean ± SEM.
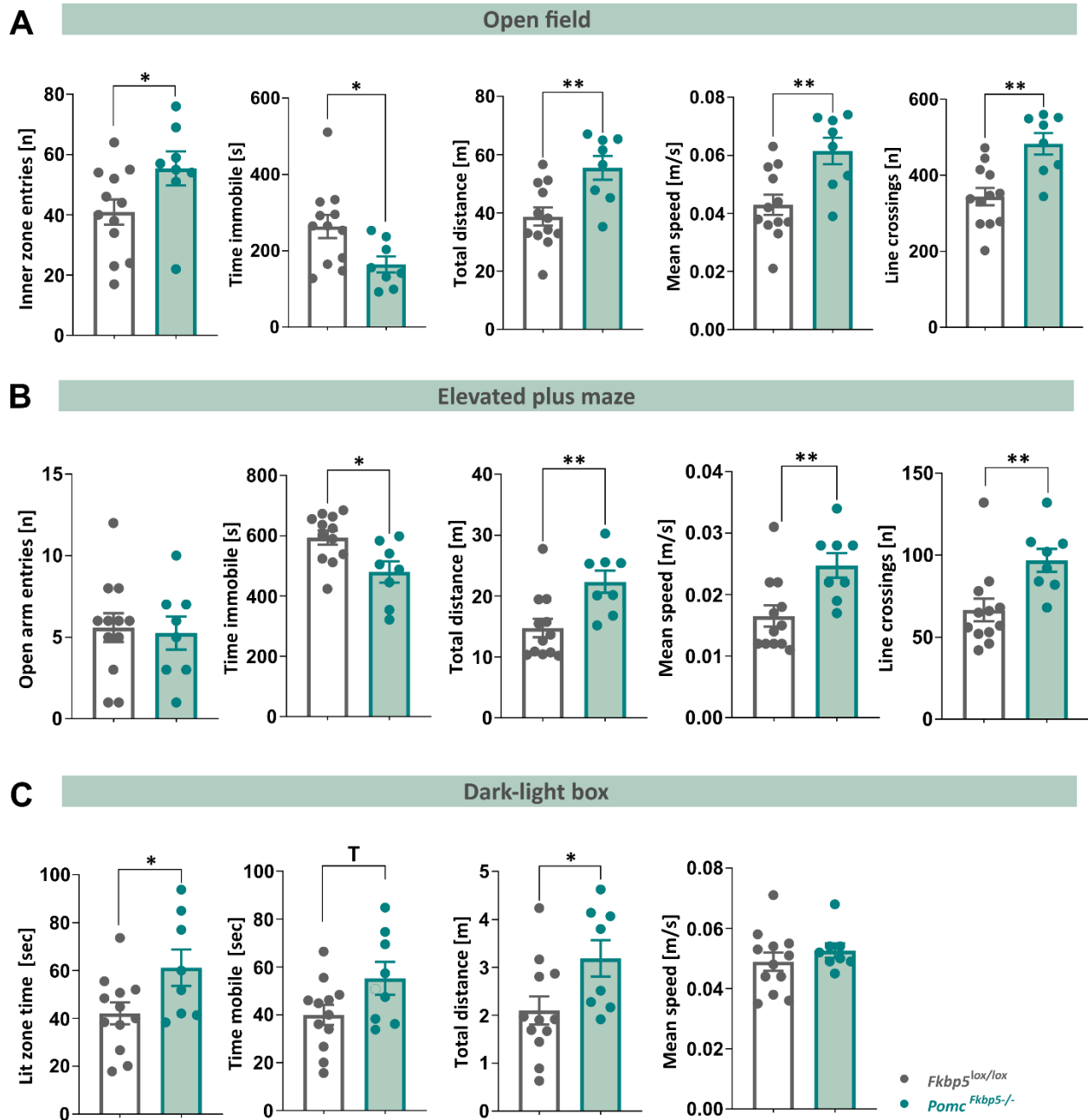
Suppl. Figure 2: Loss of FKBP51 induces a hyperlocomotion and mild anxiolytic phenotype in young $Pomc^{Fkbp5-/-}$.

A In the open field test, young knockdown animals ($n_{PomcFkbp5-/-}$ = 8, $n_{Fkbp5lox/lox}$ = 12) entered the inner zone significantly more often than controls, spent less time immobile, covered a higher total distance with significantly greater mean speed and more line crossings. **B** In the elevated plus maze, time immobile,

total distance, mean speed and line crossings were significantly increased in young $Pomc^{Fkbp5-/-}$, whereas there was no difference in open arm entries between genotypes. **C** Time spent in the lit zone and total distance travelled were significantly increased in $Pomc^{Fkbp5-/-}$ with a significant trend towards higher mobility in the dark-light box. Behavioral data are received from the 2nd cohort of young mice between 3 to 4 months of age and are presented as mean ± SEM. *p < 0.05, **p < 0.01, T < 0.1.
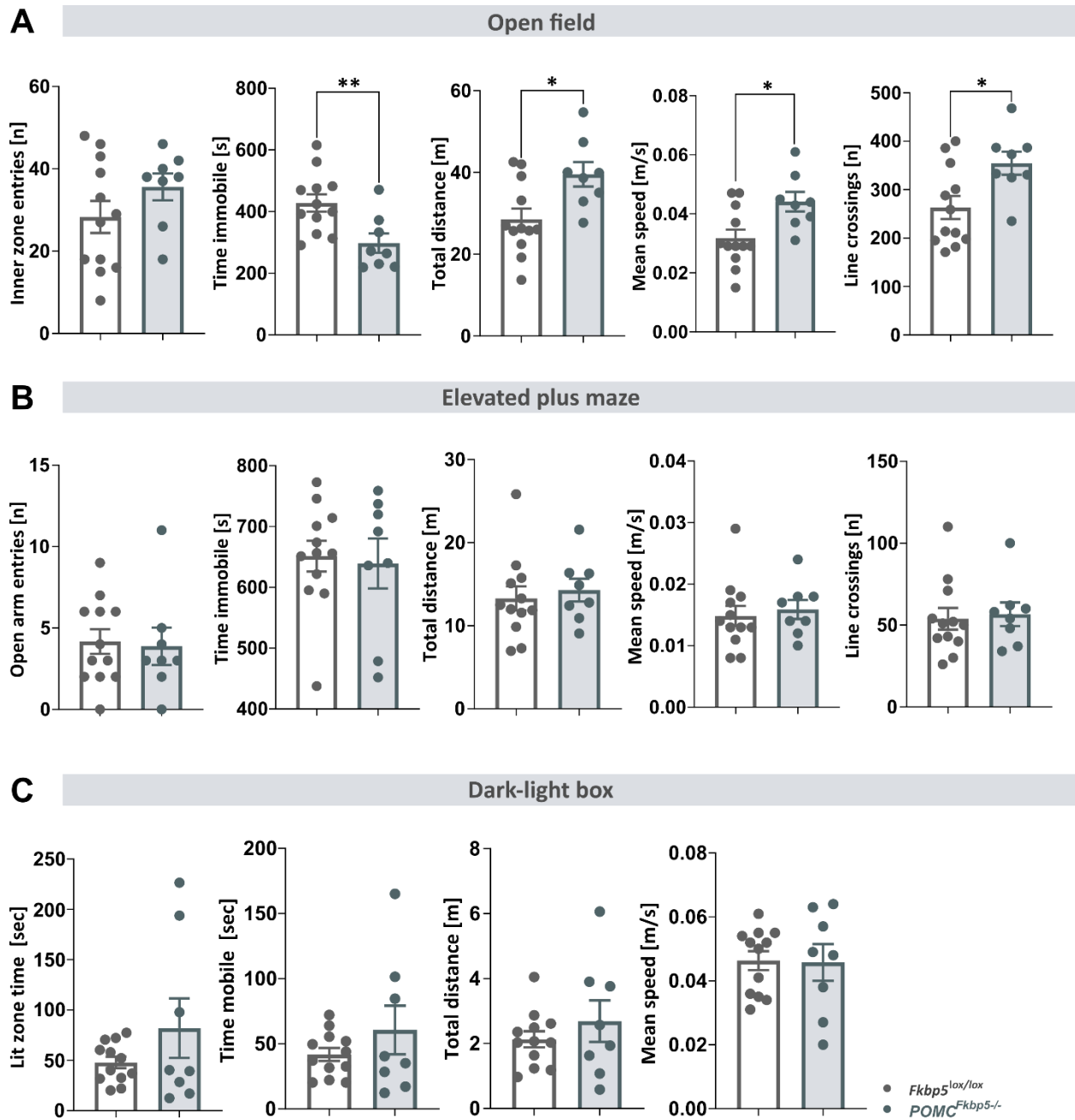
Suppl. Figure 3: Aged *Pomc^Fkbp5-/-* animals confirm hyperlocomotion but do not display mild anxiolytic phenotype of young animals.

A Aged *Pomc^Fkbp5-/-* (n*_PomcFkbp5-/-* = 8, n*_Fkbp5lox/lox* = 12) mirrored the open field hyperlocomotion phenotype observed in young animals with less time immobile, higher total distance, significantly greater mean speed and more line crossings. However, the number of inner zone entries did not differ between genotypes in

aged animals. **B, C** Mild anxiolytic phenotypes in the dark-light box and elevated plus maze observed in young mice were abolished with aging. Data are received from the 2nd cohort of aged mice between 7 to 8 months of age and are presented as mean ± SEM. *p < 0.05, **p < 0.01.

2.3 Mediobasal hypothalamic FKBP51 acts as a molecular switch linking autophagy to whole-body metabolism

Häusl, A.S., Bajaj, T., <u>Brix, L.M.,</u> Pöhlmann, M.L., Hafner, K., De Angelis, M., Nagler, J., Dethloff, F., Balsevich, G., Schramm, K.W., Giavalisco, P., Chen, A., Schmidt, M.V. & Gassen, N.C.

CELL BIOLOGY

Mediobasal hypothalamic FKBP51 acts as a molecular switch linking autophagy to whole-body metabolism

Alexander S. Häusl[1]†, Thomas Bajaj[2]†, Lea M. Brix[1,3], Max L. Pöhlmann[1], Kathrin Hafner[4], Meri De Angelis[5], Joachim Nagler[5], Frederik Dethloff[6], Georgia Balsevich[1], Karl-Werner Schramm[5], Patrick Giavalisco[6], Alon Chen[7,8], Mathias V. Schmidt[1]*‡, Nils C. Gassen[2,4]*‡

The mediobasal hypothalamus (MBH) is the central region in the physiological response to metabolic stress. The FK506-binding protein 51 (FKBP51) is a major modulator of the stress response and has recently emerged as a scaffolder regulating metabolic and autophagy pathways. However, the detailed protein-protein interactions linking FKBP51 to autophagy upon metabolic challenges remain elusive. We performed mass spectrometry–based metabolomics of FKBP51 knockout (KO) cells revealing an increased amino acid and polyamine metabolism. We identified FKBP51 as a central nexus for the recruitment of the LKB1/AMPK complex to WIPI4 and TSC2 to WIPI3, thereby regulating the balance between autophagy and mTOR signaling in response to metabolic challenges. Furthermore, we demonstrated that MBH FKBP51 deletion strongly induces obesity, while its overexpression protects against high-fat diet (HFD)–induced obesity. Our study provides an important novel regulatory function of MBH FKBP51 within the stress-adapted autophagy response to metabolic challenges.

INTRODUCTION

An adequate response to nutritional changes requires a well-coordinated interplay between the central nervous system and multiple peripheral organs and tissues to maintain energy homeostasis. High-caloric food intake and chronic overnutrition strongly challenge this system on a cellular and organismic level and are main drivers in the development of obesity, a hallmark of the metabolic syndrome (1).

Autophagy is an evolutionarily conserved process that efficiently degrades cellular components, like unfolded proteins or organelles, to provide internal nutrients and building blocks for cellular fitness (2). Dysfunctional autophagy is associated with many diseases, such as neurodegeneration, liver disease, cancer, and metabolic syndrome (3–5). In obesity, however, the alterations of autophagy are not fully explored yet. Autophagic signaling in obese individuals is suppressed in pancreatic B cells, liver, and muscle, whereas other studies demonstrated enhanced autophagy signaling in adipose tissue (3, 6, 7). Autophagy initiation is tightly controlled by a series of proteins encoded by autophagy-related genes (ATGs) and regulatory heteroprotein complexes, including the systemic energy sensor adenosine 5′-monophosphate (AMP)–activated protein kinase (AMPK) that is in balance with the mechanistic target of rapamycin (mTOR) (8). Amino acid surplus activates mTOR signaling, which further suppresses autophagy by inhibiting the UNC51-like kinase 1 (ULK1) complex [composed of ULK1, ATG13, FIP200 (FAK family

kinase-interacting protein of 200 kDa), and ATG101]. In the course of nutrient deprivation, elevated AMP activates AMPK to initiate autophagy via the ULK1 complex and in turn diminishes mTOR signaling (9, 10). It has recently been shown that the tryptophan-aspartic acid (WD)–repeat proteins that interact with the phosphoinositide protein family (WIPI proteins) act as subordinate scaffolders of the liver kinase B1 (LKB1)/AMPK/TSC2 (tuberous sclerosis complex 2)/FIP200 network linking AMPK and mTOR signaling to the control of autophagy upon metabolic stress (11).

In the mediobasal hypothalamus (MBH), the brain's central region for metabolic control, the deletion of ATG7 (a ubiquitin E1-like ligase, downstream of the ULK1 complex) in proopiomelanocortin (POMC)–expressing neurons resulted in obesity and dampened sympathetic outflow to white adipose tissue (WAT) (12), while ATG7 deficiency exclusively in agouti-related protein (AgRP)–expressing neurons resulted in decreased body weight (13). Together, these data indicate a role of MBH autophagy in the development of obesity, but key regulatory proteins remain largely elusive.

The FK506-binding protein 51 (FKBP51, encoded by *Fkbp5*) is the main modulator of the stress response and is best characterized as a co-chaperone to HSP90, thereby orchestrating diverse pathways important to maintain homeostatic control (14–17). We and others have provided evidence that FKBP51 is associated with type 2 diabetes and have shed light on its role as a fundamental regulator of obesity and glucose metabolism (18–22). Following the identification of FKBP51 as a negative regulator of the serine/threonine kinase AKT in cancer cells (23), we showed that FKBP51 acts as a modulator of glucose uptake by mediating the AKT2/PHLPP (PH domain leucine-rich repeat-containing protein phosphatase)/AS160 (AKT substrate of 160 kDa) complex specifically in muscle (18). Furthermore, we demonstrated that FKBP51 induces autophagy through autophagy-promoting beclin-1 (BECN1) in two ways: (i) FKBP51 limits AKT-directed inhibitory phosphorylation of BECN1 at S234 and S295 (24, 25), and (ii) it reduces AKT-mediated phosphorylation of S-phase kinase-associated protein 2 (SKP2) at S72 and thereby lowering its E3-ligase activity, preventing BECN1 from proteasomal degradation (26). Autophagy and FKBP51 are involved in the regulatory role of

[1]Research Group Neurobiology of Stress Resilience, Max Planck Institute of Psychiatry, 80804 Munich, Germany. [2]Neurohomeostasis Research Group, Department of Psychiatry and Psychotherapy, Bonn Clinical Center, University of Bonn, 53127 Bonn, Germany. [3]International Max Planck Research School for Translational Psychiatry (IMPRS-TP), Kraepelinstr. 2-10, 80804 Munich, Germany. [4]Department of Translational Research in Psychiatry, Max Planck Institute of Psychiatry, 80804 Munich, Germany. [5]Helmholtz Center Munich Germany Research Center for Environmental Health, Molecular EXposomics, Neuherberg, Germany. [6]Max Planck Institute for Biology of Ageing, 50931 Cologne, Germany. [7]Department of Stress Neurobiology and Neurogenetics, Max Planck Institute of Psychiatry, 80804 Munich, Germany. [8]Department of Neurobiology, Weizmann Institute of Science, Rehovot, Israel.
*Corresponding author. Email: mschmidt@psych.mpg.de (M.V.S.); nils.gassen@ukbonn.de (N.C.G.)
†These authors contributed equally to this work as first authors.
‡These authors contributed equally to this work as senior authors.

adipocyte differentiation and mass development (*19*, *27–29*) and are up-regulated in the MBH following starvation (*13*, *30*, *31*). The data indicate converging mechanisms of FKBP51-directed protein scaffolding and autophagy, and therefore, we hypothesized a subordinate role of FKBP51 in concert with members of the autophagy signaling network in shaping central and peripheral autophagy signaling. In the current study, we set out to identify the molecular interplay of FKBP51 with cellular autophagic signaling and tested whether FKBP51 shapes the in vivo whole-body response to an obesogenic challenge. Our study unravels the tissue specificity of autophagy signaling in response to obesity and reveals FKBP51 as a previously unknown regulatory link between the stress-induced LKB1/AMPK-mediated autophagy induction and WIPI protein scaffolds.

RESULTS

FKBP51 deletion increases AMPK and mTOR-associated amino acid and polyamine biosynthesis

As a first approach to broaden our insights into the contribution of FKBP51 under basal (1× glucose) and metabolically challenging (2× glucose) conditions, we performed a multilevel mass spectrometry (MS)–based metabolomics profiling analysis of human neuroblastoma SH-SY5Y cells lacking FKBP51 [(FKBP51 knockout (KO)] and wild-type (WT) controls. FKBP51 KO cells showed an increase in multiple metabolites compared to WT cells to different extents under basal and high glucose conditions (fig. S1, A to D). Most frequent and pronounced alterations could be attributed to biosynthetic and metabolic pathways of various amino acids, including but not limited to arginine, valine, leucine, and isoleucine biosynthesis and histidine, cysteine, and methionine metabolism (Fig. 1A and fig. S1E). It is well known that amino acids signal to mTOR and that mTOR itself actively participates in the sensing of amino acids in the lysosomal lumen. Particularly, the branched-chain amino acids (BCAAs) leucine, valine, and isoleucine, all elevated in FKBP51 KO cells (Fig. 1B, top right), can activate mTOR and thereby block the autophagy pathway (*32–34*). On the other hand, the pathway analysis showed increased AMP/adenosine 5′-triphosphate (ATP) ratio and strongly increased levels of polyamines and their metabolites in FKBP51 KO cells (Fig. 1B, left and bottom right). AMP/ATP ratio was strongly reduced in FKBP51 KO cells under metabolically challenging conditions (fig. S2E).

The overall increase in amino acids most likely results from ubiquitous protein degradation, in line with enhanced cellular catabolic processes. We performed isotope tracing with ^{13}C-labeled glucose to determine the intracellular flux in FKBP51 KO cells. Here, we observed no substantial differences between both cell types (fig. S1F), corroborating the fact that cellular catabolic processes rather dominate over anabolic processes. To exclude that the observed effects are specific to a human cell line, we performed the metabolomics profiling also in mouse Neuro2a (N2a) cells (fig. S2, A to E). While the effects of amino acid biosynthesis are more pronounced in the human cell line following FKBP51 deletion, the data nonetheless point in the same direction and support our hypothesis that FKBP51 affects autophagy and mTOR signaling. We were therefore further encouraged to disentangle the underlining metabolic pathways.

FKBP51 is essential for homeostatic autophagy following nutrient deprivation

Because autophagy and FKBP51 expression levels are highly induced after starvation (*4*, *31*), we tested whether deletion of FKBP51,

in turn, affects the induction of autophagy after nutrient deprivation. To do so, we exposed FKBP51 KO or WT cells to Hank's balanced salt solution (HBSS) for 4 hours to induce cellular starvation. FKBP51 KO cells showed less phosphorylated AMPK (pAMPK) at T172 and lower levels of LKB1 compared to WT cells already under nutrient-rich conditions (Fig. 2A and fig. S3A), while there was a significant increase in activating phosphorylation of SKP2 at S72 and AKT at S473 (fig. S3, B and C). These changes in upstream signaling resulted in the slight but not significant accumulation of the autophagy receptor and substrate p62 (Fig. 2B), which is an important measure to determine autophagic activity (*35*). On the other hand, we could observe increased levels of pp70S6K at T389 in FKBP51 KO cells (Fig. 2C). These data imply a reduction of autophagy signaling and increased mTOR signaling after FKBP51 deletion under basal conditions (*36*). The deletion of FKBP51 blocked the starvation-induced increase in LKB1 protein and the activation of AMPK at T172 (Fig. 2A and fig. S3A) and thereby reduced the level of autophagy signaling. These data underline the importance of FKBP51 in the autophagic stress response after starvation and suggest a tight regulation of FKBP51 on AMPK and LKB1.

Next, we investigated whether FKBP51 up-regulation can enhance autophagy by moderately overexpressing (OE) Flag-tagged FKBP51 in N2a cells (fig. S3D). In line with our hypothesis, FKBP51 OE resulted in highly increased phosphorylation of AMPK at T172 and enhanced levels of LKB1 (Fig. 2E and fig. S3E), which indicate an increase of upstream autophagy initiation, further evidenced by increased phosphorylation of ULK1 at S555 (fig. S3E). Consequently, there was an increase in proautophagic phosphorylation of BECN1 at S14 and S91/S94 (in humans at S93/S96) through kinases ULK1 and AMPK, respectively (fig. S3E) (*37*). Previous literature has shown that increased LKB1/AMPK signaling also activates the TSC1/TSC2 complex, which, in turn, inhibits mTOR activity (*38*). In line with that, phosphorylation of TSC2 at S1387 was significantly enhanced (fig. S3E), and the phosphorylation of AKT at S473, SKP2 at S72, and the mTOR substrate pp70S6K at T389 was significantly decreased (Fig. 2F and fig. S2F). In addition, we validated autophagy signaling by the increase in phosphorylation of ATG16L1 at S278, a recently described marker for autophagy induction (*39*), and the decrease in the autophagy substrate p62 (Fig. 2G and fig. S2G). Last, we assessed autophagic flux by the quantification of LC3B-II (lipidated microtubule-associated proteins 1A/1B light chain 3B) accumulation in response to starvation (HBSS) and the autophagy inhibitor bafilomycin A1 (BafA1) in FKBP51 OE, KO, and FKBP51 KO + OE N2a cells (Fig. 2, I and J, and fig. S3, H and I). BafA1 led to a significant increase in LC3B-II levels in FKBP51 WT and FKBP51 OE N2a cells, but not in FKBP51 KO and FKBP51 KO + OE N2a cells, as compared to FKBP51 WT N2a cells during baseline conditions. Under starvation conditions (HBSS treatment), BafA1 caused a significant accumulation of LC3B-II in all genotypes; however, this increase was attenuated in FKBP51 KO N2a cells.

The data from our metabolomic analysis indicated that alteration in FKBP51 levels might enhance hypusination of the translation factor eIF5A and thereby positively regulate autophagy via nuclear translocation of transcription factor EB (TFEB) (*40*). To test this hypothesis, we measured the translocation of TFEB into the nucleus using a TFEB–green fluorescent protein (GFP) reporter assay in N2a cells. Here, we observed reduced baseline levels of nuclear TFEB in FKBP51 KO N2a cells and diminished nuclear translocation of TFEB after starvation (HBSS) of FKBP51 KO cells compared
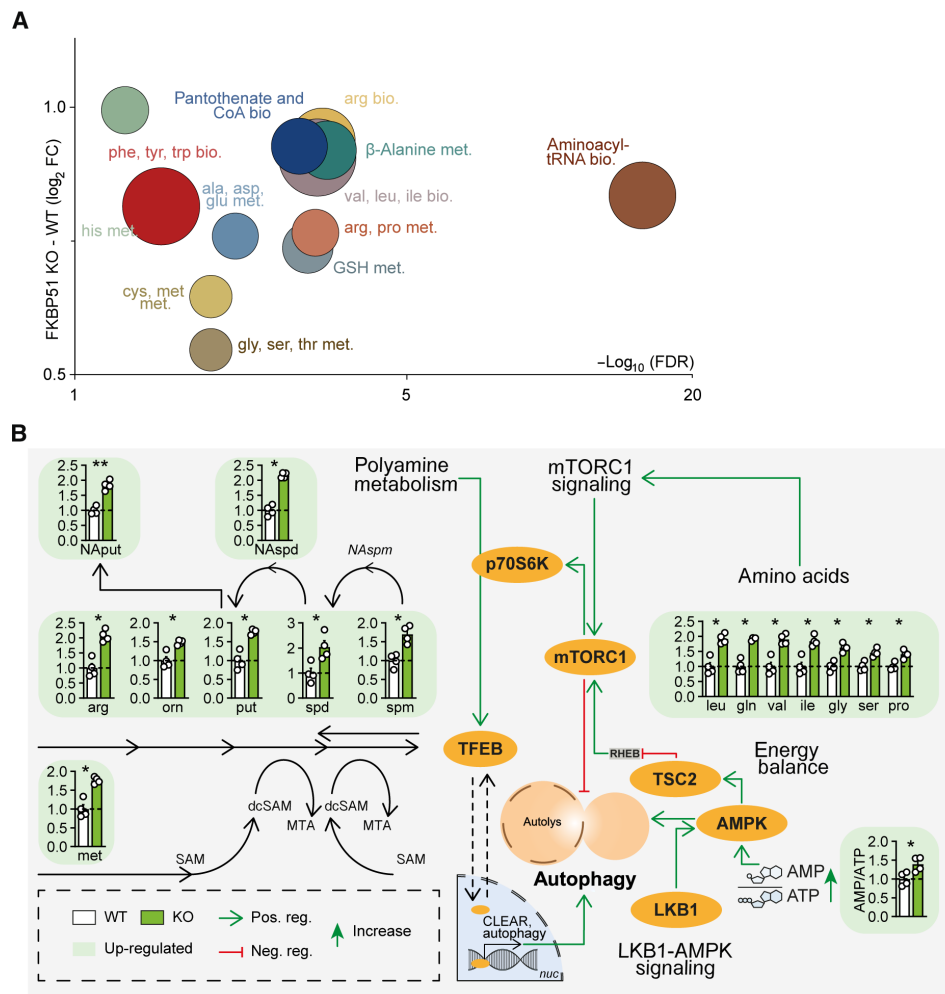
Fig. 1. FKBP51 associates with amino acids and polyamine biosynthesis pathways. (A) Analysis and regulation of significantly altered pathways of FKBP51 KO and WT cells. The $f(x)$ axis shows the (median) $\log_2$ fold change (FC) of all significantly altered metabolites of the indicated pathway, and the false discovery rate (FDR) (equals the $-\log_{10}$–adjusted P value) is shown on the x axis. The size of the circles represents the amount of significantly changed metabolites in comparison to all metabolites of a particular pathway. tRNA, transfer RNA. **(B)** FKBP51 deletion increases metabolites of the polyamine pathway, the AMP/ATP ratio, and enhances levels of amino acids associated with mTOR signaling. Data in (B) are shown as means + SEM and were analyzed by a two-way analysis of variance (ANOVA) and a subsequent Bonferroni multiple comparison analysis. ala, alanine; AMPK, AMP-activated protein kinase; arg, arginine; asp, asparagine; bio., biosynthesis; CoA, coenzyme A; cys, cysteine; dcSAM, decarboxylated *S*-adenosylmethione; gln, glutamine; glu, glutamic acid; gly, glycine; GSH, glutathione (reduced); his, histidine; ile, isoleucine; leu, leucine; LKB1, liver kinase B1; met, methionine; met., metabolism; MTA, 5′-methylthioadenosine; mTORC1, mechanistic target of rapamycin complex 1; NAput, *N*-acetylputrescine; NAspd, *N*-acetylspermidine; NAspm, *N*- acetylspermine; orn, ornithine pro, proline; phe, phenylalanine; put, putrescine; SAM, *S*- adenosylmethionine; ser, serine; spd, spermidine; spm, spermine; TFEB, transcription factor EB; TSC2, tuberous sclerosis complex 2; thr, threonine; trp, tryptophan; tyr, tyrosine; val, valine. *$P < 0.05$, **$P < 0.01$.

to the control (Fig. 2, K and L). OE of FKBP51 in WT cells could further increase nuclear TFEB under basal conditions. The nuclear TFEB signal could not be further increased by OE under starvation compared to the WT control (Fig. 2, K and L). We could not detect any differences in the hypusination of eIF5A (fig. S4, A and B).

Together, these findings demonstrate that FKBP51 regulates autophagy induction, especially after a metabolic challenge. However, it is still unclear whether FKBP51 shapes the autophagic response via direct protein-protein interactions to AMPK and LKB1. Given the fact that FKBP51 was previously shown to interact with several signaling molecules within the autophagy pathway (Fig. 3A), we were encouraged to unravel the underlying molecular mechanism and identify potential novel interactions of FKBP51 with members of the autophagy signaling network.

FKBP51 associates with LKB1/AMPK/WIPI4 and TSC2/WIPI3 heteroprotein complexes to regulate autophagy and mTOR signaling

A recent study by Bakula and colleagues (*11*) investigated the role of the four WIPI proteins on autophagy, and the WIPI protein interactome revealed an association of WIPI4 with FKBP51, AMPKα1, and AMPKγ2 (*11*). WIPI proteins are essential scaffolding proteins that function as central molecular hubs to link key regulatory elements of autophagy with proteins that are sensitive to main metabolic cascades such as amino acid and glucose metabolism (*41*). On the basis of our FKBP51 starvation and OE experiments, we hypothesized that FKBP51 might scaffold WIPI4 and AMPK to induce autophagy initiation and therefore performed co-immunoprecipitation (co-IP) studies using N2a cells, with FKBP51-Flag OE.
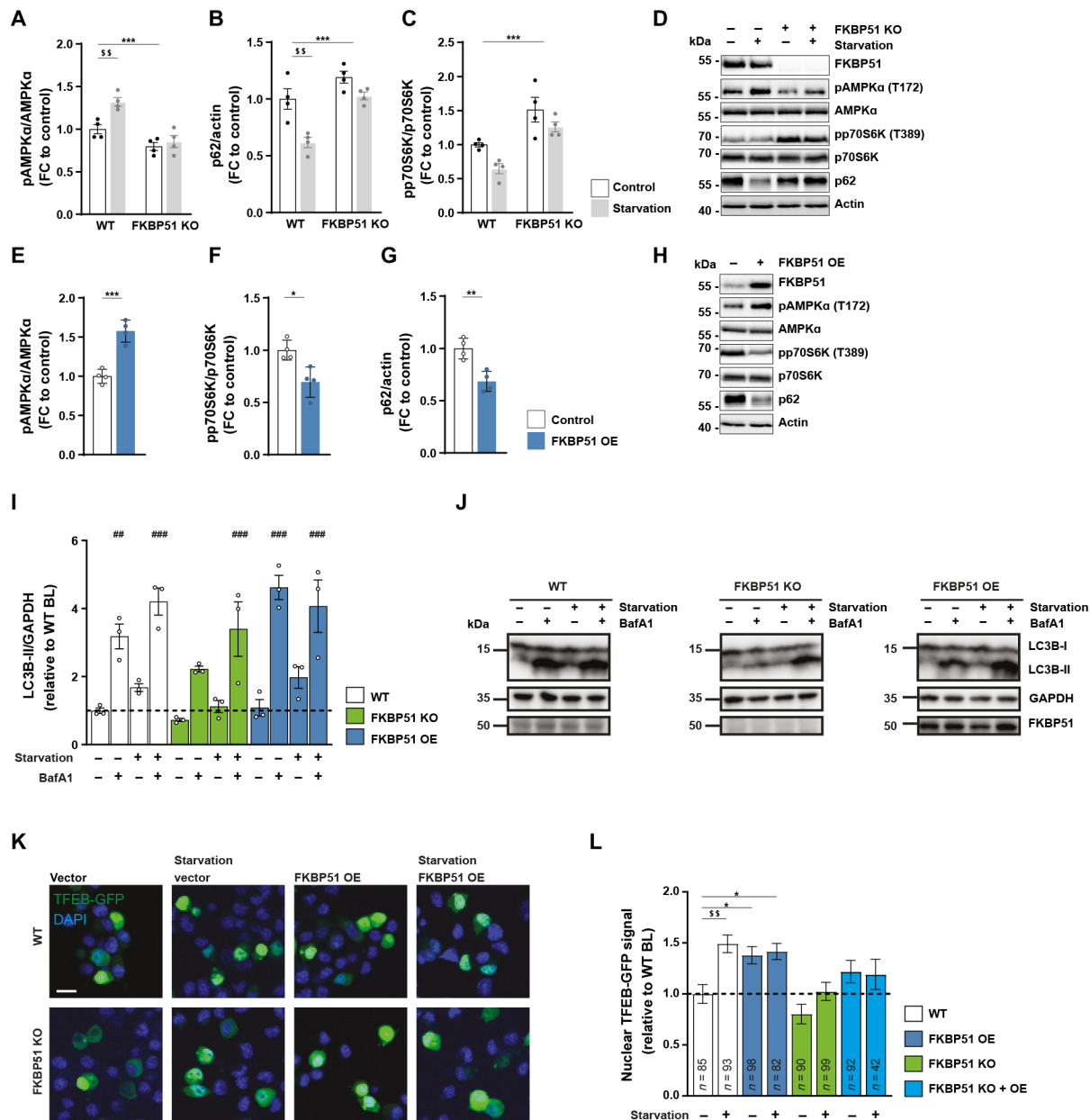
Fig. 2. FKBP51 regulates AMPK and mTOR activity following nutrient deprivation. (**A**) WT or FKBP51 KO cells were starved in HBSS medium for 4 hours to induce autophagy, followed by quantification of pAMPKα (T172), (**B**) p62, and (**C**) pp70S6K (T389). Representative blots are shown in (**D**). FKBP51 overexpression (FKBP51 OE) in N2a cells (see fig. S3D for validation) enhanced autophagy signaling. Quantification of (**E**) pAMPKα (T172), (**F**) pp70S6K (T389), (**G**) p62, and (**H**) representative blots. (**I**) Quantification of autophagic flux in FKBP51 KO and FKBP51 OE cells in response to starvation. GAPDH, glyceraldehyde-3-phosphate dehydrogenase. (**J**) Representative blots of autophagic flux measurements. (**K**) Representative pictures of TFEB nuclear localization/translocation. DAPI, 4′,6-diamidino-2-phenylindole. Scale bar, 10 μm. (**L**) Quantification of TFEB reporter assay. BL, baseline. All data (A to J) are shown as relative fold change compared to control condition; ± SEM; *$P < 0.05$, **$P < 0.01$, ***$P < 0.001$; ##$P < 0.01$, ###$P < 0.001$; $$$P < 0.01$. Two-way ANOVA was performed in (A) to (C) and followed by a Tukey's multiple comparisons test. One-way ANOVA was performed for (I) and (L), followed by a Dunnett's multiple comparison test. The unpaired Student's *t* test was performed for (E) to (G). *, significant genotype effect; $, significant starvation effect; #, significant treatment effect.

These experiments confirmed that FKBP51 associates with WIPI4 but not with WIPI1 and WIPI2 (Fig. 3B), as suggested by Bakula and colleagues (*11*). Intriguingly, our experiments revealed a previously unidentified association of FKBP51 with WIPI3 (Fig. 3B). Next, we assessed the association of FKBP51 with various isoforms of AMPK

and validated the expected interactions of FKBP51 with AMPKα1 and AMPKγ2 and further revealed a interaction with AMPKβ1 (Fig. 3C). We validated the previously unknown interactions of FKBP51 with WIPI3, WIPI4, AMPKα, and LKB1 in mouse WT N2a neuroblastoma cells performing IPs and co-IPs from endogenous proteins (fig. S5A).
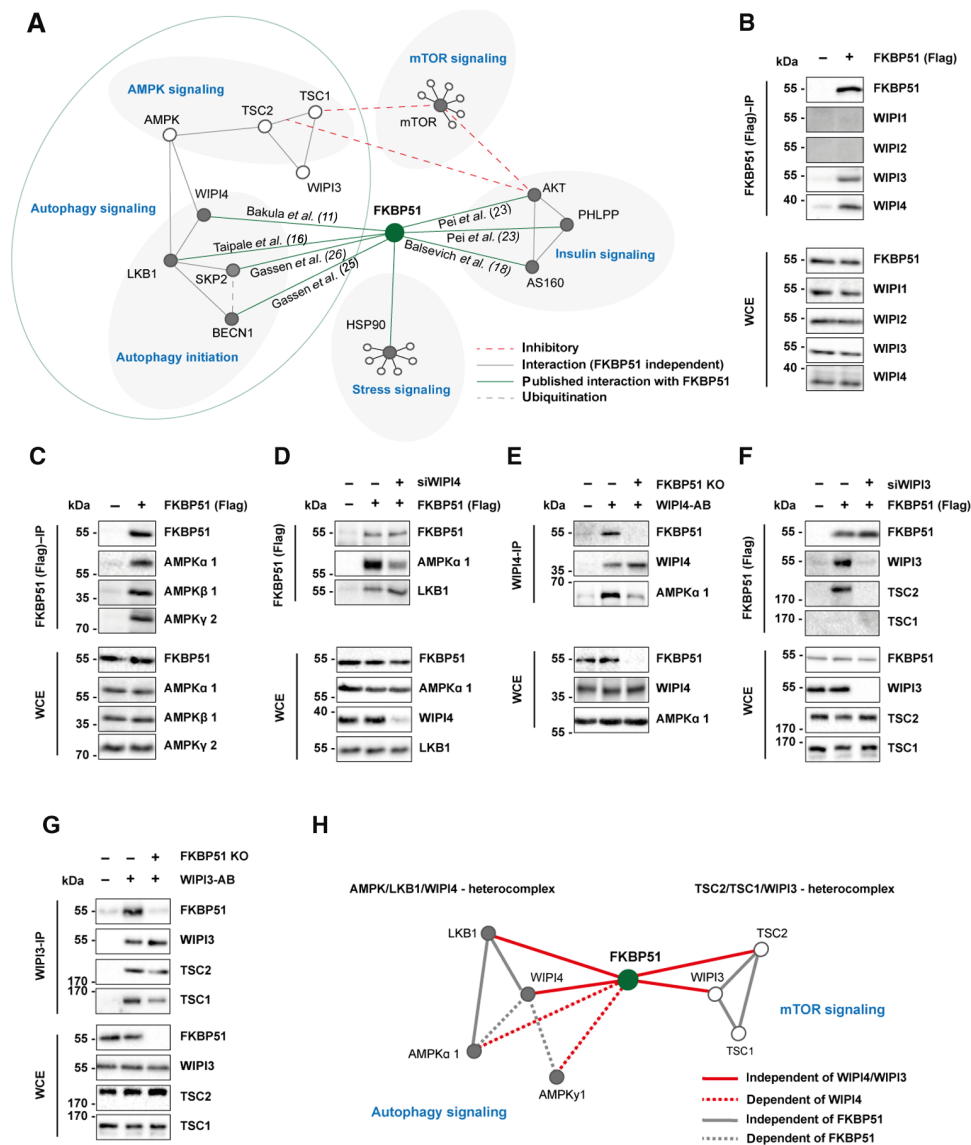
Fig. 3. FKBP51 associates with AMPK, TSC2, and WIPI3 and WIPI4 to regulate autophagy and mTOR signaling. (**A**) Published protein-protein interactions of FKBP51. (**B**) FKBP51 associates with WIPI3 and WIPI4, but not with WIPI1 and WIPI2. WCE, whole-cell extract; IP, immunoprecipitation. (**C**) Interaction of FKBP51 with AMPK subunits. (**D**) Interaction of FKBP51 with LKB1 and AMPKα in WIPI4 KD cells. (**E**) Interaction of WIPI4 with AMPKα in FKBP51-lacking cells. (**F**) FKBP51 interacts with TSC2 in dependency of WIPI3. (**G**) WIPI3 interacts with TSC2 and TSC1 in the presence or absence of FKBP51. (**H**) Identified associations of FKBP51 in the regulation of autophagy and mTOR signaling and the proposed model of interaction. FKBP51 recruits LKB1 to the AMPK-WIPI4 complex and thereby facilitates AMPK activation. Furthermore, FKBP51 scaffolds TSC2-WIPI3 binding to alter mTOR signaling. AB, antibody.

To investigate the functional relevance of WIPI4 in the association of FKBP51 with AMPK, we generated WIPI4 knockdown (KD) N2a cells using small interfering RNA (siRNA) cotransfected with FKBP51-Flag (fig. S5B). We observed that FKBP51 binding to AMPK was reduced in cells lacking WIPI4 (Fig. 3D and fig. S5C). Our precipitation studies further demonstrated that FKBP51 interacts with LKB1, which confirmed the finding of a previous interactomics-based screening experiment by Taipale and colleagues (*16*) and further revealed that this interaction is independent of WIPI4 (Fig. 3D and fig. S5, D and A). Furthermore, we could demonstrate that WIPI4 deletion blocked the phosphorylation effect of FKBP51 OE on pAMPK at T172 (fig. S5E), suggesting that FKBP51 binds to AMPK in dependency of WIPI4. In addition, studies in FKBP51 KO cells revealed that the WIPI4

interaction to AMPK depends on the presence of FKBP51 (Fig. 3E), indicating a subordinate role of FKBP51 as a molecular bridge that links the autophagy-relevant WIPI network to AMPK signaling.

Last, we assessed the functional relevance of WIPI3-FKBP51 binding. Performing co-IP studies in N2a cells in the presence or absence of WIPI3 (fig. S5F), we observed that FKBP51 interacts with TSC2 but not TSC1 (Fig. 3F), which are upstream master regulators of mTOR (*42*). Further, we confirmed the association of FKBP51 with TSC2, which depends on the presence of WIPI3 (Fig. 3F), whereas the interaction of WIPI3 to TSC2 and TSC1 is independent of FKBP51 (Fig. 3G).

Collectively, we demonstrate that FKBP51 regulates autophagy in concert with the WIPI protein family, specifically WIPI3 and

WIPI4 via interactions with the mTOR and AMPK cascades (Fig. 3H). The combined interpretation of our molecular and metabolomic analyses led us to hypothesize that FKBP51 regulates autophagy and consequently whole-body metabolism in vivo, especially after a metabolic challenge.

MBH FKBP51 is a regulator of body weight and food intake
We and others have previously shown that FKBP51 acts in a tissue-specific manner in soleus muscle (SM), epididymal WAT (eWAT), and the hypothalamus to regulate metabolism (*18, 19, 22, 30*). However, the interconnected response of autophagy and FKBP51 to a metabolic stressor, such as HFD, remains elusive and encouraged us to investigate the possible relationship between FKBP51 expression and autophagic flux (the protein turnover through catabolic autophagy).

Our analysis revealed that C57BL/6N mice showed significantly increased FKBP51 protein levels (Fig. 4A) and diminished accumulation of the autophagy substrate p62 in the MBH upon 10 weeks of HFD (58% kcal from fat) (Fig. 4B). HFD per se did not affect the lipidation of the autophagosome-spiking protein light chain 3 (LC3B-I) to LC3B-II (Fig. 4C), which binds the autophagosome and is a reliable marker to analyze autophagic flux (*35*). However, levels of LC3B-II were similarly increased in both conditions after treatment with chloroquine (50 mg/kg), an inhibitor of lysosomal acidification and autophagosome-lysosome fusion that, in turn, blocks degradation of autophagosome cargo (*35*). In line with the reduced levels of p62, these results indicate an active central autophagic flux after HFD.

In peripheral eWAT and SM, however, chloroquine treatment did increase LC3B-II levels only in chow-fed animals (fig. S6, A and B), implying reduced or even blocked autophagy signaling under HFD conditions. This hypothesis is supported by an increased accumulation of p62 in these peripheral tissues with a significant increase in SM (fig. S6C). FKBP51 protein levels were unaffected in eWAT and slightly but not significantly decreased in SM (fig. S6D). These data suggested a possible interconnected role of FKBP51 and autophagy flux, particularly in the MBH. We, therefore, decided to further test the effects of FKBP51 on autophagy signaling and its relevance for whole-body metabolism in vivo by manipulating FKBP51 in the MBH.

First, we injected a *Cre*-expressing virus into the MBH of FKB-P51^lox/lox animals (Fig. 4D) to evaluate the effects of central FKBP51 deletion. FKBP51^MBH-KO animals showed a massive increase in body weight 6 weeks after surgery, despite their regular chow diet (Fig. 4E). The bodyweight increase was accompanied by increased food intake and decreased glucose tolerance (Fig. 4, F and G). These findings were unexpected, considering the lean phenotype of full-body FKBP51-deficient mice after prolonged exposure to an HFD (*18, 19*) and further highlight the tissue specificity of FKBP51.

Next, we injected an adeno-associated virus (AAV)–mediated FKBP51 OE virus into the MBH of C57/Bl6 mice (FKBP51^MBH-OE, Fig. 4H). FKBP51^MBH-OE animals showed no substantial differences in body weight gain within the first 4 weeks after surgery. Therefore, we challenged FKBP51^MBH-OE animals with a metabolic stressor by feeding them an HFD for 8 weeks. Animals overexpressing FKBP51 displayed significantly reduced body weight gain compared to the control group (Fig. 4I), paralleled by a reduction in food intake (Fig. 4J). In a second cohort of FKBP51^MBH-OE animals [with an identical body weight phenotype (fig. S6E)], we investigated whether glucose

metabolism was altered and observed improved glucose tolerance and insulin sensitivity compared to the control group under HFD but not under normal chow diet (Fig. 4K and fig. S6, F to H). Together, these experiments reveal an essential role of MBH FKBP51 in central coping mechanisms with an obesogenic stressor and position MBH FKBP51 as a key regulator of whole-body metabolism.

MBH FKBP51 fine-tunes autophagy signaling in an inversed U-shaped manner
Given the opposing phenotypes of FKBP51^MBH-KO and FKBP51^MBH-OE animals and the discovered regulatory function of FKBP51 in the metabolic control of autophagy, we were interested in the underlying regulation of autophagy signaling. In our KO experiment, viral injection resulted in a high-deletion rate within the MBH of FKBP51^MBH-KO animals (Fig. 5, A and B). According to our hypothesis, we observed a reduced binding of LKB1 and AMPK to WIPI4 (Fig. 5C and see fig. S7A for quantification), which was accompanied by a reduction in the phosphorylation of AMPK at T172, causing less active AMPK (Fig. 5D). Downstream of AMPK, we monitored diminished phosphorylation of ULK1 at S555, BECN1 at S91/S94, and TSC2 at S1387 (fig. S7, B to D). Parallel to the effects of AMPK downstream proteins, we detected reduced levels of TSC2 binding to WIPI3 (Fig. 5E and see fig. S7E for quantification). Furthermore, we observed increased levels of phosphorylated AKT at S473 and phosphorylated ULK1 at S757 (fig. S7, F and G), indicating increased AKT/mTOR signaling. The increased mTOR activity could be validated by increased levels of pp70S6K (Fig. 5F). Last, loss of FKBP51 resulted in decreased levels of LC3B-II and the accumulation of p62 (Fig. 5, G and H). Together, these data suggest that FKBP51 deletion reduced autophagy signaling in the MBH via the reduction of AMPK activity and an increased mTOR signaling, which is in line with our in vitro data.

Animals overexpressing FKBP51 in the MBH showed an excessive up-regulation of FKBP51 (Fig. 5, I and J). Co-IP studies indicated that following the excessive overexpression (OE) of FKBP51, AMPK binding to WIPI4 was decreased. Furthermore, LKB1 levels were strongly reduced and binding of LKB1 to WIPI4 vanished (Fig. 5K and fig. S7A). Consequently, phosphorylation of AMPK at T172 was significantly reduced (Fig. 5L). Downstream of AMPK, we observed a decrease in phosphorylation of ULK1 at S555 and no changes of phosphorylated BECN1 levels (fig. S7, B and C). Phosphorylation of TSC2 at S1387 and the binding of TSC2 to WIPI3 were significantly decreased (Fig. 5M and fig. S7, D and E). Phosphorylation of AKT at S473 was unchanged (fig. S7F). On the other hand, FKBP51^MBH-OE animals showed increased mTOR signaling, indicated by increased phosphorylation of ULK1 at S757 and elevated levels of pp70S6K (Fig. 5N and fig. S7G). Last, FKBP51 OE animals showed increased levels of LC3B-II. However, treatment with chloroquine (50 mg/kg) did not further increase the LC3B-II levels in FKBP51^MBH-OE animals (Fig. 5O), indicating that the fusion of autophagosomes with lysosomes is impaired and central autophagic flux is blocked. This hypothesis is supported by the fact that FKBP51 OE resulted in the accumulation of the autophagy substrate p62 (Fig. 5P). These data are in contrast to our previously observed findings and imply that FKBP51^MBH-OE animals, despite their highly elevated FKBP51 levels, have blocked autophagy signaling in the MBH.

The observation that viral overexpression of FKBP51 in the MBH resulted in a massive overexpressing of FKBP51 led us to hypothesize that the level of FKBP51 expression directly correlates with the degree
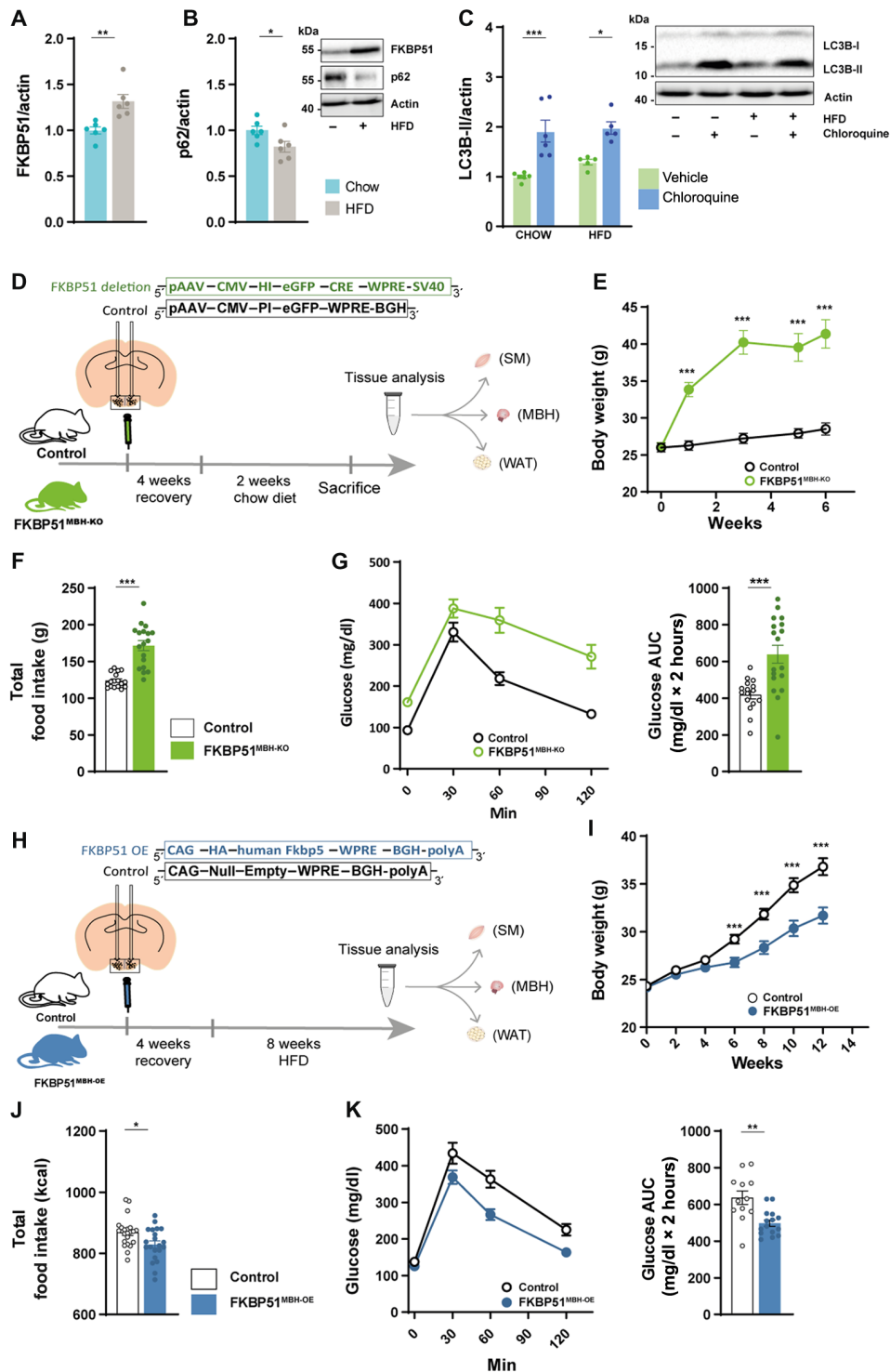
Fig. 4. MBH FKBP51 regulates body weight gain, food intake and glucose metabolism. (**A**) Ten weeks of HFD increased hypothalamic FKBP51 in the MBH [n (chow) = 6 versus n (HFD) = 6]. (**B**) Effects of HFD on the accumulation of p62. (**C**) Treatment with chloroquine (50 mg/kg) increased LC3B-II level under chow and HFD conditions. (**D**) FKBP51$^{lox/lox}$ animals were injected with 200 nl of Cre-expressing virus and fed a chow diet for 6 weeks. (**E**) FKBP51^{MBH-KO} showed significant body weight increase after virus injection on a regular chow diet. (**F**) FKBP51^{MBH-KO} animals showed increased food intake and (**G**) enhanced glucose intolerance. AUC, area under the curve. (**H**) For FKBP51 overexpression, animals were injected with an AAV virus into the MBH. (**I**) FKBP51^{MBH-OE} animals showed reduced body weight gain on an HFD diet compared to their control animals (**J**) FKBP51^{MBH-OE} animals showed reduced food intake. (**K**) FKBP51^{MBH-OE} animals showed improve glucose tolerance under HFD conditions. For (A), (B), (F), (G), (J), and (K), an unpaired Student's t test was performed. For (C), a two-way ANOVA was performed, followed by a Tukey's multiple comparison test. For (E) and (I), a repeated measurements ANOVA was performed. ± SEM; *$P < 0.05$, **$P < 0.01$, and ***$P < 0.001$.

Fig. 5. MBH FKBP51 regulates autophagy in an inversed U-shaped manner. FKBP51 deletion is depicted in green, and FKBP51 overexpression is depicted in blue. (**A**) Representative blots of autophagy and mTOR markers in FKBP51[MBH-KO] mice. (**B**) Quantification of FKBP51 dele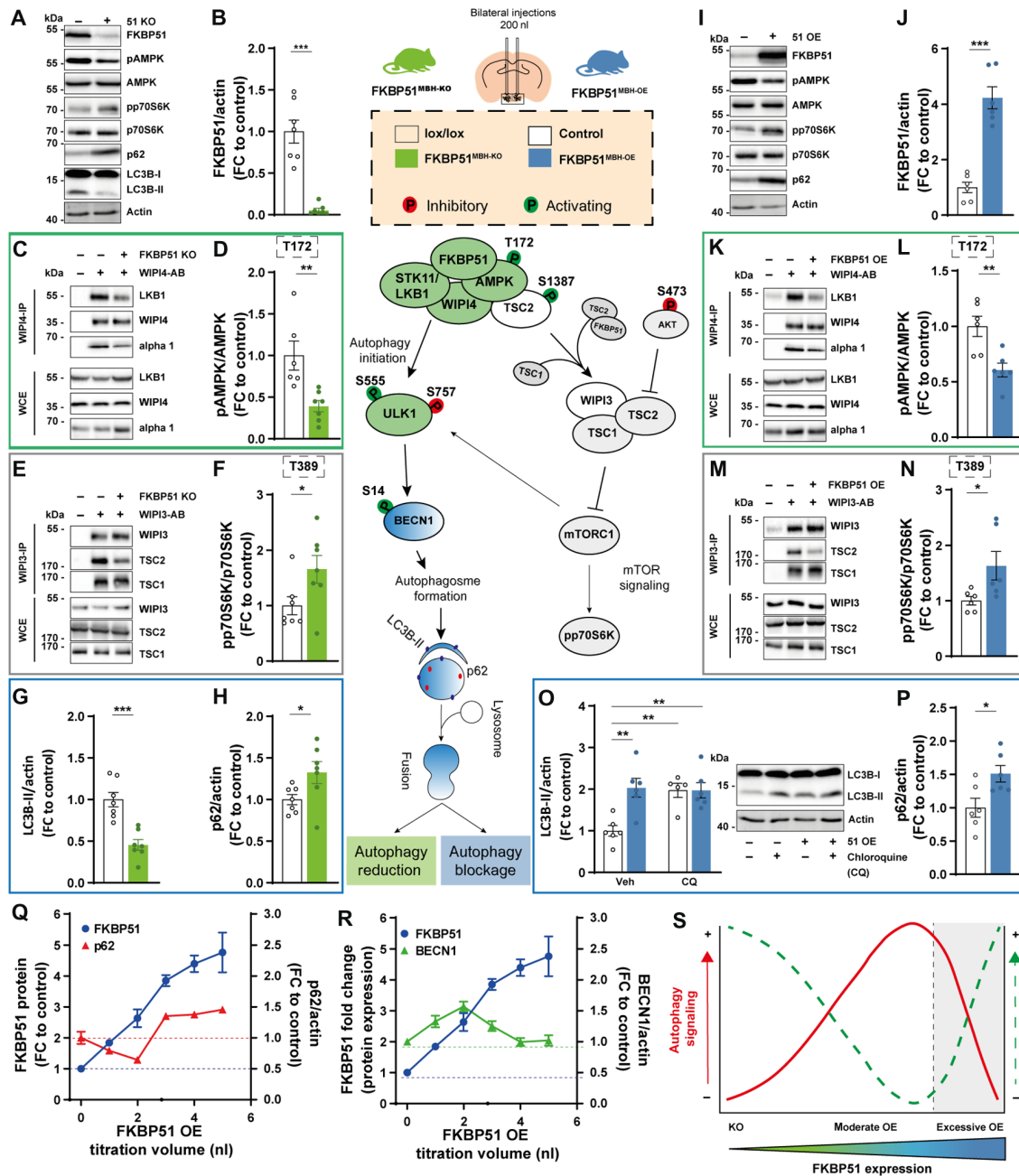tion. (**C**) FKBP51 deletion reduced LKB1 and AMPK binding to WIPI4 as well as (**D**) AMPK phosphorylation at T172. (**E**) TSC2-WIPI3 binding was decreased in FKBP51[MBH-KO] animals. (**F**) Quantification of mTOR substrate pp70S6K (T389). (**G**) LC3B-II and (**H**) p62 levels in the MBH. (**I**) Representative blots of autophagy and mTOR marker in FKBP51[MBH-OE] mice. (**J**) Quantification of viral FKBP51 overexpression. (**K**) FKBP51 overexpression reduced LKB1 and AMPK binding to WIPI4. (**L**) Quantification of AMPK phosphorylation at T172. (**M**) TSC2-WIPI3 binding was decreased. (**N**) Quantification of pp70S6K phosphorylation at T389. (**O**) To assess autophagic flux FKBP51MBH-OE, animals were treated with chloroquine (50 mg/kg), and LC3B-II levels were analyzed 4 hours after treatment. (**P**) FKBP51 overexpression blocked autophagic flux and resulted in an accumulation of p62. (**Q** and **R**) Quantification of FKBP51, p62, and BECN1, while titrating AAV-HA-FKBP51 virus into mouse neuroblastoma cells. (**S**) MBH FKBP51 regulates autophagy and mTOR signaling in a dose-dependent manner. All data are shown as ±SEM. Data are shown as the relative protein expression compared to control; for (A) to (N), an unpaired Student's *t* test was performed. *$P < 0.05$, **$P < 0.01$, and ***$P < 0.001$.

of autophagy signaling. Therefore, we gradually increased FKBP51 levels in N2a cells by the titration of AAV–hemagglutinin tag (HA)–FKBP51. Following a moderate increase of FKBP51, we observed a decrease in the accumulation of p62 and an increase in BECN1, supporting the activating role of FKBP51. In parallel, we could observe a slight decrease in p70S6K phosphorylation. However, upon a stimulus threshold (at approximately three- to fourfold FKBP51), we observed an inhibitory effect on autophagy with decreased protein level of BECN1 and an increased phosphorylation of p70S6K and enhanced accumulation of p62 (Fig. 5, Q and R, and fig. S7H).

Our pathway analysis demonstrates that deletion of FKBP51 reduces autophagy signaling, and excessive levels of FKBP51 protein results in a total block of autophagy, causing a substantial shift from autophagy to mTOR signaling. In conclusion, we suggest that FKBP51 dose dependently regulates autophagy signaling in an inversed U-shaped manner (Fig. 5S).

MBH FKBP51 alters sympathetic outflow and thereby regulates autophagy signaling in the periphery

The MBH is an established regulatory center for sympathetic outflow to peripheral tissues (43). Consequently, we were interested whether the sympathetic tone of the brain into peripheral tissues was affected in FKBP51^{MBH-OE} animals. To do so, we treated FKBP51^{MBH-OE} mice with a single dose of the norepinephrine (NE) synthesis inhibitor α-methyl-p-tyrosine (α-MPT) to block NE synthesis in the periphery, thereby enabling the assessment of the catecholamine turnover rate (cTR) (44, 45). MBH FKBP51 OE led to a reduction in the cTR in muscle and eWAT (Fig. 6, A and B). Further, inguinal WAT (iWAT) of FKBP51^{MBH-OE} animals showed significant differences in initial NE levels, but not in cTR (fig. S8A). We also observed a mildly but not significantly decreased cTR in brown adipose tissue (BAT) (fig. S8B), whereas no effects were detected in the pancreas or heart tissue (fig. S8, C and D). Together, these data demonstrate that MBH FKBP51 OE dampens the sympathetic outflow especially to muscle and fat tissue and encouraged us to investigate changes in autophagy signaling in both tissues.

In FKBP51^{MBH-OE} animals, we observed increased levels of FKBP51 in SM and eWAT (fig. S8E), which resulted in increased AMPK activity (Fig. 6C) by enhanced binding of AMPK and LKB1 to WIPI4 (fig. S8, F and G). Downstream of AMPK, we observed increased phosphorylation of ULK1, BECN1, and TSC2, indicating enhanced autophagy initiation in the periphery (fig. S8, H to J). We again assessed mTOR signaling and observed increased binding of TSC2 to WIPI3 (fig. S8K) and a strong reduction in the phosphorylation of AKT at S473 and ULK1 at S757 (fig. S8, L and M), which resulted in reduced levels of pp70S6K (T389) (Fig. 6D). Furthermore, we monitored reduced levels of p62 (Fig. 6, E and F). To verify the increase in autophagy signaling, we analyzed LC3B-II levels before and after chloroquine treatment. Here, we detected a true increase in LC3B-II levels after chloroquine treatment (Fig. 6, G to I). These data imply an increase in autophagy flux in the periphery of FKBP51^{MBH-OE} animals. This is in line with our hypothesis that moderately elevated levels of FKBP51 increase autophagy signaling and suggest that the balance between active mTOR signaling in the MBH and active autophagy signaling in the periphery is one driving factor of the lean phenotype of the FKBP51^{MBH-OE} animals.

In FKBP51^{MBH-KO} mice, we observed an opposing phenotype with reduced autophagy signaling in SM, whereas autophagy signaling in eWAT was unaltered. In both tissues, we did not observe significant changes in FKBP51 protein level (fig. S8N). However, we could detect less phosphorylation of AMPK at T172 (Fig. 6J) and reduced binding of AMPK/LKB1 to WIPI4 (fig. S8, O and P). These findings were accompanied by reduced levels of ULK1, BECN1, and TSC2 (fig. S8, Q to S). Furthermore, we monitored increased levels of pp70S6K (T389), pULK1 (S757), and pAKT (S473), suggesting increased mTOR signaling (Fig. 6K and fig. S8, U and V). Last, LC3B-II levels were significantly reduced (Fig. 6L) in combination with elevated levels of p62 in SM (Fig. 6, M and N), which is indicative of reduced autophagy signaling solely in this peripheral tissue.

We could not detect any differences in autophagy signaling in other peripheral tissues, such as the liver (fig. S9, A and B). In summary, we suggest that the combined reduction of autophagy in the MBH and peripheral tissues, such as muscle and adipose tissue, is driving the observed body weight phenotype in FKBP51^{MBH-KO} mice.

DISCUSSION

In the current study, we examined the role of stress-activated chaperone FKBP51 as a molecular master switch linking autophagy and whole-body metabolism. We here present that FKBP51 actively modulates the response of the AMPK-mTOR network to an HFD by scaffolding autophagy-upstream AMPK/LKB1/WIPI4 and TSC2/WIPI3 heteroprotein complexes. We identify a tissue-specific function of FKBP51 by providing in vivo evidence that hypothalamic FKBP51 acts as a dose-specific mediator of whole-body metabolism.

Metabolomic profiling of neuronal-like cells lacking FKBP51 revealed a substantial increase for several metabolites and amino acids and suggests a role of FKBP51 in BCAA metabolism. BCAAs are important regulators of neurotransmitters and protein synthesis as well as food intake (46, 47). The increase of multiple BCAAs have been associated with obesity and insulin resistance (48, 49). In our in vitro metabolomic profiling analysis, isoleucine, leucine, valine, and tyrosine were strongly elevated in FKBP51 KO cells under normal and high glucose concentrations, which is indicative of constantly active mTOR signaling (50). Furthermore, it has been shown that excess leucine can reduce abdominal fat loss, whereas leucine deprivation promotes fat loss via cyclic AMP response element-binding protein signaling and increased expression of CRH (corticotropin-releasing hormone) in the hypothalamus. This effect is conveyed by the activation of the sympathetic nervous system (51). Leucine is an important regulator of mTOR and negatively affects the biogenesis of autophagosomes through its metabolite acetyl coenzyme A, which thereby enhances acetylation of the regulatory-associated protein of MTOR (RPTOR) via acetyltransferase EP300 in neurons and other cell types. This cascade of events ultimately leads to autophagy inhibition and mTOR activation (52, 53). At the same time, the increased levels of polyamines, observed in FKBP51 KO cells, are in contrast to autophagy inhibition. In particular, spermidine was shown to be capable of autophagy induction via inhibition of EP300 (54). Nevertheless, cell type–specific effects have to be taken into account as studies suggest an increased expression of EP300 in response to spermidine supplementation in aged and osteoarthritic chondrocytes (55).

To gain further insight into the underlying mechanisms, we built on already existing knowledge about FKBP51 regarding its regulatory role on single autophagy-related proteins [like BECN1, WIPIs, and SKP2 (11, 16, 26)], which further positions FKBP51 as a major upstream regulator of autophagy. AMPK is activated by the phosphorylation of T172, which is regulated by LKB1 (56), and increased LKB1/AMPK signaling activates the TSC1/TSC2 complex, which, in turn, inhibits mTOR activity (38). Recently, Bakula and colleagues (11) showed that the WIPI protein family members WIPI3 and WIPI4 are essential scaffolders of the LKB1/AMPK/TSC1/2 signaling network thereby regulating autophagy and mTOR signaling. Here, we extended this knowledge by revealing that FKBP51 recruits LKB1 to the WIPI4-AMPK regulatory platform to induce AMPK phosphorylation at T172, which further increases autophagy initiation by direct phosphorylation of ULK1 at S555 (10). On the other hand, FKBP51 associates with the TSC2/WIPI3 heterocomplex to coregulate
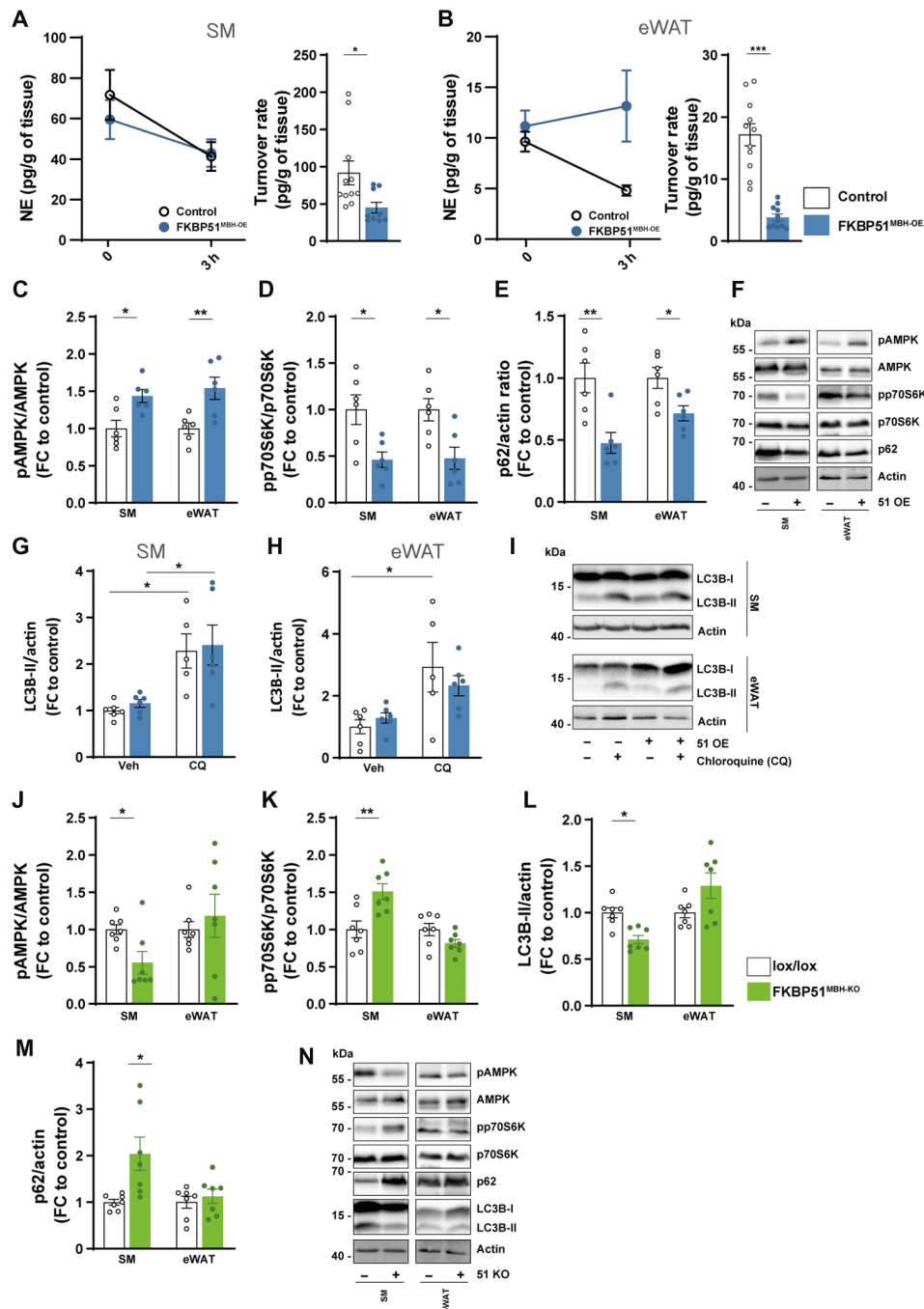
Fig. 6. MBH FKBP51 affects sympathetic outflow and peripheral autophagy signaling. FKBP51 overexpression is depicted in blue, and FKBP51 deletion is depicted in green. (**A** and **B**) Representative decrease in tissue NE content after α-MPT injection (left) and turnover rate (right) were determined on SM and eWAT (see fig. S8 for pancreas, heart, iWAT, and BAT tissues). Quantification of (**C**) pAMPK (T172) and (**D**) pp70S6K (T389), and (**E**) p62 level in the SM and eWAT. (**F**) Representative blots. (**G** to **H**) FKBP51 overexpression increased autophagic flux and in SM and eWAT. (**I**) Representative blots of chloroquine the experiment. Quantification of (**J**) pAMPK (T172), (**K**) pp70S6K (T389), (**L**) LC3B-II, and (**M**) p62 levels in SM and eWAT in animals lacking FKBP51 in the MBH. (**N**) Representative blots of FKBP51[MBH-KO] protein analysis. All data are shown as ±SEM. Protein data are shown as the relative protein expression compared to control. A two-way ANOVA was performed, followed by a Tukey's multiple comparison test in (F) and (G). For (A) to (E) and (I) to (L), an unpaired Student's t test was performed. *$P < 0.05$, **$P < 0.01$, and ***$P < 0.001$.

mTOR signaling and thus position FKBP51 as a main regulatory switch between autophagy initiation and mTOR signaling. Our experiments in vivo and in vitro led us to propose a model in which physiological levels of FKBP51 are essential for normal cellular autophagy-mediated homeostasis. Hereby, the absence of FKBP51 reduces autophagy signaling and capacity in contrast to excessive, nonphysiological levels of FKBP51, which block autophagy in favor of mTOR signaling. The relative amounts of FKBP51 complexed with autophagy regulators within a cell govern the threshold for a transition from cell homeostasis to impaired autophagy in an inversed U-shaped manner.

FKBP51 has been shown to act tissue-specific to control adipocyte differentiation, browning (*19*, *57*), and glucose metabolism (*18*). Most studies investigated global FKBP51 KO mice and observed a lean phenotype after an HFD regimen. These observations would imply that hypothalamic FKBP51 OE increases body weight gain, whereas deletion reduces body weight. We here observed that the acute FKBP51 manipulation in the MBH acts in an opposing manner with a central deletion leading to obesity and an overexpression to a lean phenotype, emphasizing its tissue specificity. These data suggest that hypothalamic FKBP51 regulates body weight and food intake in a U-shaped manner, which is supported by the fact that HFD increases FKBP51 expression and that a modest increase of hypothalamic FKBP51 induces body weight gain (*30*).

Several studies have already addressed the functional role of hypothalamic autophagy in the regulation of whole-body metabolism. Mice challenged with a chronic HFD showed impaired autophagy in the arcuate nucleus, and a deletion of ATG7 in the MBH resulted in hyperphagia and increased body weight (*58*). The MBH, however, is a complex brain region with multiple different nuclei, which have various opposing roles in the control of whole-body metabolism (*1*, *59*). Here, we targeted FKBP51 nonselectively in various nuclei within the MBH, which is a limitation of the study. However, it also raises the question, which nuclei or neuronal subpopulations are the driving force behind our observed phenotypes. Previous studies have shown that specific deletion of autophagy in POMC neurons leads to hyperphagia and obesity (*12*). These findings are in line with our data of the FKBP51^{MBH-KO} animals, which develop obesity and hyperphagia on a regular chow diet in combination with decreased activity of central autophagy. Intriguingly, animals overexpressing FKBP51 in the MBH have a reduced body weight progression, increased glucose tolerance, and insulin sensitivity under an HFD regimen despite the hypothalamic autophagy blockage. The deletion of autophagy in AgRP neurons resulted in decreased body weight and food intake in response to fasting (*13*). The current study, however, cannot fully address whether the observed effects on obesity and the sympathetic effect output are purely driven by FKBP51 manipulation and whether autophagy is required for this effect. Future studies should emphasize the specific neuronal action of FKBP51 on autophagy to regulate body weight progression and food intake and investigate whether a blockade of autophagy can indeed counteract the effects of FKBP51 overexpression and vice versa.

Last, we suggest that the altered balance between hypothalamic and peripheral autophagy–mTOR signaling is a major contributor to the observed phenotype of FKBP51^{MBH-OE} and FKBP51^{MBH-KO} animals. FKBP51^{MBH-KO} animals showed decreased autophagy and increased mTOR signaling in the periphery (eWAT and SM), whereas peripheral autophagy signaling in FKBP51^{MBH-OE} animals displayed the opposite phenotype. The importance of central-peripheral mTOR and autophagy signaling has already been studied intensely. For instance, peripheral mTOR activity was shown to be involved in the pathogenesis of obesity and is enhanced in muscle and adipose tissue in obese animals (*60*, *61*), whereas the activation of central mTOR can reduce food intake and body weight gain (*62*). In particular, the mTOR substrate p70S6K was shown to regulate body weight by mediating the sensitivity of leptin to AMPK via PI3K/AKT1/mTOR pathway (*63*, *64*). Here, we extend this finding by the fact that the combination of peripheral and central p70S6K activity is an important contributor to the development of obesity. One has to keep in mind, although, that FKBP51 is highly dynamically regulated by stressful situations and acts in concert with other chaperone proteins in a cell type– and tissue-specific manner. This may also explain apparent minor inconsistencies in our data and warrants further investigation.

In conclusion, this study provides a conceptual framework for the regulatory function of the stress-responsive co-chaperone FKBP51 on autophagy signaling and establishes a physiological role of MBH FKBP51 in the regulation of food intake and body weight regulation. We further suggest that FKBP51 is a crucial sensor linking signaling pathways controlling the stress response, autophagy, and metabolism. The ability of FKBP51 to regulate autophagy and energy homeostasis might therefore open new promising treatment avenues for metabolic disorders, such as obesity and type 2 diabetes.

MATERIALS AND METHODS
Antibodies
The following antibodies were used: goat polyclonal anti-actin (I-19) (sc-1616, Santa Cruz Biotechnology), rabbit polyclonal anti-FKBP51 (A301-430A, Bethyl Laboratories), rabbit monoclonal anti-FKBP5 (D5G2, #12210, Cell Signaling Technology), rabbit monoclonal anti-LKB1 (D60C5, #3047, Cell Signaling Technology), rabbit polyclonal anti-pAMPKα^{T172} (#2531, Cell Signaling Technology), rabbit polyclonal anti-pAMPKα (#2532, Cell Signaling Technology), rabbit polyclonal anti-SKP2 (L70, #4313, Cell Signaling Technology), rabbit anti-pSKP2^{S72} (was a gift from Cell Signaling Technology), rabbit polyclonal anti-AKT (#9272, Cell Signaling Technology), rabbit monoclonal anti-pAKT^{S473} (D9E, #4060, Cell Signaling Technology), rabbit polyclonal anti-p62 (#5114, Cell Signaling Technology), rabbit monoclonal anti-LC3B (D11, #3868, Cell Signaling Technology), rabbit polyclonal anti-pULK1^{S757} (#6888, Cell Signaling Technology), rabbit monoclonal anti-pULK1^{S555} (D1H4, #5869, Cell Signaling Technology), rabbit monoclonal anti-ULK1 (D8H5, #8054, Cell Signaling Technology), anti-pBECN1$^{S93/S96}$ (in mouse S91/S94) (#12476, Cell Signaling Technology), rabbit polyclonal anti-pBECN1^{S15} (#84966, Cell Signaling Technology), rabbit polyclonal anti-BECN1 (#3738, Cell Signaling Technology), rabbit polyclonal anti-TSC2 (#3612, Cell Signaling Technology), rabbit polyclonal anti-pTSC2^{S1387} (#5584, Cell Signaling Technology), rabbit monoclonal anti-pATG16L1^{S278} (EPR19016, ab195242, Abcam), rabbit polyclonal anti-WIPI4 (WDR45) (19194-1-AP, Proteintech), mouse monoclonal anti-WIPI4 (G12, sc-398272, Santa Cruz Biotechnology), rabbit polyclonal anti-WIPI3 (WDR45L) (SAB2102704, Sigma-Aldrich), mouse monoclonal anti-WIPI3 (B-7, sc-514194, Santa Cruz Biotechnology), rabbit polyclonal anti-WIPI2 (#8567, Cell Signaling Technology), rabbit polyclonal anti-WIPI1 (HPA007493, Sigma-Aldrich), rabbit polyclonal anti-AMPKα1 (#2795, Cell Signaling Technology), rabbit polyclonal anti-AMPKγ2 (#2536, Cell Signaling Technology), rabbit polyclonal anti-AMPKα2 (#2757, Cell Signaling Technology), rabbit monoclonal anti-AMPKβ1 (71C10, #4178, Cell Signaling Technology), rabbit polyclonal anti-AMPKγ1 (#4187, Cell Signaling Technology), rabbit polyclonal anti-AMPKβ2 (#4188, Cell Signaling Technology), rabbit polyclonal anti-AMPKγ3 (#2550, Cell Signaling Technology), rabbit monoclonal anti-TSC1 (D43E2, #6935, Cell Signaling Technology), rabbit polyclonal anti-Flag (600-401-383, Rockland Inc.), rabbit polyclonal anti-hypusine (ABS1046, Merck Millipore), rabbit monoclonal anti-eIF5A (D8L8Q, #20765, Cell Signaling Technology), and rabbit polyclonal anti-TFEB (ab245350, Abcam).

Animals and animal housing

All experiments and protocols were approved by the committee for the Care and Use of Laboratory Animals of the Government of Upper Bavaria and were performed in accordance with the European Communities' Council Directive 2010/63/EU. All animals were kept singly housed in individually ventilated cages (IVCs) (30 cm by 16 cm by 16 cm; 501 cm^2) with ad libitum access to water and food and constant environmental conditions (12-hour light/12-hour dark cycle, 23° ± 2°C, and humidity of 55%) during all times. All IVCs had sufficient bedding and nesting material as well as a wooden tunnel for environmental enrichment. All animals were fed with a standard research chow diet (Altromin 1318, Altromin GmbH, Germany) or an HFD (58% kcal from fat; D12331, Research Diets, New Brunswick, NJ, USA). For all experiments, male C57BL/6N or male *Fkbp5*$^{lox/lox}$ mice [described in (*65*)] aged between 2 and 5 months were used.

Viral overexpression and knockdown of FKBP51

For overexpression of FKBP51, we injected an AAV vector containing a CAG-HA–tagged FKBP51-WPRE-BGH-polyA expression cassette (containing the coding sequence of human FKBP51 National Center for Biotechnology Information CCDS ID CCDS4808.1) in C57BL/6N mice. The same vector construct without expression of FKBP51 (CAG-Null/Empty-WPRE-BGH-polyA) was used as a control. Virus production, amplification, and purification were performed by GeneDetect. A viral vector containing a *Cre*-expressing cassette (pAAV-CMV-HI-eGFP-Cre-WPRE-SV40, #105545, Addgene) was used to induce FKBP51 deletion in FKBP51$^{lox/lox}$ mice. Control animals were injected with a control virus (pAAV-CMV-PI-eGFP-WPRE-bGH, #105530, Addgene). For both experiments, stereotactic injections were performed as described previously (*66*). Briefly, mice were anesthetized with isoflurane prior surgery, and 0.2 μl of the abovementioned viruses (titers: $1.6 \times 10^{12–13}$ genomic particles/ml) was bilaterally injected in the MBH at 0.05 μl/min by glass capillaries with a tip resistance of 2 to 4 megohm in a stereotactic apparatus. The following coordinates were used: −1.5 mm anterior to bregma, 0.4 mm lateral from midline, and 5.6 mm below the surface of the skull, targeting the MBH. After surgery, mice were treated for 3 days with Metacam via intraperitoneal injections and were housed for 3 to 4 weeks for total recovery before the actual experiments. Successful overexpression and KD of FKBP51 were verified by Western blot.

Autophagic flux

We investigated the autophagic flux by the injection of chloroquine (50 mg/kg), an inhibitor of lysosomal acidification and autophagosome-lysosomal fusion that blocks degradation of autophagosome cargo (*35*). We injected C57BL/6N mice in the morning with chloroquine (50 mg/kg) or saline as control. Multiple tissues were removed and shock-frozen 4 hours after injection and stored at −80°C until protein analysis of LC3B-II normalized to glyceraldehyde-3-phosphate dehydrogenase or actin. Lipidation of LC3B in protein homogenates obtained from animals treated with chloroquine (fusion block) was compared to LC3B lipidation of animals treated with vehicle.

Sample collection

On the day of euthanization, animals were deeply anesthetized with isoflurane and euthanized by decapitation. Trunk blood was collected in labeled 1.5-ml EDTA-coated microcentrifuge tubes (Sarstedt) and kept on ice until centrifugation. After centrifugation (4°C, 8000 rpm

for 1 min), the plasma was removed and transferred to new, labeled tubes and stored at −20°C until hormone quantification. For protein analysis, the MBH, skeletal muscle (SM), and WAT (eWAT) were collected and immediately shock-frozen and stored at −80°C until protein analysis.

cTR determination

Catecholamine turnover was measured on the basis of the decline in tissue NE content after the inhibition of catecholamine biosynthesis with α-methyl-DL-tyrosine (α-MPT) (200 mg/kg i.p. injection; Sigma-Aldrich, ST, Quentin, France), as described previously (*44*).

In the morning, bedding was changed, and C57BL/6N mice were food-deprived for 3 hours to insure postprandial state and injected with α-methyl-DL-tyrosine (α-MPT; a tyrosine hydroxylase inhibitor) to block catecholamine synthesis. Before (time = 0) and 3 hours after the injection (time = 3 hours), animals were euthanized, and the tissues were removed, flash-frozen in liquid nitrogen, and stored at −80°C for monoamine and metabolite analysis.

Catecholamine content at time = 0 [NE (0)] was determined on a group of animals receiving a saline injection. Because the concentration of catecholamine in tissues declined exponentially, we could obtain the rate constant of NE efflux (expressed in h − 1). Comprehensive analysis of NE was carried out by reverse-phase liquid chromatography (LC) with electrochemical detection as described in (*67*). The values obtained were expressed as nanogram per milligram wet tissue and were logarithmically transformed for calculation of linearity of regression, SE of the regression coefficients, and significance of differences between regression coefficients.

Glucose tolerance and insulin tolerance

Alteration of glucose metabolism in FKBP51^{MBH-OE} and FKBP51^{MBH-KO} mice was investigated by a glucose (glucose tolerance test) and insulin tolerance (insulin tolerance test) test as described previously (*18*).

Hormone assessment

Corticosterone concentrations were determined by radioimmunoassay using a corticosterone double antibody ^{125}I radioimmunoassay kit (sensitivity: 12.5 ng/ml; MP Biomedicals Inc.) and were used following the manufacturers' instructions. Radioactivity of the pellet was measured with a gamma counter (Packard Cobra II Auto Gamma, PerkinElmer). Final corticosterone levels were derived from the standard curve.

Cell lines and transfection

N2a WT, N2a FKBP51 KO, SH-SY5Y WT, and FKBP51 KO (*68*) cells were maintained in Dulbecco's modified Eagle's medium supplemented with 10% fetal bovine serum and 1× penicillin-streptomycin antibiotics at 37°C in a humidified atmosphere with 5% CO2. At 90% confluency, N2a cells were detached from the plate, and 2×10^6 cells were resuspended in 100 μl of transfection buffer [50 nM Hepes (pH 7.3), 90 mM NaCl, 5 mM KCl, and 0.15 mM CaCl2]. A total of 2.5 μg of plasmid DNA or 80 ng of siRNA (siWIPI3, EMU081491 or siWIPI4, EMU007321 or siControl, and SIC001, all Sigma-Aldrich) was used per transfection. Electroporation was performed using the Amaxa Nucleofector System 2b (program T-020). For OE experiments, N2a cells were transfected with FKBP51-Flag expression or TFEB-GFP reporter plasmid using Lipofectamine 2000 (Thermo Fisher Scientific) according to the manufacturer's instructions.

Generation of FKBP51 KO N2a cells

N2a (Sigma-Aldrich) FKBP51 KO cell line was generated with the Alt-R CRISPR-Cas9 System from Integrated DNA Technologies (IDT) according to the manufacturer's instructions. Briefly, RNA oligos [Alt-R CRISPR-Cas9 crispr RNA (crRNA) against murine FKBP51 and Alt-R CRISPR-Cas9 trans-activating crRNA (tracrRNA)] were mixed in nuclease-free duplex buffer (IDT) in equimolar concentrations yielding a final duplex of 1 μM and then heated at 95°C for 5 min and combined with 1 μM Alt-R S.p. HiFi Cas9 Nuclease V3 diluted in Opti-MEM (Thermo Fisher Scientific). Ribonucleoprotein (RNP) complexes were assembled at room temperature (RT) for 5 min and mixed with Lipofectamine RNAiMAX reagent (Thermo Fisher Scientific) and Opti-MEM (Thermo Fisher Scientific) and incubated for 20 min at RT to form transfection complexes. Subsequently, 40,000 N2a cells per well were reverse-transfected using complete culture media without antibiotics in a 96-well tissue culture plate with a final RNP concentration of 10 nM. After 48 hours (37°C, 5% CO2), single-cell clones were obtained by array dilution method, expanded, and analyzed by Western blotting. FKBP51 WT control cells were identified by immunoblotting after single-cell cloning procedures and, therefore, underwent the same transfection and isolation procedure as the FKBP51 KO cells. Predesigned Alt-R CIRSPR Cas9 guide RNAs (IDT) were used for KO generation (protospacer adjacent motif sequence in italics). Mm.Cas9.*FKBP5*.1.AA: CGATC-CCAATCGGAATGTCG*TGG*.

Treatment of N2a cells

Treatments of N2a cell cultures included glutocorticoid receptor (GR) stimulation with dexamethasone (Sigma-Aldrich) ranging from 1 to 100 nM for 24 hours, HBSS (Thermo Fisher Scientific)–induced starvation for 4 hours, and inhibition of autophagosome-lysosome fusion by BafA1 (100 nM, 4 hours; Alfa Aesar).

Co-immunoprecipitation

IPs of endogenous proteins were performed from protein extracts (n = 3 to 4 per group) derived from N2a cells, SH-SY5Y WT or FKBP51 KO cells, SM, eWAT, and MBH. For co-IPs, 500 μg of lysate was incubated with 2 μg of the appropriate IP antibody [anti-Flag (FKBP51), anti-FKBP51, anti-WIPI4, and anti-WIPI3] at 4°C overnight. A total of 20 μl of rabbit immunoglobulin G–conjugated protein G Dynabeads (Invitrogen, 100-03D) were blocked with bovine serum albumin and subsequently added to the lysate-antibody mixture and allowed to incubate at 4°C for 3 hours to mediate binding between Dynabeads and the antibody-antigen complex of interest. Beads were then washed three times with ice-cold phosphate-buffered saline, and the protein antibody complexes were eluted with 60 μl of Laemmli loading buffer. Thereafter, the eluate was boiled for 5 min at 95°C. Then, 2 to 5 μl of each immunoprecipitate were separated by SDS–polyacrylamide gel electrophoresis (SDS-PAGE) and electro-transferred onto nitrocellulose membranes. For assessing protein complexes, immunoblotting against WIPI1-WIPI4, FKBP51, LKB1, AMPK, TSC1, and TSC2 was performed.

Western blot analysis

Protein extracts were obtained by lysing cells [in radioimmunoprecipitation assay buffer (150 mM NaCl, 1% IGEPAL CA-630, 0.5% sodium deoxycholate, 0.1% SDS, and 50 mM tris (pH 8.0)] freshly supplemented with protease inhibitor (Merck Millipore, Darmstadt, Germany), benzonase (Merck Millipore), 5 mM dithiothreitol

(Sigma-Aldrich, Munich, Germany), and phosphatase inhibitor cocktail (Roche, Penzberg, Germany). Proteins were separated by SDS-PAGE and electro-transferred onto nitrocellulose membranes. Blots were placed in tris-buffered saline supplemented with 0.05% Tween (Sigma-Aldrich) and 5% nonfat milk for 1 hour at RT and then incubated with primary antibody (diluted in tris-buffered saline/0.05% Tween) overnight at 4°C.

Subsequently, blots were washed and probed with the respective horseradish peroxidase or fluorophore-conjugated secondary antibody for 1 hour at RT. The immunoreactive bands were visualized either using an enhanced chemiluminesence detection reagent (Millipore, Billerica, MA, USA) or directly by excitation of the respective fluorophore. Determination of the band intensities was performed with Bio-Rad, ChemiDoc MP.

LC-MS analysis of amine-containing metabolites

The benzoyl chloride derivatization method was used for amino acid analysis (69). Briefly, the dried metabolite pellets were resuspended in 90 μl of the LC-MS grade water (Milli-Q 7000 equipped with an LC-Pak and a Millipak filter, Millipore). Then, 20 μl of the resuspended sample was mixed with 10 μl of 100 mM sodium carbonate (Sigma-Aldrich), followed by the addition of 10 μl of 2% benzoyl chloride (Sigma-Aldrich) in acetonitrile (Optima-Grade, Fisher Scientific). Samples were vortexed before centrifugation for 10 min at 21,300g at 20°C. Clear supernatants were diluted 1:10 with LC-MS grade water and transferred to fresh autosampler tubes with conical glass inserts (Chromatographie Zubehoer Trott) and analyzed using a Vanquish UHPLC (Thermo Fisher Scientific) connected to a Q-Exactive HF (Thermo Fisher Scientific).

For the analysis, 1 μl of the derivatized sample were injected onto a 100 × 2.1 mm HSS T3 UPLC column (Waters). The flow rate was set to 400 μl/min using a buffer system consisting of buffer A [10 mM ammonium formate (Sigma-Aldrich) and 0.15% formic acid (Sigma-Aldrich) in LC-MS grade water] and buffer B (acetonitrile, Optima-grade, Fisher Scientific). The LC gradient was 0% buffer B at 0 min, 0 to 15% buffer B at 0 to 0.1 min, 15 to 17% buffer B at 0.1 to 0.5 min, 17 to 55% buffer B at 0.5 to 7 min, 55 to 70% buffer B at 7 to 7.5 min, 70 to 100% buffer B at 7.5 to 9 min, 100% buffer B at 9 to 10 min, 100 to 0% buffer B at 10 to 10.1 min, and 0% buffer B at 10.1 to 15 min. The mass spectrometer was operating in positive-ionization mode monitoring the mass range, mass/charge ratio of 50 to 750. The heated electrospray ionization (ESI) source settings of the mass spectrometer were as follows: spray voltage of 3.5 kV, capillary temperature of 250°C, sheath gas flow of 60 arbitrary units (AU), and auxiliary gas flow of 20 AU at a temperature of 250°C. The S-lens was set to a value of 60 AU.

Data analysis was performed using the TraceFinder software (version 4.2, Thermo Fisher Scientific). Identity of each compound was validated by authentic reference compounds, which were analyzed independently. Peak areas were analyzed using extracted ion chromatogram (XIC) of compound-specific $[M + nBz + H]^+$, where n corresponds to the number of amine moieties, which can be derivatized with a benzoyl chloride (Bz). XIC peaks were extracted with a mass accuracy (<5 parts per million) and a retention time tolerance of 0.2 min.

Anion-exchange chromatography MS of the analysis of tricarboxylic acid cycle and glycolysis metabolites

Anion-exchange chromatography was performed simultaneously to the LC-MS analysis. First, 50 μl of the resuspended sample was diluted 1:5 with LC-MS grade water and analyzed using a Dionex

ion chromatography system (ICS-5000, Thermo Fisher Scientific). The applied protocol was adopted from (70). Briefly, 10 μl of polar metabolite extract was injected in full-loop mode using an overfill factor of 3, onto a Dionex IonPac AS11-HC column (2 mm by 250 mm, 4-μm particle size, Thermo Fisher Scientific) equipped with a Dionex IonPac AS11-HC guard column (2 mm by 50 mm, 4 μm, Thermo Fisher Scientific). The column temperature was held at 30°C, while the autosampler was set to 6°C. A potassium hydroxide gradient was generated by the eluent generator using a potassium hydroxide cartridge that was supplied with deionized water. The metabolite separation was carried at a flow rate of 380 μl/min, applying the following gradient: 0 to 5 min, 10 to 25 mM KOH; 5 to 21 min, 25 to 35 mM KOH; 21 to 25 min, 35 to 100 mM KOH, 25 to 28 min, 100 mM KOH; and 28 to 32 min, 100 to 10 mM KOH. The column was re-equilibrated at 10 mM for 6 min. The eluting metabolites were detected in negative ion mode using ESI MRM (multireaction monitoring) on a Xevo TQ (Waters) triple quadrupole mass spectrometer applying the following settings: capillary voltage of 1.5 kV, desolvation temperature of 550°C, desolvation gas flow of 800 liters/hour, and collision cell gas flow of 0.15 ml/min. All peaks were validated using two MRM transitions, one for quantification of the compound, while the second ion was used for qualification of the identity of the compound. Data analysis and peak integration were performed using the TargetLynx Software (Waters).

Analysis of nuclear translocation of TFEB

Images for assessment of nuclear translocation of TFEB-GFP in paraformaldehyde-fixed N2a cells were acquired using the VisiScope CSU-W1 spinning disk confocal microscope and the VisiView Software (Visitron Systems GmbH). Settings for laser and detector were maintained constant for the acquisition of each image. For analysis, at least three images were acquired using the 20× objective. For quantification of nuclear TFEB- GFP translocation, GFP intensity was determined in ImageJ by manually drawing a border around randomly selected, 4′,6-diamidino-2-phenylindole–positive nuclei of N2a cells with a GFP signal.

Statistical analysis

The data presented are shown as means ± SEM, and samples sizes are indicated in the figure legends. All data were analyzed by the commercially available software SPSS v17.0 and GraphPad v8.0. The unpaired Student's *t* test was used when two groups were compared. For four-group comparisons, two-way analysis of variance (ANOVA) was performed, followed by Tukey's or Dunnett's multiple comparisons test, as appropriate. *P* values of less than 0.05 were considered statistically significant.

SUPPLEMENTARY MATERIALS

Supplementary material for this article is available at https://science.org/doi/10.1126/sciadv.abi4797

View/request a protocol for this paper from *Bio-protocol*.

REFERENCES AND NOTES

1. G. J. Morton, T. H. Meek, M. W. Schwartz, Neurobiology of food intake in health and disease. *Nat. Rev. Neurosci.* **15**, 367–378 (2014).
2. L. Galluzzi, J. M. Bravo-San Pedro, B. Levine, D. R. Green, G. Kroemer, Pharmacological modulation of autophagy: Therapeutic potential and persisting obstacles. *Nat. Rev. Drug Discov.* **16**, 487–511 (2017).
3. Y. Zhang, J. R. Sowers, J. Ren, Targeting autophagy in obesity: From pathophysiology to management. *Nat. Rev. Endocrinol.* **14**, 356–376 (2018).
4. J. D. Rabinowitz, E. White, Autophagy and metabolism. *Science* **330**, 1344–1348 (2010).
5. B. Levine, G. Kroemer, Biological functions of autophagy genes: A disease perspective. *Cell* **176**, 11–42 (2019).
6. Y. Potes, B. de Luxán-Delgado, S. Rodriguez-González, M. R. M. Guimarães, J. J. Solano, M. Fernández-Fernández, M. Bermúdez, J. A. Boga, I. Vega-Naredo, A. Coto-Montes, Overweight in elderly people induces impaired autophagy in skeletal muscle. *Free Radic. Biol. Med.* **110**, 31–41 (2017).
7. Y. Mizunoe, Y. Sudo, N. Okita, H. Hiraoka, K. Mikami, T. Narahara, A. Negishi, M. Yoshida, R. Higashibata, S. Watanabe, H. Kaneko, D. Natori, T. Furuichi, H. Yasukawa, M. Kobayashi, Y. Higami, Involvement of lysosomal dysfunction in autophagosome accumulation and early pathologies in adipose tissue of obese mice. *Autophagy* **13**, 642–653 (2017).
8. K. Inoki, J. Kim, K.-L. Guan, AMPK and mTOR in cellular energy homeostasis and drug targets. *Annu. Rev. Pharmacol. Toxicol.* **52**, 381–400 (2012).
9. M. M. Mihaylova, R. J. Shaw, The AMPK signalling pathway coordinates cell growth, autophagy and metabolism. *Nat. Cell Biol.* **13**, 1016–1023 (2011).
10. J. Kim, M. Kundu, B. Viollet, K. L. Guan, AMPK and mTOR regulate autophagy through direct phosphorylation of Ulk1. *Nat. Cell Biol.* **13**, 132–141 (2011).
11. D. Bakula, A. J. Müller, T. Zuleger, Z. Takacs, M. Franz-Wachtel, A. K. Thost, D. Brigger, M. P. Tschan, T. Frickey, H. Robenek, B. Macek, T. Proikas-Cezanne, WIPI3 and WIPI4 β-propellers are scaffolds for LKB1-AMPK-TSC signalling circuits in the control of autophagy. *Nat. Commun.* **8**, 15637 (2017).
12. S. Kaushik, E. Arias, H. Kwon, N. M. Lopez, D. Athonvarangkul, S. Sahu, G. J. Schwartz, J. E. Pessin, R. Singh, Loss of autophagy in hypothalamic POMC neurons impairs lipolysis. *EMBO Rep.* **13**, 258–265 (2012).
13. S. Kaushik, J. A. Rodriguez-Navarro, E. Arias, R. Kiffin, S. Sahu, G. J. Schwartz, A. M. Cuervo, R. Singh, Autophagy in hypothalamic AgRP neurons regulates food intake and energy balance. *Cell Metab.* **14**, 173–183 (2011).
14. D. L. Riggs, P. J. Roberts, S. C. Chirillo, J. Cheung-Flynn, V. Prapapanich, T. Ratajczak, R. Gaber, D. Picard, D. F. Smith, The Hsp90-binding peptidylprolyl isomerase FKBP52 potentiates glucocorticoid signaling in vivo. *EMBO J.* **22**, 1158–1167 (2003).
15. G. M. Wochnik, J. Rüegg, G. A. Abel, U. Schmidt, F. Holsboer, T. Rein, FK506-binding proteins 51 and 52 differentially regulate dynein interaction and nuclear translocation of the glucocorticoid receptor in mammalian cells. *J. Biol. Chem.* **280**, 4609–4616 (2005).
16. M. Taipale, G. Tucker, J. Peng, I. Krykbaeva, Z. Y. Lin, B. Larsen, H. Choi, B. Berger, A. C. Gingras, S. Lindquist, A quantitative chaperone interaction network reveals the architecture of cellular protein homeostasis pathways. *Cell* **158**, 434–448 (2014).
17. M. V. Schmidt, M. Paez-Pereda, F. Holsboer, F. Hausch, The prospect of FKBP51 as a drug target. *ChemMedChem* **7**, 1351–1359 (2012).
18. G. Balsevich, A. S. Häusl, C. W. Meyer, S. Karamihalev, X. Feng, M. L. Pöhlmann, C. Dournes, A. Uribe-Marino, S. Santarelli, C. Labermaier, K. Hafner, T. Mao, M. Breitsamer, M. Theodoropoulou, C. Namendorf, M. Uhr, M. Paez-Pereda, G. Winter, F. Hausch, A. Chen, M. H. Tschöp, T. Rein, N. C. Gassen, M. V. Schmidt, Stress- responsive FKBP51 regulates AKT2-AS160 signaling and metabolic function. *Nat. Commun.* **8**, 1725 (2017).
19. L. A. Stechschulte, B. Qiu, M. Warrier, T. D. Hinds, M. Zhang, H. Gu, Y. Xu, S. S. Khuder, L. Russo, S. M. Najjar, B. Lecka-Czernik, W. Yong, E. R. Sanchez, FKBP51 null mice are resistant to diet-induced obesity and the PPARγ agonist rosiglitazone. *Endocrinology* **157**, 3888–3900 (2016).
20. M. J. Pereira, J. Palming, M. K. Svensson, M. Rizell, J. Dalenbäck, M. Hammar, T. Fall, C. O. Sidibeh, A. Svensson, J. W. Eriksson, FKBP5 expression in human adipose tissue increases following dexamethasone exposure and is associated with insulin resistance. *Metabolism* **63**, 1198–1208 (2014).
21. C. O. Sidibeh, M. J. Pereira, X. M. Abalo, G. J. Boersma, S. Skrtic, P. Lundkvist, P. Katsogiannos, F. Hausch, C. Castillejo-López, J. W. Eriksson, FKBP5 expression in human adipose tissue: Potential role in glucose and lipid metabolism, adipogenesis and type 2 diabetes. *Endocrine* **62**, 116–128 (2018).
22. A. S. Häusl, G. Balsevich, N. C. Gassen, M. V. Schmidt, Focus on FKBP51: A molecular link between stress and metabolic disorders. *Mol. Metab.* **29**, 170–181 (2019).
23. H. Pei, L. Li, B. L. Fridley, G. D. Jenkins, K. R. Kalari, W. Lingle, G. Petersen, Z. Lou, L. Wang, FKBP51 affects cancer cell response to chemotherapy by negatively regulating Akt. *Cancer Cell* **16**, 259–266 (2009).
24. R. C. Wang, Y. Wei, Z. An, Z. Zou, G. Xiao, G. Bhagat, M. White, J. Reichelt, B. Levine, Akt-mediated regulation of autophagy and tumorigenesis through Beclin 1 phosphorylation. *Science* **338**, 956–959 (2012).
25. N. C. Gassen, J. Hartmann, M. V. Schmidt, T. Rein, FKBP5/FKBP51 enhances autophagy to synergize with antidepressant action. *Autophagy* **11**, 578–580 (2015).
26. N. C. Gassen, D. Niemeyer, D. Muth, V. M. Corman, S. Martinelli, A. Gassen, K. Hafner, J. Papies, K. Mösbauer, A. Zellner, A. S. Zannas, A. Herrmann, F. Holsboer, R. Brack-Werner, M. Boshart, B. Müller-Myhsok, C. Drosten, M. A. Müller, T. Rein, SKP2 attenuates autophagy through Beclin1-ubiquitination and its inhibition reduces MERS-Coronavirus infection. *Nat. Commun.* **10**, 5770 (2019).

27. R. Singh, S. Kaushik, Y. Wang, Y. Xiang, I. Novak, K. Komatsu, K. Tanaka, A. M. Cuervo, M. J. Czaja, Autophagy regulates lipid metabolism. *Nature* **458**, 1131–1135 (2009).

28. J. Toneatto, S. Guber, N. L. Charo, S. Susperreguy, J. Schwartz, M. D. Galigniana, G. Piwien-Pilipuk, Dynamic mitochondrial-nuclear redistribution of the immunophilin FKBP51 is regulated by the PKA signaling pathway to control gene expression during adipocyte differentiation. *J. Cell Sci.* **126**, 5357–5368 (2013).

29. Y. Zhang, S. Goldman, R. Baerga, Y. Zhao, M. Komatsu, S. Jin, Adipose-specific deletion of autophagy-related gene 7 (atg7) in mice reveals a role in adipogenesis. *Proc. Natl. Acad. Sci. U.S.A.* **106**, 19860–19865 (2009).

30. L. Yang, F. Isoda, K. Yen, S. P. Kleopoulos, W. Janssen, X. Fan, J. Mastaitis, A. Dunn-Meynell, B. Levin, R. McCrimmon, R. Sherwin, S. Musatov, C. V. Mobbs, Hypothalamic Fkbp51 is induced by fasting, and elevated hypothalamic expression promotes obese phenotypes. *AJP Endocrinol. Metab.* **302**, E987–E991 (2012).

31. S. H. Scharf, C. Liebl, E. B. Binder, M. V. Schmidt, M. B. Müller, Expression and regulation of the Fkbp5 gene in the adult mouse brain. *PLOS ONE* **6**, e16883 (2011).

32. R. L. Wolfson, D. M. Sabatini, The dawn of the age of amino acid sensors for the mTORC1 pathway. *Cell Metab.* **26**, 301–309 (2017).

33. S. M. Son, S. J. Park, H. Lee, F. Siddiqi, J. E. Lee, F. M. Menzies, D. C. Rubinsztein, Leucine signals to mTORC1 via its metabolite acetyl-coenzyme A. *Cell Metab.* **29**, 192–201.e7 (2019).

34. D. Meng, Q. Yang, H. Wang, C. H. Melick, R. Navlani, A. R. Frank, J. L. Jewell, Glutamine and asparagine activate mTORC1 independently of Rag GTPases. *J. Biol. Chem.* **295**, 2890–2899 (2020).

35. D. J. Klionsky, Guidelines for the use and interpretation of assays for monitoring autophagy (3rd edition). *Autophagy* **12**, 1–222 (2016).

36. A. Arif, J. Jia, B. Willard, X. Li, P. L. Fox, Multisite phosphorylation of S6K1 directs a kinase phospho-code that determines substrate selection. *Mol. Cell.* **73**, 446–457.e6 (2019).

37. J. Kim, Y. C. Kim, C. Fang, R. C. Russell, J. H. Kim, W. Fan, R. Liu, Q. Zhong, K. L. Guan, Differential regulation of distinct Vps34 complexes by AMPK in nutrient stress and autophagy. *Cell* **152**, 290–303 (2013).

38. D. B. Shackelford, R. J. Shaw, The LKB1-AMPK pathway: Metabolism and growth control in tumour suppression. *Nat. Rev. Cancer* **9**, 563–575 (2009).

39. W. Tian, R. Alsaadi, Z. Guo, A. Kalinina, M. Carrier, M. E. Tremblay, B. Lacoste, D. Lagace, R. C. Russell, An antibody for analysis of autophagy induction. *Nat. Methods* **17**, 232–239 (2020).

40. H. Zhang, G. Alsaleh, J. Feltham, Y. Sun, G. Napolitano, T. Riffelmacher, P. Charles, L. Frau, P. Hublitz, Z. Yu, S. Mohammed, A. Ballabio, S. Balabanov, J. Mellor, A. K. Simon, Polyamines control eIF5A hypusination, TFEB translation, and autophagy to reverse B cell senescence. *Mol. Cell.* **76**, 110–125.e9 (2019).

41. W. Wan, Z. You, L. Zhou, Y. Xu, C. Peng, T. Zhou, C. Yi, Y. Shi, W. Liu, mTORC1-regulated and HUWE1-mediated WIPI2 degradation controls autophagy Flux. *Mol. Cell.* **72**, 303–315.e6 (2018).

42. G. Y. Liu, D. M. Sabatini, mTOR at the nexus of nutrition, growth, ageing and disease. *Nat. Rev. Mol. Cell Biol.* **21**, 183–203 (2020).

43. C. Broberger, Brain regulation of food intake and appetite: Molecules and networks. *J. Intern. Med.* **258**, 301–327 (2005).

44. B. B. Brodie, E. Costa, A. Dlabac, N. H. Neff, H. H. Smookler, Application of steady state kinetics to the estimation of synthesis rate and turnover time of tissue catecholamines. *J. Pharmacol. Exp. Ther.* **154**, 493–498 (1966).

45. A. Joly-Amado, R. G. P. Denis, J. Castel, A. Lacombe, C. Cansell, C. Rouch, N. Kassis, J. Dairou, P. D. Cani, R. Ventura-Clapier, A. Prola, M. Flamment, F. Foufelle, C. Magnan, S. Luquet, Hypothalamic AgRP-neurons control peripheral substrate utilization and nutrient partitioning. *EMBO J.* **31**, 4276–4288 (2012).

46. J. E. Sperringer, A. Addington, S. M. Hutson, Branched-chain amino acids and brain metabolism. *Neurochem. Res.* **42**, 1697–1709 (2017).

47. J. D. Fernstrom, *Journal of Nutrition* (American Institute of Nutrition, 2005; https://academic.oup.com/jn/article/135/6/1539S/4663842), vol. 135, pp. 1539S–1546S.

48. C. B. Newgard, J. An, J. R. Bain, M. J. Muehlbauer, R. D. Stevens, L. F. Lien, A. M. Haqq, S. H. Shah, M. Arlotto, C. A. Slentz, J. Rochon, D. Gallup, O. Ilkayeva, B. R. Wenner, W. S. Yancy, H. Eisenson, G. Musante, R. S. Surwit, D. S. Millington, M. D. Butler, L. P. Svetkey, A branched-chain amino acid-related metabolic signature that differentiates obese and lean humans and contributes to insulin resistance. *Cell Metab.* **9**, 311–326 (2009).

49. T. J. Wang, M. G. Larson, R. S. Vasan, S. Cheng, E. P. Rhee, E. McCabe, G. D. Lewis, C. S. Fox, P. F. Jacques, C. Fernandez, C. J. O'Donnell, S. A. Carr, V. K. Mootha, J. C. Florez, A. Souza, O. Melander, C. B. Clish, R. E. Gerszten, Metabolite profiles and the risk of developing diabetes. *Nat. Med.* **17**, 448–453 (2011).

50. M. S. Yoon, The emerging role of branched-chain amino acids in insulin resistance and metabolism. *Nutrients.* **8**, 405 (2016).

51. Y. Cheng, Q. Zhang, Q. Meng, T. Xia, Z. Huang, C. Wang, B. Liu, S. Chen, F. Xiao, Y. Du, F. Guo, Leucine deprivation stimulates fat loss via increasing CRH expression

52. G. Mariño, F. Pietrocola, T. Eisenberg, Y. Kong, S. A. Malik, A. Andryushkova, S. Schroeder, T. Pendl, A. Harger, M. Niso-Santano, N. Zamzami, M. Scoazec, S. Durand, D. P. Enot, Á. F. Fernández, I. Martins, O. Kepp, L. Senovilla, C. Bauvy, E. Morselli, E. Vacchelli, M. Bennetzen, C. Magnes, F. Sinner, T. Pieber, C. López-Otín, M. C. Maiuri, P. Codogno, J. S. Andersen, J. A. Hill, F. Madeo, G. Kroemer, Regulation of autophagy By cytosolic acetyl-coenzyme A. *Mol. Cell* **53**, 710–725 (2014).

53. S. M. Son, S. J. Park, E. Stamatakou, M. Vicinanza, F. M. Menzies, D. C. Rubinsztein, Leucine regulates autophagy via acetylation of the mTORC1 component raptor. *Nat. Commun.* **11**, 3148 (2020).

54. F. Pietrocola, S. Lachkar, D. P. Enot, M. Niso-Santano, J. M. Bravo-San Pedro, V. Sica, V. Izzo, M. C. Maiuri, F. Madeo, G. Mariño, G. Kroemer, Spermidine induces autophagy by inhibiting the acetyltransferase EP300. *Cell Death Differ.* **22**, 509–516 (2015).

55. P. K. Sacitharan, S. Lwin, G. B. Gharios, J. R. Edwards, Spermidine restores dysregulated autophagy and polyamine synthesis in aged and osteoarthritic chondrocytes via EP300. *Exp. Mol. Med.* **50**, 1–10 (2018).

56. D. G. Hardie, AMP-activated/SNF1 protein kinases: Conserved guardians of cellular energy. *Nat. Rev. Mol. Cell Biol.* **8**, 774–785 (2007).

57. L. A. Stechschulte, T. D. Hinds, S. S. Khuder, W. Shou, S. M. Najjar, E. R. Sanchez, FKBP51 controls cellular adipogenesis through p38 kinase-mediated phosphorylation of GRα and PPARγ. *Mol. Endocrinol.* **28**, 1265–1275 (2014).

58. Q. Meng, D. Cai, Defective hypothalamic autophagy directs the central pathogenesis of obesity via the IκB kinase β(IKKβ)/NF-κB pathway. *J. Biol. Chem.* **286**, 32324–32332 (2011).

59. M. G. Myers, D. P. Olson, Central nervous system control of metabolism. *Nature* **491**, 357–363 (2012).

60. S. H. Um, F. Frigerio, M. Watanabe, F. Picard, M. Joaquin, M. Sticker, S. Fumagalli, P. R. Allegrini, S. C. Kozma, J. Auwerx, G. Thomas, Absence of S6K1 protects against age- and diet-induced obesity while enhancing insulin sensitivity. *Nature* **431**, 200–205 (2004).

61. L. Khamzina, A. Veilleux, S. Bergeron, A. Marette, Increased activation of the mammalian target of rapamycin pathway in liver and skeletal muscle of obese rats: Possible involvement in obesity-linked insulin resistance. *Endocrinology* **146**, 1473–1481 (2005).

62. D. Cota, K. Proulx, K. A. B. Smith, S. C. Kozma, G. Thomas, S. C. Woods, R. J. Seeley, Hypothalamic mTOR signaling regulates food intake. *Science* **312**, 927–930 (2006).

63. C. Blouet, H. Ono, G. J. Schwartz, Mediobasal hypothalamic p70 S6 kinase 1 modulates the control of energy homeostasis. *Cell Metab.* **8**, 459–467 (2008).

64. Y. Dagon, E. Hur, B. Zheng, K. Wellenstein, L. C. Cantley, B. B. Kahn, P70S6 kinase phosphorylates AMPK on serine 491 to mediate leptin's effect on food intake. *Cell Metab.* **16**, 104–112 (2012).

65. A. Häusl, J. Hartmann, M. Pöhlmann, L. Brix, J.-P. Lopez, E. Brivio, C. Engelhardt, S. Roeh, L. Rudolph, R. Stoffel, K. Hafner, H. Goss, J. Reul, J. Deussing, K. Ressler, N. Gassen, A. Chen, M. Schmidt, The co-chaperone Fkbp5 shapes the acute stress response in the paraventricular nucleus of the hypothalamus. *bioRxiv*, 824664 (2019).

66. M. V. Schmidt, J.-P. Schulke, C. Liebl, M. Stiess, C. Avrabos, J. Bock, G. M. Wochnik, H. A. Davies, N. Zimmermann, S. H. Scharf, D. Trumbach, W. Wurst, W. Zieglgansberger, C. Turck, F. Holsboer, M. G. Stewart, F. Bradke, M. Eder, M. B. Muller, T. Rein, Tumor suppressor down-regulated in renal cell carcinoma 1 (DRR1) is a stress-induced actin bundling factor that modulates synaptic efficacy and cognition. *Proc. Natl. Acad. Sci.* **108**, 17213–17218 (2011).

67. J. Nagler, S. C. Schriever, M. De Angelis, P. T. Pfluger, K. W. Schramm, Comprehensive analysis of nine monoamines and metabolites in small amounts of peripheral murine (C57Bl/6 J) tissues. *Biomed. Chromatogr.* **32**, e4151 (2018).

68. S. Martinelli, E. A. Anderzhanova, S. Wiechmann, F. Dethloff, K. Weckmann, T. Bajaj, J. Hartmann, K. Hafner, M. L. Pöhlmann, L. Jollans, G. Maccarrone, F. Hausch, C. W. Turck, A. Philipsen, M. V. Schmidt, B. Kuster, N. C. Gassen, Stress-primed secretory autophagy drives extracellular BDNF maturation. *bioRxiv* **2020**, 2020.05.13.090514 (2020).

69. J. M. T. Wong, P. A. Malec, O. S. Mabrouk, J. Ro, M. Dus, R. T. Kennedy, Benzoyl chloride derivatization with liquid chromatography-mass spectrometry for targeted metabolomics of neurochemicals in biological samples. *J. Chromatogr. A* **1446**, 78–90 (2016).

70. M. Schwaiger, E. Rampler, G. Hermann, W. Miklos, W. Berger, G. Koellensperger, Anion-exchange chromatography coupled to high-resolution mass spectrometry: A powerful tool for merging targeted and non-targeted metabolomics. *Anal. Chem.* **89**, 7667–7674 (2017).

ScienceAdvances

Mediobasal hypothalamic FKBP51 acts as a molecular switch linking autophagy to whole-body metabolism

Alexander S. HäuslThomas BajajLea M. BrixMax L. PöhlmannKathrin HafnerMeri De AngelisJoachim NaglerFrederik DethloffGeorgia BalsevichKarl-Werner SchrammPatrick GiavaliscoAlon ChenMathias V. SchmidtNils C. Gassen

View the article online
https://www.science.org/doi/10.1126/sciadv.abi4797
Permissions
https://www.science.org/help/reprints-and-permissions

Use of this article is subject to the Terms of service

Science Advances
NAAAS

Supplementary Materials for

Mediobasal hypothalamic FKBP51 acts as a molecular switch linking autophagy to whole-body metabolism

Alexander S. Häusl*, Thomas Bajaj*, Lea M. Brix, Max L. Pöhlmann, Kathrin Hafner,
Meri De Angelis, Joachim Nagler, Frederik Dethloff, Georgia Balsevich, Karl-Werner Schramm,
Patrick Giavalisco, Alon Chen, Mathias V. Schmidt, Nils C. Gassen

*Corresponding author. Email: mschmidt@psych.mpg.de (M.V.S.); nils.gassen@ukbonn.de (N.C.G.)

The PDF file includes:

Figs. S1 to S10

Other Supplementary Material for this manuscript includes the following:

Data S1

Supplementary figure 1: FKBP51 deletion alters AMPK and mTOR-associated amino acid metabolic and biosynthetic pathways.
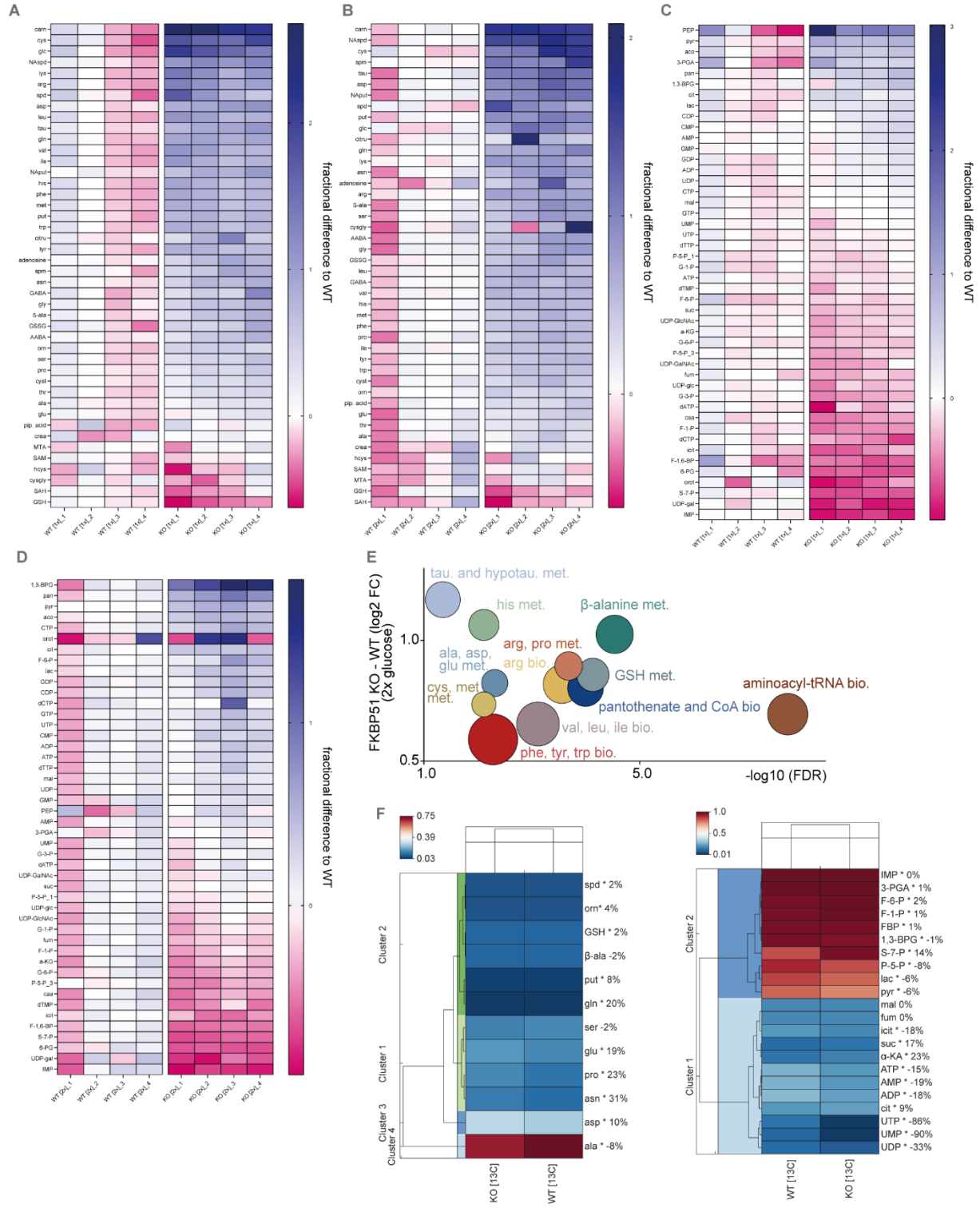
Fig. S1: FKBP51 deletion alters AMPK and mTOR-associated amino acid metabolic and biosynthetic pathways. A) Heatmap of altered amine-containing (Bz) metabolites in SH-SY5Y cells lacking FKBP51 and WT control cells cultured under normal glucose condition (1x, 4.5 g/l) and **(B)** increased glucose condition (2x, 9 g/l). **(C)** Heatmaps of altered anionic (IC) metabolites in SH-SY5Y cells lacking FKBP51 compared to WT control cells under normal and **(D)** increased glucose culturing conditions. The fractional differences of each replicate are shown for all metabolites comparing the genotype and the different glucose conditions. **(E)** Analysis and regulation of significantly altered pathways of FKBP51 KO and WT cells under excessive glucose conditions. The f(x)-axis shows the (median) log2 fold change (FC) of all significantly altered metabolites of the indicated pathway and the false discovery rate (FDR, equals the –log10 adjusted p-value) is shown on the x-axis. The size of the circles represents the amount of significantly changed metabolites in comparison to all metabolites of a particular pathway. **(F)** Analysis of the metabolic flux in FKBP51 KO cells compared to WT cells using C13 glucose as tracer. The enrichment of C13 is displayed for each metabolite investigated.

Fig. S2: FKBP51 deletion alters AMPK and mTOR-associated amino acid metabolic and biosynthetic pathways in murine neuroblastoma cells.
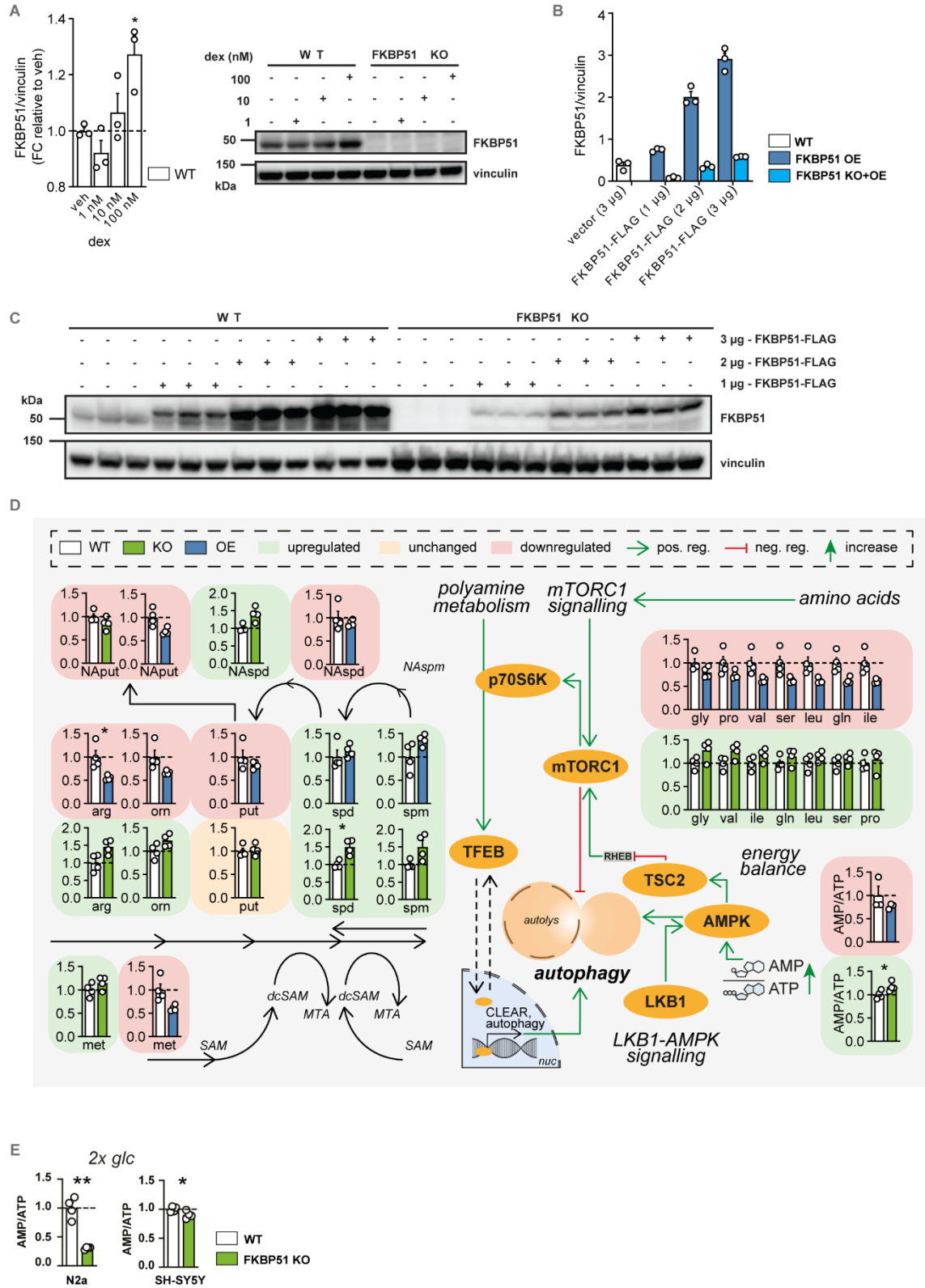
Fig. S2: FKBP51 deletion alters AMPK and mTOR- associated amino acid metabolic and biosynthetic pathways in murine neuroblastoma cells. (A, B) Validation of FKPB51 responsiveness in WT N2a cells to dexamethasone stimulation. **(C)** Titration of FKBP51-FLAG expression construct in FKBP51 WT and KO N2a cells (n=3). **(D)** FKBP51 deletion and overexpression (OE) in N2a cells alters metabolites of the polyamine pathway and levels of amino acids associated with mTOR signaling. **(E)** AMP/ATP ratio in N2a and SH-SY5Y FKBP51 KO cells under increased glucose conditions. All data are shown as relative fold change compared to control condition; ± s.e.m.; One-way ANOVA followed by Dunnett's multiple comparison test for **A**, the paired student's t-test was performed in **D** and **E**. * $p < 0.05$, **$p < 0.01$, ***$p < 0.001$; Abbreviations: AMP, adenosine monophosphate; AMPK, AMP-activated protein kinase; arg, arginine; ATP, adenosine triphosphate; dex, dexamethasone; dcSAM, decarboxylated S-adenosylmethione; glc, glucose; gln, glutamine; gly, glycine; ile, isoleucine; leu, leucine; LKB1, liver kinase B 1; met, methionine; MTA, 5'-methylthioadenosine; mTORC1, mechanistic target of rapamycin complex 1; NAput, N-acetylputrescine; NAspd, N-acetylspermidine; NAspm, N-acetylspermine; orn, ornithine pro; proline; put, putrescine; SAM, S-adenosylmethionine; ser, serine; spd, spermidine; spm, spermine; TFEB, transcription factor EB; TSC2, tuberous sclerosis complex 2; val, valine; veh, vehicle.

Fig. S3: *In-vitro* manipulation of FKBP51 and its effects on autophagy signaling.
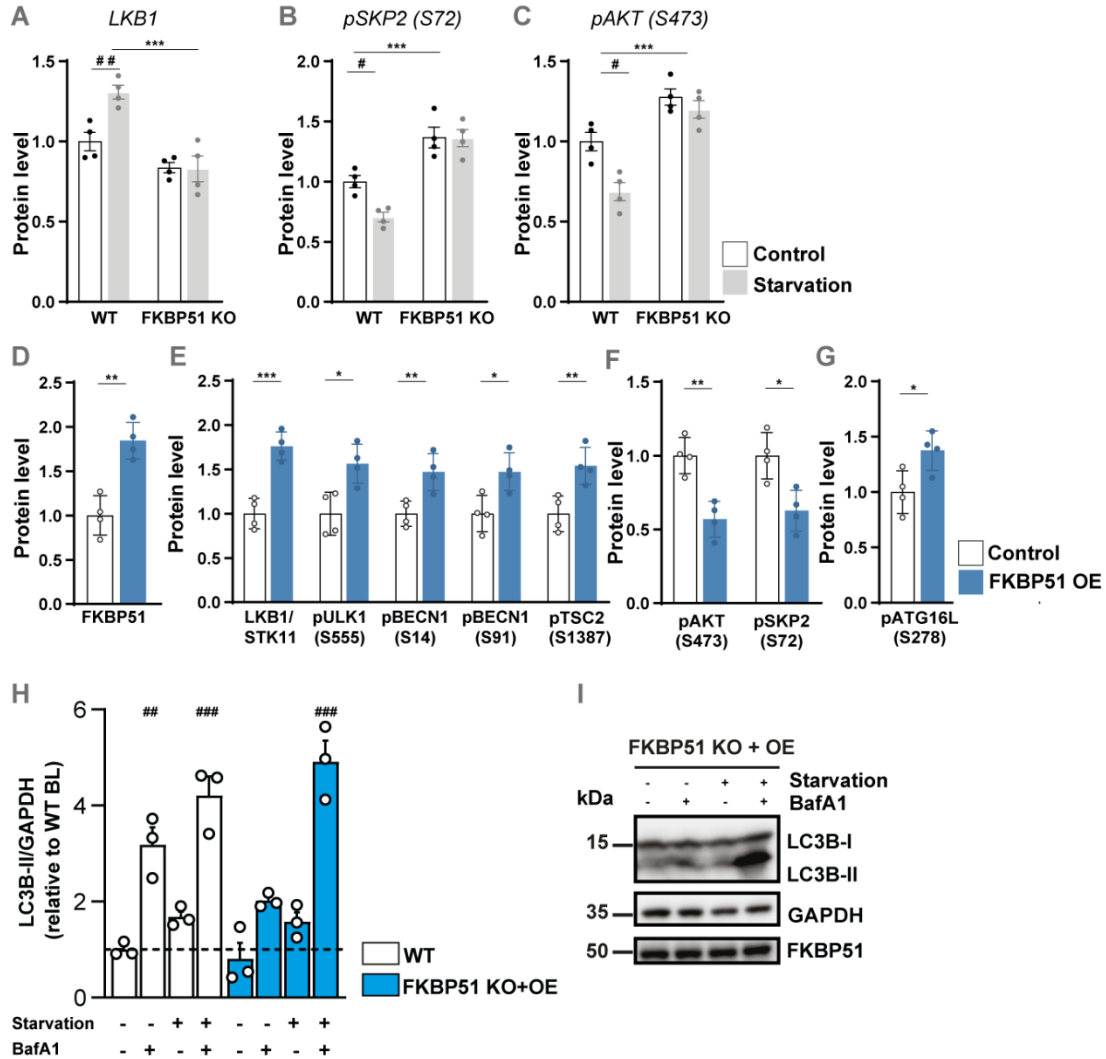
Fig. S3: In-vitro manipulation of FKBP51 and its effects on autophagy signaling. Wildtype (WT) or FKBP51 knockout (FKBP51 KO) cells were starved in HBSS medium for 4 h to induce autophagy. The levels of autophagy markers were determined by immunoblotting. **(A)** Quantification of LKB1, **(B)** pSKP2 (S72), and **(C)** pAKT (S473). **(D)** Validation of FKBP51 overexpression (FKBP51 OE) in mouse neuroblastoma cells. **(E)** FKBP51 OE in N2a cells enhanced phosphorylation of autophagy markers regulating autophagy initiation. **(F)** Quantification of pAKT (S473) and pSKP2 (S72). **(G)** Phosphorylation of ATGL16L1 at S278. **(H)** LC3B-II accumulation in FKBP51 KO+OE N2a cells in response to starvation and in the

presence or absence of BafA1 to assess autophagy flux **(I)**. Representative blots of autophagy flux assay. All data are shown as relative fold change compared to control condition; ± s.e.m.; a two-way ANOVA was performed in **(A-C)** and followed by a Tukey's multiple comparison test. One-way ANOVA followed by a Dunnett's multiple comparison test was performed for **(I)**. The unpaired student's t-test was performed in **(D-L)**. *$p < 0.05$, **$p < 0.01$, ***$p < 0.001$; # $p < 0.05$, ## $p < 0.01$. * = significant genotype effect; # = significant treatment effect.

Fig. S4: FKBP51 does not alter hypusination of elF5A.
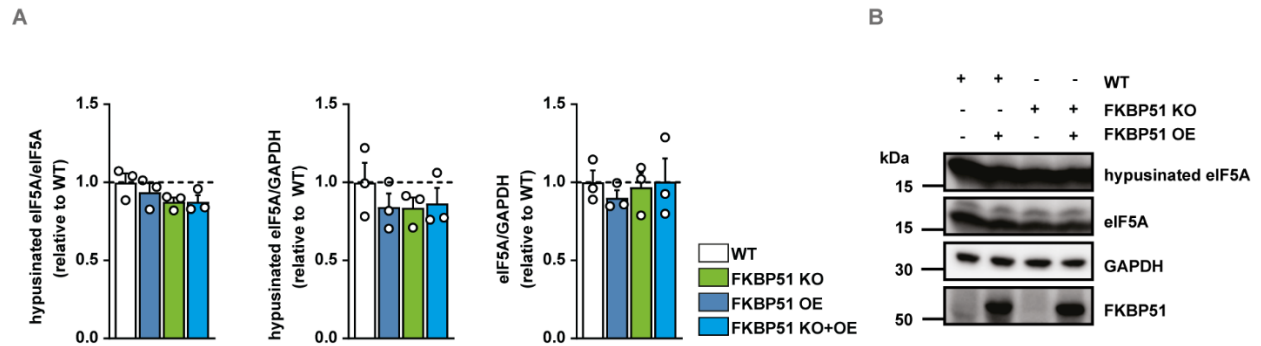
Fig. S4: FKBP51 does not alter hypusination of elF5A.

(A) Hypusination of elF5A is not affected by FKBP51 KO or expression level in N2a cells.

(B) Representative blots of hypusinated elF5A, total elF5A, GAPDH and FKBP51.

Fig. S5: *In-vitro* **manipulation of FKBP51 and its effects on autophagy signaling.**
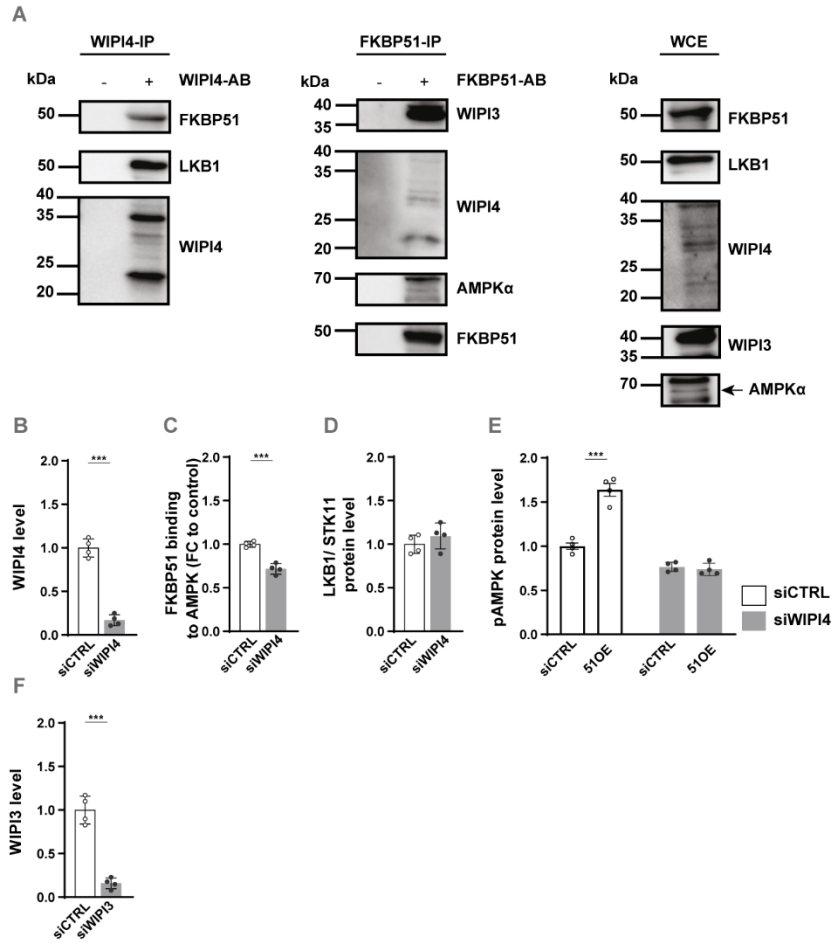
Fig. S5: FKBP51 associates with AMPK, TSC2, and WIPI3 & 4 to regulate autophagy and mTOR signaling. (A) Endogenously expressed FKBP51 associates with WIPI4, LKB1, WIPI3 and AMPKα in WT N2a cells. **(B)** Confirmation of WIPI4 KD in N2a cells. **(C)** FKBP51 binding to AMPKα1 in WIPI4 KD cells. **(D)** LKB1 binding to FKBP51 was not affected in WIPI4-KD cells**. (E)** WIPI4 KD blocked the FKBP51 overexpressing (51OE) effect on pAMPK at T172 **(F)** WIPI3 KD in N2a cells. All data are shown as relative fold change compared to control condition and were analyzed with an unpaired t-test.; ± SEM; * $p < 0.05$, **$p < 0.01$, ***$p < 0.001$.

Fig. S6: FKBP51 overexpression in the MBH affects sympathetic outflow to muscle and fat tissue.
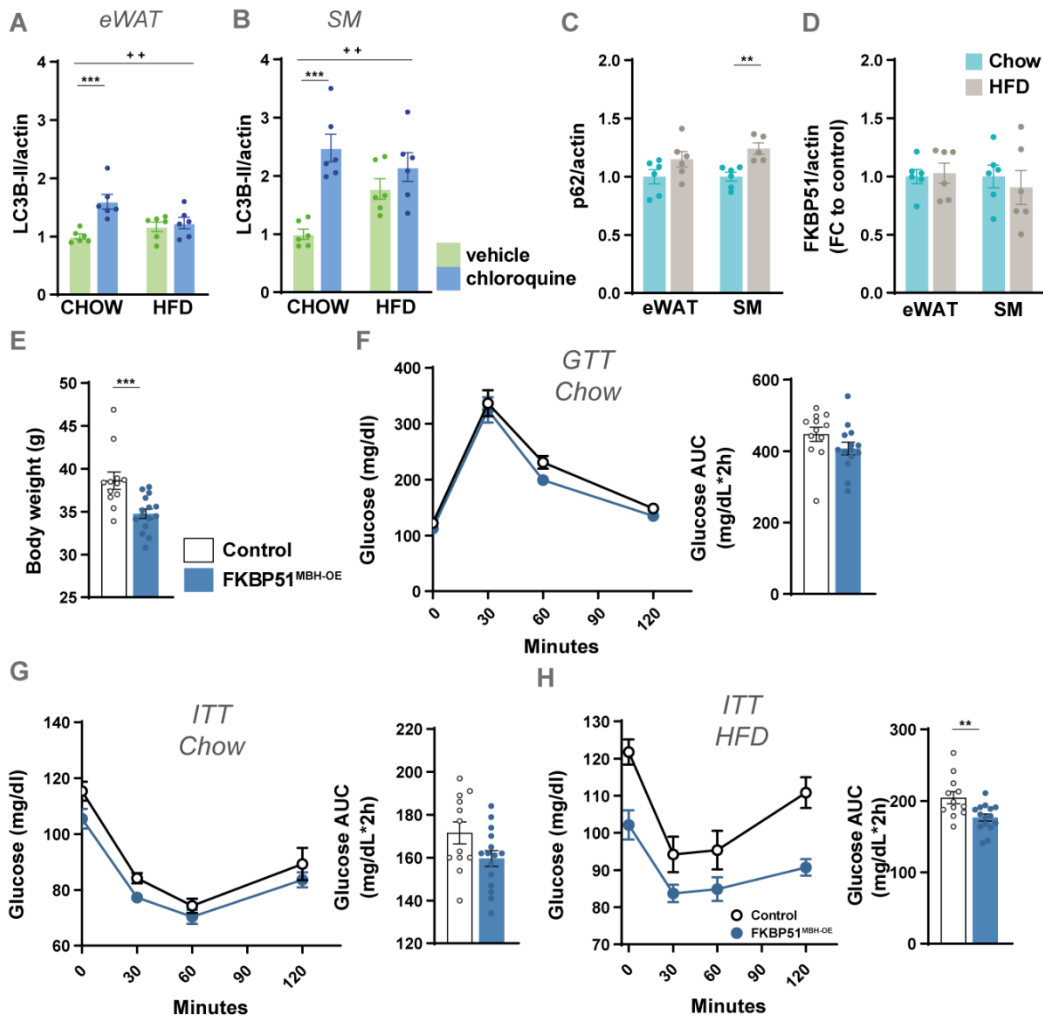
Fig. S6: FKBP51 overexpression in the MBH affects sympathetic outflow to muscle and fat tissue. (A) LC3B-II levels before and after chloroquine treatment (50 mg/kg) in eWAT and **(B)** soleus muscle under chow and HFD conditions **(C)** 10 weeks of HFD increased the accumulation of the autophagy receptor p62 in SM, but not in eWAT. **(D)** FKBP51 expression in soleus muscle (SM) and epididymal white adipose tissue (eWAT) after 10 weeks of HFD. **(E)** Overexpression of FKBP51 in a second cohort of C57/Bl6 animals resulted in a lean body weight phenotype after 10 weeks of HFD**. (F-H)** Differences in glucose metabolism were investigated by performing a

glucose tolerance test (GTT) and an insulin tolerance test (ITT) under chow and HFD conditions. For **(A, B)** a two-way ANOVA was performed followed by a Tukey's multiple comparisons test and data are shown as relative fold change compared to control condition. For **(C - H)** an unpaired student's t-test was performed. ± SEM; * $p < 0.05$, **$p < 0.01$, ***$p < 0.001$; + $p < 0.05$, ++ $p < 0.01$. * = significant treatment effect; + = significant treatment x diet interaction.

Fig. S7: FKBP51 regulates autophagy signaling in the MBH.
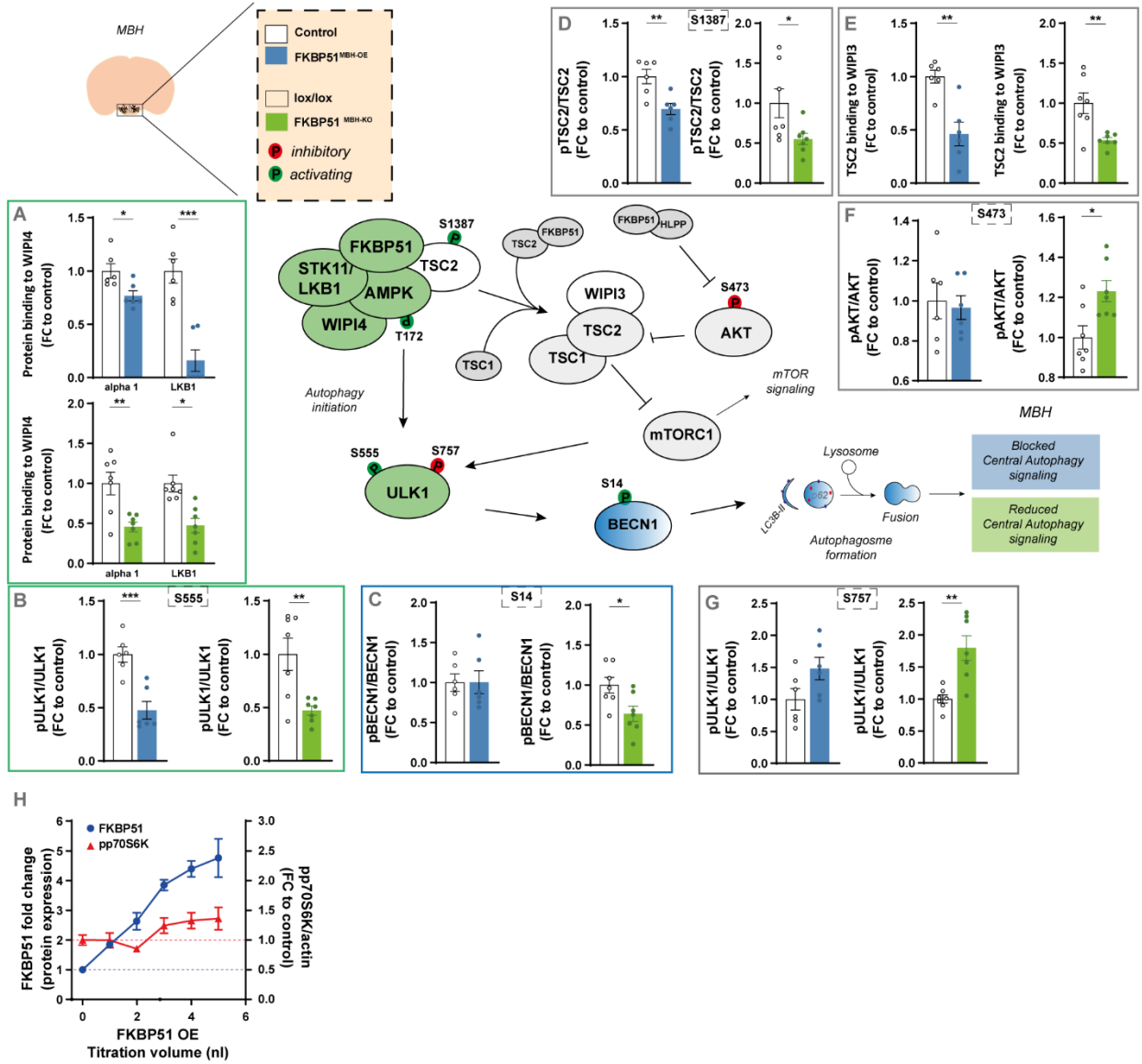
Fig. S7: FKBP51 regulates autophagy signaling in the MBH. Pathway analysis of main autophagy and mTOR regulators in the mediobasal hypothalamus (MBH). FKBP51 overexpression is depicted in blue and FKBP51 deletion is depicted in green. **(A)** Quantification of LKB1 and AMPK binding to WIPI4. **(B)** Phosphorylation of ULK1 at S555**, (C)** pBECN1 at S14, **(D)** pTSC2 at S1387. **(E)** Quantification of TSC2 binding to WIPI3. **(F)** Phosphorylation of AKT at S473, and **(G)** ULK1 at S757. **(H)** Quantification of pp70S6K while titrating AAV-HA-

FKBP51 virus into N2a cells. All data are shown as relative fold change compared to control condition and were analyzed with an unpaired t-test.; $\pm$ SEM; $*$ $p < 0.05$, $**p < 0.01$, $***p < 0.001$.

Fig. S8: Effects of hypothalamic FKBP51 overexpression on peripheral autophagy signaling.
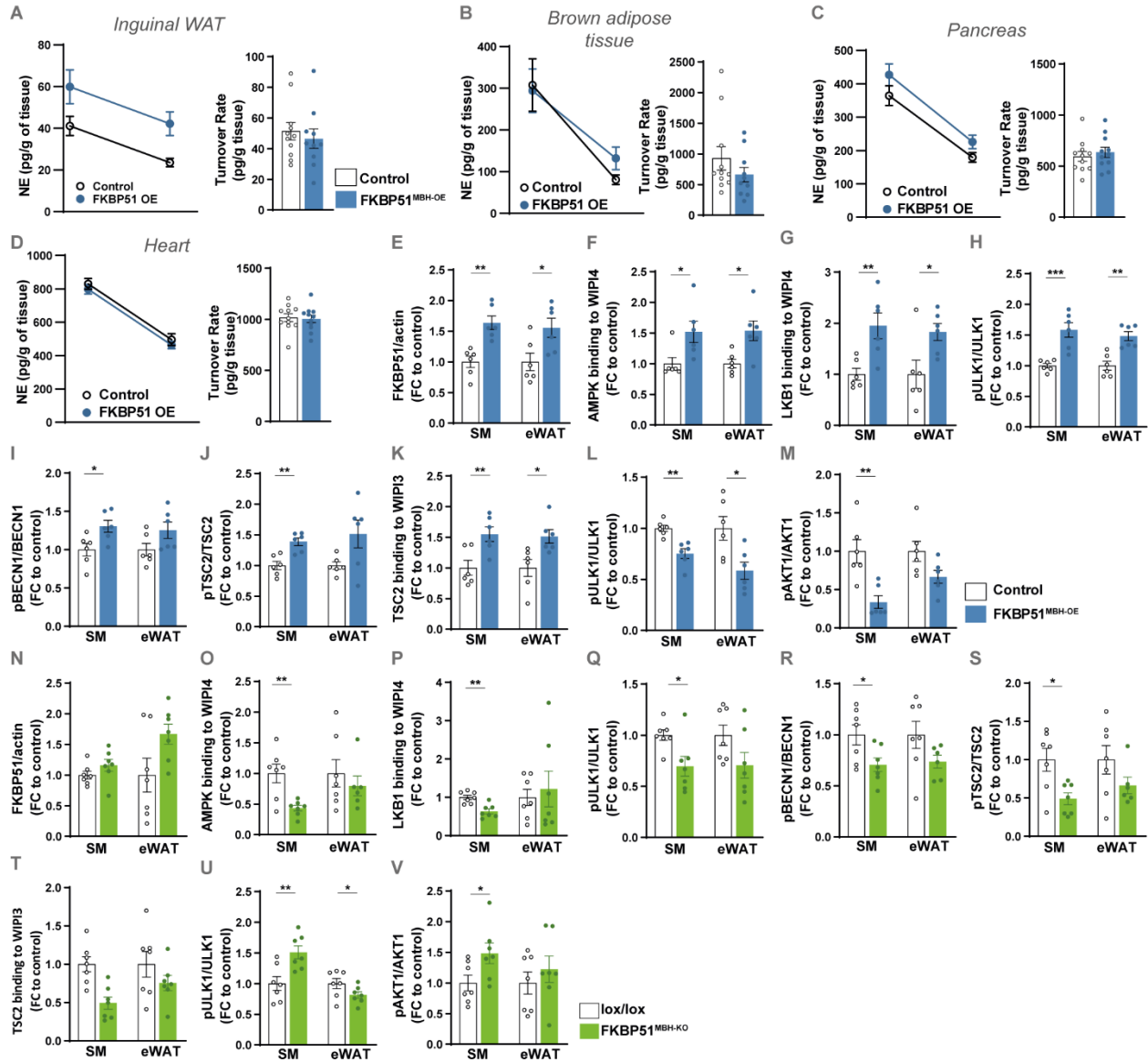
Fig. S8: Effects of hypothalamic FKBP51 overexpression on peripheral autophagy signaling.

(A-D) Representative decrease in tissue NE content after MPT injection (left panel) and turnover rate (right panel) were determined on inguinal WAT and brown adipose tissue (BAT), pancreas, and heart. **(E-V)** Pathway analysis of main autophagy and mTOR marker in the soleus muscle (SM) and epididymal white adipose tissue (eWAT). FKBP51 overexpression is depicted in blue and FKBP51 deletion is depicted in green. **(E)** Quantification of FKBP51 protein level. **(F)**

Quantification of AMPK and **(G)** LKB1 binding to WIPI4. **(H)** Phosphorylation of ULK1 at S555**,** **(I)** pBECN1 at S14, **(J)** TSC2 at S1387. **(K)** Quantification of TSC2 binding to WIPI3. **(L)** Phosphorylation of ULK1 at S757, and **(M)** AKT1 at S473. **(N)** FKBP51 level in SM and eWAT of FKBP51$^{\text{MBH-KO}}$ mice. **(O)** Quantification of AMPK and **(P)** LKB1 binding to WIPI4. **(Q)** Phosphorylation of ULK1 at S555**, (R)** pBECN1 at S14, **(S)** TSC2 at S1387. **(T)** Quantification of TSC2 binding to WIPI3. **(U)** Phosphorylation of ULK1 at S757, and **(V)** AKT1 at S473. All data are shown as relative fold change compared to control condition and were analyzed with an unpaired t-test.; ± SEM; * $p < 0.05$, **$p < 0.01$, ***$p < 0.001$.

Fig. S9: AMPK and mTOR signaling was not affected in in liver tissue of FKBP51$^{\text{MBH-KO}}$ mice.
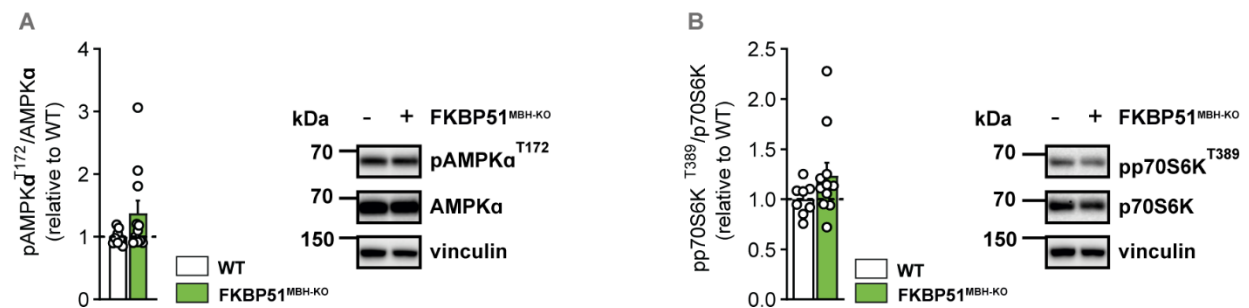
Fig. S9: AMPK and mTOR signaling was not affected in liver tissue of FKBP51$^{\text{MBH-KO}}$ mice. **(A)** Representative blots and quantification of AMPK phosphorylation at T172 and **(B)** p70S6K in liver tissue of FKBP51$^{\text{MBH-KO}}$ mice (n = 8 for WT, n = 11 for KO). All data are shown as relative fold change compared to control condition and were analyzed with an unpaired t-test.; ± SEM; * $p < 0.05$, **$p < 0.01$, ***$p < 0.001$.

Fig. S10:
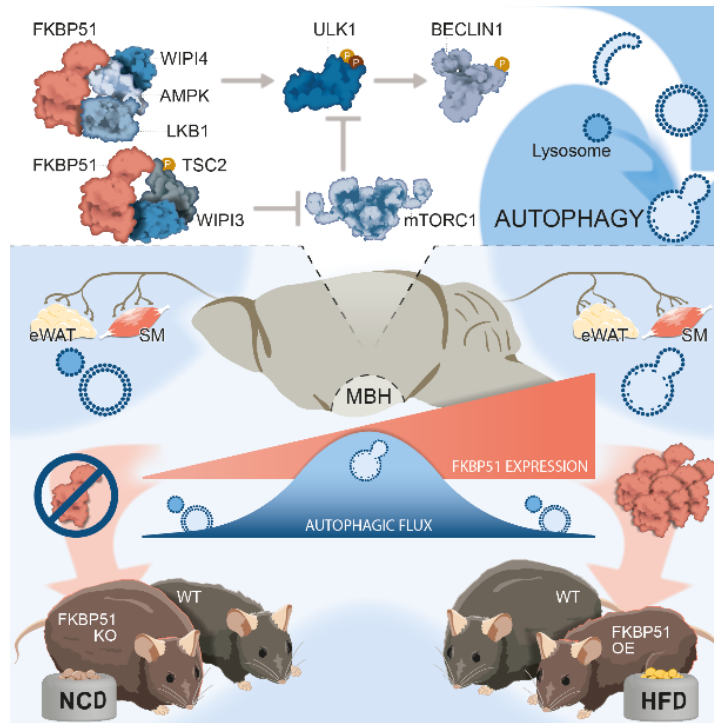
Fig. S10: The stress-responsive FKBP51 controls body weight gain by regulating the balance between autophagy and mTOR signaling. We identified FKBP51 as a central nexus for the recruitment of the LKB1/AMPK complex to WIPI4 and TSC2 to WIPI3, thereby regulating the balance between autophagy and mTOR signaling in response to metabolic challenges. MBH FKBP51 dose-dependently regulates autophagy both in the brain as well as in peripheral metabolic tissues. Consequently, deletion of MBH FKBP51 strongly induces obesity, while its overexpression protects against high-fat diet (HFD) induced obesity.

2.4 Contribution of the co-chaperone FKBP51 in the ventromedial hypothalamus to metabolic homeostasis in male and female mice

Brix, L.M., Toksöz, I., Aman, L., Bordes, J., Doeselaar, L.V., Engelhardt, C., Häusl, A.S., Kovarova, V., Narayan, S., Springer, M., Sterlemann, Yang, H., Deussing, J.M. & Schmidt, M.V.

Abstract

Objective: Steroidogenic factor 1 (SF1) expressing neurons in the ventromedial hypothalamus (VMH) have been directly implicated in whole-body metabolism and in the onset of obesity. The co-chaperone FKBP51 is abundantly expressed in the VMH and was recently linked to type 2 diabetes, insulin resistance, adipogenesis, browning of white adipose tissue (WAT) and bodyweight regulation.

Methods: We investigated the role of FKBP51 in the VMH by conditional deletion and virus-mediated overexpression of FKBP51 in SF1-positive neurons. Baseline and high fat diet (HFD)-induced metabolic- and stress-related phenotypes in male and female mice were obtained.

Results: In contrast to previously reported robust phenotypes of FKBP51 manipulation in the entire mediobasal hypothalamus (MBH), selective deletion or overexpression of FKBP51 in the VMH resulted in only a moderate alteration of HFD-induced bodyweight gain and body composition, independent of sex.

Conclusions: Overall, this study shows that animals lacking and overexpressing *Fkbp5* in *Sf1*-expressing cells within the VMH display only a mild metabolic phenotype compared to an MBH-wide manipulation of this gene, suggesting that FKBP51 in SF1 neurons within this hypothalamic nucleus plays a subsidiary role in controlling whole-body metabolism.

1. Introduction

Since the ventromedial hypothalamus (VMH) was first described as a site for body weight regulation and food intake in 1942 by Hetherington and Ranson (Hetherington and Ranson, 1942) it has been convincingly demonstrated that this mediobasal hypothalamic (MBH) nucleus directly steers food intake, whole-body metabolism, and energy homeostasis (Choi et al., 2013; King, 2006). Hetherington's and other early VMH lesion studies concurringly observed hyperphagia, insulin resistance, and dramatic body weight gain following the loss of VMH function (Anand and Brobeck, 1951; Brobeck, 1946; Kennedy, 1950).

The heterogenous cytoarchitecture of the VMH is comprised of various cell types with different gene expression patterns (McClellan et al., 2006). Intriguingly, the ubiquitously expressed *Nr5a1* gene, encoding steroidogenic factor 1 (SF1), is specifically and exclusively expressed within the VMH in the brain. Here, it acts as a transcription factor, which expression is essential for both VMH development and function (Kurrasch et al., 2007; Parker et al., 2002; Segal et al., 2005). Studies using postnatal VMH-specific SF1 knockout (KO) mice mirrored the metabolic phenotype of VMH lesion in rats, highlighting the cruciality of SF1 in the VMH for healthy energy homeostasis; together with its role as a primary satiety center (Dhillon et al., 2006; Kim et al., 2011). Chemo- and optogenetic techniques, allowing for spatiotemporal neuronal manipulation, revealed that inactivation of *Sf1*-expressing neurons increased feeding behavior, reduced energy expenditure and thermogenesis, and blocked recovery from insulin-induced hypoglycemia via a plethora of different hormone receptors, including leptin- (LepR) and insulin receptor (IR), nutrient sensors and sympathetic nervous system (SNS) activation (Fosch et al., 2021). A recent study by Coupé et al. further demonstrated the importance of autophagy signaling within the VMH in response to fasting: mice lacking the autophagy-related gene 7 (*Atg7*) within the VMH displayed altered leptin sensitivity and disrupted energy expenditure in response to fasting. Additionally, from a cellular metabolism perspective, they had impaired mitochondrial morphology and activity (Coupé et al., 2021).

In the periphery, SF1 is expressed in steroidogenic tissue of the adrenal cortex, in gonadotrope cells of the anterior pituitary, and gonads with differential roles during development. A global SF1 KO was shown to be lethal, with animals exhibiting a complex endocrine phenotype including gonadal and adrenal agenesis, impaired expression of pituitary gonadotropes and ablation of the VMH. Altogether, indicating that SF1 acts at multiple levels of this hypothalamic-pituitary-steroidogenic organ axis to regulate

steroidogenesis, reproduction and energy homeostasis (Hoivik et al., 2010; Majdic et al., 2002; Sadovsky et al., 1995; Zhao et al., 2004).

Another gene expressed at described sites along this axis, including the VMH, adrenal and pituitary is the FKBP506 binding protein 51 (FKBP51), encoded by the *Fkbp5* gene (Balsevich et al., 2014; Brix et al., 2022; Jenkins et al., 2013; Scharf et al., 2011). This protein belongs to the superfamily of immunophilins, and as a co-chaperone of heat-shock protein 90 (Hsp90) it regulates the responsiveness of steroid hormone receptors (Sinars et al., 2003). Several studies identified FKBP51 as a strong inhibitor of glucocorticoid receptor (GR) function by reducing glucocorticoid (GC) binding, delaying nuclear translocation and decreasing GR-dependent transcriptional activity, thereby shaping (GR)-mediated negative feedback of the hormonal stress response system, the hypothalamic-pituitary-adrenal (HPA) axis (De Kloet et al., 2005; Denny et al., 2000; Scammell et al., 2001; Westberry et al., 2006; Wochnik et al., 2005). The first cell type-specific murine KO studies recently published by our lab found that FKBP51 in the paraventricular nucleus (PVN) of the hypothalamus and in corticotrope proopiomelanocortin (POMC) cells of the anterior pituitary shape negative feedback and (re)activity of the HPA axis (Brix et al., 2022; Häusl et al., 2021).

Besides its function along the HPA axis in humans and rodents, FKBP51 is abundantly expressed in metabolically relevant tissues in the periphery, such as adipocytes and skeletal muscle (Balsevich et al., 2017; Baughman et al., 1997; Pereira et al., 2014; Sidibeh et al., 2018) and brain regions, like the arcuate nucleus (ARC) and VMH, both well-established as neuronal hubs controlling energy balance (Balsevich et al., 2014; Gautron et al., 2015; Scharf et al., 2011). Today, there is an increasing body of research providing evidence on the role of FKBP51 in type 2 diabetes, insulin resistance, adipogenesis, browning of white adipose tissue (WAT), and bodyweight regulation (Häusl et al., 2019; Smedlund et al., 2021). We and other colleagues showed that FKBP51-null mice are resistant to diet-induced obesity and demonstrate improved glucose tolerance and increased insulin-signaling in skeletal muscle. Furthermore, chronic treatment with a highly selective FKBP51 antagonist, SAFit2, recapitulates the effects of FKBP51 deletion on both body weight regulation and glucose tolerance (Balsevich et al., 2017; Hartmann et al., 2012; Stechschulte et al., 2016). The investigation of central *Fkbp5* mRNA expression in response to a metabolic challenge, either a high-fat diet (HFD) or fasting, revealed that hypothalamic *Fkbp5* in the VMH, PVN, and arcuate nucleus (ARC) is increased following a metabolic stressor (Balsevich et al., 2014;

Scharf et al., 2011; Yang et al., 2012). Based on the molecular interplay of FKBP51 with cellular autophagy (Gassen et al., 2015, 2014; Häusl et al., 2019), our lab recently uncovered that FKBP51 in the rodent MBH represents a novel regulatory link between central and peripheral autophagy signaling and the *in vivo* whole-body response to an obesogenic challenge, and that KO of *Fkbp5* in the MBH results in opposite metabolic phenotypes to those observed in FKBP51-null mice (Häusl et al., 2022).

Overall, there is strong evidence that central and peripheral FKBP51 is a molecular player in human and rodent metabolism, with a powerful role in MBH-mediated control of autophagy signaling. Thus, strategies aimed at manipulating FKBP51 could provide a new therapy approach to treat metabolic disorders such as obesity and type 2 diabetes. However, the MBH-specific FKBP51 manipulation study by Häusl and colleagues (Häusl et al., 2022) once again exhibited the highly tissue-specific manner this protein acts in, together with its dynamic regulation by the environment. To address the lack of central cell type-specific studies on the role of FKBP51 on whole-body metabolism, we here investigated baseline and HFD-induced metabolic- and stress-related phenotypes in male and female mice with a conditional KO of *Fkbp5* in all *Sf1*-expressing cells ($Sf1^{Fkbp5-/-}$), mainly involving the VMH, adrenals, and pituitary (Balsevich et al., 2014; Jenkins et al., 2013; Scharf et al., 2011). To narrow down metabolic effects observed in $Sf1^{Fkbp5-/-}$ mice to the VMH, we virally overexpressed *Fkbp5* exclusively in *Sf1*-expressing ($Sf1^{Fkbp5\ OE}$) cells within this nucleus. Overall, our results show that while a KO and OE of *Fkbp5* in the VMH induced a slightly increased HFD-induced BW gain and decreased adrenal weights in $Sf1^{Fkbp5-/-}$ and $Sf1^{Fkbp5\ OE}$ males and females, this nucleus does not account for the robust metabolic alterations observed following whole MBH FKBP51 manipulations.

2. Materials and Methods

2.1 Animals and animal housing

All experiments and protocols were performed in accordance with the European Communities' Council Directive 2010/63/EU and were approved by the committee for the Care and Use of Laboratory animals of the Government of Upper Bavaria. All effort was made to minimize any suffering of the animals throughout the experiments. The mouse lines *Fkbp5^lox/lox^*, *Sf1^Fkbp5-/-^* and *Sf1-Cre* were obtained from the in-house breeding facility of the Max Planck Institute of Psychiatry and are all bred on C57/BL6N background. All animals were between 12 – 20 months old at the onset of the experiments. Male *Sf1^Fkbp5-/-^* animals were kept single housed and female mice were group housed throughout the experiments, unless indicated otherwise. All animals were held in individually ventilated cages (IVC; 30cm x 16 cm x 16 cm; 501 cm^2) serviced by a central airflow system (Tecniplast, IVC Green Line – GM500). Animals had *ad libitum* access to water (tap water) and food (see 2.3) and were maintained under constant environmental conditions (12:12 hr light/dark cycle, 23 ± 2 °C and humidity of 55%). All IVCs had sufficient bedding and nesting material as well as a wooden tunnel for environmental enrichment. Animals were allocated to experimental groups in a semi-randomized fashion, data analysis and execution of experiments were performed blinded to group allocation.

2.2 Generation of *Fkbp5^lox/lox^* and *Sf1^Fkbp5-/-^* lines

Mice with a floxed *Fkbp5* gene designated as *Fkbp5^lox/lox^* (*Fkbp5^tm1c(KOMP)Wtsi^*) were obtained by breeding *Fkbp5^Frt/Frt^* full KO mice to Deleter-Flpe mice (Rodríguez et al., 2000). The conditional *Fkbp5^Frt/Frt^* KO mice are derived from embryonic stem cell clone EPD0741_3_H03 which was targeted by the KO mouse project (KOMP). Frozen sperm obtained from the KOMP repository at UC Davis was used to generate KO mice (*Fkbp5^tm1a(KOMP)Wtsi^*) by *in vitro* fertilization. Finally, mice lacking *Fkbp5* in SF1 cells (*Sf1^Fkbp5-/-^*) were obtained by breeding *Fkbp5^lox/lox^* mice to *Sf1-Cre* mice that express *Cre* recombinase under the control of the *Sf1* promoter (approved mouse gene name, *Nr5a1*) (Dhillon et al., 2006). Genotyping details are available upon request.

2.3 Diet for induced obesity

Baseline metabolic characterization of all experimental cohorts was performed under a standard chow diet (standard research diet by Altromin 1318, Altromin GmbH, Germany) with the following nutritional values: 14 % fat and sucrose, 27 % protein, and 59 % carbohydrates. Animals under dietary challenge received a HFD diet (HFD, D12331, Research Diets, New Brunswick, NJ, USA) over a period of several weeks to induce overweight. Nutritional values HFD: 58 % fat and sucrose, 17 % protein, 25 % carbohydrates. Bodyweight and food intake were measured weekly in all experimental cohorts.

2.4 Viral overexpression of *Fkbp5* in the VMH

SF1-specific overexpression (OE) of human *Fkbp5* ($Sf1^{Fkbp5\ OE}$) was achieved by bilateral injections of the Cre-dependent viral vector AAV1/2-Cre-dept-HA-FKBP51 (rAAV1/2-Cre-dependent-CAG-HA-human wildtype FKBP51 WPRE-BGH-polyA, titer: 1.3 x 10^{12} genomic particles/ml, Gene Detect GD1001-RV) into the VMH of male *Sf1-Cre* mice. As controls, *Cre*-negative animals of this mouse line were injected with an AAV2-eSyn-GFP control virus (CMV-hSYN1-eGFP, titer: 1.3 x 10^{12} genomic particles/ml, Vector Biolabs VB1107) for neuronal expression of a fluorescent reporter. Stereotactic surgeries were performed as described previously (Häusl et al., 2021). In brief, male mice between 3 to 5 months of age were anesthetized with isoflurane and fixated in a stereotactic apparatus. Then, 0.2 µl of the above-mentioned viruses were bilaterally injected into the VMH at a 0.05 µl/min flow rate with glass capillaries with a tip resistance of 2 – 4 MΩ. To target the VMH the following coordinates were used: - 1.5 mm anterior to bregma, ± 0.4 mm lateral from midline, and 5.6 mm below the surface of the skull. After surgery, animals were treated with meloxicam for three days and were allowed to recover for four weeks before initiating the experimental phase.

2.5 RNAScope – Validation of *Fkbp5* KO and OE

To validate successful KO of *Fkbp5* mRNA in $Sf1^+$ cells, we performed a RNAScope experiment on tissue sections of male $Sf1^{Fkbp5-/-}$ and $Fkbp5^{lox/lox}$ animals under basal conditions (3 – 4 months of age). Frozen tissue was sectioned at 20 µm at -20 °C in a cryostat microtome. Sections were thaw mounted on Super Frost Plus slides, dried, and stored at -80 °C. The RNA Scope Fluorescent Multiplex Reagent kit (cat. no. 320850, Advanced Cell Diagnostics, Newark,

CA, USA) was used for mRNA staining. Probes used for staining were; *Fkbp5* (Mm-Fkbp5-C1) for native *Fkbp5* expression, human *Fkbp5* (H-Fkbp5-C1) for detection of viral OE and *Sf1* (Mm-Nr5a1-C2). The *Fkpb5* probe targets Exon 9, which is deleted in our model, but the probe also spans neighboring exons. Consequently, the probe may still bind to truncated mRNA leading to a residual *Fkbp5* mRNA signal in knock-out cells, even though no functional FKBP51 protein can be expressed. The staining procedure was performed according to the manufacturer's specifications and as performed previously (Häusl et al., 2021). Images of the VMH (left and right side), pituitary, and adrenal were acquired by an experimenter blinded to the condition of the animals. Sixteen-bit images of each section were acquired on a Zeiss confocal microscope using a 20x and 40x objective (n = 2 animals per marker and condition). For every section, all images were acquired using identical settings for laser power, detector gain, and amplifier offset. *Fkbp5* mRNA expression was analyzed using ImageJ with the experimenter blinded to the genotype of the animals and was counted manually. Each *Sf1*^{+} cell containing one or more *Fkbp5* mRNA puncta was counted as positive and calculated as a percentage of *Fkbp5* positive cells from total number of *Sf1*-expressing cells.

2.6 *In-situ* hybridization in *Sf1*[Fkbp5 OE]

To quantify viral *Fkbp5* mRNA OE, we performed *in-situ* hybridization (ISH). Frozen brains were processed as described for RNAScope and ISH using a ^{35}S UTP labeled *Fkbp5* ribonucleotide probe was performed as described previously (Häusl et al., 2021; Schmidt et al., 2007). All primer details are available upon request. For signal detection, the slides were exposed to Kodak Biomax MR films (Eastman Kodak Co., Rochester, NY) and developed. The autoradiographs were digitized, and expression was determined by optical densitometry utilizing the freely available NIH ImageJ software (NIH, Bethesda, MD, USA). The grey value of the left and the right side of the VMH was measured within a circular template (16 width x 16 height) in every slice analyzed (1 slice per animal, 2 animals per group). The data were analyzed blindly, always subtracting the background signal of a nearby structure not expressing the gene of interest from the measurements.

2.8 Acute restraint stress paradigm

The acute restraint stress paradigm is perceived as a severe stressor robustly inducing the entire spectrum of known allostatic responses in rodents and was, therefore, the stress paradigm of choice. At 8:00 AM, one hour after the lights were switched on, each animal was placed in a custom-made restrainer (50 ml falcon tube with holes at the bottom and the lid to provide enough oxygen and space for tail movement) for 15 minutes in their home cage. After 15 minutes, animals were removed from the tube and the first blood sample was collected by a tail cut. Subsequent blood samples were collected at 15, 30, and 60 minutes post stress in the home cage via tail cut. The animals were left undisturbed in between sampling procedures.

2.9 Hormone assessment

Baseline morning (measured between 08:00 – 12:00 a.m.) and post stress plasma CORT (ng/mL) and baseline ACTH (pg/mL) concentrations were determined by radioimmunoassay using CORT ^{125}I RIA kit (sensitivity: 12.5 ng/ml, MP Biomedicals Inc) and ACTH ^{125}I RIA kit (sensitivity: 10 pg/ml, MP Biomedicals Inc) following the manufacturers' instructions. The radioactivity of the pellet was measured with a gamma counter (Packard Cobra II Auto Gamma; Perkin-Elmer). Final CORT and ACTH levels were derived from the standard curve.

2.10 Nuclear magnetic resonance

In addition to weekly measures of BW, the animal's body composition was assessed with a body composition analyzer (LF50 BCA NMR Minispec Analyzer, Bruker Optik) after several weeks on chow and HFD. This method applies time domain nuclear magnetic resonance (TD - NMR) to measure lean tissue mass, fat mass, and free fluids non-invasively and *in vivo* without the need for anesthetics in small rodents (Halldorsdottir et al., 2009). Body constituents were normalized to bodyweight for each group and the ratio of fat to lean mass was calculated.

2.11 Intraperitoneal glucose (GTT) and insulin (ITT) tolerance test

After several weeks under a chow diet, an intraperitoneal glucose tolerance test (GTT) was carried out after lights-on. A 20% D-(+)-Glucose solution (Sigma Aldrich, Merck, Darmstadt)

was prepared, and animals were subjected to an overnight fast of 14 hours (6 p.m. until 8 a.m.) prior to the experiment. Every animal was weighed and intraperitoneally injected with 2 g glucose per kg bodyweight. Blood glucose concentrations were measured from tail stitches at 0, 15, 30, 60, 90, and 120 minutes after the glucose injection using a handheld XT glucometer (Bayer Health Care, Basel, Switzerland).

An intraperitoneal insulin tolerance test (ITT) was performed 14 days after the GTT to ensure a complete recovery from the overnight fast. A similar procedure as for the GTT was applied as follows: An insulin stock solution of 0.5 IU/mL (Actrapid® Penfill®, Novo Nordisk Pharma GmbH, Bagsværd, Denmark) was prepared, and animals were fasted for 4 hours (7 until 11 a.m.) before the onset of the ITT. Every animal was weighed and intraperitoneally injected with 1IU insulin per kg bodyweight. Blood glucose concentrations were measured at 0, 15, 30, 60, 90, and 120 minutes after the insulin injection.

2.12 Indirect calorimetry

Metabolic phenotyping and food intake after several weeks on HFD challenge was conducted by an automated PhenoMaster open-circuit indirect calorimetry system (TSE Systems) in single housed male $Sf1^{Fkbp5-/-}$ and $Fkbp5^{lox/lox}$ mice. All animals were allowed to acclimatize to the experimental setup for 2 days with a total experimental duration and data acquisition of 7 days. The statistical analysis was performed exclusively on data from day 3 to day 6 (total of 72 hours) for all animals. The time plots were generated from hourly averages of all parameters over 72 hours. Totals were calculated as the average of all measures over 72 hours. HFD and water were available ad libitum. The data acquisition was carried out by TSE Phenomaster version 7.2.8.

2.13 Statistical analysis

The data presented are shown as means ± standard error of the mean (SEM) and samples sizes are indicated in the figure legends and the main text. All data were analyzed by the commercially available GraphPad Prism 9.0 software (GraphPad Software, San Diego, California, USA). When two groups were compared, the unpaired two-tailed *student's t test* was applied. If data were not normally distributed the non-parametric *Mann-Whitney test* (*MW test*) was used. Data based on repeated observations comparing two groups were tested

by repeated measures ANOVA. P values of less than 0.05 were considered statistically significant. Statistical significance was defined as: $*p \leq 0.05$, $**p \leq 0.01$. A statistical trend was accepted with a p value of $0.05 \leq p \leq 0.1$ and indicated in the figures with the symbol "T". Outliers were assessed with the online available Graph Pad outlier calculator performing the two-sided *Grubb's* outlier test. As this was an exploratory study, no statistical methods were used to predetermine sample sizes.

3. Results

3.1 Validation of successful *Fkbp5* KO in VMH and metabolic phenotyping of male and female *Sf1$^{Fkbp5-/-}$* mice

As hypothalamic *Fkbp5* mRNA levels are highly responsive to dietary challenges such as prolonged HFD (Balsevich et al., 2014) and food restriction (Guarnieri et al., 2012; Scharf et al., 2011; Yang et al., 2012), this protein seems to sense the nutrient environment and to adjust its central expression to the given dietary conditions. Further, our group could show that hypothalamic FKBP51 can shape whole-body metabolism and steer central and peripheral autophagy (Häusl et al., 2022). Therefore, we hypothesized that a KO of *Fkbp5* specifically in VMH SF1 neurons could alter homeostasis and resemble observed metabolic phenotypes following *Fkbp5* manipulation in the whole MBH.

To study the effects of FKBP51 in *Sf1*-expressing neurons within the VMH on whole-body metabolism, we generated a SF1-specific conditional *Fkbp5* KO mouse line (*Sf1$^{Fkbp5-/-}$*). Qualitative co-expression analysis of *Fkbp5* and *Sf1$^+$* neurons in the VMH revealed that *Fkbp5* is almost exclusively expressed in *Sf1$^+$* neurons **(Fig. 1 A)**. Subsequent quantification of co-expression revealed that the number of *Sf1$^+$* cells expressing *Fkbp5* within the VMH is significantly reduced in *Sf1$^{Fkbp5-/-}$* mice compared to control *Fkbp5$^{lox/lox}$* mice ($t_6 = 3.13$, $p = 0.02$) confirming successful KO of *Fkbp5* in this neuronal population **(Fig. 1 B)**. Note that the residual *Fkbp5* signal in *Sf1$^{Fkbp5-/-}$* mice is likely due to the detection of truncated *Fkbp5* mRNA expression that does not lead to a functional protein. Assessment of weekly BW in a first cohort revealed non-significant but slightly increased HFD-induced BW gain in mice with a KO of *Fkbp5* (n = 13) compared to controls (n = 12), indicating a higher metabolic vulnerability to the dietary challenge ($F_{1,23} = 2.63$, $p = 0.12$) **(Fig. 1 C)**. This slight increase of BW-gain in *Sf1$^{Fkbp5-/-}$* animals could be confirmed by a significantly higher ratio of fat to lean mass in the KO animals after 8 weeks on a HFD (chow: $U = 49$, $p = 0.12$; HFD: $t_{23} = 2.36$, $p = 0.03$) **(Fig. 1 D)**. To assess the effects of our KO on glucose tolerance and insulin sensitivity under chow diet, we performed a GTT and ITT in a separate cohort **(Fig. 1 E)**, first confirming that these animals had the same phenotype as our 1st cohort (n$_{Sf1Fkbp5-/-}$ = 5; n$_{Fkbp5lox/lox}$ = 9) **(Supl. Fig. 1 A – B)**. Further, we performed a GTT and ITT after several weeks on a HFD (GTT: 16 weeks, ITT: 18 weeks) in the 1st cohort **(Fig. 1 F)**. Under both dietary regimens, KO and control animals showed typical blood glucose curve progression after a single glucose or insulin bolus, but no

difference between genotypes was detected (Chow: GTT t_{12} = 0.85, p = 0.42, ITT t_{12} = 1.67, p = 0.12; HFD: GTT t_{21} = 0.24, p = 0.81, ITT t_{23} = 0.66, p = 0.52). To allow deeper metabolic phenotyping, the animal's energy expenditure (EE), respiratory exchange ratio (RER), activity and food intake were measured in metabolic cages via indirect calorimetry. Repeated measures ANOVA did not detect significant differences between $Sf1^{Fkbp5-/-}$ KO animals and controls in any of the parameters assessed (RER: $F_{1,14}$ = 0.91, p = 0.36, t_{13} = 0.4, p = 0.7; EE: $F_{1,14}$ = 0.35, p = 0.56, t_{13} = 1.02, p = 0.33; activity: $F_{1,14}$ = 0.02, p = 0.9, t_{13} = 0.04, p = 0.1; food intake: $F_{1,12}$ = 0.91, p = 0.36, t_{12} = 1.26, p = 0.23) (Suppl. Fig. 2 A – H).
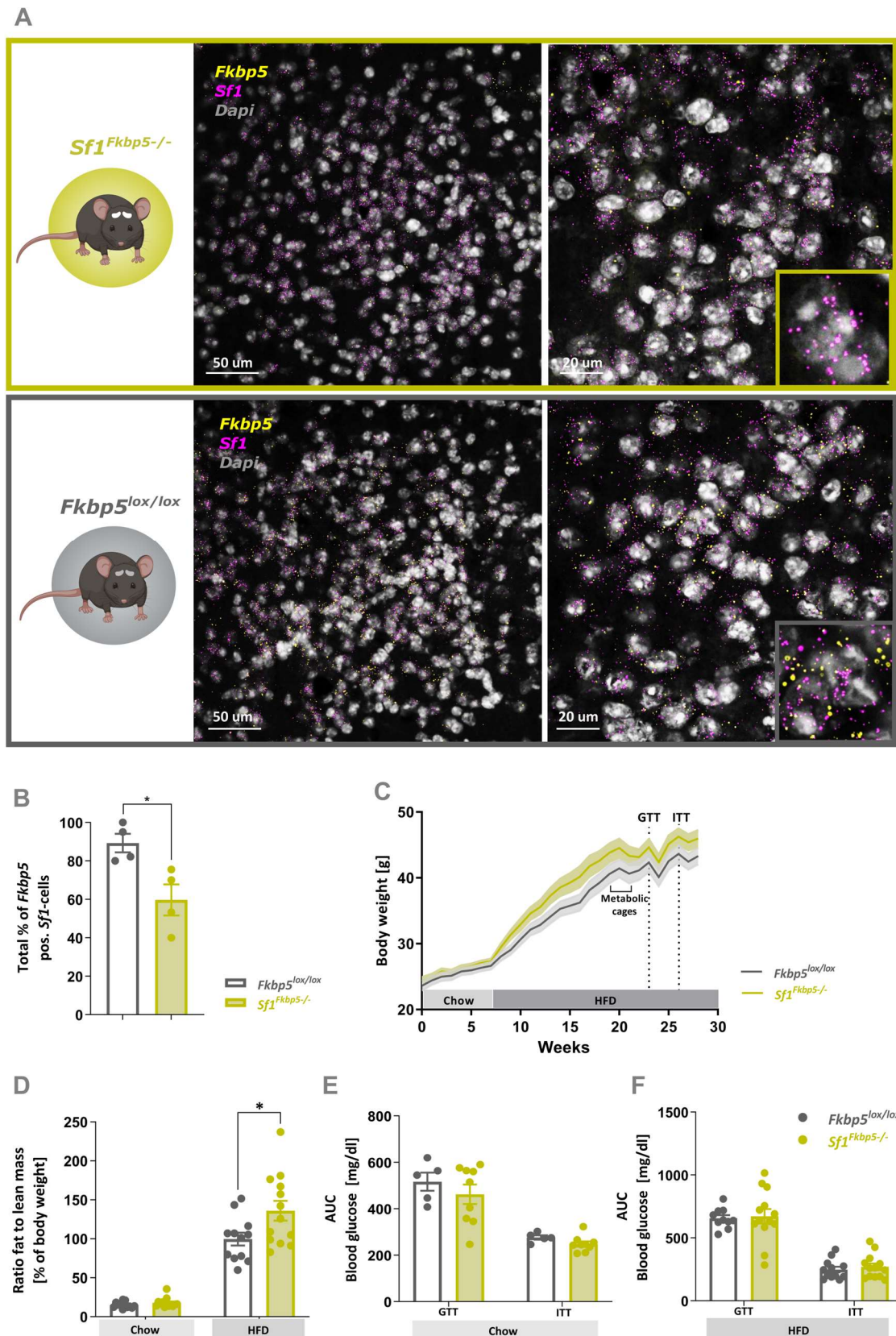
Figure 1: Conditional KO of *Fkbp5* in *Sf1*-expressing cells slightly increases BW gain under a HFD challenge in male mice

(A) Representative RNAScope confocal images of endogenous *Fkbp5* mRNA expression in SF1 neurons within the VMH of *Sf1Fkbp5-/-* (green panel) and *Fkbp5lox/lox* controls (grey panel). (B) Quantification of the

total percentage of *Fkbp5* positive cells that co-express *Sf1* mRNA revealed significant reduction of *Fkbp5* expression in the *Sf1$^{Fkbp5-/-}$* KO line (n = number of analyzed 40x confocal images of either left or right VMH, n$_{KO}$ = 4, n$_{Control}$ = 4; 2 animals/genotype). **(C)** In a first cohort under SD for 8 weeks and HFD for 21 weeks, *Sf1$^{Fkbp5-/-}$* mice *(n = 13)* displayed slightly increased HFD-induced BW gain compared to controls *(n = 12)* which was stable over time but non-significant. **(D)** Higher BW was reflected in a significant increase in the ratio of fat to lean mass in *Sf1$^{Fkbp5\ OE}$* in this cohort compared to controls after 8 weeks on a HFD. Blood glucose levels remained unchanged in the GTT and ITT under chow, which were assessed in a separate cohort (n$_{Sf1Fkbp5-/-}$ = 5; n$_{Fkbp5lox/lox}$ = 9) **(E),** and HFD in the first cohort **(F)**. Data are received from mice between 12 to 20 weeks of age and are presented as mean ± SEM. * p < 0.05. AUC area under the curve, GTT glucose tolerance test, ITT insulin tolerance test

Conditional KO of *Fkbp5* in female mice resembled metabolic phenotypes of male *Sf1$^{Fkbp5-/-}$* with a non-significant mild increase in HFD-induced BW gain over time ($F_{1,19}$ = 2.74, *p* = 0.11) **(Fig. 2 A)**, and an increase in the ratio of fat to lean mass already under chow (t_{18} = 2.48, *p* = 0.02) and after 8 weeks on HFD challenge (U = 29, *p* = 0.08) (n$_{Sf1Fkbp5-/-}$ = 9; n$_{Fkbp5lox/lox}$ = 12) **(Fig. 2 B)**. The group housing of mixed KO and control litters did not allow us to measure food intake in females.

In order to exclude that the mild metabolic phenotype of male and female *Sf1$^{Fkbp5-/-}$* KO animals was affected by the deletion of *Fkbp5* in *Sf1*-expressing cells of the pituitary (t_{12} = 3.08, *p* = 0.0097) and the adrenal gland (t_8 = 5.48, *p* = 0.0006) **(Suppl. Fig. 3 A - D)**, we assessed common HPA axis parameters in all experimental cohorts **(Suppl. Fig. 4 A – I)**. Adrenal weight was measured at the endpoint of each experiment and statistical analysis revealed significantly reduced relative adrenal weights in male KO mice under chow (t_8 = 3.49, *p* = 0.008) and after 21 weeks on a HFD (t_{12} = 2.41, *p* = 0.03) in two individual cohorts **(Suppl. Fig. 4 A)**. To determine if the function of the HPA axis was impaired by a KO of *Fkbp5* in cortical adrenal- and gonadotrope pituitary SF1 cells, morning CORT on chow and HFD and morning ACTH on HFD were assessed between 08:00 – 12:00 a.m. Both endocrine measures remained unchanged in male *Sf1$^{Fkbp5-/-}$* KO animals (CORT chow: U = 10, *p* = 0.37; CORT HFD: U = 67, *p* = 0.57; ACTH HFD: t_{23} = 1.25, *p* = 0.22) **(Suppl. Fig. 4 B and C)**. In line with the effects observed in male KO mice, relative adrenal weight was significantly decreased in female *Sf1$^{Fkbp5-/-}$* after 15 weeks on HFD (t_{11} = 4.09, *p* = 0.002) **(Suppl. Fig. 4 D)** without altering baseline CORT post HFD (t_{19} = 0.75, *p* = 0.46) **(Suppl. Fig. 4 E)**, indicating that HPA axis function is unaffected by a KO of *Fkbp5* in both sexes.

Together, data from male and female cohorts indicate that the KO of *Fkbp5* in *Sf1*-expressing cells has a mild impact on BW progression under a dietary challenge without altering other metabolic parameters assessed by indirect calorimetry. Interestingly, relative adrenal weight was significantly reduced in *Sf1Fkbp5-/-* males and females under chow and after HFD, but this had no consequences on HPA axis (re)activity.
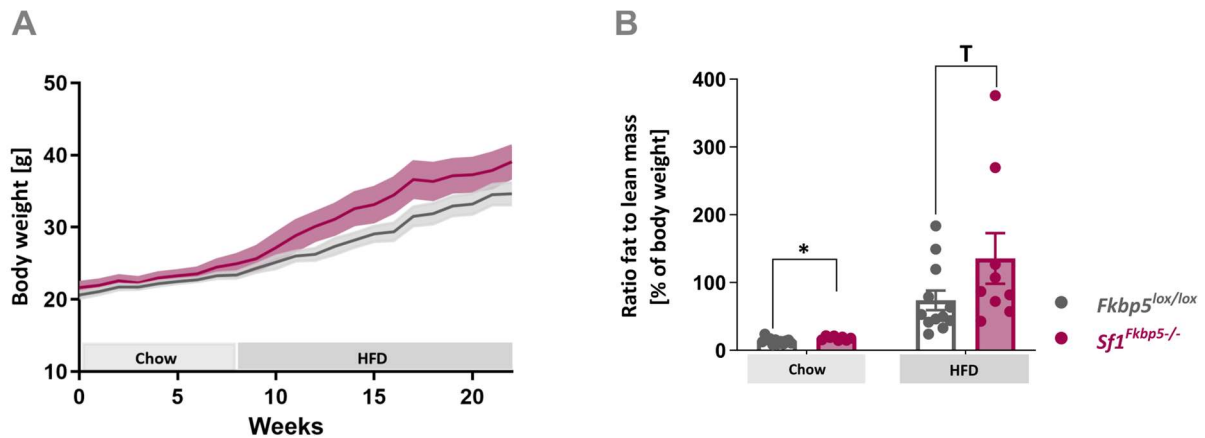
Figure 2: Conditional KO of *Fkbp5* in *Sf1*-expressing cells of female mice resembles male metabolic phenotype

(A) Female *Sf1Fkbp5-/-* (n = 9) mice displayed higher HFD-induced weight gain than control *Fkbp5lox/lox* (n = 12), thus resemble BW phenotype of the male KO cohort. (B) Female *Sf1Fkbp5-/-* ratio fat to lean mass is higher under a chow diet and after a dietary HFD challenge (15 weeks total). Data are received from mice between 8 to 12 weeks of age and are presented as mean ± SEM. * p < 0.05, T < 0.1.

3.2 Viral *Fkbp5* OE in SF1 neurons within the VMH induces similar phenotype to *Sf1Fkbp5-/-* males

To gain deeper understanding of how changes in *Fkbp5* expression levels within the VMH may control BW progression and changes in adrenal weight, and to narrow down observed effects on the VMH, we virally overexpressed *Fkbp5* exclusively in VMH SF1 neurons. SF1-specific OE of *Fkbp5* (*Sf1Fkbp5 OE*, n = 15) was achieved by bilateral injections of a *Cre*-dependent *Fkbp5* OE virus into the VMH of male *Sf1-Cre* mice. Controls (n = 16), were injected with an AAV2-eSyn-GFP control virus **(Fig. 3 A)**. Qualitative analysis of viral *Fkbp5* mRNA OE in RNAScope confocal images **(Fig. 3 B)** and *ISH* autoradiographs **(Fig. 3 C)** revealed a robust and SF1-specific increase of *Fkbp5* expression in the VMH of *Sf1Fkbp5 OE* mice. Quantification of *ISH* *Fkbp5* mRNA expression within the VMH revealed a significant 1.6-fold increase of gene expression in *Sf1Fkbp5 OE* animals (t_2 = 9.5, p = 0.01) **(Fig. 3 D)**. Comparable to *Sf1Fkbp5-/-* KO mice,

HFD-induced BW gain was mildly but non-significantly increased in group housed OE animals ($F_{1,29}$ = 2.27, p = 0.14) **(Fig. 3 E)** with a significantly higher ratio of fat to lean mass in $Sf1^{Fkbp5\ OE}$ after 6 weeks on HFD (chow: U = 95, p = 0.34; HFD: t_{26} = 2.18, p = 0.04) **(Fig. 3 F)**. Blood glucose levels assessed in the GTT and ITT were unaltered under chow diet (GTT t_{29} = 0.43, p = 0.67; ITT t_{29} = 0.08, p = 0.94) **(Fig. 3 G)**. However, on a HFD challenge, animals overexpressing $Fkbp5$ in their VMH displayed slightly impaired glucose tolerance and insulin sensitivity (GTT U = 60, p = 0.02; ITT t_{29} = 1.87, p = 0.07) **(Fig. 3 H)**. The group housing of mixed OE and control litters did not allow us to measure food intake in this cohort. As observed in male and female $Sf1^{Fkbp5-/-}$ animals, relative adrenal weight was significantly decreased in $Sf1^{Fkbp5\ OE}$ after 13 weeks on HFD (t_{26} = 2.65, p = 0.01) **(Suppl. Fig. 4 F)**, without affecting morning baseline CORT levels on chow (U = 88.5, p = 0.48) and HFD (t_{30} = 0.28, p = 0.79) nor ACTH on HFD (t_{29} = 1.05, p = 0.3) (assessed between 08:00 – 12:00 a.m.) **(Suppl. Fig. 4 G - H)**. With an acute restraint stress and subsequent CORT measures at 15, 30, and 60 minutes post stress, we further confirmed that endocrine- and HPA axis function is unaffected by the OE of $Fkbp5$ in the VMH (T15: t_{28} = 0.2, p = 0.84; T30 t_{28} = 0.75, p = 0.46; T60 U = 91, p = 0.79) **(Suppl. Fig. 4 I)**.
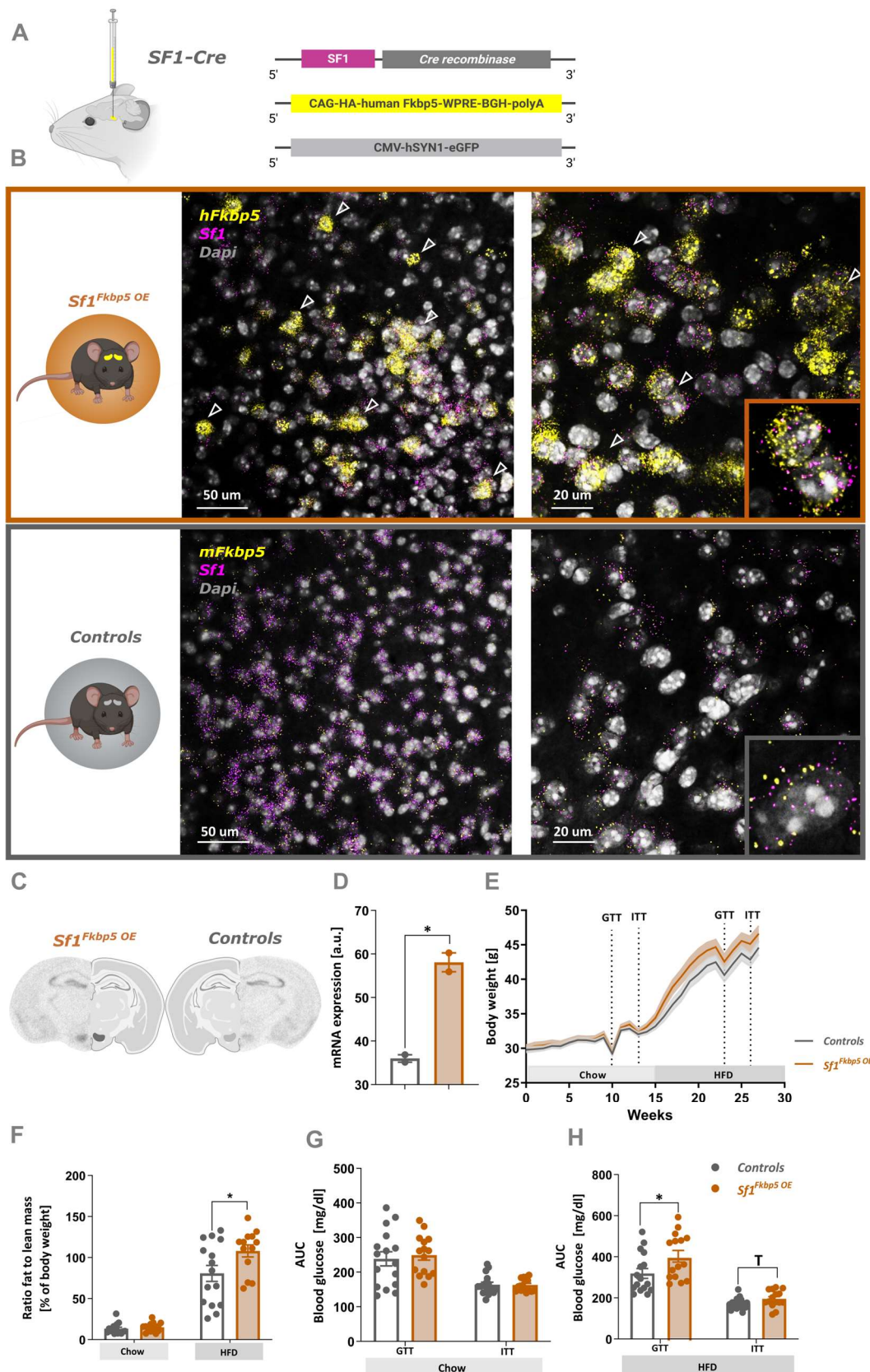
Figure 3: Viral OE of *Fkbp5* exclusively in SF1 neurons within the VMH induces a similar metabolic phenotype to the KO under a HFD challenge

(A) VMH-specific *Fkbp5* OE was achieved by bilateral injections of a *Cre*-dependent human *Fkbp5* OE virus into the VMH of *Sf1-Cre* mice (*Sf1*^*Fkbp5 OE*^; n = 15). Control *Sf1-Cre* received an eGFP control virus

(n = 16). **(B)** Representative RNAScope confocal images of *Fkbp5* mRNA expression in SF1 neurons within the VMH of *Sf1^{Fkbp5 OE}* (human *Fkbp5*; upper orange panel) and controls (mouse *Fkbp5;* lower grey panel). Arrowheads highlighting viral *Fkbp5* OE in *Sf1* positive neurons. **(C)** Qualitative and quantitative **(D)** *ISH* analysis confirmed successful viral *Fkbp5* OE with a ~ 1.6fold increase of *Fkbp5* expression in *Sf1^{Fkbp5 OE}* animals (n = 2) compared to controls (n =2). **(E)** *Sf1^{Fkbp5 OE}* mice displayed a higher HFD-induced BW gain over time compared to controls. **(F)** Higher BW was reflected in a significant increase in the ratio of fat to lean mass in *Sf1^{Fkbp5 OE}* after 6 weeks on a HFD. **(G)** Blood glucose levels in the GTT and ITT were unaltered under a chow diet but after 9 weeks on a HFD KO animals displayed significantly increased blood glucose levels in the GTT and a trend towards increased levels in the ITT **(H)**. Data are received from mice between 16 to 20 weeks of age and are presented as mean ± SEM. * $p < 0.05$, $T < 0.1$. AUC area under the curve, GTT glucose tolerance test, ITT insulin tolerance test

4. Discussion

Since a study led by Eriksson and colleagues in 2014 first revealed the metabolic impact of *Fkbp5* expression in adipose tissue (Pereira et al., 2014), our understanding of the peripheral role of this co-chaperone in adipogenesis, insulin signaling, autophagy, and type 2 diabetes (T2D) has rapidly improved. Preclinical full FKBP51 KO studies in rodents have further uncovered the role of this co-chaperone in regulating whole-body metabolism *in vivo* (Häusl et al., 2019). Despite this progress over the past 10 years and our knowledge that FKBP51 is highly expressed in metabolic brain centers such as the VMH, PVN, and ARC (Balsevich et al., 2014; Brix et al., 2022; Häusl et al., 2021), the role of FKBP51 in these nuclei remains unexplored as cell type-specific studies are completely lacking. Here we manipulated FKBP51 in a cell type- and nucleus-specific manner to further narrow down its potential sites of action in whole-body metabolism; an indispensable step towards the development of targeted therapeutic interventions for metabolic disorders. Using a combination of systemic endogenous KO of FKBP51 in *Sf1*-expressing cells and viral OE of the gene exclusively in the VMH, we demonstrate that FKBP51 in VMH SF1 neurons induces only a mild metabolic phenotype triggered by a dietary challenge in male and female mice.

We have recently shown that deletion of FKBP51 in the MBH results in massive obesity within a few weeks already under chow conditions, while MBH-specific *Fkbp5* OE resulted in protection from diet-induced obesity (Häusl et al., 2022). In this recent study, however, all cell types and regions of the MBH were affected. Data from the current study clearly indicate that while FKBP51 is strongly expressed in almost all SF1-positive neurons of the VMH, deletion of FKBP51 in these cells only had a moderate effect on weight gain and body composition under a HFD challenge, albeit in the same direction as a full MBH FKBP51 deletion. This effect was largely independent of sex and did not result in significant alterations of glucose or insulin tolerance in the animals. We can thus conclude that SF1 neurons in the VMH are not the main driver of an MBH FKBP51 deletion-induced obesity, and at most act in concert with other cell types or nuclei in the MBH to drive this phenotype. Interestingly, mice with a VMH-specific KO of SF1 showed increased weight gain and impaired thermogenesis, and in agreement with our results, a dietary challenge was necessary to induce this SF1-driven metabolic phenotype (Dhillon et al., 2006; Kim et al., 2011). Since prolonged nutrient overload is considered a metabolic stressor activating inflammatory processes at metabolically active sites in the brain, it can trigger a central and behavioral stress response (Aslani et al., 2015). This response could

in turn amplify the effects of stress-and diet-responsive *Fkbp5* (Balsevich et al., 2014; Scharf et al., 2011; Yang et al., 2012) in our KO model.

To gain a deeper understanding of the dose-dependent actions of FKBP51 in the VMH and its implications on homeostatic control, we overexpressed FKBP51 exclusively in *Sf1*-expressing neurons of the VMH by *Cre*-specific viral injections. Intriguingly, these male *Sf1^Fkbp5 OE* developed a similar BW phenotype to our male and female *Sf1^Fkbp5-/-* cohorts with a slightly accelerated weight gain under a HFD challenge, resulting in a significantly higher fat to lean mass ratio in animals overexpressing FKBP51 in the VMH. Further, viral *Fkbp5* OE and mild differences in BW resulted in impaired glucose tolerance and insulin signaling only under HFD. In line with MBH FKBP51 OE results, the BW phenotype was induced exclusively by a high-calorie challenge. However, resulting phenotypes diverged in opposite directions as the MBH FKBP51 OE mice were protected against an HFD-induced weight gain compared to controls. These results further underline that SF1 neurons in the VMH are not the main contributor to the overall metabolic role of FKBP51 in the MBH.

Interestingly, the recent paper by Häusl and colleagues (Häusl et al., 2022) does offer possible explanations for the unexpected phenotypes observed in the current study. First, they detected an altered balance between hypothalamic and peripheral autophagy-mTOR signaling as a major contributor to the observed metabolic phenotype of MBH *Fkbp5* OE and KO mice (Häusl et al., 2022). Recently, a knockout study of autophagy gene 7 (*Atg7*) in mouse VMH-SF1 neurons reported that loss of this gene alters the homeostatic response to fasting and that this metabolic challenge triggers autophagy in the VMH (Coupé et al., 2021). However, within the MBH, a role for proopiomelanocortin (POMC) and agouti-related protein (AGRP) neurons of the ARC in autophagy signaling has also been described. *Atg7* deletion in POMC neurons of the ARC implied an obesogenic phenotype, especially when fed a HFD (Coupé et al., 2012; Quan et al., 2012), whereas loss of this autophagy gene in AGRP neurons promoted leanness (Kaushik et al., 2011). These studies suggest that autophagy signaling and homeostatic control within the MBH are regulated in a cell type-specific manner, and the resulting metabolic effects are highly dependent on the types of neurons involved. Nonetheless, it is tempting to speculate that alterations of autophagic signaling in the VMH are causally linked to the mild phenotype induced by FKBP51 manipulations in this region. Second, Häusl and colleagues described the effects of FKBP51 on autophagy in the MBH in an inversed u-shaped manner. Both deletion and robust OE of FKBP51 lead to significant

reductions in autophagy in the MBH, while a moderate FKBP51 increase in the periphery of MBH OE mice stimulated autophagy and induced their lean phenotype (Häusl et al., 2022). It is therefore feasible that our current manipulations of FKBP51 in SF1 neurons both lead to a cell-type specific reduction of autophagic signaling. This could explain the similar metabolic phenotype of mice with either a SF1-specific *Fkbp5* OE or deletion.

To rule out an impact of our *Fkbp5* KO in *Sf1*-expressing cells within the adrenal and pituitary (Brix et al., 2022; Hoivik et al., 2010; Sadovsky et al., 1995; Zhao et al., 2004) on described phenotypes, we assessed adrenal weights and endocrine parameters of the HPA axis, including baseline and post-stress CORT and ACTH under HFD and SD in our cohorts. Intriguingly, adrenal weights were consistently lower in the experimental group, irrespective of sex, dietary condition and genetic manipulation. Since our viral OE exclusively affected the VMH and yet produced the same phenotype in the adrenal glands as the KO supports the hypothesis of a VMH-driven effect rather than a result of *Fkbp5* KO in this organ itself. Further, there were no functional consequences of *Fkbp5* manipulation on the HPA axis function in either cohort. Intriguingly, there are early studies demonstrating that compensatory adrenal growth after unilateral adrenalectomy, a common method to study adult adrenal growth mechanisms, is mediated by a neural loop including afferent and efferent limbs between the adrenals and the VMH (Beuschlein et al., 2002). Further, VMH-lesion studies indicated a gradual but strong increase in the efferent activity of the adrenal sympathetic nerves and increased catecholamine secretion from the adrenal medulla which could be involved in the development of metabolic disorders observed during the VMH syndrome (Yoshimatsu et al., 1985). A study by King et al. further established a key role for adrenal glucocorticoids in the development of obese phenotypes that resulted from VMH lesions (King and Smith, 1985). However, the involvement of FKBP51 in the described VMH-mediated adrenal growth mechanisms and functions in the onset of obesogenic phenotypes is speculative at the moment. Nevertheless, our study opens a promising new avenue to study our mouse models in the context of VMH-induced metabolic phenotypes.

This study also comes with some limitations: Due to experimental restrictions, we could not show the KO of FKBP51 in *Sf1^Fkbp5-/-^* animals at the protein level. However, a recent study by Häusl et. al (Häusl et al., 2021), which also used the Cre-lox breeding approach to generate a KO of FKBP51 in single-minded homolog 1 (*Sim1*) expressing neurons within the PVN, successfully confirmed their KO at the protein level by western blot analysis. Since the two

targeted neuronal cell types (Sim1 and SF1) have comparable expression levels in their respective nuclei (Kurrasch et al., 2007; Michaud et al., 1998) and the exact same strategy was used to generate the conditional FKBP51 KO mouse lines, we can assume that KO efficiency at the protein level is in the same range; with non-detectable FKBP51 protein level in the KO animals (Häusl et al., 2021). Further, it is important to note that the two approaches used for genetic manipulation of *Fkbp5* expression, might target a different set of neuronal subpopulations within the VMH: Developmental KO of *Fkbp5* affects the entire VMH as SF1 acts as a transcription factor, which expression is essential for both VMH development and function (Kurrasch et al., 2007; Parker et al., 2002; Segal et al., 2005). Adult, viral OE of *Fkbp5*, on the other hand, only targets *Sf1*-expressing cells in the dorsomedial and central parts of the VMH (Cheung et al., 2013).

5. Conclusion

In summary, this study shows that animals lacking and overexpressing *Fkbp5* in *Sf1*-expressing cells within the VMH display a mild metabolic phenotype compared to an MBH-wide manipulation of this gene. Therefore, suggesting that FKBP51 in this hypothalamic nucleus plays a minor role in controlling whole-body metabolism. Therefore, future studies involving MBH cell type-specific KO and OE studies will shed light on MBH nuclei and cell populations that contribute significantly to the metabolic effects achieved with MBH-wide manipulation of FKBP51. Two promising candidates are POMC and AGRP populations within the ARC (Coupé et al., 2012; Kaushik et al., 2011; Quan et al., 2012) and the ongoing metabolic phenotyping of FKBP51-specific KO mouse lines that we have generated (Brix et al., 2022) will help to further unravel the FKBP51 driven effects on MBH metabolism.

Author contributions

L.M.B and M.V.S.: Conceived the project and designed the experiments. J.M.D.: Provided scientific expertise for establishing the $Sf1^{Fkbp5-/-}$ mouse line. L.M.B. managed the mouse lines. L.M.B, I.T., and L.A. designed and performed RNAScope and *ISH* experiments and manual counting of cells. L.M.B. and I.T. performed experiments, surgeries and analysis of data. A.H., J.B., L.v.D., C.E., S.N., M.S., V.S., H.Y. and V.K. assisted with the experiments. L.M.B.: Wrote the initial version of the manuscript. M.V.S.: Supervised the research and all authors revised the manuscript.

Acknowledgments

References

Anand, B.K., Brobeck, J.R., 1951. Hypothalamic Control of Food Intake in Rats and Cats. Yale J. Biol. Med. 24, 123.

Aslani, S., Vieira, N., Marques, F., Costa, P.S., Sousa, N., Palha, J.A., 2015. The effect of high-fat diet on rat's mood, feeding behavior and response to stress. Transl. Psychiatry 2015 511 5, e684–e684. https://doi.org/10.1038/tp.2015.178

Balsevich, G., Häusl, A.S., Meyer, C.W., Karamihalev, S., Feng, X., Pöhlmann, M.L., Dournes, C., Uribe-Marino, A., Santarelli, S., Labermaier, C., Hafner, K., Mao, T., Breitsamer, M., Theodoropoulou, M., Namendorf, C., Uhr, M., Paez-Pereda, M., Winter, G., Hausch, F., Chen, A., Tschöp, M.H., Rein, T., Gassen, N.C., Schmidt, M. V., 2017. Stress-responsive FKBP51 regulates AKT2-AS160 signaling and metabolic function. Nat. Commun. 2017 81 8, 1–12. https://doi.org/10.1038/s41467-017-01783-y

Balsevich, G., Uribe, A., Wagner, K. V, Hartmann, J., Santarelli, S., Labermaier, C., Schmidt, M. V, 2014. Interplay between diet-induced obesity and chronic stress in mice: potential role of FKBP51. J. Endocrinol. 222, 15–26. https://doi.org/10.1530/JOE-14-0129

Baughman, G., Wiederrecht, G.J., Chang, F., Martin, M.M., Bourgeois, S., 1997. Tissue Distribution and Abundance of Human FKBP51, an FK506-Binding Protein That Can Mediate Calcineurin Inhibition. Biochem. Biophys. Res. Commun. 232, 437–443. https://doi.org/10.1006/BBRC.1997.6307

Beuschlein, F., Mutch, C., Bayers, D.L., Ulrich-Lai, Y.M., Engeland, W.C., Keegan, C., Hammer, G.D., 2002. Steroidogenic Factor-1 Is Essential for Compensatory Adrenal Growth Following Unilateral Adrenalectomy. Endocrinology 143, 3122–3135. https://doi.org/10.1210/ENDO.143.8.8944

Brix, L.M., Häusl, A.S., Toksöz, I., Bordes, J., van Doeselaar, L., Engelhardt, C., Narayan, S., Springer, M., Sterlemann, V., Deussing, J.M., Chen, A., Schmidt, M. V., 2022. The co-chaperone FKBP51 modulates HPA axis activity and age-related maladaptation of the stress system in pituitary proopiomelanocortin cells. Psychoneuroendocrinology 138, 105670. https://doi.org/10.1016/J.PSYNEUEN.2022.105670

Brobeck, J.R., 1946. MECHANISM OF THE DEVELOPMENT OF OBESITY IN ANIMALS WITH HYPOTHALAMIC LESIONS. https://doi.org/10.1152/physrev.1946.26.4.541 26, 541–559. https://doi.org/10.1152/PHYSREV.1946.26.4.541

Cheung, C.C., Kurrasch, D.M., Liang, J.K., Ingraham, H.A., 2013. Genetic labeling of

steroidogenic factor-1 (SF-1) neurons in mice reveals ventromedial nucleus of the hypothalamus (VMH) circuitry beginning at neurogenesis and development of a separate non-SF-1 neuronal cluster in the ventrolateral VMH. J. Comp. Neurol. 521, 1268–1288. https://doi.org/10.1002/CNE.23226

Choi, Y.H., Fujikawa, T., Lee, J., Reuter, A., Kim, K.W., 2013. Revisiting the ventral medial nucleus of the hypothalamus: The roles of SF-1 neurons in energy homeostasis. Front. Neurosci. 0, 71. https://doi.org/10.3389/FNINS.2013.00071/BIBTEX

Coupé, B., Ishii, Y., Dietrich, M.O., Komatsu, M., Horvath, T.L., Bouret, S.G., 2012. Loss of Autophagy in Pro-opiomelanocortin Neurons Perturbs Axon Growth and Causes Metabolic Dysregulation. Cell Metab. 15, 247–255. https://doi.org/10.1016/J.CMET.2011.12.016

Coupé, B., Leloup, C., Asiedu, K., Maillard, J., Pénicaud, L., Horvath, T.L., Bouret, S.G., 2021. Defective autophagy in Sf1 neurons perturbs the metabolic response to fasting and causes mitochondrial dysfunction. Mol. Metab. 47, 101186. https://doi.org/10.1016/J.MOLMET.2021.101186

De Kloet, E.R., Joëls, M., Holsboer, F., 2005. Stress and the brain: From adaptation to disease. Nat. Rev. Neurosci. https://doi.org/10.1038/nrn1683

Denny, W.B., Valentine, D.L., Reynolds, P.D., Smith, D.F., Scammell, J.G., 2000. Squirrel monkey immunophilin FKBP51 is a potent inhibitor of glucocorticoid receptor binding. Endocrinology 141, 4107–4113. https://doi.org/10.1210/endo.141.11.7785

Dhillon, H., Zigman, J.M., Ye, C., Lee, C.E., McGovern, R.A., Tang, V., Kenny, C.D., Christiansen, L.M., White, R.D., Edelstein, E.A., Coppari, R., Balthasar, N., Cowley, M.A., Chua, S., Elmquist, J.K., Lowell, B.B., 2006. Leptin directly activates SF1 neurons in the VMH, and this action by leptin is required for normal body-weight homeostasis. Neuron 49, 191–203. https://doi.org/10.1016/J.NEURON.2005.12.021/ATTACHMENT/61A9488A-C3F9-4A89-BBFF-7A603A5E7DEF/MMC1.PDF

Fosch, A., Zagmutt, S., Casals, N., Rodríguez-Rodríguez, R., 2021. New Insights of SF1 Neurons in Hypothalamic Regulation of Obesity and Diabetes. Int. J. Mol. Sci. 2021, Vol. 22, Page 6186 22, 6186. https://doi.org/10.3390/IJMS22126186

Gassen, N.C., Hartmann, J., Schmidt, M. V., Rein, T., 2015. FKBP5/FKBP51 enhances autophagy to synergize with antidepressant action. Autophagy 11, 578. https://doi.org/10.1080/15548627.2015.1017224

Gassen, N.C., Hartmann, J., Zschocke, J., Stepan, J., Hafner, K., Zellner, A., Kirmeier, T., Kollmannsberger, L., Wagner, K. V., Dedic, N., Balsevich, G., Deussing, J.M., Kloiber, S., Lucae, S., Holsboer, F., Eder, M., Uhr, M., Ising, M., Schmidt, M. V., Rein, T., 2014. Association of FKBP51 with Priming of Autophagy Pathways and Mediation of Antidepressant Treatment Response: Evidence in Cells, Mice, and Humans. PLoS Med. 11. https://doi.org/10.1371/JOURNAL.PMED.1001755

Gautron, L., Elmquist, J.K., Williams, K.W., 2015. Neural Control of Energy Balance: Translating Circuits to Therapies. Cell 161, 133. https://doi.org/10.1016/J.CELL.2015.02.023

Guarnieri, D.J., Brayton, C.E., Richards, S.M., Maldonado-Aviles, J., Trinko, J.R., Nelson, J., Taylor, J.R., Gourley, S.L., Dileone, R.J., 2012. Gene profiling reveals a role for stress hormones in the molecular and behavioral response to food restriction. Biol. Psychiatry 71, 358. https://doi.org/10.1016/J.BIOPSYCH.2011.06.028

Halldorsdottir, S., Carmody, J., Boozer, C.N., Leduc, C.A., Leibel, R.L., 2009. Reproducibility and accuracy of body composition assessments in mice by dual energy x-ray absorptiometry and time domain nuclear magnetic resonance. Int. J. Body Compos. Res. 7, 147.

Hartmann, J., Wagner, K., Liebl, C., Scharf, S., Wang, X., Wolf, M., Hausch, F., Rein, T., Schmidt, U., Touma, C., Cheung-Flynn, J., Cox, M., Smith, D., Holsboer, F., Müller, M., Schmidt, M., 2012. The involvement of FK506-binding protein 51 (FKBP5) in the behavioral and neuroendocrine effects of chronic social defeat stress. Neuropharmacology 62, 332–339. https://doi.org/10.1016/J.NEUROPHARM.2011.07.041

Häusl, A.S., Bajaj, T., Brix, L.M., Pöhlmann, M.L., Hafner, K., Angelis, M. De, Nagler, J., Dethloff, F., Balsevich, G., Schramm, K.-W., Giavalisco, P., Chen, A., Schmidt, M. V., Gassen, N.C., 2022. Mediobasal hypothalamic FKBP51 acts as a molecular switch linking autophagy to whole-body metabolism. Sci. Adv. 8, 4797. https://doi.org/10.1126/SCIADV.ABI4797

Häusl, A.S., Balsevich, G., Gassen, N.C., Schmidt, M. V., 2019. Focus on FKBP51: A molecular link between stress and metabolic disorders. Mol. Metab. 29, 170–181. https://doi.org/10.1016/J.MOLMET.2019.09.003

Häusl, A.S., Brix, L.M., Hartmann, J., Pöhlmann, M.L., Lopez, J.-P., Menegaz, D., Brivio, E., Engelhardt, C., Roeh, S., Bajaj, T., Rudolph, L., Stoffel, R., Hafner, K., Goss, H.M., Reul, J.M.H.M., Deussing, J.M., Eder, M., Ressler, K.J., Gassen, N.C., Chen, A., Schmidt, M. V., 2021. The co-chaperone Fkbp5 shapes the acute stress response in the paraventricular nucleus of the hypothalamus of male mice. Mol. Psychiatry 2021 1–17. https://doi.org/10.1038/s41380-021-01044-x

Hetherington, A.W., Ranson, S.W., 1942. The relation of various hypothalamic lesions to adiposity in the rat. J. Comp. Neurol. 76, 475–499. https://doi.org/10.1002/CNE.900760308

Hoivik, E.A., Lewis, A.E., Aumo, L., Bakke, M., 2010. Molecular aspects of steroidogenic factor 1 (SF-1). Mol. Cell. Endocrinol. 315, 27–39. https://doi.org/10.1016/J.MCE.2009.07.003

Jenkins, S.A., Ellestad, L.E., Mukherjee, M., Narayana, J., Cogburn, L.A., Porter, T.E., 2013. Glucocorticoid-induced changes in gene expression in embryonic anterior pituitary cells. Physiol. Genomics 45, 422–433. https://doi.org/10.1152/physiolgenomics.00154.2012

Kaushik, S., Rodriguez-Navarro, J.A., Arias, E., Kiffin, R., Sahu, S., Schwartz, G.J., Cuervo, A.M., Singh, R., 2011. Autophagy in Hypothalamic AgRP Neurons Regulates Food Intake and Energy Balance. Cell Metab. 14, 173–183. https://doi.org/10.1016/J.CMET.2011.06.008

Kennedy, G.C., 1950. The hypothalamic control of food intake in rats. Proc. R. Soc. London. Ser. B - Biol. Sci. 137, 535–549. https://doi.org/10.1098/RSPB.1950.0065

Kim, K.W., Zhao, L., Donato, J., Kohno, D., Xu, Y., Eliasa, C.F., Lee, C., Parker, K.L., Elmquist, J.K., 2011. Steroidogenic factor 1 directs programs regulating diet-induced thermogenesis and leptin action in the ventral medial hypothalamic nucleus. Proc. Natl. Acad. Sci. U. S. A. 108, 10673–10678. https://doi.org/10.1073/PNAS.1102364108

King, B.M., 2006. The rise, fall, and resurrection of the ventromedial hypothalamus in the regulation of feeding behavior and body weight. Physiol. Behav. 87, 221–244. https://doi.org/10.1016/J.PHYSBEH.2005.10.007

King, B.M., Smith, R.L., 1985. Hypothalamic obesity after hypophysectomy or adrenalectomy: dependence on corticosterone. https://doi.org/10.1152/ajpregu.1985.249.5.R522 18. https://doi.org/10.1152/AJPREGU.1985.249.5.R522

Kurrasch, D.M., Cheung, C.C., Lee, F.Y., Tran, P. V., Hata, K., Ingraham, H.A., 2007. The Neonatal Ventromedial Hypothalamus Transcriptome Reveals Novel Markers with Spatially Distinct Patterning. J. Neurosci. 27, 13624. https://doi.org/10.1523/JNEUROSCI.2858-07.2007

Majdic, G., Young, M., Gomez-Sanchez, E., Anderson, P., Szczepaniak, L.S., Dobbins, R.L., McGarry, J.D., Parker, K.L., 2002. Knockout Mice Lacking Steroidogenic Factor 1 Are a Novel Genetic Model of Hypothalamic Obesity. Endocrinology 143, 607–614. https://doi.org/10.1210/ENDO.143.2.8652

McClellan, K.M., Parker, K.L., Tobet, S., 2006. Development of the ventromedial nucleus of the hypothalamus. Front. Neuroendocrinol. 27, 193–209. https://doi.org/10.1016/J.YFRNE.2006.02.002

Michaud, J.L., Rosenquist, T., May, N.R., Fan, C.M., 1998. Development of neuroendocrine lineages requires the bHLH–PAS transcription factor SIM1. Genes Dev. 12, 3264–3275. https://doi.org/10.1101/GAD.12.20.3264

Parker, K.L., Rice, D.A., Lala, D.S., Ikeda, Y., Luo, X., Wong, M., Bakke, M., Zhao, L., Frigeri, C., Hanley, N.A., Stallings, N., Schimmer, B.P., 2002. Steroidogenic factor 1: an essential mediator of endocrine development. Recent Prog. Horm. Res. 57, 19–36. https://doi.org/10.1210/RP.57.1.19

Pereira, M.J., Palming, J., Svensson, M.K., Rizell, M., Dalenbäck, J., Hammar, M., Fall, T., Sidibeh, C.O., Svensson, P.A., Eriksson, J.W., 2014. FKBP5 expression in human adipose tissue increases following dexamethasone exposure and is associated with insulin resistance. Metabolism 63, 1198–1208. https://doi.org/10.1016/J.METABOL.2014.05.015

Quan, W., Kim, H.K., Moon, E.Y., Kim, S.S., Choi, C.S., Komatsu, M., Jeong, Y.T., Lee, M.K., Kim, K.W., Kim, M.S., Lee, M.S., 2012. Role of Hypothalamic Proopiomelanocortin Neuron Autophagy in the Control of Appetite and Leptin Response. Endocrinology 153, 1817–1826. https://doi.org/10.1210/EN.2011-1882

Rodríguez, C.I., Buchholz, F., Galloway, J., Sequerra, R., Kasper, J., Ayala, R., Stewart, A.F., Dymecki, S.M., 2000. High-efficiency deleter mice show that FLPe is an alternative to Cre-loxP. Nat. Genet. https://doi.org/10.1038/75973

Sadovsky, Y., Crawford, P.A., Woodson, K.G., Polish, J.A., Clements, M.A., Tourtellotte, L.M., Simburger, K., Milbrandt, J., 1995. Mice deficient in the orphan receptor steroidogenic factor 1 lack adrenal glands and gonads but express P450 side-chain-cleavage enzyme in the placenta and have normal embryonic serum levels of corticosteroids. Proc. Natl. Acad. Sci. U. S. A. 92, 10939. https://doi.org/10.1073/PNAS.92.24.10939

Scammell, J.G., Denny, W.B., Valentine, D.L., Smiths, D.F., 2001. Overexpression of the FK506-binding immunophilin FKBP51 is the common cause of glucocorticoid resistance in three New World primates. Gen. Comp. Endocrinol. 124, 152–165. https://doi.org/10.1006/gcen.2001.7696

Scharf, S.H., Liebl, C., Binder, E.B., Schmidt, M. V., Müller, M.B., 2011. Expression and regulation of the Fkbp5 gene in the adult mouse brain. PLoS One 6. https://doi.org/10.1371/journal.pone.0016883

Schmidt, M. V., Sterlemann, V., Ganea, K., Liebl, C., Alam, S., Harbich, D., Greetfeld, M., Uhr, M., Holsboer, F., Müller, M.B., 2007. Persistent neuroendocrine and behavioral effects of a novel, etiologically relevant mouse paradigm for chronic social stress during adolescence. Psychoneuroendocrinology 32, 417–429. https://doi.org/10.1016/j.psyneuen.2007.02.011

Segal, J.P., Stallings, N.R., Lee, C.E., Zhao, L., Socci, N., Viale, A., Harris, T.M., Soares, M.B., Childs, G., Elmquist, J.K., Parker, K.L., Friedman, J.M., 2005. Use of Laser-Capture Microdissection for the Identification of Marker Genes for the Ventromedial Hypothalamic Nucleus. J. Neurosci. 25, 4181. https://doi.org/10.1523/JNEUROSCI.0158-05.2005

Sidibeh, C.O., Pereira, M.J., Abalo, X.M., J. Boersma, G., Skrtic, S., Lundkvist, P., Katsogiannos, P., Hausch, F., Castillejo-López, C., Eriksson, J.W., 2018. FKBP5 expression in human adipose tissue: potential role in glucose and lipid metabolism, adipogenesis and type 2 diabetes. Endocrine 1–13. https://doi.org/10.1007/s12020-018-1674-5

Sinars, C.R., Cheung-Flynn, J., Rimerman, R.A., Scammell, J.G., Smith, D.F., Clardy, J., 2003. Structure of the large FK506-binding protein FKBP51, an Hsp90-binding protein and a component of steroid receptor complexes. Proc. Natl. Acad. Sci. U. S. A. 100, 868–873. https://doi.org/10.1073/pnas.0231020100

Smedlund, K.B., Sanchez, E.R., Hinds, T.D., 2021. FKBP51 and the molecular chaperoning of metabolism. Trends Endocrinol. Metab. 32, 862–874. https://doi.org/10.1016/J.TEM.2021.08.003

Stechschulte, L.A., Qiu, B., Warrier, M., Hinds, T.D., Zhang, M., Gu, H., Xu, Y., Khuder, S.S., Russo, L., Najjar, S.M., Lecka-Czernik, B., Yong, W., Sanchez, E.R., 2016. FKBP51 Null Mice Are Resistant to Diet-Induced Obesity and the PPARγ Agonist Rosiglitazone. Endocrinology 157, 3888. https://doi.org/10.1210/EN.2015-1996

Westberry, J.M., Sadosky, P.W., Hubler, T.R., Gross, K.L., Scammell, J.G., 2006. Glucocorticoid resistance in squirrel monkeys results from a combination of a transcriptionally incompetent glucocorticoid receptor and overexpression of the glucocorticoid receptor co-chaperone FKBP51. J. Steroid Biochem. Mol. Biol. 100, 34–41. https://doi.org/10.1016/J.JSBMB.2006.03.004

Wochnik, G.M., Rüegg, J., Abel, G.A., Schmidt, U., Holsboer, F., Rein, T., 2005. FK506-binding proteins 51 and 52 differentially regulate dynein interaction and nuclear translocation of the glucocorticoid receptor in mammalian cells. J. Biol. Chem. 280, 4609–4616. https://doi.org/10.1074/jbc.M407498200

Yang, L., Isoda, F., Yen, K., Kleopoulos, S.P., Janssen, W., Fan, X., Mastaitis, J., Dunn-Meynell, A., Levin, B., McCrimmon, R., Sherwin, R., Musatov, S., Mobbs, C. V., 2012. Hypothalamic Fkbp51 is induced by fasting, and elevated hypothalamic expression promotes obese phenotypes. Am. J. Physiol. - Endocrinol. Metab. 302, E987. https://doi.org/10.1152/AJPENDO.00474.2011

Yoshimatsu, H., Oomura, Y., Katafuchi, T., Niijima, A., Sato, A., 1985. Lesions of the ventromedial hypothalamic nucleus enhance sympatho-adrenal function. Brain Res. 339, 390–392. https://doi.org/10.1016/0006-8993(85)90112-X

Zhao, L., Bakke, M., Hanley, N.A., Majdic, G., Stallings, N.R., Jeyasuria, P., Parker, K.L., 2004. Tissue-specific knockouts of steroidogenic factor 1. Mol. Cell. Endocrinol. 215, 89–94. https://doi.org/10.1016/J.MCE.2003.11.009

Supplementary Figures
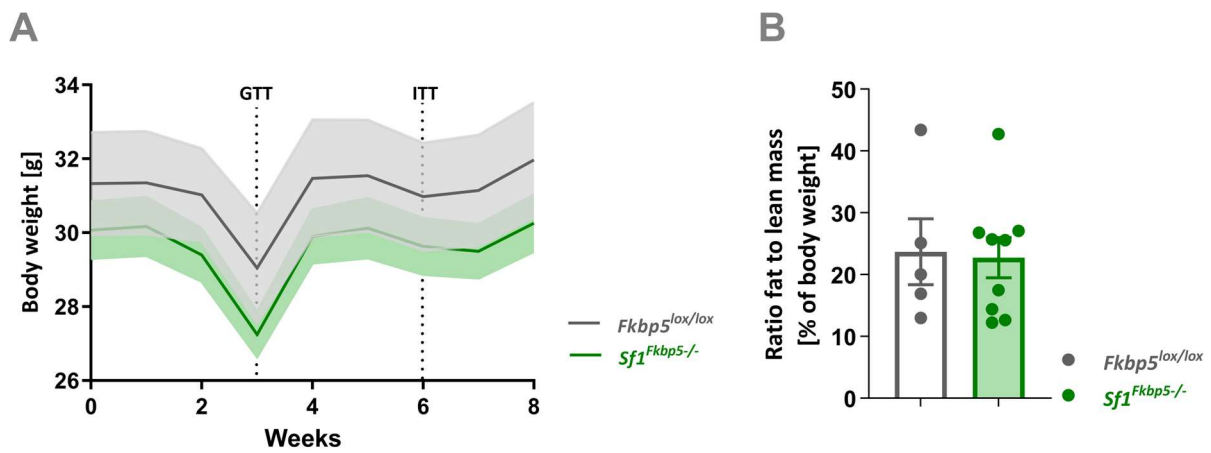
Suppl. Figure 1: Separate cohort of *Sf1^Fkbp5-/-* male mice under a chow diet to assess glucose tolerance- and insulin signaling

(A) In a separate cohort of *Sf1^Fkbp5-/- (n = 9) and Fkbp5^lox/lox* (n = 5) under chow diet, bodyweight (BW) was assessed over a total period of 8 weeks to ensure a comparable BW phenotype as in the 1st cohort **(Fig. 1 C)**. Glucose tolerance (GTT) and insulin tolerance test (ITT) after 3 and 6 weeks respectively did not reveal differences between *Sf1^Fkbp5-/-* KO animals and controls. **(B)** The body composition scan in week 2 of the experiment did not reveal differences between the two groups. Data are received from mice between 18 to 24 weeks of age and are presented as mean ± SEM.
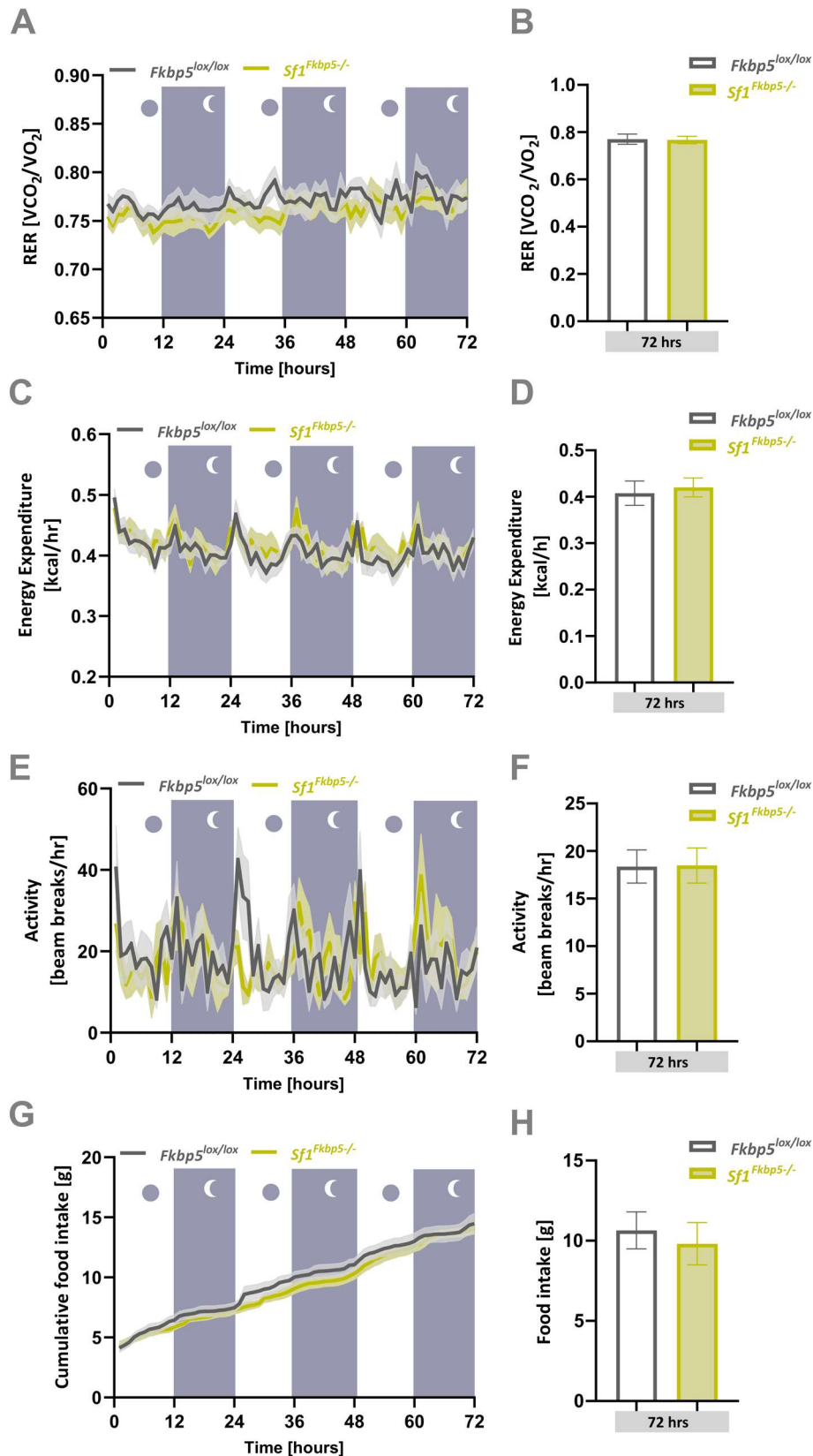
Suppl. Figure 2: Knockout of *Fkbp5* in *Sf1*-expressing cells did not alter the metabolic phenotype assessed by indirect calorimetry

(A) Respiratory exchange ratio (RER) over a time course of 72 hours (average/hour) and the total average of RER over 72 hours (B) was not different between *Sf1^Fkbp5-/-^* (n = 8) and *Fkbp5^lox/lox^* (n = 8). (C)

Energy Expenditure (EE) and the average EE over three days **(D)** were unchanged between both groups. **(E)** Activity over 72 hours and average activity over three days **(F)** were unaffected by a knockout of *Fkbp5* in SF1 neurons. **(G)** Cumulative food intake and average total food intake (average over 72 hours) **(H)** were the same between both genotypes. Data are received from mice between 16 to 20 weeks of age and are presented as mean ± SEM. RER respiratory exchange ratio, VO_2 oxygen intake, VCO_2 carbon dioxide release
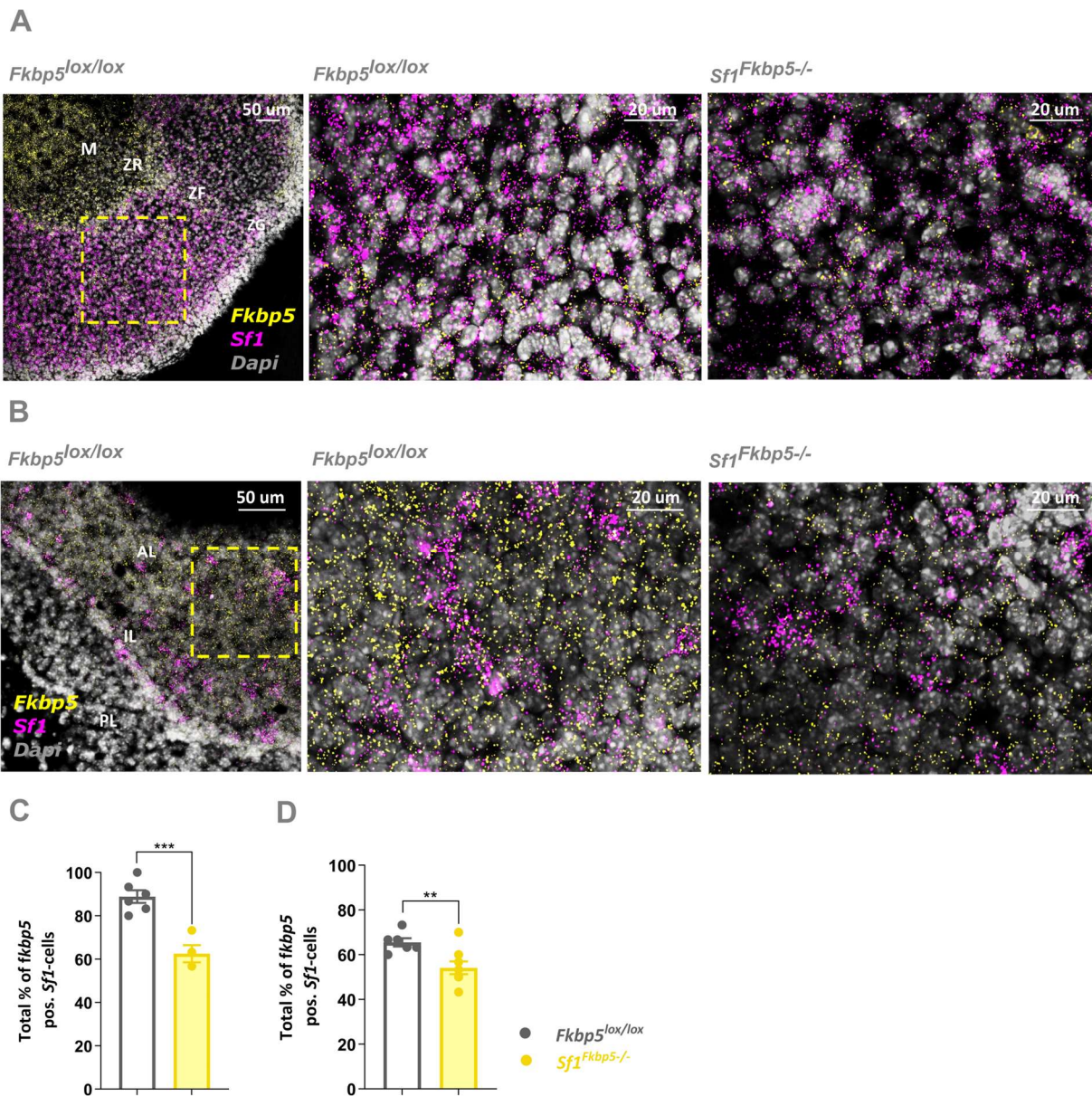
Suppl. Figure 3: Knockout validation of *Fkbp5* in *Sf1*-expressing cells in the adrenal zona fasciculata and anterior pituitary

(A) Representative RNAscope confocal images of *Fkbp5* mRNA expression in SF1 cells in the zona fasciculata (ZF) of the adrenal cortex and anterior lobe (AL) of the pituitary **(B)** in *Fkbp5^{lox/lox}* and *Sf1^{Fkbp5-/-}* knockout male mice. Yellow dashed squares represent area chosen for 40 x confocal images for quantification. Significant decrease in the total percentage of *Sf1*-positive cells that co-express *Fkbp5*

mRNA in adrenal cortex **(C)** and anterior pituitary **(D)** of *Sf1*^{Fkbp5-/-} knockout animals compared to *Fkbp5*^{lox/lox} controls (n = number of analyzed 40x confocal images of pituitary AL: n_{KO} = 4, $n_{Control}$ = 6 and adrenal ZF: n_{KO} = 8, $n_{Control}$ = 6; 1 - 2 animals/genotype). Data are received from mice between 10 to 16 weeks of age and are presented as mean ± SEM. ** p < 0.01, *** p < 0.001. AL anterior lobe, IL intermediate lobe, M medulla, PL posterior lobe, ZF zona fasciculata, ZG zona glomerulosa, ZR zona reticulata
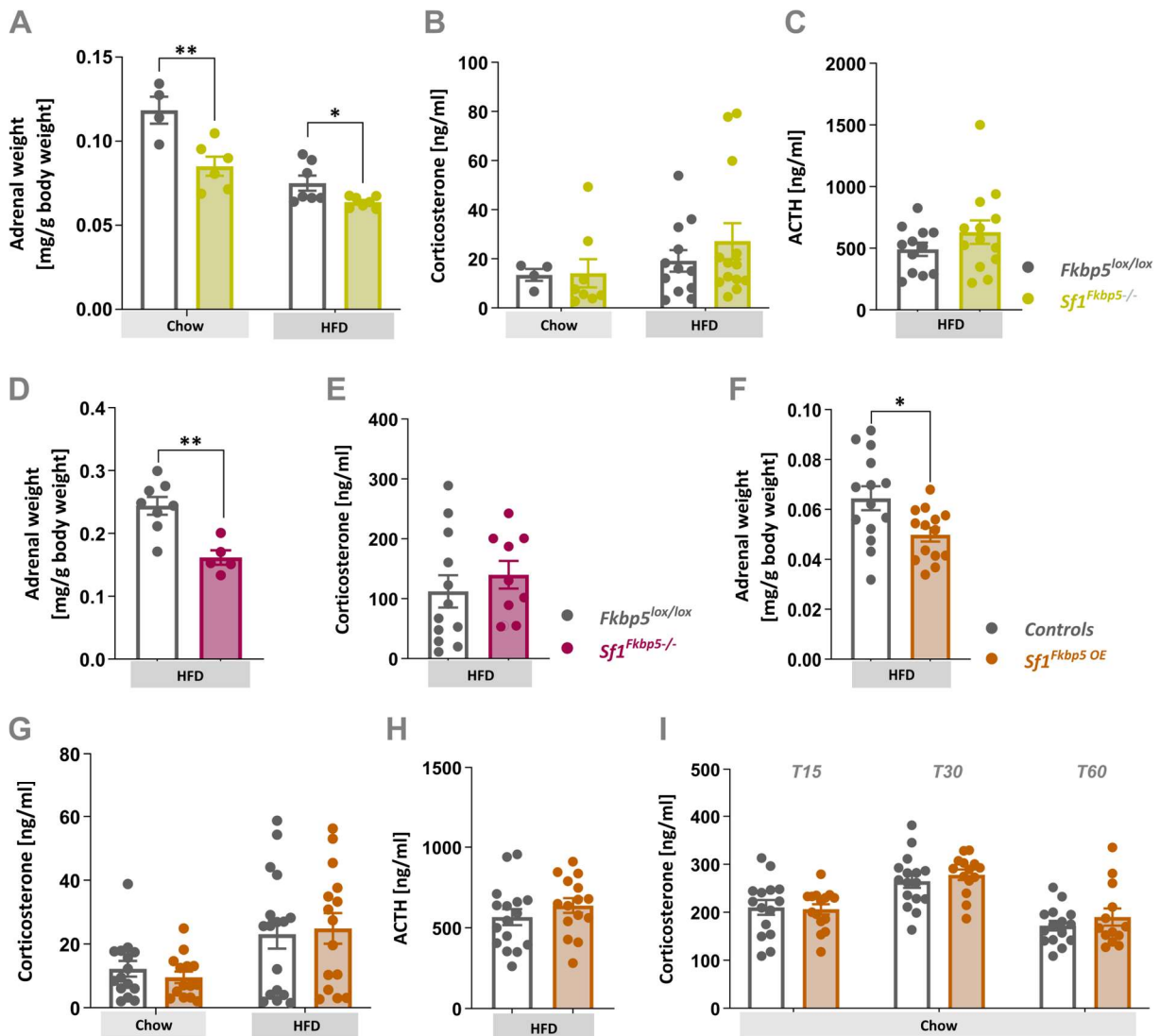
Suppl. Figure 4: Endocrine phenotyping of *Sf1*^{Fkbp5-/-} males and females, and male mice overexpressing *Fkbp5* in SF1 neurons within the VMH reveals decreased adrenal weights in all three cohorts with an intact HPA axis function

(A) Relative adrenal weight was significantly lower in male knockout animals under chow and after 21 weeks on a HFD ($n_{Sf1^{Fkbp5-/-}}$ = 13; $n_{Fkbp5^{lox/lox}}$ = 12). **(B)** Baseline morning CORT (measured between 08:00 – 12:00 a.m.) under chow diet and after 21 weeks on HFD was unaltered between *Sf1*^{Fkbp5-/-} (n = 13) and *Fkbp5*^{lox/lox} (n = 12) male mice with unaffected morning baseline ACTH post HFD **(C)**. **(D)** Relative adrenal weight of female animals with a knockout of *Fkbp5* was significantly reduced after 15 weeks on a HFD

with unaltered baseline corticosterone levels **(E)**. **(F)** Relative adrenal weight of *Sf1^Fkbp5 OE^* was significantly lower than that of controls after 13 weeks on a HFD. **(G)** Baseline morning CORT under chow diet and after 13 weeks on HFD were not different between *Sf1^Fkbp5 OE^* (n = 15) and controls (n = 16). **(H)** Morning baseline ACTH levels after 13 weeks on HFD are equal in both groups. **(I)** Both *Sf1^Fkbp5 OE^* and control animals displayed a functioning stress response post restraint stress with an increase in CORT at T15 and T30 post restraint and a recovery at T60 but there were no differences between groups observed. Data are received from mice between 16 to 20 weeks of age and are presented as mean ± SEM. * p < 0.05, ** p < 0.01. ACTH adrenocorticotropin releasing hormone, CORT corticosterone, HFD high-fat diet, T time point

2.5 Deletion of the co-chaperone FKBP51 in POMC- but not AgRP neurons of the arcuate nucleus improves whole-body metabolism in male and female mice

Brix., L.M., Häusl, A.S., Toksöz, I., Aman, L., Bordes, J., Doeselaar, L.V., Engelhardt, Kovarova, V., Narayan, S., Springer, M., Sterlemann, Yang, H., Deussing, J.M. & Schmidt, M.V.

Manuscript in preparation

Abstract

FKBP51 in the mediobasal hypothalamus (MBH) has been recently described as a central regulator of whole-body metabolism and energy homeostasis. However, the contribution of FKBP51 in specific MBH cell types to robust and distinct phenotypes remains elusive. Two promising candidates in this context are agouti related protein (*AgRP*)- and proopiomelanocortin (*Pomc*)-expressing neurons within the arcuate nucleus (ARC), as they are the driving force of the melanocortin signaling pathway and thus control food intake and energy homeostasis. In the current study we therefore manipulated *Fkbp5* expression in POMC- (*Pomc*$^{Fkbp5-/-}$) and AgRP neurons (*AgRP*$^{Fkbp5-/-}$) within the ARC by means of endogenous knockout (KO) (*AgRP*$^{Fkbp5-/}$ and *Pomc*$^{Fkbp5-/-}$) and viral overexpression (OE) (*Pomc*$^{Fkbp5\ OE}$), and assessed the animal's baseline and high fat diet (HFD)-induced metabolic phenotypes. Our data reveal that only a KO of *Fkbp5* in POMC cells induced beneficial metabolic, behavioral and neuroendocrine phenotypes in these animals, regardless of sex. Our study therefore identifies the first cell type in rodents that benefits from attenuation of *Fkbp5* expression in the context of metabolic control, opening a new avenue of research for the development of targeted therapeutic interventions in the treatment of metabolic diseases and their comorbidities.

1. Introduction

The prevalence of overweight and obesity has reached epidemic proportions worldwide but the environmental and internal factors, molecular players and underlying genetics that contribute to obese phenotypes remain elusive (WHO, 2022). The main cause of this disease is a long-term energy imbalance between too many calories consumed and too few calories expended, which is owed to our modern sedentary life style, a lack of physical activity and, the over-consumption of high-calorie food (Blüher, 2019). Our bodies must constantly fine-tune energy homeostasis via an unceasing process of communication between the brain and peripheral organs to maintain a stable body weight throughout life (Lenard and Berthoud, 2008).

The relevant role of the arcuate nucleus (ARC) in the mediobasal hypothalamus (MBH) in fine-tuning energy balance and adapting feeding behavior has been known since decades. Peripheral nutrients and hormonal signals, like insulin, leptin and glucagon like peptide (Glp1) are sensed by two functionally distinct and antagonistic neuronal subpopulations within the ARC (Xu et al., 2011): The orexigenic (appetite-stimulating) AgRP/NPY neurons expressing agouti-related peptide (AgRP) and neuropeptide Y (NPY), and the anorexigenic (appetite-suppressing) neurons that express pro-opiomelanocortin (POMC) and amphetamine-related transcript (CART) (Myers and Olson, 2012). The homeostatic regulatory neurocircuit that underlies the interplay of these two subpopulations is the central melanocortin pathway (Timper and Brüning, 2017). Activation of POMC neurons by adipostatic signaling molecules insulin or leptin promotes satiety, increases energy expenditure, and suppresses food intake through the release of POMC-derived neuropeptide alpha-melanocyte stimulating hormone (α-MSH) (Timper and Brüning, 2017). α-MSH mediates its effects through transmembrane melanocortin receptors 3 and 4 (MC3R/MC4R) on downstream targets, such as the paraventricular nucleus (PVN) and the lateral mediobasal hypothalamus (LHA) (Harno et al., 2018; Millington, 2007). AgRP acts as a high-affinity antagonist on these receptors, thereby promoting food intake and decreasing energy expenditure (Morton and Schwartz, 2001). Beyond this simplistic view on POMC function, this ARC population is well known for its high neuronal heterogeneity, which may have originated as an adaptive mechanism to orchestrate competing emotional states and food foraging. Hence, POMC neurons can affect a plethora of physiological and behavioral responses associated with the evolutionary survival of our species, including locomotion, pain, fear, and stress (Quarta et al., 2021).

Best known for its role as a negative regulator of the glucocorticoid receptor (GR), co-chaperone FK506-binding protein 51 (FKBP51, encoded by *Fkbp5)* shapes GR-mediated negative feedback of the hormonal stress response system, the hypothalamic-pituitary-adrenal (HPA) axis in complex with heat-shock protein 90 (Hsp90) (Wochnik et al., 2005). In this context, our lab found that FKBP51 in the PVN of the hypothalamus and in POMC cells of the anterior pituitary shapes negative feedback and (re)activity of the HPA axis (Brix et al., 2022; Häusl et al., 2021). Besides its role as a genetic risk factor in the occurrence of stress-related psychiatric disorders (Binder et al., 2008, 2004; Matosin et al., 2018; Zannas and Binder, 2014), there is evidence that FKBP51 is associated with type 2 diabetes, insulin resistance, adipogenesis, browning of white adipose tissue, glucose metabolism and bodyweight regulation (Häusl et al., 2019; Smedlund et al., 2021). Further, we and others could show that *Fkbp5* is abundantly expressed in metabolically relevant tissues in the periphery, such as adipocytes and skeletal muscle (Balsevich et al., 2017; Baughman et al., 1997; Pereira et al., 2014; Sidibeh et al., 2018), and brain regions, like the ARC and ventromedial hypothalamus (VMH), which are considered neuronal centers controlling energy metabolism (Balsevich et al., 2014; Gautron et al., 2015; Scharf et al., 2011). The investigation of central *Fkbp5* mRNA expression in response to a prolonged metabolic challenge revealed that hypothalamic *Fkbp5* mRNA expression is increased in the VMH, PVN and ARC (Balsevich et al., 2014; Scharf et al., 2011; Yang et al., 2012). Further, we know from preclinical studies in mice with a full knockout (KO) of FKBP51 that these animals are resistant to diet-induced obesity and demonstrate improved glucose tolerance, and increased insulin-signaling in skeletal muscle (Balsevich et al., 2017; Hartmann et al., 2012; Stechschulte et al., 2016). Publications by our lab shed light on the region- and cell-type specificity of FKBP51 in mediating whole-body metabolism: A recent study by Häusl and colleagues revealed that FKBP51 in the rodent MBH represents a novel regulatory link between central and peripheral autophagy signaling and the *in vivo* whole-body response to an obesogenic challenge, and that KO of *Fkbp5* in the MBH results in opposite metabolic phenotypes to those observed in FKBP51-null mice (Häusl et al., 2022). Further, we could show that cell-type specific KO and overexpression (OE) of *Fkbp5* in steroidogenic factor 1 (*Sf1*)-expressing neurons of the VMH induced only a mild metabolic phenotype compared to an MBH-wide manipulation of this gene. This suggests that FKBP51 in SF1 neurons plays a subsidiary role in controlling whole-body metabolism (Brix et al. 2022, in submission).

The exclusion of the VMH as the driving force behind metabolic effects in the Häusl study (Häusl et al., 2022) raises the question of other MBH subpopulations responsible for the observed changes in whole-body metabolism. Therefore, we here investigated homeostatic, metabolic, and behavioral effects of an endogenous *Fkbp5* KO in *Pomc*- (*Pomc*^{Fkbp5-/-}) and *AgRP*-expressing neurons (*AgRP*^{Fkbp5-/-}). Central *AgRP* expression was shown to be restricted to neurons within the ARC (Tong et al., 2008). Successful deletion of *Fkbp5* in POMC neurons of the ARC, as the primary central site of *Pomc*-expression, and corticotroph cells of the anterior pituitary, was recently confirmed by our lab (Brix et al., 2022; Toda et al., 2017). Within the brain, *Pomc* is also expressed in a small population in the nucleus of the solitary tract (NTS) (Georgescu et al., 2020). To assess dose-dependent effects of FKBP51 and to induce a region- and cell-type specific genetic manipulation, we virally overexpressed the gene in POMC neurons of the ARC. Our data revealed, that only a KO of *Fkbp5* in POMC cells triggers beneficial metabolic, behavioral and neuroendocrine phenotypes in these animals, independent of sex. Therefore, positioning FKBP51 in POMC neurons as a promising target in the future development of novel therapy approaches to treat metabolic disorders and their comorbidities.

2. Materials and Methods

2.1 Animals and animal housing

The mouse lines *Fkbp5$^{lox/lox}$*, *Pomc$^{Fkbp5-/-}$* and *AgRP$^{Fkbp5-/-}$* were obtained from the in-house breeding facility of the Max Planck Institute of Psychiatry and are all bred on C57/BL6n background. Males and females in all *Fkbp5$^{lox/lox}$*, *Pomc$^{Fkbp5-/-}$* and *AgRP$^{Fkbp5-/-}$* cohorts were aged 2 - 7 months at the onset of the experiments. Male *Pomc$^{Fkbp5-/-}$* and *AgRP$^{Fkbp5-/-}$* animals were kept single housed (Fig. 1 and Fig. 4), female *Pomc$^{Fkbp5-/-}$* (Fig. 2) and male *Pomc$^{Fkbp5\ OE}$* (Fig. 3) were kept in groups of 3 - 5 animals per cage. All animals were held in individually ventilated cages (IVC; 30cm x 16 cm x 16 cm; 501 cm^2) serviced by a central airflow system (Tecniplast, IVC Green Line – GM500). Animals had *ad libitum* access to water (tap water) and food (see 2.2) and were maintained under constant environmental conditions (12:12 hr light/dark cycle, 23 ± 2 °C and humidity of 55%). All IVCs had sufficient bedding and nesting material as well as a wooden tunnel for environmental enrichment. Animals were allocated to experimental groups in a semi-randomized fashion, data analysis and execution of experiments were performed blinded to group allocation. All experiments and protocols were approved by the committee for the Care and Use of Laboratory animals of the Government of Upper Bavaria and were performed in accordance with the European Communities' Council Directive 2010/63/EU. Throughout the experiments, all effort was made to minimize animal suffering during the experiments.

2.2 Generation of *Fkbp5$^{lox/lox}$*, *Pomc$^{Fkbp5-/-}$* and *AgRP$^{Fkbp5-/-}$* lines

Mouse lines with deletion of FKBP51 in POMC neurons of the ARC and POMC cells in the pituitary (*Pomc$^{Fkbp5-/-}$*) were generated by breeding mice with a floxed exon 9 in the *Fkbp5* gene locus designated as *Fkbp5$^{lox/lox}$* (*Fkbp5$^{tm1c(KOMP)Wtsi}$*) to *Pomc-Cre* mice (Balthasar et al., 2004). Animals lacking FKBP51 in AgRP neurons in the ARC were generated by crossing *Fkbp5$^{lox/lox}$* to *AgRP-Cre* animals (Tong et al., 2008). Genotyping details are available upon request.

2.3 Diet for induced obesity

Baseline metabolic characterization of all experimental cohorts was performed under a standard chow diet (standard research diet by Altromin 1318, Altromin GmbH, Germany) with the following nutritional values: 14 % fat, 27 % protein and 59 % carbohydrates. Dietary challenge was induced with a HFD diet (HFD, D12331, Research Diets, New Brunswick, NJ, USA) over a period of several weeks to induce overweight. Nutritional values HFD: 58 % fat and sucrose, 17 % protein, 25 % carbohydrates. Bodyweight and food intake were measured on a regular basis in all experimental cohorts.

2.4 Viral overexpression of *Fkbp5* in the ARC of *Pomc-Cre* mice

Pomc-specific overexpression (OE) of *Fkbp5* (*Pomc^Fkbp5 OE*) was achieved by bilateral injections of a *Cre*-dependent *Fkbp5* OE virus (pAAV-Cre-dependent-CAG-HA-human wildtype FKBP51 WPRE-BGH-polyA, titer: 1.3×10^{12} genomic particles/ml, Gene Detect GD1001-RV) into the ARC of male *Pomc-Cre* mice. Control *Pomc-Cre* mice were injected with an AAV2-eSyn-GFP control virus (titer: 1.3×10^9 genomic particles/ml, Vector Biolabs VB1107). Stereotactic surgeries were performed as described previously (Häusl et al., 2021). In brief, male mice between 6 to 7 months of age were anesthetized with isoflurane and fixated in a stereotactic apparatus. Then, 0.5 µl of above-mentioned viruses were bilaterally injected into the ARC at a 0.05 µl/min flow rate with glass capillaries with a tip resistance of 2 – 4 MΩ. To target the ARC the following coordinates were used: - 1.5 mm anterior to bregma, ± 0.35 mm lateral from midline, and 5.8 mm below the surface of the skull. After surgery, animals were treated with meloxicam for three days and were allowed to recover for four weeks before initiating the experimental phase.

2.5 RNAScope – Validation of *Fkbp5* KO in *AgRP^Fkbp5-/-* and OE in *Pomc^Fkbp5 OE*

To validate successful KO of *Fkbp5* in *AgRP*-expressing neurons of the ARC and to confirm viral OE of *Fkbp5* in *Pomc^+* neurons, we performed an RNAScope experiment on tissue sections of male *AgRP^Fkbp5-/-* and *Pomc^Fkbp5 OE* animals. Frozen tissue was sectioned at 20 µm at -20 °C in a cryostat microtome. Sections were thaw mounted on Super Frost Plus slides, dried and stored at -80 °C. The RNA Scope Fluorescent Multiplex Reagent kit (cat. no. 320850, Advanced Cell Diagnostics, Newark, CA, USA) was used for mRNA staining. Probes used for

staining were; *Fkbp5* (Mm-Fkbp5-C1) for native *Fkbp5* expression, human *Fkbp5* (H-Fkbp5-C1) for detection of viral OE, *Pomc* (Mm-Pomc-C2) and *AgRP* (Mm-AgRP-C2). The provided *Fkpb5* probe spans Exon 9, which is deleted in *AgRP*$^{Fkbp5-/-}$ and Pomc$^{Fkbp5-/-}$ line, but also targets neighboring exons. Consequently, the *Fkbp5* probe may still bind to truncated mRNA leading to a residual *Fkbp5* mRNA signal in knock-out cells, even though no functional FKBP51 protein can be expressed. The staining procedure was performed according to manufacturer's specifications and as performed previously (Häusl et al., 2021). Images of the ARC (left and right side) were acquired by an experimenter blinded to the condition of the animals. Sixteen-bit images of each section were acquired on a Zeiss confocal microscope using a 20x and 40x objective (n = 2 animals per experimental group). For every section, all images were acquired using identical settings for laser power, detector gain, and amplifier offset. *Fkbp5* mRNA expression in animals with a KO in AgRP neurons was analyzed using ImageJ with the experimenter blinded to the genotype of the animals and was counted manually. *AgRP*$^+$ cells were split up in 5 bins according to the amount of *Fkbp5* mRNA puncta counted inside the cell: Bin 0 (0 puncta), Bin 1 (1 - 3), Bin 2 (4 – 9), Bin 3 (10 – 15) and Bin 4 (> 15). Then, the percentage of *AgRP*$^+$ neurons in each bin was calculated from a total amount of 30 *AgRP*-expressing cells per image.

2.6 Tissue sampling procedure and hormone assessment

On the day of sacrifice, animals were weighed, deeply anesthetized with isoflurane and sacrificed by decapitation. For mRNA analyses, brains were removed and snap-frozen in isopentane at -40°C and stored at -80°C until further processing. Trunk blood (basal morning and basal adrenocorticotropin hormone (ACTH)) was collected in labeled 1.5 ml EDTA-coated microcentrifuge tubes (Kabe Labortechnik, Germany) and kept on ice until centrifugation. After centrifugation (4°C, 8,000 rpm for 15 min) plasma was removed and transferred to new, labeled 2 mL tubes and stored at -80°C until hormone quantification. Post stress CORT was collected 30 and 90 minutes post stress via tail cut and further processed like trunk blood. Baseline and post stress plasma CORT (ng/ml) and baseline ACTH (pg/ml) concentrations were determined by radioimmunoassay using CORT 125I RIA kit (sensitivity: 12.5 ng/ml, MP Biomedicals Inc) and ACTH 125I RIA kit (sensitivity: 10 pg/ml, MP Biomedicals Inc) following

the manufacturers' instructions and as described previously (Brix et al., 2022). Final CORT and ACTH levels were derived from the standard curve.

2.7 Nuclear magnetic resonance

In addition to weekly measures of BW, the animal's body composition was assessed with a body composition analyzer (LF50 BCA NMR Minispec Analyzer, Bruker Optik) after several weeks on chow and HFD. This method applies time domain nuclear magnetic resonance (TD - NMR) to measure lean tissue mass, fat mass and free fluids non-invasively and *in vivo* without the need for anesthetics in small rodents (Halldorsdottir et al., 2009). Body constituents were normalized to bodyweight for each group and ratio of fat to lean mass was calculated.

2.8 Intraperitoneal glucose (GTT) and insulin (ITT) tolerance test

After several weeks under chow diet, an intraperitoneal glucose tolerance test (GTT) was carried out as described previously after lights-on (Brix et al., 2022). A 20% D-(+)-Glucose solution (Sigma Aldrich, Merck, Darmstadt) was prepared, and animals were subjected to an overnight fast of 14 hours (6 p.m. until 8 a.m.) prior to the experiment. Every animal was weighed and intraperitoneally injected with 2 g glucose per kg bodyweight. Blood glucose concentrations were measured from tail stitches at 0, 15, 30, 60, 90, and 120 minutes after the glucose injection using a handheld XT glucometer (Bayer Health Care, Basel, Switzerland). An intraperitoneal insulin tolerance test (ITT) was performed 14 days after the GTT to ensure a complete recovery from the overnight fast. A similar procedure as for the GTT was applied as follows: An insulin stock solution of 0.5 IU/mL (Actrapid® Penfill®, Novo Nordisk Pharma GmbH, Bagsværd, Denmark) was prepared, and animals were fasted for 4 hours (7 until 11 a.m.) before the onset of the ITT. Every animal was weighed and intraperitoneally injected with 1IU insulin per kg bodyweight. Blood glucose concentrations were measured at 0, 15, 30, 60, 90, and 120 minutes after the insulin injection.

2.9 Indirect calorimetry

Metabolic phenotyping and food intake after several weeks on HFD challenge was conducted by an automated PhenoMaster version 7.2.8 open-circuit indirect, calorimetry system (TSE Systems) in single housed male and female *Pomc$^{Fkbp5-/-}$* mice as described previously (Brix et al., 2022). All animals were allowed to acclimatize to the experimental setup for 2 days with a

total experimental duration and data acquisition of 5 -7 days. Statistical analysis was performed exclusively on data from day 3 to day 6 (total of 72 hours) for all animals. Time plots were generated from hourly averages of all parameters over 72 hours. Means per day and night were calculated as the average of all measures over 72 hours. HFD and water were available ad libitum.

2.10 Behavioral assessment

Open field test

The first behavioral task of the test battery was the open field test (OF) to assess locomotor activity and anxiety-like behavior. Animals were placed in the lower left corner of the OF arenas (50 x 50 x 50 cm) right before 15 minutes of recording and tracking was started manually. Assessed parameters: inner zone entries, distance travelled, line crossings and mean speed.

Elevated plus maze

The elevated maze (50 cm above ground) consisted of two opposing open arms (30 x 5 x 0.5 cm) and two opposing enclosed arms (30 x 5 x 0.5 cm), which were connected by a central platform (5 x 5 cm) shaping a plus sign. At the beginning of the 10 minutes recording, animals were placed in the center zone, facing an enclosed arm before recording and tracking was started manually. Assessed parameters: open arm entries, distance travelled, line crossings and mean speed.

Dark-light box test

Finally, we assessed anxiety in the dark-light box test (DALI) at the third day of behavioral testing. The DALI apparatus has two compartments: One light compartment (30 x 20 x 25 cm) a dark and protected compartment (15 x 20 x 25 cm). Mice were placed in the lower left corner of the dark compartment, facing the center before manually starting the 5 minutes test. Assessed parameters: lit zone entries, distance travelled, line crossings and mean speed were analyzed.

2.11 Statistical analysis

The data presented are shown as means ± standard error of the mean (SEM) and samples sizes are indicated in the figure legends. All data were analyzed by the commercially available

GraphPad Prism 9.0 software (GraphPad Software, San Diego, California, USA). When two groups were compared, the unpaired two-tailed *student's t test* was applied. If data were not normally distributed the non-parametric *Mann-Whitney test* (*MW test*) was used. Data based on repeated observations comparing two groups were tested by repeated measures ANOVA. *P* values of less than 0.05 were considered statistically significant. Statistical significance was defined as: *p $\leq$ 0.05, **p $\leq$ 0.01, *** p $\leq$ 0.001, **** p $\leq$ 0.0001. A statistical trend was accepted with a p value of 0.05 $\leq$ p $\leq$ 0.1 and indicated in the figures with the symbol "T". Outliers were assessed with the online available Graph Pad outlier calculator performing the two-sided *Grubb's* outlier test. As this was an exploratory study, no statistical methods were used to predetermine sample sizes.

3. Results

3.1 KO of *Fkbp5* in POMC neurons of male mice increases activity and improves whole-body metabolism under HFD

The successful and specific knockout of *Fkbp5* in *Pomc*-expressing neurons of the ARC and cells within the pituitary gland was confirmed recently in a publication by our lab describing the endocrine phenotype and stress physiology of the *Pomc*$^{Fkbp5-/-}$ KO model in the context of aging (Brix et al., 2022). In the current study, we show that deletion of FKBP51 in *Pomc*-expressing neurons of the ARC does not induce metabolic changes unless challenging this model with a HFD over several weeks (16 weeks) **(Fig. 1 A – L)**. Weekly BW measures in two separate cohorts (Chow and HFD) revealed a significantly lower HFD-induced BW gain in *Pomc*$^{Fkbp5-/-}$ KO animals compared to *Fkbp5*$^{lox/lox}$ controls, which remained stable over the course of the experiment (Chow: $F_{1,39}$ = 0.89, p = 0.35; HFD: $F_{1,27}$ = 5.00, p = 0.03) **(Fig. 1 A)**. This reduction in BW gain in animals lacking FKBP51 in *Pomc* neurons was reflected in body composition scans under chow and HFD, which showed a lower fat-to-lean mass ratio in KO males compared to controls exclusively after a dietary challenge (chow: t_{29} = 0.68, p = 0.5; HFD: t_{29} = 3.53, p = 0.0014) **(Fig. 1 B)**. To assess the functional effects of deleting *Fkbp5* in POMC neurons on metabolic control, we performed GTTs and ITTs under chow and HFD showing that *Pomc*$^{Fkbp5-/-}$ mice exhibited improved insulin sensitivity compared to controls once differences in body weight became apparent (chow: GTT t_{38} = 0.50, p = 0.62, ITT U = *164*, p = 0.34; HFD: GTT t_{27} = 1.49, p = 0.15, ITT t_{27} = 2.3, p = 0.03) **(Fig. 1 C, D)**. This observation suggests that improved insulin signaling in *Pomc*$^{Fkbp5-/-}$ is a consequence rather than a cause of the differences in body weight after dietary challenge. To allow in depth metabolic phenotyping and to assess metabolic consequences of BW differences under a HFD (4.5 months), the animals' energy expenditure (EE), respiratory exchange ratio (RER), activity, speed and food intake were measured in metabolic cages via indirect calorimetry **(Fig. 1 E – L)**. RER ($F_{1,14}$ = 0.62, p = 0.44) and EE ($F_{1,14}$ = 2.0, p = 0.18) were unaffected by a deletion of FKBP51 **(Fig. 1 E, F)**. Interestingly, male *Pomc*$^{Fkbp5-/-}$ displayed increased activity during the day- and active night phase ($F_{1,14}$ = 0.72, p = 0.2; day: U = 36012, p = 0.015; night: U = 33966, p = 0.0007) **(Fig. 1 G – H)**. Mean speed was slightly but non-significantly increased during day and night ($F_{1,14}$ = 1.64, p = 0.22; day: U = 38579, p = 0.25; night: U = 37648, p = 0.11) **(Fig. 1 I – J)**. Food intake over the course of 72 hours did not differ between the two groups ($F_{1,12}$ = 0.002,

$p = 0.97$; day: $U = 81901$, $p = 0.29$; night: $U = 84209$, $p = 0.7$) **(Fig. 1 K, L)**. To assess the impact of a dietary challenge on the animal's endocrine phenotype, adrenal weights and CORT were measured at baseline under both dietary regimens. Other than a trend towards reduced baseline CORT levels on HFD $t_{27} = 0.16$, $p = 0.09$), $Pomc^{Fkbp5-/-}$ males did not display differences in adrenal size (chow: $t_{30} = 0.86$, $p = 0.4$; HFD: $t_{27} = 0.16$, $p = 0.87$) and chow baseline CORT $(U = 106.5$, $p = 0.61)$ **(Suppl. Fig. 1 A, B)**.
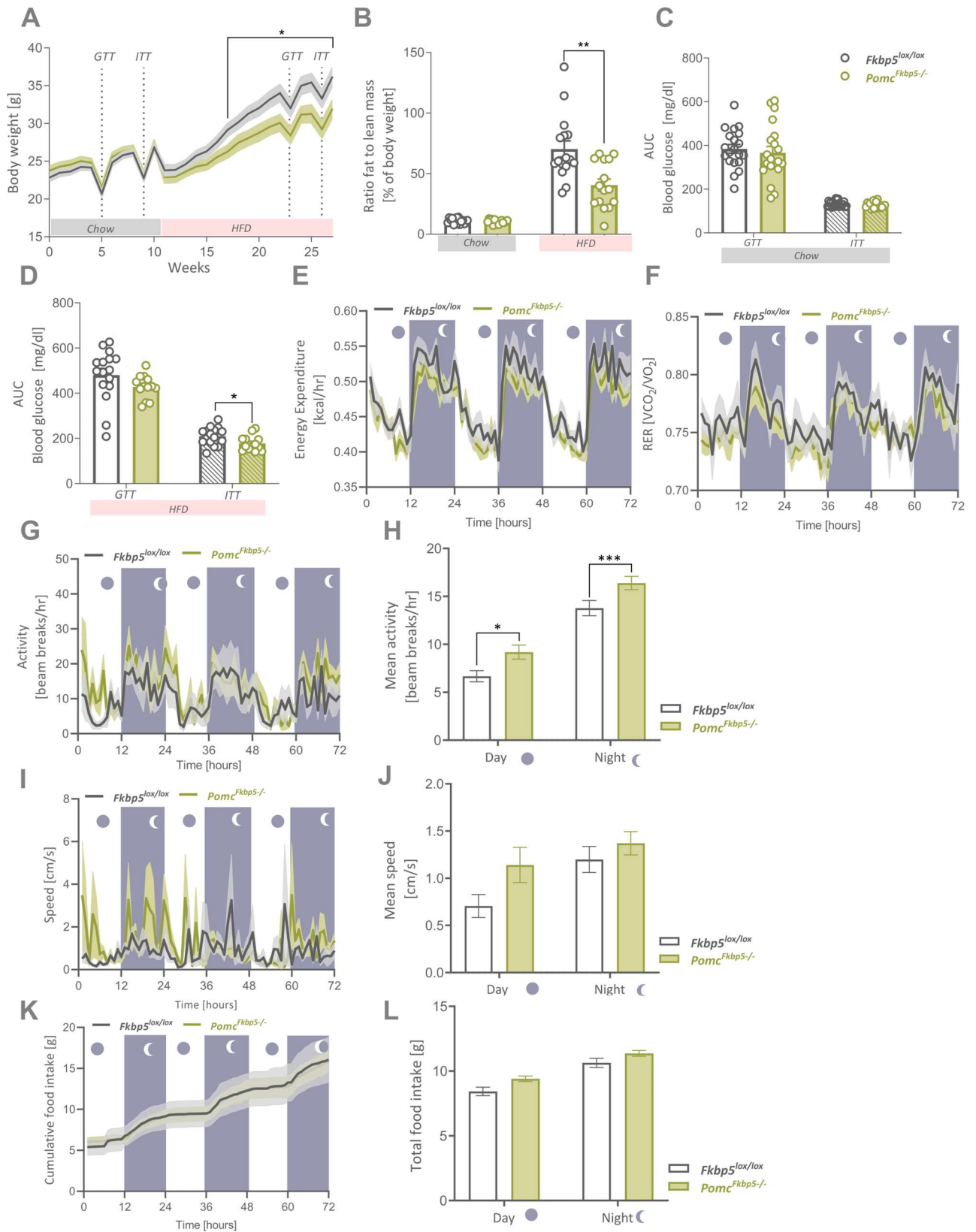
Figure 1: KO of *Fkbp5* in POMC neurons of male mice alters whole-body metabolism by increasing locomotion under HFD

(A) Endogenous KO of *Fkbp5* in *Pomc*-expressing neurons within the ARC increased HFD-induced BW gain (chow (11 weeks): n*Fkbp5lox/lox* = 21, n*PomcFkbp5-/-* = 20; HFD (16 weeks): n*Fkbp5lox/lox* = 16, n*PomcFkbp5-/-* =

13). **(B)** Higher BW was reflected in a significantly lower ratio of fat-to-lean mass in $Pomc^{Fkbp5-/-}$ KO males exclusively under high calorie load once differences in BW were present. **(C)** Blood glucose level in the GTT and ITT were unaltered after 5 and 7 weeks on chow diet. **(D)** After 15 weeks on a HFD, animals with a deletion of FKBP51 in $Pomc$-expressing ARC neurons developed improved insulin signaling but no changes in glucose tolerance were observed. EE **(E)** and RER **(F)** assessed over a time course of 72 hours via indirect calorimetry were unchanged between $Pomc^{Fkbp5-/-}$ and $Fkbp5^{lox/lox}$ animals. **(G), (H)** Activity and mean speed **(I, J)** were increased during both day and night in animals with a deletion of FKBP51. **(K, L)** Food intake was not different between groups ($n_{Fkbp5lox/lox}$ = 7, $n_{PomcFkbp5-/-}$ = 9). Data are received from male mice between 8 to 24 weeks of age and are presented as mean ± SEM. * p < 0.05, ** p < 0.01, *** p < 0.001, T 0.05 ≤ p ≤ 0.1. AUC area under the curve, EE energy expenditure, GTT glucose tolerance test, HFD high-fat diet, ITT insulin tolerance test, RER respiratory exchange ratio

3.2 KO of $Fkbp5$ in POMC neurons of female mice resembles male $Pomc^{Fkbp5-/-}$ metabolic phenotype

As sex differences in metabolic traits such as obesity, diabetes and cardiovascular disease have been extensively described in preclinical animal- and patient studies (Krishnan et al., 2018), we set out to characterize female $Pomc^{Fkbp5-/-}$ mice on a chow diet and after several weeks on a HFD (16 weeks). Under chow diet, BW **(Fig. 2 A)**, body composition (t_{27} = 0.22, p = 0.83) **(Fig. 2 B)**, glucose (t_{26} = 0.24, p = 0.81)- and insulin tolerance (U = 0.85, p = 0.54) **(Fig. 2 C)** were unaltered between female KO and control animals ($n_{Fbkp5lox/lox}$ = 18, $n_{PomcFkbp-/-}$ = 11). Comparable to the male mice, female KO mice showed differences in BW exclusively after a high-caloric load (Chow: $F_{1,27}$ = 1.12, p = 0.3; HFD: $F_{1,33}$ = 34.74, p < 0.0001) **(Fig. 2 A)**, which is why we went on to examine metabolic parameters under HFD in a second cohort of females ($n_{Fkbp5lox/lox}$ = 13, $n_{PomcFkbp5-/-}$ = 23). A body composition scan after 7 weeks on HFD consequently reflected differences in BW with a higher fat-to-lean mass ratio in $Fkbp5^{lox/lox}$ controls compared to $Pomc^{Fkbp5-/-}$ (t_{32} = 3.53, p = 0.0013) **(Fig. 2 B)**. As in males, female KO mice developed improved insulin signaling but no changes in glucose tolerance under HFD (HFD: GTT t_{33} = 0.04, p = 0.96; ITT t_{32} = 3.73, p = 0.0008) **(Fig. 2 D)**. EE ($F_{1,13}$ = 1.35, p = 0.27) and RER ($F_{1,13}$ = 0.77, p = 0.4) assessed by indirect calorimetry were unaffected by a KO of FKBP51 in POMC neurons of the ARC and could therefore not explain observed differences in BW **(Fig. 2 E, F)**. In line with findings in males, females with a KO of FKBP51 displayed significantly increased activity exclusively during their active phase at night ($F_{1,13}$ = 0.59, p = 0.46; day: U = 34614, p = 0.35; night: U = 31956, p = 0.02) **(Fig. 2 G, H)**. Further supporting this notion,

Pomc^Fkbp5-/- mice moved with significantly higher speed during the night ($F_{1,13}$ = 0.09, p = 0.76; day: U = 34231, p = 0.26; night: U = 32381, p = 0.03) **(Fig. 2 I, J)**. Food intake, was slightly but not significantly lower in *Pomc^Fkbp5-/-* females during the night ($F_{1,11}$ = 0.23, p = 0.64; day: U = 26114, p = 0.45; night: U = 25017, p = 0.13) **(Fig. 2 K, L)**. Together, assessment of metabolic parameters and in-depth phenotyping in metabolic cages indicate that animals lacking FKBP51 develop increased activity and speed, which appear to be causative for the observed protection against HFD-induced weight gain and subsequent metabolic complications. Relative adrenal weights were significantly increased after a HFD challenge in female *Pomc^Fkbp5-/-* (t_{32} = 2.78, p = 0.009) together with a trend towards increased morning CORT (t_{27} = 1.78, p = 0.09), and decreased ACTH levels (t_{33} = 2.37, p = 0.02) **(Suppl. Fig. 1 C – E)**.
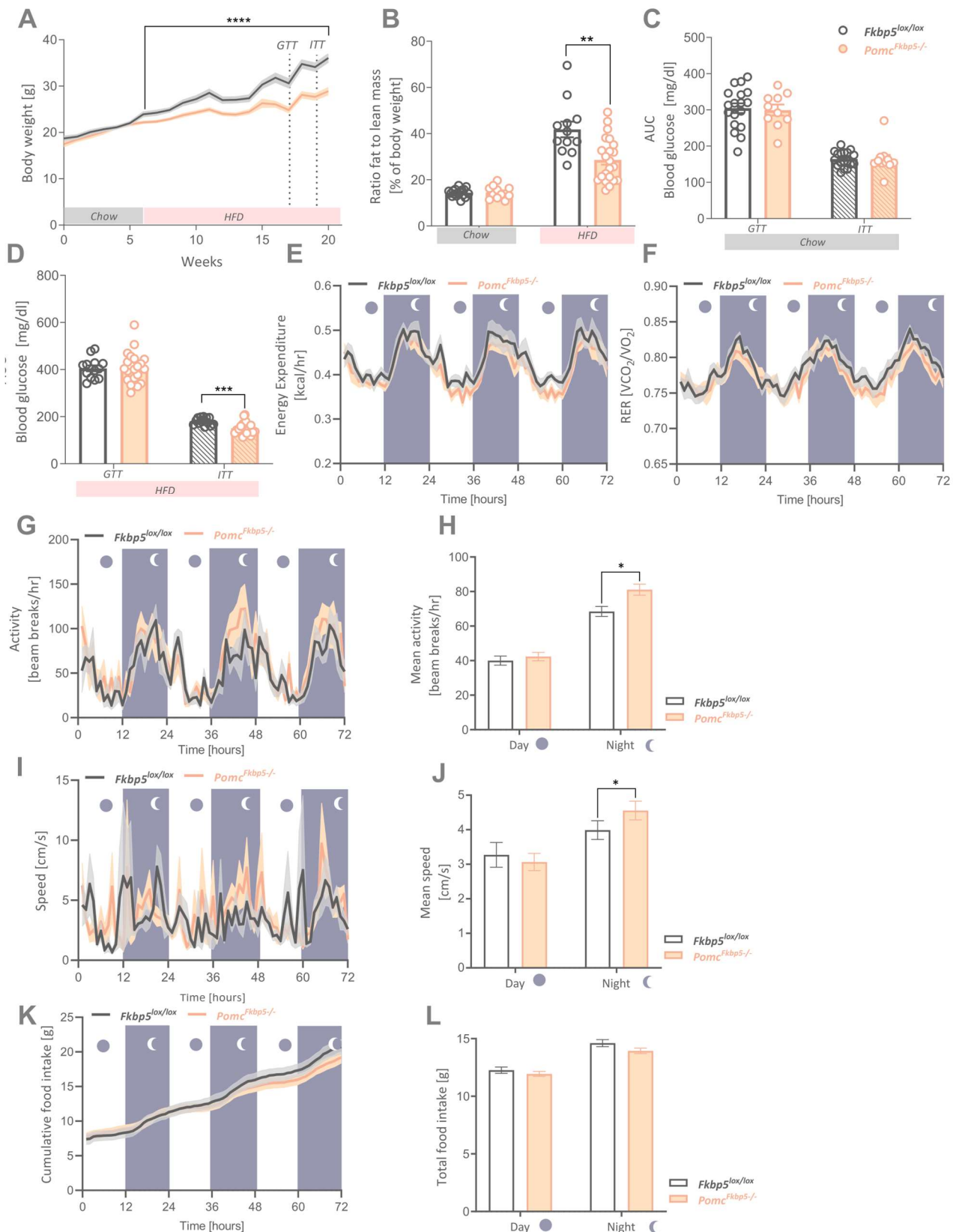
Figure 2: KO of *Fkbp5* in POMC neurons of female mice resembles male *Pomc^Fkbp5-/-* HFD-induced metabolic and locomotion phenotype

(A) Weekly assessment of BW over a period of 6 weeks on chow and 16 weeks on HFD revealed a blunted HFD-induced BW increase in female *Pomc^Fkbp5-/-* mice compared to *Fkbp5^lox/lox* controls (chow:

$n_{Fkbp5lox/lox}$ = 18, $n_{PomcFkbp5-/-}$ = 11; HFD: $n_{Fkbp5lox/lox}$ = 13, $n_{PomcFkbp5-/-}$ = 23). **(B)** A body composition scan after 7 weeks on HFD confirmed lower BW with a decreased ratio of fat-to-lean mass in females with a KO with no changes under chow diet. **(C)** There were no differences in glucose- and insulin tolerance under chow diet. **(D)** As in males, $Pomc^{Fkbp5-/-}$ KO mice showed improved insulin signaling after 13 weeks on HFD but there were no effects on glucose tolerance observed. EE **(E)** and RER **(F)** assessed over a time course of 72 hours by indirect calorimetry remained unaffected by a deletion of FKBP51 in POMC neurons. KO animals displayed higher activity **(G, H)** and speed **(I, J)** at night during their active phase. **(K – L)** Food intake was not different between KO and control animals in the metabolic cages (n = 8 animals per genotype). Data are received female mice per genotype between 4 to 10 weeks of age and are presented as mean ± SEM. * $p < 0.05$, ** $p < 0.01$, **** $p < 0.0001$. AUC area under the curve, EE energy expenditure, GTT glucose tolerance test, HFD high-fat diet, ITT insulin tolerance test, RER respiratory exchange ratio

3.3 Viral overexpression of *Fkbp5* in POMC neurons of male mice does not alter metabolism

Since there is solid evidence that mRNA expression of *Fkpb5* in the central MBH is increased during prolonged metabolic challenge (Balsevich et al., 2014; Scharf et al., 2011; Yang et al., 2012), we set out to investigate metabolic effects of *Fkbp5* OE exclusively within POMC neurons of the ARC. *Pomc*-specificity ($Pomc^{Fkbp5\ OE}$) was achieved by bilateral injections of a *Cre*-dependent *Fkbp5* OE virus into the ARC of male *Pomc-Cre* mice. Control mice received an AAV2-eSYN-GFP control virus **(Fig. 3 A)**. Qualitative analysis of viral *Fkbp5* mRNA OE in RNAScope images revealed a robust and very strong OE of the gene which in *Pomc*-expressing neurons within the ARC **(Fig. 3 B, C)**. Metabolic phenotyping under chow and HFD did however not reveal any effects of the *Fkbp5* OE on BW progression under dietary load ($F_{1,29}$ = 0.61, p = 0.44), body composition (U = 85, p = 0.18), glucose tolerance (Chow: U = 85, p = 0.44; HFD: U = 112, p = 0.77) and insulin signaling (Chow: t_{29} = 0.45, p = 0.22; HFD: U = 109, p = 0.68) **(Fig. 3 D – G)**. Further, viral OE of FKBP51 in POMC neurons of the ARC did not alter adrenal weights (after HFD) (t_{26} = 0.5, p = 0.62), morning CORT on chow (U = 111, p = 0.96) and HFD (t_{30} = 1.18, p = 0.25) and ACTH post dietary challenge (t_{28} = 1.0, p = 0.33) **(Suppl. Fig. 1F – H)**. Therefore, viral overexpression of *Fkbp5* in POMC neurons revealed that, in contrast to a deletion of this gene, unphysiologically high levels of this co-chaperone do not affect central MBH-regulated control of whole-body metabolism.

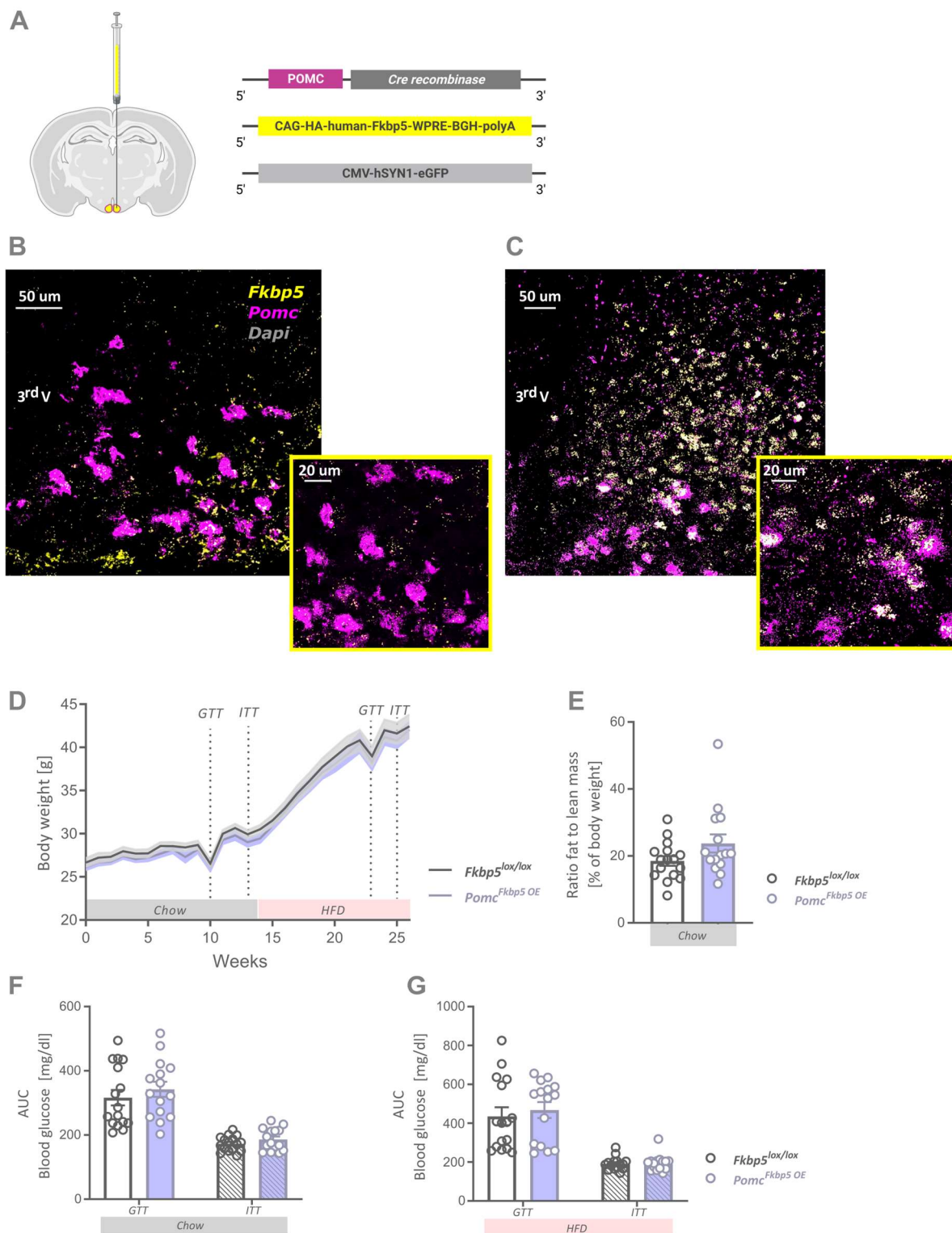Figure 3: Viral overexpression of *Fkbp5* in POMC neurons of male mice does not alter metabolism

(A) *Pomc*-specific *Fkbp5* OE was achieved by bilateral injections of a *Cre*-dependent human *Fkbp5* OE virus into the ARC of *Pomc-Cre* male mice (*Pomc$^{Fkbp5\ OE}$*; n = 15). Control *Pomc-Cre* animals received an eGFP control virus (n = 16). Representative RNAScope confocal images of *Fkbp5* mRNA expression in

Pomc^{+} neurons within the ARC in control *Fkbp5*[lox/lox] **(B)** and *Pomc*[Fkbp5 OE] animals (n = 1 male per group) **(C)**. Dashed yellow squares indicate areas chosen for 40x close-up images. **(D)** Assessment of weekly BW over a period of 14 weeks on chow and 13 weeks on HFD showed no differences in BW development in animals overexpressing *Fkbp5* in POMC neurons. **(E)** OE did not induce changes in body composition in *Pomc*[Fkbp5 OE] animals compared to controls. **(F – G)** Glucose tolerance and insulin signaling remained unaffected by OE of *Fkbp5* under both dietary conditions. Data are received from male mice between 24 to 28 weeks of age and are presented as mean ± SEM. AUC area under the curve, GTT glucose tolerance test, HFD high-fat diet, ITT insulin tolerance test

3.4 KO of *Fkbp5* in AgRP neurons of male mice does not affect metabolic control nor locomotion

Another neuronal population within the ARC, which has been studied extensively in the context of hypothalamic control of food intake and metabolism, expresses *AgRP* and is described to counteract *Pomc* neurons in the melanocortin pathway (Yeo et al., 2021). Therefore, we hypothesized that endogenous KO of *Fkbp5* in *AgRP*-expressing neurons could induce a metabolic phenotype that contrasts with the described effects observed in our *Pomc*[Fkbp5-/-] mice. *AgRP*-specific conditional KO (*AgRP*[Fkbp5-/-]) was achieved by crossing the *Fkbp5*[lox/lox] with the *AgRP-Cre* line (Tong et al., 2008), which expresses *Cre*-recombinase under the *AgRP* promoter. Qualitative and semi-quantitative analysis of RNAScope images **(Fig. 4 A)** revealed successful and *AgRP*-specific KO of *Fkbp5* in the ARC (Bin 1 (1-3 puncta): t_{20} = 2.39, p < 0.03; Bin 2 (4-9 puncta): U = 26, p = 0.04) **(Fig. 4 B)**. Contrary to our expectations, FKBP51 deletion in this neuronal subpopulation within the ARC did not trigger differences in BW ($F_{1,29}$ = 0.34, p = 0.57) nor food intake ($F_{1,29}$ = 0.81, p = 0.38) under both dietary conditions **(Fig. 4 C - D)**. Further, glucose- (t_{29} = 0.42, p = 0.68) and insulin tolerance (t_{28} = 1.13, p = 0.27) on chow diet remained unaffected by FKBP51 deletion **(Fig. 4 E)**. Besides their well described role in hypothalamic control of food intake and energy homeostasis (Deem et al., 2021), *AgRP/Npy*-expressing neurons within the MBH were shown to engage in HPA axis activity (Chong et al., 2015; Li et al., 2019; Perry et al., 2019; Rutters et al., 2012; Xiao et al., 2003). Therefore, we investigated potential changes in HPA axis function in our KO model by measuring relative adrenal weights under chow (t_{29} = 0.62, p = 0.54) and HFD (t_{12} = 0.03, p = 0.98) and performed an acute 15 minutes restraint stress challenge (basal: U = 85, p = 0.34; T30 min t_{29} = 0.27, p = 0.79; T90 min U = 72, p = 0.19) **(Suppl. Fig. 1 I – J)**, neither of which showed any functional

consequences of the KO. A behavioral test battery with an open field test (OF) (inner zone entries: U = 105.5, p = 0.58; distance travelled: t_{30} = 0.25, p = 0.81; line crossings: t_{30} = 0.07, p = 0.94; mean speed: t_{30} = 0.23, p = 0.82), elevated plus maze (EPM) (inner zone entries: t_{29} = 1.5, p = 0.14; distance travelled: t_{29} = 0.14, p = 0.89; line crossings: t_{29} = 0.55, p = 0.58; mean speed: t_{29} = 0.16, p = 0.88) and a dark-light (DALI) test (lit zone entries: t_{24} = 0.30, p = 0.77; distance travelled: U = 95, p = 0.7; line crossings: U = 94.5, p = 0.85; mean speed: t_{28} = 0.5, p = 0.62) did not reveal any effects on anxiety-related- and locomotion phenotypes in KO mice compared to controls (Suppl. Fig. 2 A – C). In summary, KO of *Fkbp5* in AgRP neurons of the ARC did not induce changes in whole-body metabolism, left HPA axis function intact and did not elicit behavioral changes as described in *Pomc*$^{Fkbp5-/-}$ animals in this and a recently published study from our lab (Brix et al., 2022).
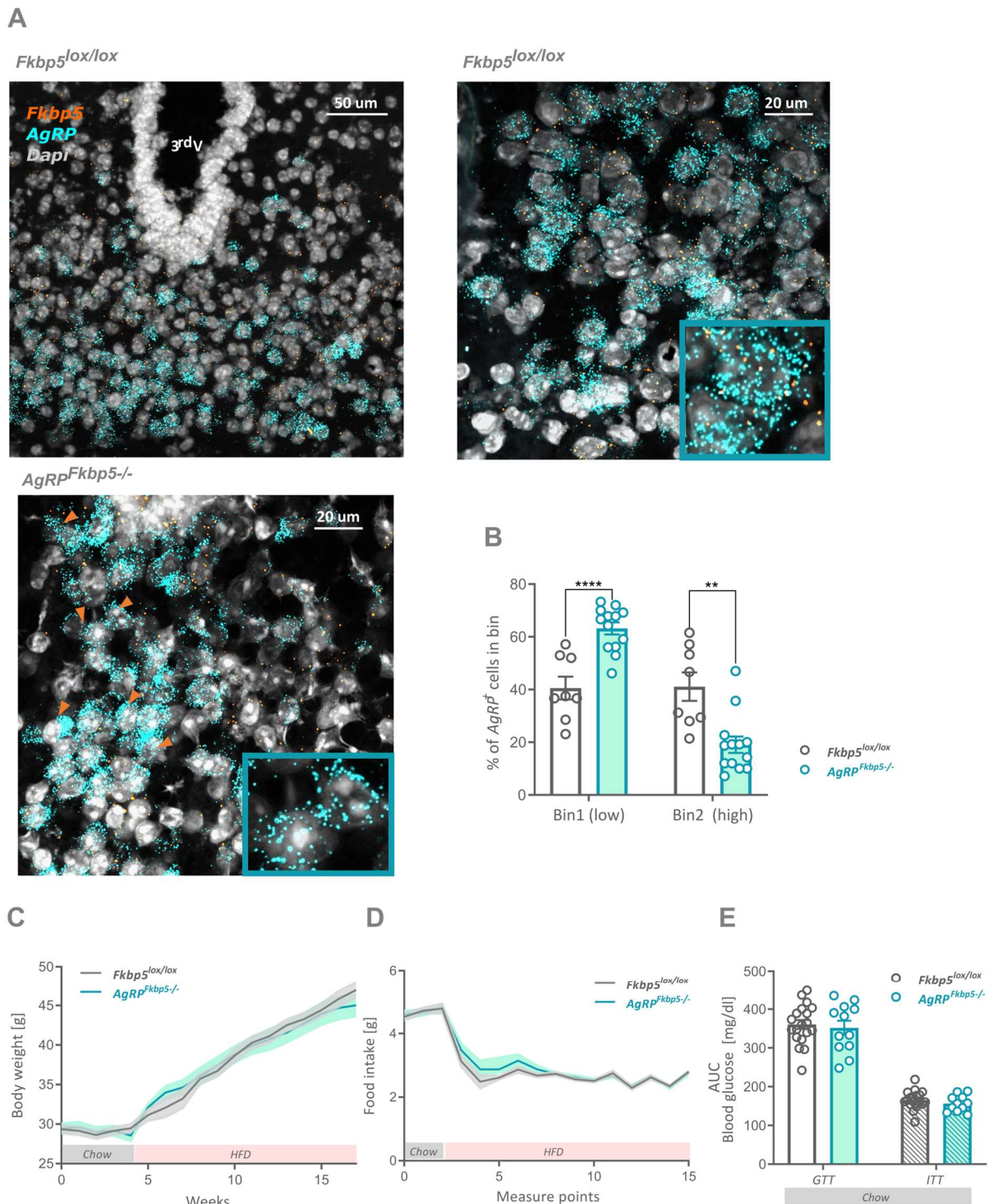
Figure 4: KO of *Fkbp5* in AgRP neurons of the ARC does not affect metabolism in male mice

(A) Representative RNAScope confocal images show co-expression of *Fkbp5* mRNA with *AgRP⁺* neurons in the ARC of male *Fkbp5^lox/lox* and *AgRP^Fkbp5-/-* KO mice. Orange arrow heads indicate *AgRP⁺* neurons with a complete KO of *Fkbp5*. (B) Semi-quantitative analysis of *Fkbp5* mRNA expression in AgRP neurons revealed a significant increase in *AgRP⁺* cells expressing a low number of *Fkbp5* mRNA puncta (Bin 1: 1 – 3 puncta) and a significantly lower percentage of high-expressors (Bin 2: 4 – 9 puncta) in

AgRP^Fkbp5-/- KO mice (n = number of analyzed 40x confocal images of either left or right ARC, n_{KO} = 14, $n_{Control}$ = 8; 2 males per genotype). Irrespective of the dietary regimen, BW **(C)** and food intake **(D)** were not affected by a KO of *Fkbp5* in AgRP neurons of the ARC. **(E)** Glucose- and insulin tolerance under chow diet remained unaffected in *AgRP^Fkbp5-/-* males compared to controls ($n_{Fkbp5lox/lox}$ = 19; $n_{AgRPFkbp5-/-}$ = 12). Data are received from male mice between 16 to 20 weeks of age and are presented as mean ± SEM. AgRP agouti-related protein, AUC area under the curve, GTT glucose tolerance test, HFD high-fat diet, ITT insulin tolerance test

4. Discussion

While recent work from our lab revealed that *Sf1*-expressing neurons in the VMH are not the driving force (Brix et al., 2022, in submission) behind strong (and opposing) phenotypes achieved with an MBH-wide (Häusl et al., 2022) or a full KO of *Fkbp5* (Balsevich et al., 2017; Hartmann et al., 2012; Stechschulte et al., 2016), this study is the first to identify a cell-type specific role of this co-chaperone in robust metabolic phenotypes. Endogenous KO in *Pomc*-(*Pomc^{Fkbp5-/-}*) and *AgRP*-expressing (*AgRP^{Fkbp5-/-}*) neurons, and viral cell-type specific OE of *Fkbp5* in the ARC, suggested a beneficial effect of FKBP51 deletion exclusively in the *Pomc^{Fkbp5-/-}* mouse model, in both sexes. Male and female mice with a KO of FKBP51 in *Pomc*-expressing cells were protected from HFD-induced bodyweight gain, which was reflected in a higher ratio of fat to lean mass and improved insulin signaling. Intriguingly, described metabolic improvements were absent under a chow diet and were dependent on a HFD trigger. It is known that diet-induced obesity undermines the ability of POMC neurons to appropriately respond to nutrients and hormones, and chronic exposure to high-fat feeding decreased the electrophysiological properties of these neurons (Quarta et al., 2020). Further, our lab revealed that central *Fkbp5* is upregulated in the MBH in response to a high-fat diet challenge (Balsevich et al., 2014). Therefore, our model suggests that FKBP51 could be involved in intra- and intercellular pathogenic alterations underlying HFD-induced POMC dysfunction. In line with this hypothesis, a KO of *Fkbp5* in this vulnerable neuronal population of the ARC should have a protective effect against HFD-induced maladaptation of this system, which is what we show in our *Pomc^{Fkbp5-/-}* model.

A prolonged HDF and resulting obese phenotypes were shown to induce hypothalamic inflammatory pathways and increased autophagic activity, particularly at the level of POMC neurons (Le Thuc et al., 2017; Thaler et al., 2012). These long-term neuronal alterations induced by elevated pro-inflammatory signaling, such as the inhibitor of κB kinase-β (IKKβ)-nuclear factor kappa B (NFκB) pathway (Jais and Brüning, 2017), can eventually lead to apoptotic events and therefore to POMC neuron death (Moraes et al., 2009; Thaler et al., 2012). Ultimately this results in HFD-induced insulin and leptin resistance and supports obesity and related metabolic complications (Ullah et al., 2021).

At this stage, we can only speculate about the possible involvement of FKBP51 in these maladaptive processes in POMC neurons, but there are two promising lines of thought. **1)** A direct mechanistic role of FKBP51 in inflammatory signaling: Immunoprecipitation studies in

cell culture by Kästle and colleagues described the presence of a complex of FKBP51, Hsp90, GR, and members of the IKK family. Intriguingly, RNAi-mediated silencing of *Fkbp5* reduced NFκB signaling, demonstrating FKBP51s potential for a broad anti-inflammatory profile (Kästle et al., 2018). In line with this, human genome-wide association studies by Zannas et al. linked higher *Fkbp5* mRNA in human blood cells with a pro-inflammatory profile and altered NFκB-related gene networks (Zannas et al., 2019). Hence, the KO of *Fkbp5* in our *Pomc*^Fkbp5-/- mouse model could protect animals from HFD-induced inflammation. **2)** A role of FKBP51 in the inflammation-driven increase of autophagic signaling and cell-death (Thaler et al., 2012): While, described HFD-induced increase in autophagic signaling in the MBH may serve to minimize neuronal inflammation and injury (Meng and Cai, 2011), there is emerging evidence that autophagy is a primary mechanism of cell death (autophagic cell death) (Jung et al., 2020). As for the role of FKBP51 in autophagy signaling, there is ample evidence that this co-chaperone is an important upstream regulator of this pathway (Gassen et al., 2019, 2014; Häusl et al., 2022). The MBH-wide FKBP51 manipulation study by Häusl revealed that FKBP51 steers autophagy pathways in the MBH in a dose-dependent inversed u-shaped manner. Hereby, the absence of FKBP51(KO) reduced MBH autophagy signaling in contrast to excessive, non-physiological levels (OE), which block autophagy (Häusl et al., 2022).

Metabolic cage experiments revealed that *Pomc*^Fkbp5-/- females and males had a higher voluntary locomotor activity, an effect that had already been shown in full FKBP51 KO males (Balsevich et al., 2017). Intriguingly, we have observed this phenomenon before in our *Pomc*^Fkbp5-/- model in classical behavioral tasks to assess locomotion and anxiety-related phenotypes (Brix et al., 2022). Zhan and colleagues showed that one of the downstream metabolic effects of POMC deletion in the ARC, which mimics a malfunctioning or cell-death of this neuronal population, is a reduction in voluntary locomotion, along with a decrease in food intake and increase in bodyweight. Interestingly, this POMC deletion study excluded a role of POMC neurons in the NTS in mediating these effects, suggesting that the ARC is the neuronal hub that enables changes in locomotion and energy metabolism in our model (Zhan et al., 2013). In this sense, there is ample evidence for the role of ARC POMC neurons and the melanocortin signaling pathway in controlling rodent locomotor activity (Adage et al., 2001; Caron et al., 2018; Huo et al., 2009; Lute et al., 2014; Marie et al., 2000; Pei et al., 2019; Reinoß et al., 2020). The potential underlying mechanism causing changes in locomotor activity could be described HFD-induced inflammation of POMC neurons, as hypothalamic induction of

inflammatory pathways in mice via bacterial lipopolysaccharide (LPS) injections decreased locomotor activity (Le Thuc et al., 2017). Therefore, it is tempting to speculate that the deletion of FKBP51 in our *Pomc^Fkbp5-/-* mice prevents inflammation-induced autophagic cell death and the associated decrease in locomotor activity, thus protecting the animals from POMC-mediated dysregulation of energy metabolism under HFD.

A possible explanation for the lack of an FKBP51 OE effect (*Pomc^Fkbp5 OE*) is the high age of the animals at the beginning of the experiments (8 – 9 months), which is a major limitation of this study. In this age range, studies show that aging can accelerate obesity-induced comorbidities and that aged mice are more vulnerable to the effects of a prolonged HFD (Azzu and Valencak, 2017; Moreno-Fernandez et al., 2021). Further, FKBP51 was shown to increase with aging (Sabbagh et al., 2014; Zannas et al., 2019) and under a HFD challenge (Balsevich et al., 2014). Hence, age-related metabolic perturbations could override any beneficial or detrimental effects of our genetic manipulation in this experiment, as the potential of FKBP51 to drive underlying mechanisms in POMC neurons could be limited (ceiling-effect).

The absence of a metabolic phenotype in our *AgRP^Fkbp5-/-* mouse model was surprising in light of AgRP's important role in energy metabolism, food intake, locomotion and food foraging (Dietrich et al., 2015; Huang et al., 2013; Timper and Brüning, 2017). One possible explanation is that AgRP neurons are activated most prominently and robustly under food deprivation and in fasted states, driving food foraging- and intake (Dietrich et al., 2015; Takahashi and Cone, 2005). Therefore, it is likely that we are overlooking FKBP51-related effects in AgRP neurons with our experimental set up, and future experiments in this mouse model should include an assessment of homeostatic states in fasted and food deprived animals.

In summary, we demonstrate that male and female mice with a KO of FKBP51 in POMC neurons of the ARC exhibit improved whole-body metabolism, a phenotype that is most likely driven by increased voluntary locomotor activity. Considering that the disruption of FKBP51 in POMC neurons of the ARC is consistent with a full FKBP51 KO (Balsevich et al., 2017; Stechschulte et al., 2016) and in contrast to an MBH-specific central *Fkbp5* KO (Häusl et al., 2022), this study highlights the complexity of tissue- and cell type-specific, but also cross-tissue effects of FKBP51 in whole-body metabolism. With this study, we are opening up a new research avenue for the development of targeted therapeutic interventions for the treatment of metabolic diseases and their comorbidities.

Author contributions

L.M.B., A.S.H. and M.V.S.: Conceived the project and designed the experiments. J.M.D.: Provided scientific expertise for establishing the *Pomc*$^{Fkbp5-/-}$ and *AgRP*$^{Fkbp5-/-}$ mouse lines. L.M.B. and A.S.H. managed the mouse lines. L.M.B., I.T. and L.A. designed and performed RNAscope experiments and manual counting of cells. L.M.B. performed surgeries and L.M.B. and V.K. performed experiments and analysis of data. I.T., L.A., J.B., L.v.D., C.E., V.K., S.N., M.S., V.S. and H.Y. assisted with the experiments. L.M.B.: Wrote the initial version of the manuscript. M.V.S.: Supervised the research and all authors revised the manuscript.

Acknowledgments

References

Adage, T., Scheurink, A.J.W., De Boer, S.F., De Vries, K., Konsman, J.P., Kuipers, F., Adan, R.A.H., Baskin, D.G., Schwartz, M.W., Van Dijk, G., 2001. Hypothalamic, Metabolic, and Behavioral Responses to Pharmacological Inhibition of CNS Melanocortin Signaling in Rats. J. Neurosci. 21, 3639–3645. https://doi.org/10.1523/JNEUROSCI.21-10-03639.2001

Azzu, V., Valencak, T.G., 2017. Energy Metabolism and Ageing in the Mouse: A Mini-Review. Gerontology 63, 327–336. https://doi.org/10.1159/000454924

Balsevich, G., Häusl, A.S., Meyer, C.W., Karamihalev, S., Feng, X., Pöhlmann, M.L., Dournes, C., Uribe-Marino, A., Santarelli, S., Labermaier, C., Hafner, K., Mao, T., Breitsamer, M., Theodoropoulou, M., Namendorf, C., Uhr, M., Paez-Pereda, M., Winter, G., Hausch, F., Chen, A., Tschöp, M.H., Rein, T., Gassen, N.C., Schmidt, M. V., 2017. Stress-responsive FKBP51 regulates AKT2-AS160 signaling and metabolic function. Nat. Commun. 2017 81 8, 1–12. https://doi.org/10.1038/s41467-017-01783-y

Balsevich, G., Uribe, A., Wagner, K. V, Hartmann, J., Santarelli, S., Labermaier, C., Schmidt, M. V, 2014. Interplay between diet-induced obesity and chronic stress in mice: potential role of FKBP51. J. Endocrinol. 222, 15–26. https://doi.org/10.1530/JOE-14-0129

Balthasar, N., Coppari, R., McMinn, J., Liu, S.M., Lee, C.E., Tang, V., Kenny, C.D., McGovern, R.A., Chua, S.C., Elmquist, J.K., Lowell, B.B., 2004. Leptin receptor signaling in POMC neurons is required for normal body weight homeostasis. Neuron 42, 983–991. https://doi.org/10.1016/j.neuron.2004.06.004

Baughman, G., Wiederrecht, G.J., Chang, F., Martin, M.M., Bourgeois, S., 1997. Tissue Distribution and Abundance of Human FKBP51, an FK506-Binding Protein That Can Mediate Calcineurin Inhibition. Biochem. Biophys. Res. Commun. 232, 437–443. https://doi.org/10.1006/BBRC.1997.6307

Binder, E.B., Bradley, R.G., Liu, W., Epstein, M.P., Deveau, T.C., Mercer, K.B., Tang, Y., Gillespie, C.F., Heim, C.M., Nemeroff, C.B., Schwartz, A.C., Cubells, J.F., Ressler, K.J., 2008. Association of FKBP5 polymorphisms and childhood abuse with risk of posttraumatic stress disorder symptoms in adults. JAMA - J. Am. Med. Assoc. 299, 1291–1305. https://doi.org/10.1001/jama.299.11.1291

Binder, E.B., Salyakina, D., Lichtner, P., Wochnik, G.M., Ising, M., Pütz, B., Papiol, S., Seaman, S., Lucae, S., Kohli, M.A., Nickel, T., Künzel, H.E., Fuchs, B., Majer, M., Pfennig, A., Kern, N., Brunner, J., Modell, S., Baghai, T., Deiml, T., Zill, P., Bondy, B., Rupprecht, R., Messer, T., Köhnlein, O., Dabitz, H., Brückl, T., Müller, N., Pfister, H., Lieb, R., Mueller, J.C., Lõhmussaar,

E., Strom, T.M., Bettecken, T., Meitinger, T., Uhr, M., Rein, T., Holsboer, F., Muller-Myhsok, B., 2004. Polymorphisms in FKBP5 are associated with increased recurrence of depressive episodes and rapid response to antidepressant treatment. Nat. Genet. 36, 1319–1325. https://doi.org/10.1038/ng1479

Blüher, M., 2019. Obesity: global epidemiology and pathogenesis. Nat. Rev. Endocrinol. 2019 155 15, 288–298. https://doi.org/10.1038/s41574-019-0176-8

Brix, L.M., Häusl, A.S., Toksöz, I., Bordes, J., van Doeselaar, L., Engelhardt, C., Narayan, S., Springer, M., Sterlemann, V., Deussing, J.M., Chen, A., Schmidt, M. V., 2022. The co-chaperone FKBP51 modulates HPA axis activity and age-related maladaptation of the stress system in pituitary proopiomelanocortin cells. Psychoneuroendocrinology 138, 105670. https://doi.org/10.1016/J.PSYNEUEN.2022.105670

Caron, A., Lemko, H.M.D., Castorena, C.M., Fujikawa, T., Lee, S., Lord, C.C., Ahmed, N., Lee, C.E., Holland, W.L., Liu, C., Elmquist, J.K., 2018. POMC neurons expressing leptin receptors coordinate metabolic responses to fasting via su

ppression of leptin levels. Elife 7. https://doi.org/10.7554/ELIFE.33710
Chong, A.C.N., Vogt, M.C., Hill, A.S., Brüning, J.C., Zeltser, L.M., 2015. Central insulin signaling modulates hypothalamus–pituitary–adrenal axis responsiveness. Mol. Metab. 4, 83–92. https://doi.org/10.1016/J.MOLMET.2014.12.001

Deem, J.D., Faber, C.L., Morton, G.J., 2021. AgRP neurons: Regulators of feeding, energy expenditure, and behavior. FEBS J. https://doi.org/10.1111/FEBS.16176

Dietrich, M.O., Zimmer, M.R., Bober, J., Horvath, T.L., 2015. Hypothalamic Agrp Neurons Drive Stereotypic Behaviors beyond Feeding. Cell 160, 1222–1232. https://doi.org/10.1016/J.CELL.2015.02.024

Gassen, N.C., Hartmann, J., Zschocke, J., Stepan, J., Hafner, K., Zellner, A., Kirmeier, T., Kollmannsberger, L., Wagner, K. V., Dedic, N., Balsevich, G., Deussing, J.M., Kloiber, S., Lucae, S., Holsboer, F., Eder, M., Uhr, M., Ising, M., Schmidt, M. V., Rein, T., 2014. Association of FKBP51 with Priming of Autophagy Pathways and Mediation of Antidepressant Treatment Response: Evidence in Cells, Mice, and Humans. PLoS Med. 11. https://doi.org/10.1371/JOURNAL.PMED.1001755

Gassen, N.C., Niemeyer, D., Muth, D., Corman, V.M., Martinelli, S., Gassen, A., Hafner, K., Papies, J., Mösbauer, K., Zellner, A., Zannas, A.S., Herrmann, A., Holsboer, F., Brack-Werner, R., Boshart, M., Müller-Myhsok, B., Drosten, C., Müller, M.A., Rein, T., 2019. SKP2 attenuates autophagy through Beclin1-ubiquitination and its inhibition reduces MERS-Coronavirus

infection. Nat. Commun. 2019 101 10, 1–16. https://doi.org/10.1038/s41467-019-13659-4

Gautron, L., Elmquist, J.K., Williams, K.W., 2015. Neural Control of Energy Balance: Translating Circuits to Therapies. Cell 161, 133. https://doi.org/10.1016/J.CELL.2015.02.023

Georgescu, T., Lyons, D., Doslikova, B., Garcia, A.P., Marston, O., Burke, L.K., Chianese, R., Lam, B.Y.H., Yeo, G.S.H., Rochford, J.J., Garfield, A.S., Heisler, L.K., 2020. Neurochemical Characterization of Brainstem Pro-Opiomelanocortin Cells. Endocrinology 161, 1–13. https://doi.org/10.1210/ENDOCR/BQAA032

Halldorsdottir, S., Carmody, J., Boozer, C.N., Leduc, C.A., Leibel, R.L., 2009. Reproducibility and accuracy of body composition assessments in mice by dual energy x-ray absorptiometry and time domain nuclear magnetic resonance. Int. J. Body Compos. Res. 7, 147.

Harno, E., Ramamoorthy, T.G., Coll, A.P., White, A., 2018. POMC: The Physiological Power of Hormone Processing. https://doi.org/10.1152/physrev.00024.2017 98, 2381–2430. https://doi.org/10.1152/PHYSREV.00024.2017

Hartmann, J., Wagner, K., Liebl, C., Scharf, S., Wang, X., Wolf, M., Hausch, F., Rein, T., Schmidt, U., Touma, C., Cheung-Flynn, J., Cox, M., Smith, D., Holsboer, F., Müller, M., Schmidt, M., 2012. The involvement of FK506-binding protein 51 (FKBP5) in the behavioral and neuroendocrine effects of chronic social defeat stress. Neuropharmacology 62, 332–339. https://doi.org/10.1016/J.NEUROPHARM.2011.07.041

Häusl, A.S., Bajaj, T., Brix, L.M., Pöhlmann, M.L., Hafner, K., Angelis, M. De, Nagler, J., Dethloff, F., Balsevich, G., Schramm, K.-W., Giavalisco, P., Chen, A., Schmidt, M. V., Gassen, N.C., 2022. Mediobasal hypothalamic FKBP51 acts as a molecular switch linking autophagy to whole-body metabolism. Sci. Adv. 8, 4797. https://doi.org/10.1126/SCIADV.ABI4797

Häusl, A.S., Balsevich, G., Gassen, N.C., Schmidt, M. V., 2019. Focus on FKBP51: A molecular link between stress and metabolic disorders. Mol. Metab. 29, 170–181. https://doi.org/10.1016/J.MOLMET.2019.09.003

Häusl, A.S., Brix, L.M., Hartmann, J., Pöhlmann, M.L., Lopez, J.-P., Menegaz, D., Brivio, E., Engelhardt, C., Roeh, S., Bajaj, T., Rudolph, L., Stoffel, R., Hafner, K., Goss, H.M., Reul, J.M.H.M., Deussing, J.M., Eder, M., Ressler, K.J., Gassen, N.C., Chen, A., Schmidt, M. V., 2021. The co-chaperone Fkbp5 shapes the acute stress response in the paraventricular nucleus of the hypothalamus of male mice. Mol. Psychiatry 2021 1–17. https://doi.org/10.1038/s41380-021-01044-x

Huang, H., Lee, S.H., Ye, C., Lima, I.S., Oh, B.C., Lowell, B.B., Zabolotny, J.M., Kim, Y.B., 2013. ROCK1 in AgRP Neurons Regulates Energy Expenditure and Locomotor Activity in Male Mice. Endocrinology 154, 3660–3670. https://doi.org/10.1210/EN.2013-1343

Huo, L., Gamber, K., Greeley, S., Silva, J., Huntoon, N., Leng, X.H., Bjørbæk, C., 2009. Leptin-Dependent Control of Glucose Balance and Locomotor Activity by POMC Neurons. Cell Metab. 9, 537–547. https://doi.org/10.1016/J.CMET.2009.05.003

Jais, A., Brüning, J.C., 2017. Hypothalamic inflammation in obesity and metabolic disease. J. Clin. Invest. 127, 24. https://doi.org/10.1172/JCI88878

Jung, S., Jeong, H., Yu, S.W., 2020. Autophagy as a decisive process for cell death. Exp. Mol. Med. 2020 526 52, 921–930. https://doi.org/10.1038/s12276-020-0455-4

Kästle, M., Kistler, B., Lamla, T., Bretschneider, T., Lamb, D., Nicklin, P., Wyatt, D., 2018. FKBP51 modulates steroid sensitivity and NFκB signalling: A novel anti-inflammatory drug target. Eur. J. Immunol. 48, 1904. https://doi.org/10.1002/EJI.201847699

Krishnan, K.C., Mehrabian, M., Lusis, A.J., 2018. Sex differences in metabolism and cardiometabolic disorders. Curr. Opin. Lipidol. 29, 404. https://doi.org/10.1097/MOL.0000000000000536

Le Thuc, O., Stobbe, K., Cansell, C., Nahon, J.L., Blondeau, N., Rovère, C., 2017. Hypothalamic Inflammation and Energy Balance Disruptions: Spotlight on Chemokines. Front. Endocrinol. (Lausanne). 8, 1. https://doi.org/10.3389/FENDO.2017.00197

Lenard, N.R., Berthoud, H.R., 2008. Central and Peripheral Regulation of Food Intake and Physical Activity: Pathways and Genes. Obesity (Silver Spring). 16, S11. https://doi.org/10.1038/OBY.2008.511

Li, C., Hou, Y., Zhang, J., Sui, G., Du, X., Licinio, J., Wong, M.L., Yang, Y., 2019. AGRP neurons modulate fasting-induced anxiolytic effects. Transl. Psychiatry 2019 91 9, 1–10. https://doi.org/10.1038/s41398-019-0438-1

Lute, B., Jou, W., Lateef, D.M., Goldgof, M., Xiao, C., Piñol, R.A., Kravitz, A. V., Miller, N.R., Huang, Y.G., Girardet, C., Butler, A.A., Gavrilova, O., Reitman, M.L., 2014. Biphasic Effect of Melanocortin Agonists on Metabolic Rate and Body Temperature. Cell Metab. 20, 333–345. https://doi.org/10.1016/J.CMET.2014.05.021

Marie, L.S., Miura, G.I., Marsh, D.J., Yagaloff, K., Palmiter, R.D., 2000. A metabolic defect promotes obesity in mice lacking melanocortin-4 receptors. Proc. Natl. Acad. Sci. U. S. A.

97, 12339–12344. https://doi.org/10.1073/PNAS.220409497

Matosin, N., Halldorsdottir, T., Binder, E.B., 2018. Understanding the Molecular Mechanisms Underpinning Gene by Environment Interactions in Psychiatric Disorders: The FKBP5 Model. Biol. Psychiatry. https://doi.org/10.1016/j.biopsych.2018.01.021

Meng, Q., Cai, D., 2011. Defective Hypothalamic Autophagy Directs the Central Pathogenesis of Obesity via the IκB Kinase β (IKKβ)/NF-κB Pathway. J. Biol. Chem. 286, 32324–32332. https://doi.org/10.1074/JBC.M111.254417

Millington, G.W.M., 2007. The role of proopiomelanocortin (POMC) neurones in feeding behaviour. Nutr. Metab. 2007 41 4, 1–16. https://doi.org/10.1186/1743-7075-4-18

Moraes, J.C., Coope, A., Morari, J., Cintra, D.E., Roman, E.A., Pauli, J.R., Romanatto, T., Carvalheira, J.B., Oliveira, A.L.R., Saad, M.J., Velloso, L.A., 2009. High-Fat Diet Induces Apoptosis of Hypothalamic Neurons. PLoS One 4, e5045. https://doi.org/10.1371/JOURNAL.PONE.0005045

Moreno-Fernandez, M.E., Sharma, V., Stankiewicz, T.E., Oates, J.R., Doll, J.R., Damen, M.S.M.A., Almanan, M.A.T.A., Chougnet, C.A., Hildeman, D.A., Divanovic, S., 2021. Aging mitigates the severity of obesity-associated metabolic sequelae in a gender independent manner. Nutr. Diabetes 2021 111 11, 1–13. https://doi.org/10.1038/s41387-021-00157-0

Morton, G.J., Schwartz, M.W., 2001. The NPY/AgRP neuron and energy homeostasis. Int. J. Obes. Relat. Metab. Disord. 25 Suppl 5, S56–S62. https://doi.org/10.1038/SJ.IJO.0801915

Myers, M.G., Olson, D.P., 2012. Central nervous system control of metabolism. Nat. 2012 4917424 491, 357–363. https://doi.org/10.1038/nature11705

Pei, H., Patterson, C.M., Sutton, A.K., Burnett, K.H., Myers, M.G., Olson, D.P., 2019. Lateral Hypothalamic Mc3R-Expressing Neurons Modulate Locomotor Activity, Energy Expenditure, and Adiposity in Male Mice. Endocrinology 160, 343–358. https://doi.org/10.1210/EN.2018-00747

Pereira, M.J., Palming, J., Svensson, M.K., Rizell, M., Dalenbäck, J., Hammar, M., Fall, T., Sidibeh, C.O., Svensson, P.A., Eriksson, J.W., 2014. FKBP5 expression in human adipose tissue increases following dexamethasone exposure and is associated with insulin resistance. Metabolism 63, 1198–1208. https://doi.org/10.1016/J.METABOL.2014.05.015

Perry, R.J., Resch, J.M., Douglass, A.M., Madara, J.C., Rabin-Court, A., Kucukdereli, H., Wu, C., Song, J.D., Lowell, B.B., Shulman, G.I., 2019. Leptin's hunger-suppressing effects are mediated by the hypothalamic–pituitary–adrenocortical axis in rodents. Proc. Natl. Acad.

Sci. U. S. A. 116, 13670–13679. https://doi.org/10.1073/PNAS.1901795116/SUPPL_FILE/PNAS.1901795116.SAPP.PDF

Quarta, C., Claret, M., Zeltser, L.M., Williams, K.W., Yeo, G.S.H., Tschöp, M.H., Diano, S., Brüning, J.C., Cota, D., 2021. POMC neuronal heterogeneity in energy balance and beyond: an integrated view. Nat. Metab. 1–10. https://doi.org/10.1038/s42255-021-00345-3

Quarta, C., Fioramonti, X., Cota, D., 2020. POMC Neurons Dysfunction in Diet-induced Metabolic Disease: Hallmark or Mechanism of Disease? Neuroscience 447, 3–14. https://doi.org/10.1016/J.NEUROSCIENCE.2019.09.031

Reinoß, P., Ciglieri, E., Minére, M., Bremser, S., Klein, A., Löhr, H., Fuller, P.M., Büschges, A., Kloppenburg, P., Fenselau, H., Hammerschmidt, M., 2020. Hypothalamic Pomc Neurons Innervate the Spinal Cord and Modulate the Excitability of Premotor Circuits. Curr. Biol. 30, 4579-4593.e7. https://doi.org/10.1016/J.CUB.2020.08.103

Rutters, F., La Fleur, S., Lemmens, S., Born, J., Martens, M., Adam, T., 2012. The Hypothalamic-Pituitary-Adrenal Axis, Obesity, and Chronic Stress Exposure: Foods and HPA Axis. Curr. Obes. Rep. 1, 199–207. https://doi.org/10.1007/S13679-012-0024-9/FIGURES/1

Sabbagh, J.J., O'Leary, J.C., Blair, L.J., Klengel, T., Nordhues, B.A., Fontaine, S.N., Binder, E.B., Dickey, C.A., 2014. Age-associated epigenetic upregulation of the FKBP5 gene selectively impairs stress resiliency. PLoS One 9, 107241. https://doi.org/10.1371/journal.pone.0107241

Scharf, S.H., Liebl, C., Binder, E.B., Schmidt, M. V., Müller, M.B., 2011. Expression and regulation of the Fkbp5 gene in the adult mouse brain. PLoS One 6. https://doi.org/10.1371/journal.pone.0016883

Sidibeh, C.O., Pereira, M.J., Abalo, X.M., J. Boersma, G., Skrtic, S., Lundkvist, P., Katsogiannos, P., Hausch, F., Castillejo-López, C., Eriksson, J.W., 2018. FKBP5 expression in human adipose tissue: potential role in glucose and lipid metabolism, adipogenesis and type 2 diabetes. Endocrine 1–13. https://doi.org/10.1007/s12020-018-1674-5

Smedlund, K.B., Sanchez, E.R., Hinds, T.D., 2021. FKBP51 and the molecular chaperoning of metabolism. Trends Endocrinol. Metab. 32, 862–874. https://doi.org/10.1016/J.TEM.2021.08.003

Stechschulte, L.A., Qiu, B., Warrier, M., Hinds, T.D., Zhang, M., Gu, H., Xu, Y., Khuder, S.S., Russo, L., Najjar, S.M., Lecka-Czernik, B., Yong, W., Sanchez, E.R., 2016. FKBP51 Null Mice Are Resistant to Diet-Induced Obesity and the PPARγ Agonist Rosiglitazone. Endocrinology

157, 3888. https://doi.org/10.1210/EN.2015-1996

Takahashi, K.A., Cone, R.D., 2005. Fasting Induces a Large, Leptin-Dependent Increase in the Intrinsic Action Potential Frequency of Orexigenic Arcuate Nucleus Neuropeptide Y/Agouti-Related Protein Neurons. Endocrinology 146, 1043–1047. https://doi.org/10.1210/EN.2004-1397

Thaler, J.P., Yi, C.X., Schur, E.A., Guyenet, S.J., Hwang, B.H., Dietrich, M.O., Zhao, X., Sarruf, D.A., Izgur, V., Maravilla, K.R., Nguyen, H.T., Fischer, J.D., Matsen, M.E., Wisse, B.E., Morton, G.J., Horvath, T.L., Baskin, D.G., Tschöp, M.H., Schwartz, M.W., 2012. Obesity is associated with hypothalamic injury in rodents and humans. J. Clin. Invest. 122, 153. https://doi.org/10.1172/JCI59660

Timper, K., Brüning, J.C., 2017. Hypothalamic circuits regulating appetite and energy homeostasis: pathways to obesity. Dis. Model. Mech. 10, 679–689. https://doi.org/10.1242/DMM.026609

Toda, C., Santoro, A., Kim, J.D., Diano, S., 2017. POMC Neurons: From Birth to Death. Annu. Rev. Physiol. https://doi.org/10.1146/annurev-physiol-022516-034110

Tong, Q., Ye, C.P., Jones, J.E., Elmquist, J.K., Lowell, B.B., 2008. Synaptic release of GABA by AgRP neurons is required for normal regulation of energy balance. Nat. Neurosci. 2008 119 11, 998–1000. https://doi.org/10.1038/nn.2167

Ullah, R., Rauf, N., Nabi, G., Yi, S., Yu-Dong, Z., Fu, J., 2021. Mechanistic insight into high-fat diet-induced metabolic inflammation in the arcuate nucleus of the hypothalamus. Biomed. Pharmacother. 142, 112012. https://doi.org/10.1016/J.BIOPHA.2021.112012

WHO, 2022. WHO European regional obesity report 2022.

Wochnik, G.M., Rüegg, J., Abel, G.A., Schmidt, U., Holsboer, F., Rein, T., 2005. FK506-binding proteins 51 and 52 differentially regulate dynein interaction and nuclear translocation of the glucocorticoid receptor in mammalian cells. J. Biol. Chem. 280, 4609–4616. https://doi.org/10.1074/jbc.M407498200

Xiao, E., Xia-Zhang, L., Vulliémoz, N.R., Ferin, M., Wardlaw, S.L., 2003. Agouti-related protein stimulates the hypothalamic-pituitary-adrenal (HPA) axis and enhances the HPA response to interleukin-1 in the primate. Endocrinology 144, 1736–1741. https://doi.org/10.1210/EN.2002-220013

Xu, Y., Elmquist, J.K., Fukuda, M., 2011. Central nervous control of energy and glucose balance: focus on the central melanocortin system. Ann. N. Y. Acad. Sci. 1243, 1.

https://doi.org/10.1111/J.1749-6632.2011.06248.X

Yang, L., Isoda, F., Yen, K., Kleopoulos, S.P., Janssen, W., Fan, X., Mastaitis, J., Dunn-Meynell, A., Levin, B., McCrimmon, R., Sherwin, R., Musatov, S., Mobbs, C. V., 2012. Hypothalamic Fkbp51 is induced by fasting, and elevated hypothalamic expression promotes obese phenotypes. Am. J. Physiol. - Endocrinol. Metab. 302, E987. https://doi.org/10.1152/AJPENDO.00474.2011

Yeo, G.S.H., Chao, D.H.M., Siegert, A.M., Koerperich, Z.M., Ericson, M.D., Simonds, S.E., Larson, C.M., Luquet, S., Clarke, I., Sharma, S., Clément, K., Cowley, M.A., Haskell-Luevano, C., Van Der Ploeg, L., Adan, R.A.H., 2021. The melanocortin pathway and energy homeostasis: From discovery to obesity therapy. Mol. Metab. 48, 101206. https://doi.org/10.1016/J.MOLMET.2021.101206

Zannas, A.S., Binder, E.B., 2014. Gene-environment interactions at the FKBP5 locus: Sensitive periods, mechanisms and pleiotropism. Genes, Brain Behav. 13, 25–37. https://doi.org/10.1111/gbb.12104

Zannas, A.S., Jia, M., Hafner, K., Baumert, J., Wiechmann, T., Pape, J.C., Arloth, J., Ködel, M., Martinelli, S., Roitman, M., Röh, S., Haehle, A., Emeny, R.T., Iurato, S., Carrillo-Roa, T., Lahti, J., Räikkönen, K., Eriksson, J.G., Drake, A.J., Waldenberger, M., Wahl, S., Kunze, S., Lucae, S., Bradley, B., Gieger, C., Hausch, F., Smith, A.K., Ressler, K.J., Müller-Myhsok, B., Ladwig, K.H., Rein, T., Gassen, N.C., Binder, E.B., 2019. Epigenetic upregulation of FKBP5 by aging and stress contributes to NF-κB-driven inflammation and cardiovascular risk. Proc. Natl. Acad. Sci. U. S. A. 166, 11370–11379. https://doi.org/10.1073/pnas.1816847116

Zhan, C., Zhou, J., Feng, Q., Zhang, J. en, Lin, S., Bao, J., Wu, P., Luo, M., 2013. Acute and Long-Term Suppression of Feeding Behavior by POMC Neurons in the Brainstem and Hypothalamus, Respectively. J. Neurosci. 33, 3624–3632. https://doi.org/10.1523/JNEUROSCI.2742-12.2013

Supplementary Figures

Suppl. Figure 1: Endocrine phenotyping of *Pomc^Fkbp5-/-* males and females, male mice overexpressing *Fkbp5* in POMC neurons and males with a KO of *Fkbp5* in AgRP neurons within the ARC

(A) Relative adrenal weight and baseline morning corticosterone (CORT) **(B)** were not altered in male knockout animals under chow and after 16 weeks on a HFD. **(C)** Relative adrenal weight of female

animals with a knockout of *Fkbp5* in POMC neurons was significantly increased after 16 weeks on a HFD with higher baseline CORT **(D)** and lower baseline ACTH levels **(E)**. **(F)** Relative adrenal weight, CORT under chow and HFD **(G)** and ACTH after HFD **(H)** remained unchanged male *Pomc^Fkbp5 OE* mice virally overexpressing *Fkbp5* in POMC neurons of the ARC. **(I)** Relative adrenal weight, CORT at baseline and after 15 minutes restraint stress **(J)** was unaltered in male *AgRP^Fkbp5-/-* mice with a knockout of *Fkbp5* in AgRP neurons. Data are received from male and female mice between 16 to 20 weeks of age and are presented as mean ± SEM. * p < 0.05, ** p < 0.01, T 0.05 ≤ p ≤ 0.1. ACTH adrenocorticotropin releasing hormone, CORT corticosterone, HFD high-fat diet
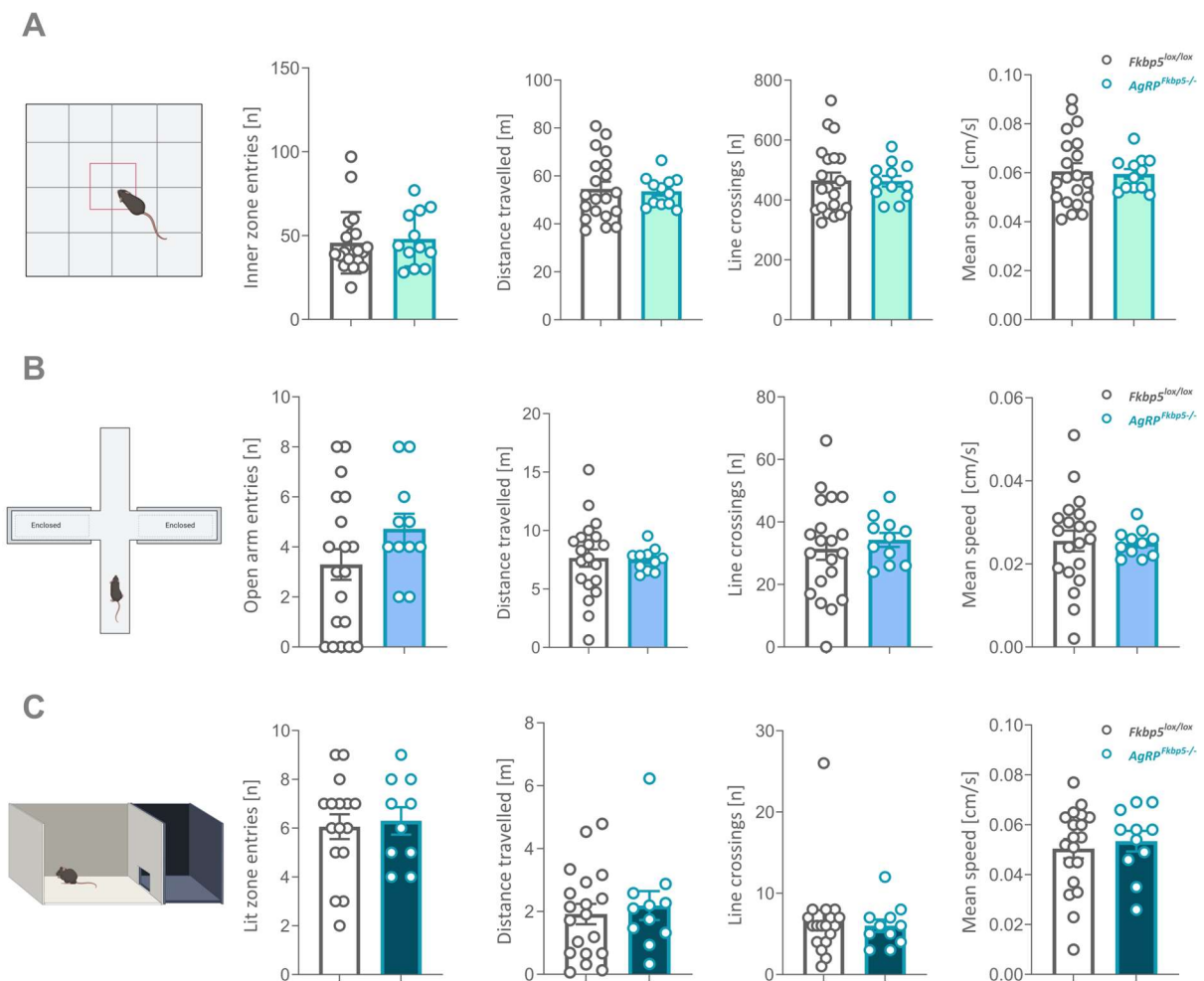
Suppl. Fig. 2: Behavioral assessment of anxiolytic phenotypes and locomotion in animals lacking FKBP51 in AgRP neurons

(A) Male *AgRP^Fkbp5-/-* mice with a deletion of FKBP51 in AgRP neurons in the arcuate nucleus did not develop an anxiolytic- nor a hyperlocomotion phenotype in the open field test as assessed with inner zone entries, distance travelled, line crossings and mean speed. The same parameters for locomotion and anxiety-related measures were unaltered between *AgRP^Fkbp5-/-* and *Fkbp5^lox/lox* in the elevated plus maze **(B)** and dark-light box **(C)**. Data are received from male mice between 12 to 16 weeks of age and are presented as mean ± SEM.

3. General Discussion

3.1 Summary

The main goal of this thesis was to decipher the tissue- and cell type-specific role of the co-chaperone FKBP51 in regulating the hormonal stress response system and energy metabolism. Since FKBP51 is best known for its critical involvement in the negative feedback control of the HPA axis, we set out to investigate the effects of its genetic manipulation in two anatomical nodes in this process. In particular, we examined its role in central negative feedback control and HPA axis (re)activity in the PVN of the hypothalamus (Chapter 2.1) and corticotrope POMC cells of the PIT (Chapter 2.2). Both studies confirmed that the loss of FKBP51 has a beneficial effect on HPA axis function by improving negative feedback, an effect that is dependent on the animals' age.

To further unravel the central role of FKBP51 in whole-body metabolism, we manipulated its expression in the MBH via viral approaches: we uncovered a novel regulatory role for FKBP51 in autophagy signaling, identifying new molecular interaction partners involved in this process (Chapter 2.3). To delve deeper into specific subnuclei of the MBH that may be involved in FKBP51-mediated actions in the MBH, we manipulated its expression in SF1 neurons of the VMH (Chapter 2.4) and POMC neurons of the ARC (Chapter 2.5). Intriguingly, the resulting phenotypes diverge in opposite directions, highlighting its cell type specificity in the regulation of energy metabolism.

These data are the first to examine the cell type-specific roles of FKBP51 in the HPA axis and metabolism *in vivo*. Therefore, they are crucial to decipher the potential of FKBP51 for targeted pharmacological interventions in treating psychiatric- and metabolic disease phenotypes. In this regard, the observed effects of FKBP51 depended mainly on the following aspects: cell type (Chapter 3.2 and 3.4), age (Chapter 3.3), dose (Chapter 3.4), and diet (Chapter 3.5).

3.2 The effects of FKBP51 on HPA axis (re)activity are unidirectional

In our first two studies (Chapter 2.1 and Chapter 2.2), we tested the hypothesis that ablation of FKBP51 in the PVN ($Fkbp5^{PVN-/-}$) and corticotrope POMC cells in the PIT ($Pomc^{Fkbp5-/-}$) improves the hormonal stress response and that this positive effect is mediated via negative feedback control of the HPA axis at the GR. This hypothesis is based on the well-established

negative regulatory role of FKBP51 at the GR (Touma et al., 2011) and FKBP51's stress-responsive nature (Zannas et al., 2019, 2015). It has been shown that the expression of *Fkbp5* is drastically increased after stress in stress-relevant brain regions, including the PVN and PIT (Jenkins et al., 2013; Scharf et al., 2011). In line with its mechanistic role in HPA axis negative feedback control, the 51KO mouse line displays decreased HPA axis (re)activity and Gr expression changes in response to acute stressors, positively shaping the neuroendocrine profile of these animals (Hartmann et al., 2012; Touma et al., 2011). Despite increasing evidence of a positive effect of FKBP51 loss on the hormonal stress response, the involvement of specific central and peripheral tissues and cell-types driving these phenotypes was previously unknown.

Therefore, we genetically and virally modulated *Fkbp5* expression in the PVN (Chapter 2.1) and PIT (Chapter 2.2), confirming findings in 51KO animals: both endogenous FKBP51 KO models *(Fkbp5$^{PVN-/-}$ and Pomc$^{Fkbp5-/-}$)* displayed improved HPA axis negative feedback control, whereas OE of the gene in the PVN (*Fkbp5$^{PVN\ OE}$*) reproduced physiological and endocrinological hallmarks of a chronic stress situation (Schmidt et al., 2007). Assessment of GR sensitivity via the DEX/CRH test produced very strong and robust phenotypes in both genetic lines, indicating the involvement of the GR in improved stress responses and negative feedback regulation. Interestingly, CORT levels were lower in *Fkbp5$^{PVN-/-}$* animals than in controls after both DEX and CRH, whereas *Pomc$^{Fkbp5-/-}$* mice showed differences exclusively after CRH. Our data suggest that this can be explained by slightly different modes of action of FKBP51 on GR activity in the two target tissues: A negative correlation between FKBP51 levels and GR activity, as determined by the phosphorylation status of the receptor, revealed that the phenotypes observed in the *Fkbp5$^{PVN-/-}$* model were due to direct involvement of FKBP51 in GR-mediated negative feedback. In *Pomc*-expressing cells of the PIT, our data suggest that KO of FKBP51 has an indirect effect on GR activity via reducing the efficiency of GCs on POMC downregulation (Kageyama et al., 2021). This proposed mechanism could explain why we did not observe differences in negative feedback regulation post DEX but rather a dampened (re)activation of the HPA axis after CRH. Taken together, both KO studies describe an improvement of GR-mediated negative feedback of the HPA axis via direct (*Fkbp5$^{PVN-/-}$*) or indirect (*Pomc$^{Fkbp5-/-}$*) actions of FKBP51 on GR activity.

Since the effects of the KO at these two anatomical sites in the periphery and in the brain are unidirectional, it is tempting to speculate that their effects on GR-mediated feedback are

additive, which would be reflected in more robust global 51KO phenotypes compared to a KO in one specific tissue. To approach this question, significance levels of the most informative HPA-related parameters (see Table 1) from two global 51KO ($Fkbp5^{-/-}$) studies by Touma et al. and Hartmann et al. (Hartmann et al., 2012; Touma et al., 2011) were qualitatively compared with our tissue specific KO studies in the PVN in chapter 2.1 (Häusl et al., 2021) and PIT in chapter 2.2 (Brix et al., 2022). The experimental procedures in the various studies are congruent for almost all endocrine parameters, as shown in the table below. What is immediately striking is that the basal CORT levels (A) in none of the four studies listed differ significantly from those of the control group. This confirms once again that FKBP51 is a stress-responsive gene whose expression must be triggered by a stressor to induce significant effects of its KO on stress physiology. Consistent with this, the 6-minute forced swim test (FST) (B) used in the Hartmann study (row 2) is not strong enough to trigger an effect compared to 15-minute restraint stress used in the other studies (except $Pomc^{Fkbp5-/-}$), underlining that the exact nature and strength of the stressor is decisive. This observation is in line with results by Scharf et al. (Scharf et al., 2011), who found that more severe stressors (24 h food deprivation) resulted in a higher expression shift of central $Fkbp5$ mRNA compared to milder and shorter stressors (15-minute restrained).

Comparing significance levels of all four studies across all parameters assessed, the KO of $Fkbp5$ in POMC cells of the PIT (row 4) was found to have the most specific effects on HPA axis activity, exclusively at CORT 60 minutes post stress, and CORT 30 minutes post CRH injection in the DEX/CRH (E) test. In contrast, the KO of $Fkbp5$ in the PVN (row 3) appears to elicit a comparable, if not stronger, stress phenotype than the global $Fkbp5^{-/-}$ KO (rows 1 and 2). It should be noted here that a global loss of FKBP51 also affects other brain regions that are crucial for the stress response, such as the amygdala, BNST, and HIP which could have counterregulatory or opposite effects. Engelhardt and colleagues showed that a KO of $Fkbp5$ in the BNST actually induced the opposite effect and increased the HPA axis (Engelhardt et al., 2021). Taken together, these results do not support the hypothesis of additive effects in global 51KO animals but instead suggest a predominantly PVN-driven effect on HPA axis function in all four studies, with a significant but not exclusive role of FKBP51 in the PIT in HPA axis (re)activity and stress recovery. This is consistent with our finding that reinstatement of $Fkbp5$ expression exclusively in the PVN of global 51KO animals raises HPA axis activity to WT

levels, demonstrating that FKBP51 in the PVN is necessary and sufficient to regulate HPA axis activity (Chapter 2.1) (Häusl et al., 2021).

Mouse line	Study	A) Basal CORT	B) CORT T^{15} post stress	C) CORT T^{60}_{90} post stress	D) CORT 6 h post DEX	E) CORT 30 min post CRH	F) Adrenals
$Fkbp5^{-/-}$ vs. $Fkbp5^{+/+}$	(Touma et al., 2011)	n.s.	***(Restraint)	* (75min)	*	***	
$Fkbp5^{-/-}$ vs. $Fkbp5^{+/+}$	(Hartmann et al., 2012)	n.s.	n.s.(FST)	* (90min)			*
$Fkbp5^{PVN-/-}$ vs. $Fkbp5^{lox/lox}$	(Häusl et al., 2021)	n.s.	***(Restraint)	* (60min)	***	***	***
$Pomc^{Fkbp5-/}$ vs. $Fkbp5^{lox/lo-}$	(Brix et al., 2022)	n.s.	n.s.(Restraint)	* (60min)	n.s.	***	n.s.

Table 1: Overview of the levels of statistical significance between different FKBP51 knockout (KO) mouse lines and their respective wildtype (WT) controls

Rows one and two show global 51KO ($Fkbp5^{-/}$) studies by Touma et al. and Hartmann et al. Rows three and four show tissue-specific KO studies by Häusl and Brix et al.: KO of $Fkbp5$ in the paraventricular nucleus (PVN; $Fkbp5^{PVN-/}$) and pro-opiomelanocortin (POMC; $Pomc^{Fkbp5-/}$) cells in the pituitary (PIT). **(A)** In all four studies, baseline plasma corticosterone (CORT) levels were assessed during the circadian nadir in the morning between 08:00 – 10:00 and were consistently unchanged between KOs and controls in each study. **(B)** Depicted are the significance levels of CORT 15 minutes after acute restraint stress. Applied stress was a 15-minute restraint stress in all studies, except for a 6-minute forced swim test (FST) in the study by Hartmann et al. **(C)** CORT levels in the recovery phase after the respective stress paradigm ranged from 60-90 minutes post stress (duration indicated in the table, column C). **(D)** With the exception of the study by Hartmann et al., all studies performed the dexamethasone/corticotropin-releasing hormone test (DEX/CRH), starting in the morning between

08:00 and 09:00 with the injections of DEX and continuing 6 hours later with a subsequent CRH injection **(E)**. **(F)** The weights of dissected adrenals were assessed in all studies at the endpoint (sacrifice).

n.s. not significant; significance levels are indicated by following asterisks: *p < 0.05, **p < 0.01, and ***p < 0.001

3.3 The effects of FKBP51 on HPA axis (re)activity are age-dependent

Male mice of our tissue-specific KO lines (Chapter 2.1 and Chapter 2.2) were tested at different ages in each study to investigate whether FKBP51-mediated effects on the HPA axis in the target regions are age-dependent. This is based on the described increase of *Fkbp5* expression levels with aging in humans (Blair et al., 2013; Zannas et al., 2019) and mice (Jinwal et al., 2010; O'Leary et al., 2011; Sabbagh et al., 2014), which contribute to reduced resilience to depression-like behavior that increases with aging mice and humans. An overview of the animals' age and their designation in both studies is given in Table 2 below.

Mouse line	Study	Age in weeks	Age designation
Fkbp5^PVN−/−	(Häusl et al., 2021)	8	Adolescent
		16 - 20	Adult
Pomc^Fkbp5-/-	(Brix et al., 2022)	12 - 16	Young
		28 - 32	Aging

Table 2: Age of animals used in paraventricular nucleus (PVN)- and pituitary (PIT)-specific knockout (KO) studies

Overview of the animal's age indicated in weeks and their respective designations in the *Fkbp5^PVN-/-* and *Pomc^Fkbp5-/-* KO studies of chapters 2.1and 2.2, respectively.

Although not the focus of this study, we were able to show that the robust effects on HPA axis (re)activity observed in adult *Fkbp5^PVN−/−* animals (16 – 20 weeks old) were not present in adolescent males that were eight weeks old at the start of the experimental phase (Chapter 2.1). The same phenomenon was observed in study 2 (Chapter 2.2), in which young (12 – 16 weeks) and aging (28 – 32 weeks) male mice with a KO of *Fkbp5* in POMC cells of the PIT

($Pomc^{Fkbp5-/-}$) were compared with respect to the significance levels of our KO. The $Fkbp5^{PVN-/-}$ mice designated as "adult" in chapter 2.1 and the "young" $Pomc^{Fkbp5-/-}$ animals in chapter 2.2 were approximately in the same age range so the results can be directly compared with each other in terms of the effect size of our KO (see 3.2). In brain lysates from mice collected at different ages, Jinwal and colleagues showed that FKBP51 protein levels gradually increased from detectable levels at 5.5 months of age to markedly elevated levels at 9 months of age (Jinwal et al., 2010). The fact that we were able to observe FKBP51-mediated effects on endocrine parameters of the HPA axis at a younger age than 5.5 months in both studies might be due to the low resolution of the technique applied in the Jinwal study: they used Western blot analyses in whole-brain lysates, which can dilute expression in particular brain regions at a young age to a point where it is no longer detectable. Overall, this dynamic of FKBP51 levels in the rodent brain over time described by Jinwal et al. fits into the overall picture of resulting phenotypes that we drew in chapters 2.1 and chapter 2.2. Unfortunately, we did not cover all three age stages (adolescent, adult, and aging) in each study. However, by combining the results from both studies, we can suggest that the strength of the effects of our FKBP51 KOs in the PVN and PIT follow the protein's gradual upregulation with aging (see Figure 6). We are therefore the first to add spatial information to these dynamics *in vivo*. Furthermore, the PIT is the first peripheral tissue in rodents in which upregulation of FKBP51 with age has been suggested.
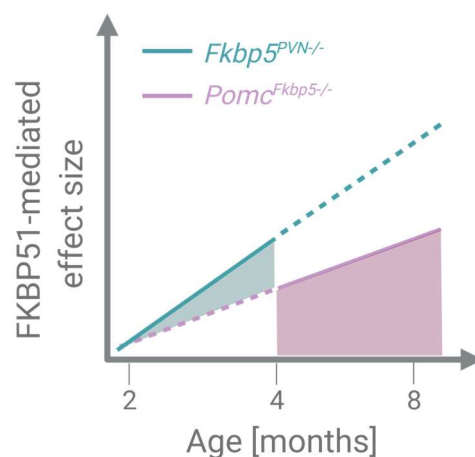
Created with BioRender.com

Figure 6: Graphical representation of the directionality of FKBP51-mediated effects in $Fkbp5^{PVN-/-}$ and $Pomc^{Fkbp5-/-}$ mice

FKBP51 KO studies in the paraventricular nucleus (PVN) and pro-opiomelanocortin (POMC) cells of the pituitary (PIT) indicate a positive linear correlation of FKBP51-mediated effects on hypothalamic-

pituitary-adrenal (HPA) axis function and age. Dotted lines and blanks below the line indicate extrapolation of the curve progression because data within these age ranges were not assessed in the respective study. Solid lines and filled spaces indicate the age ranges in which effects on HPA axis activity were evaluated in each study.

3.4 FKBP51 shapes metabolism bidirectionally dependent on tissue and cell type in a dose-dependent manner

Based on the lean phenotype and improved metabolism of global 51KO mice (Balsevich et al., 2017, 2014; Hartmann et al., 2012; Sanchez, 2012; Stechschulte et al., 2016), we were initially puzzled to observe that male mice with a viral KO in the MBH showed a massive increase in BW within a few weeks, while an OE of *Fkbp5* protected these animals from HFD-induced weight gain (Chapter 2.3; see Figure 7). The overarching mechanism that appeared to drive the differences in BW in our MBH-wide manipulation was autophagy signaling within this hypothalamic brain region. We identified FKBP51 in the MBH as a master switch linking autophagy and whole-body metabolism via the AMPK-mTOR network by scaffolding upstream hetero protein complexes in the initiation phase of autophagy signaling. By combining our *in vivo* and *in vitro* data, we revealed that FKBP51 regulates autophagy signaling within the MBH dose-dependently in an inversed u-shaped manner (see Figure 7): deletion of FKBP51 reduced autophagy signaling, and excessive levels of the protein resulted in a total block of autophagy in the MBH. However, the MBH does not regulate energy homeostasis in isolation but in concert with the periphery (Broberger, 2005). Excessive OE of *Fkbp5* in the MBH also moderately increased FKBP51 levels and autophagic flux in muscle and adipose tissue via decreased sympathetic outflow, which positively affected BW regulation.

Intriguingly, endogenous KO of *Fkbp5* in *Sf1*-expressing neurons within the VMH also resulted in slightly increased susceptibility to a dietary challenge. Still, instead of improving energy metabolism, viral OE of *Fkbp5* in *Sf1*-expressing neurons increased susceptibility to a HFD-challenge (Chapter 2.4). Thus, FKBP51-mediated BW regulation followed the described u-shaped and dose-dependent effects of FKBP51 on autophagy signaling described in chapter 2.3 (see Figure 7). Therefore, it is tempting to speculate that autophagy signaling within the MBH is the common mechanism underlying the observed metabolic phenotypes in both studies. The fact that we see opposite effects on BW in the respective FKBP51 OE experiments may also be a matter of dose: cell type-specific OE of the co-chaperone in the VMH was

probably not strong enough to induce downstream effects on sympathetic outflow and to increase FKP51 levels, and autophagy signaling in the periphery, and therefore we did not see beneficial effects on BW progression in the SF1-specific OE in chapter 2.4. The relatively mild effects on metabolic control induced by the manipulation of FKBP51 in SF1 neurons suggest that this neuronal population is not the only one, or else one of a conglomerate of MBH nuclei that drive robust phenotypes upon MBH-wide manipulation in chapter 2.3.

Adding to the complexity of the role of FKBP51 in energy metabolism, an endogenous KO in *Pomc*-expressing neurons of the ARC produced a phenotype comparable to that of global 51KO animals, while its viral OE did not have effects on metabolic control (Chapter 2.5; see Figure 7). Based on our postulated theory that FKBP51 regulates autophagy signaling in an inversed u-shaped manner, this suggests two things: 1) Loss of FKBP51 could be advantageous in pathways other than autophagy signaling, such as HFD-induced neuroinflammation in POMC neurons (Kästle et al., 2018; Zannas et al., 2019). 2) A dampening of autophagy signaling in POMC neurons could be beneficial in cases of inflammation-driven excessive autophagy, protecting the neurons from cell death (Thaler et al., 2012). The absence of a phenotype with viral POMC-specific OE might be explained by the animals' high age (8 - 9 months) at the beginning of the experiments. Age-related metabolic perturbations could override any beneficial or detrimental effects of our genetic manipulation (Azzu and Valencak, 2017; Balsevich et al., 2014; Moreno-Fernandez et al., 2021; Sabbagh et al., 2014; Zannas et al., 2019), as the potential of FKBP51 to drive underlying mechanisms in POMC neurons could be limited (ceiling effect). Although this is a major limitation of the study, it extends our hypothesis of age-dependent dynamics of FKBP51-mediated effects on stress- and metabolic phenotypes. Future studies should include young adult animals to underpin this hypothesis. In global 51KO animals, the sum of the described positive effects of FKBP51 loss (see 1.6.2) might outweigh the negative consequences on hypothalamic autophagy signaling (Chapter2.3), resulting in an overall favorable metabolic phenotype.

Taken together, these results illustrate that manipulation of FKBP51 levels can lead to opposite metabolic phenotypes, depending on cell type, tissue, and site of its loss or OE (see Figure 7), thus expanding our understanding of the cell type-specific role of this co-chaperone in energy homeostasis.
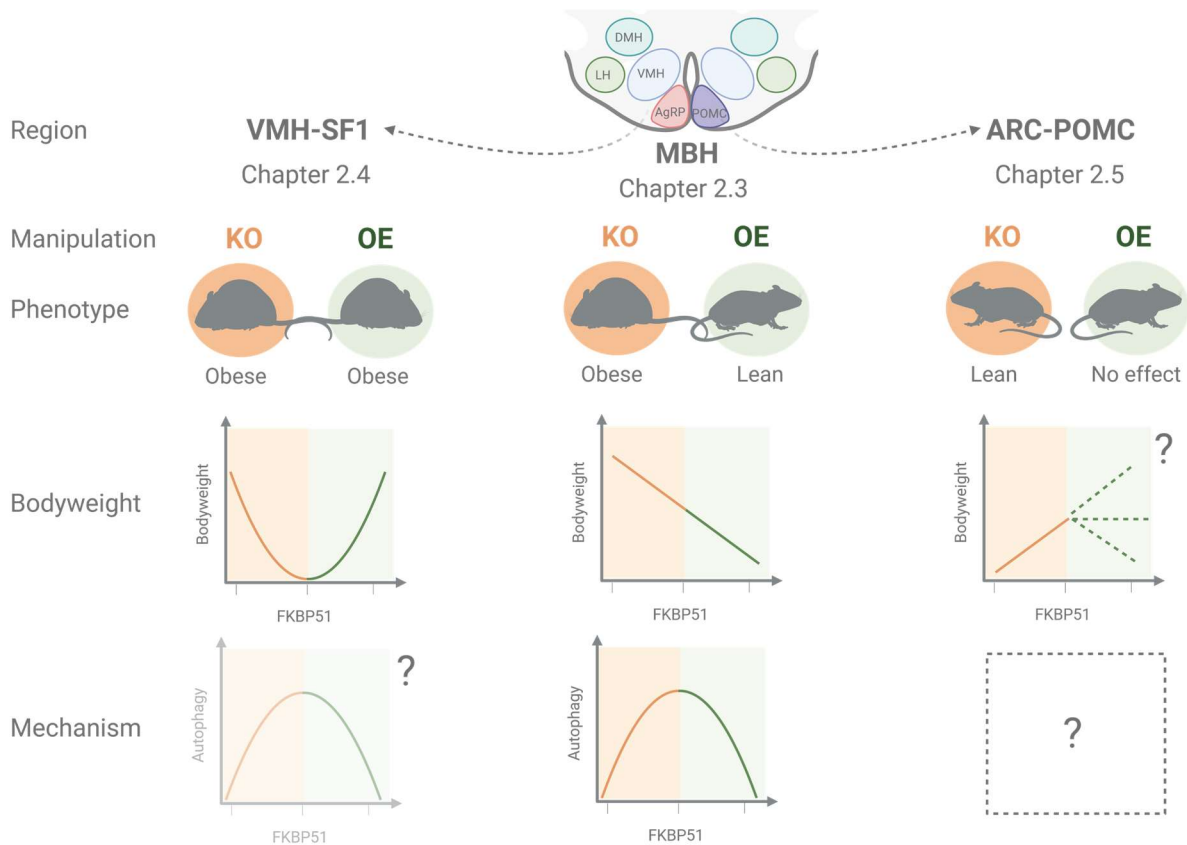
Created with BioRender.com

Figure 7: Overview of metabolic phenotypes resulting from FKBP51 manipulation in the mediobasal hypothalamus (MBH), the ventromedial hypothalamus (VMH), and the arcuate nucleus (ARC)

Knockout (KO; orange) of *Fkbp5* in the MBH and steroidogenic factor 1 (*Sf1*)-expressing cells in the VMH lead to increased body weight (BW) and obese phenotypes. In contrast, a KO in pro-opiomelanocortin (*Pomc*)-expressing neurons of the ARC protects animals from a high-fat diet (HFD)-induced BW gain. Overexpression (OE; green) in SF1 neurons results in increased susceptibility to a HFD, whereas animals with viral MBH-wide OE remain lean under dietary challenge due to moderate increases of FKBP51 and autophagy signaling in the periphery. OE in POMC neurons of aging animals had no effect on BW, which may indicate a ceiling effect in terms of the potential of FKBP51 to induce downstream effects on metabolic control. Therefore, the dynamic and thus curve progression in younger animals with an OE of FKBP51 in POMC neurons remains unknown (dashed green lines).

Overall, the effect of FKBP51 levels on the animal's BW depends strongly on the targeted cell types: The relationship between FKBP51 and BW in the VMH can be described by a u-shaped curve, and in MBH-wide manipulation, it follows a negative linear function. The BW phenotype in VMH-FKBP51 KO and OE animals suggests that autophagy signaling is the underlying mechanism, as the BW follows the same dose-dependent dynamics as this mechanism itself. The results of POMC-specific FKBP51 manipulation suggest other molecular effects responsible for the observed phenotype that are

currently unknown. All curves shown are representative, hypothetical approximations. Question marks indicate open hypothesis.

3.5 The effects of FKBP51 on whole-body metabolism are modulated by the dietary context

In chapters 2.3, 2.4, and 2.5, we investigated the effects of endogenous and viral manipulation of *Fkbp5* gene expression in the MBH and its subnuclei, the VMH and the ARC, on whole-body metabolism. What was striking and common to almost all models (except MBH-wide KO in Chapter 2.3) was that the phenotypes were only triggered after a dietary challenge (HFD) lasting several weeks. While it was known from Scharf et al. (Scharf et al., 2011) that not only a physical restraint stress but also 24 hours of fasting induce increased *Fkbp5* mRNA levels in the mouse brain, Yang and colleagues confirmed that *Fkbp5* is one of the genes that are upregulated in the hypothalamus after 48 hours fast. In particular, they observed increased FKBP51 levels in the VMH, PVN, and ARC of mice and rats. Hypothesizing that an OE of *Fkbp5* in the hypothalamus promotes obese phenotypes, they transferred the gene to the hypothalamus via an AAV and observed elevated BW on a HFD (Yang et al., 2012). This not only confirmed that hypothalamic *Fkbp5* responds to a HFD challenge but also showed that these elevated levels can trigger obese phenotypes. Two years later, Balsevich and colleagues investigated the interaction effect of an eight-week HFD followed by a psychosocial and physical chronic social defeat stress (CSDS) paradigm to assess a potential role for FKBP51 at the interface between stress reactivity and energy balance. They were the first to show an upregulation of *Fkbp5* mRNA in the MBH and HIP upon dietary challenge but could not show an interaction effect of the two stressors (Balsevich et al., 2014). Interestingly, the harmful effects of a HFD can be passed on from the damn to the offspring, leading to long-lasting impairments in anxiety-like behaviors and stress coping strategies in the next generation that correspond to the adverse effects of chronic stress exposure in adult mice. Further, they observed significant upregulation of *Fkbp5* in the PVN of the offspring (Balsevich et al., 2016). Consistent with these findings, a chronic HFD exposure was shown to elicit a stress response itself with downstream behavioral and neuroendocrine effects comparable to chronic physical and or psychosocial stress exposure (Aslani et al., 2015). Further, high calorie diets can potentiate the negative effects of chronic stressors alone, increasing neuroinflammation, cardiovascular-, endocrine-, behavioral- and cognitive deficits (Batschauer et al., 2020; Lippi,

2021; Wang et al., 2022). Overall, there is ample evidence that chronic HFD elicits a stress response and increases FKBP51 levels in hypothalamic brain regions, promoting obesity and stress-related phenotypes, so we can assume that it acts as a trigger for the observed changes in energy metabolism in our models.

The KO of *Fkbp5* in *Pomc*-expressing neurons (Chapter 2.5) follows this logic as it is known from the literature that a prolonged HFD causes detrimental effects on POMC neuron function, such as inflammation and cell death (Le Thuc et al., 2017; Moraes et al., 2009; Thaler et al., 2012), that can be boosted by higher FKBP51 levels (Gassen et al., 2014b; Kästle et al., 2018; Zannas et al., 2019). This gradual loss of POMC neuronal function can ultimately promote obesity (Ullah et al., 2021). In the VMH KO model (Chapter 2.4), where autophagy signaling is assumed to be the driving mechanism, loss and OE of *Fkbp5* have detrimental effects on BW following the dose-dependent u-shaped curve of FKBP51-mediated autophagy signaling (see Figure 7). Prolonged nutrient overload is known to increase inflammatory processes in the hypothalamus (Jais and Brüning, 2017; Thaler et al., 2012) and could amplify the effects mediated by FKBP51, ultimately leading to higher metabolic susceptibility to a HFD in our model. In contrast to all our other models, MBH-wide KO of *Fkbp5* did not require a HFD to induce obesity-related phenotypes. The reason for this is most likely the dose-dependence of FKBP51 when it comes to the magnitude of its effect on autophagy signaling: A KO of *Fkbp5* in only one cell type within the MBH (SF1 neurons; Chapter 2.4) corresponds to a moderate reduction in autophagy, whereas a KO targeting all cell types within the MBH (Chapter 2.3) results in a total block of autophagy signaling. In this sense, our "moderate" KO in the VMH requires an additional stressor to trigger FKBP51-mediated effects on metabolism. In contrast, a total block of autophagy in the MBH alone seems sufficient to increase BW.

3.6 FKBP51 shapes the stress response and energy homeostasis: Potential therapeutic implications

Soon after the discovery of antidepressant and antipsychotic medications in the mid-twentieth century, it was recognized that a lot of patients show limited to no response to these drugs. Today we know that 20 - 60 % of patients with psychiatric disorders are treatment resistant (Howes et al., 2021), which is associated with increased healthcare burden that is up to ten-fold higher relative to patients in general. While there has been an

increase in the proportion of psychiatric research focusing on treatment resistance, it is still less than 1% of the total output (Howes et al., 2021). Our world is facing a shortage of effective pharmacological treatments not only for psychiatric- but also for metabolic diseases. While enormous progress has been made in the management of obesity and its comorbidities, the treatment of this disease itself has proven largely resistant to pharmacological interventions (Müller et al., 2021). Since both diseases are comorbid (Rabasa and Dickson, 2016; Russell and Lightman, 2019; Tomiyama, 2019; van der Kooij, 2020), it is even more worrying that some of the medications have side effects that can exacerbate the other condition. A large proportion of anti-obesity drugs target the central neurochemical system, which modifies behavioral components of obesity, such as food intake, emotional- and cognitive function, and they were found to have varying adverse neuropsychiatric profiles (Nathan et al., 2011). On the other hand, pharmacological interventions for psychiatric diseases, especially antidepressants, often increase the risk of metabolic complications (Gramaglia et al., 2018). A great glimmer of hope on the horizon of this crisis is personalized medicine which is based on the assumption that an individual's unique physiologic characteristics play a significant role in disease vulnerability and in response to specific therapies. A fundamental building block of this approach is the patient's genetic profile to elucidate the molecular underpinnings of these disorders and be able to develop individualized prevention strategies (Ozomaro et al., 2013).

This is where FKBP51 comes to the table: Not only is this gene regulated via interactions among environmental stressors, genetic variants, and epigenetic modifications, which can result in psychiatric disease phenotypes (Zannas et al., 2015), but its genetic variants are also associated with obesity and insulin resistance (Fichna et al., 2018). This broad spectrum of FKBP51 action makes it a very promising target for pharmacological interventions targeting both sides of the coin. Two highly selective antagonist ligands of FKBP51, SAFit1 and SAFit2 (selective antagonist for FKBP51 by induced fit; SAFit2 is brain-permeable), have been shown to enhance neurite outgrow in mice, with SAFit2 increasing feedback inhibition of the HPA axis and stress coping (Gaali et al., 2015). Moreover, SAFit2 has anxiolytic properties (Hartmann et al., 2015), alleviates pain states (Maiarù et al., 2018, 2016), and improves stress-coping behavior in combination with escitalopram in rodent models (Pöhlmann et al., 2018). In addition to the positive effects on stress- and pain-related phenotypes, blocking FKBP51 action with SAFit2 was shown to improve insulin signaling in skeletal myotubes and protected

treated animals from diet-induced weight gain, which was comparable to the effects of a global KO of FKBP51 (Balsevich et al., 2017).

In chapters 2.1 and 2.2, we provide evidence that central and peripheral loss of FKBP51 in the PVN and corticotrope cells of the PIT, respectively, positively shapes HPA axis negative feedback regulation and (re)activity, which is consistent with the HPA axis phenotype in animals with a global loss of FKBP51 (Hartmann et al., 2012; Touma et al., 2011) (see 3.2). The unidirectionality of the central and peripheral effects of FKBP51 on the stress-response would argue for global pharmacological attenuation of FKBP51 to improve the hormonal stress response. Ideally, only in patients who have been screened for known FKBP51 SNPs to increase treatment success (Binder, 2009; Binder et al., 2008, 2004; Matosin et al., 2018; Zannas and Binder, 2014). Consistent with this, Gaali and colleagues could show that SAFit2 improved the suppression of CORT levels after DEX and CRH, which is consistent with the enhancement of GR sensitivity following FKBP51 inhibition (Gaali et al., 2015). However, our studies on the metabolic effects of central loss of FKBP51 in metabolically relevant hypothalamic nuclei in chapters 2.3 and 2.4, and 2.5 add another level of complexity to any potential pharmacological approach to attenuate FKBP51 function. Considering improved whole-body metabolism in global FKBP51 KO mice (Balsevich et al., 2017; Hartmann et al., 2012; Sanchez, 2012; Stechschulte et al., 2016) in combination with our cell type-specific loss of FKBP51 in *Pomc*-expressing neurons in the ARC (Chapter 2.5), it seems reasonable to suggest that blocking FKBP51 function (globally and/or centrally) is beneficial in both psychiatric- and metabolic diseases, bypassing the known side effects of classical antidepressant- and anti-obesity drugs. However, our central KO and OE studies in the MBH (Chapter 2.3) and VMH (Chapter 2.4), where the loss of FKBP51 impaired energy metabolism, urge caution about pharmacological attenuation of FKBP51 and suggest region- and cell type-specific fine-tuning of SAFit administration to avoid metabolic side effects.

Therefore, the work done here increases our knowledge of the potential of FKBP51 as a target in the pharmacological treatment of psychiatric- and metabolic diseases tremendously. It raises awareness for the importance of region- and cell type-specific studies in the preclinical phase of developing tailored pharmacological treatment approaches.

3.7 Limitations and future directions

This thesis provides compelling evidence that FKBP51 acts in a highly cell type-specific, dose- and age-dependent manner and that its action is modulated by the dietary context. We are the first to decipher the cell type-specific effects of FKBP51 on the HPA axis and metabolic control, and delineate the underlying mechanisms in which this co-chaperone is involved, thereby steering and fine-tuning the hormonal stress response and energy metabolism. Despite our in-depth characterization of the cell-type specificity of FKBP51 and its dynamics in modulating these two physiologic processes, there remain outstanding research questions and limitations to our current findings.

Sex differences

The cell type-specific KO and OE studies in the PVN (Chapter 2.1) and *Pomc*-expressing cells of the pituitary (Chapter 2.2) were performed exclusively in male mice, even though sex and gender differences in mental disorders are among the most common and robust findings in psychiatric research. These differences exist in the prevalence of psychiatric diseases, with depression being twice as common in females than in males, and in symptomatology, risk- and influencing factors (Riecher-Rössler, 2017). However, we still don't understand the underlying physiologic causes of these differences, and there is a lack of research in this field, which has resulted in poorer treatment outcomes for women. Often-used justification for this focus on males is that females are considered more variable (in part due to estrous cyclicity), their use will reduce statistical power, and small differences can be overemphasized. However, research shows that these concerns do not stand in-depth statistical simulations, demonstrating that females are not more variable than males and that their estrous cycle need not be considered (Beery, 2018). In particular, the PIT, which plays a central role in sexual development and modulation of various endocrine axes, is sexually dimorphic in size, gene expression and function in humans and rodents (Bjelobaba et al., 2015; MacMaster et al., 2007). Therefore, future preclinical studies in our cell type-specific KO and OE models of FKBP51 should include female phenotyping to help overcome this gap and improve future treatment outcomes for women.

Interaction effect

While this thesis suggests that FKBP51 has a high potential to act at the interface of stress-physiology and metabolism, we do not investigate this in-depth. Research shows that prolonged HFD is considered a metabolic stressor, increasing *Fkbp5* expression in hypothalamic brain regions (Balsevich et al., 2014) and eliciting similar behavioral- and endocrine profiles as a CSDS (Aslani et al., 2015) (Chapter 3.5). Even more importantly, it was shown that a dietary challenge could boosts the adverse effects of chronic physical and psychosocial stressors (Batschauer et al., 2020; Lippi, 2021; Wang et al., 2022). In this context, FKBP51 could be the molecular bridgehead at the interface of these two mechanisms, linking and amplifying the negative effects of a high-calorie diet and chronic stressors. Balsevich et al. investigated this a couple of years ago in the global 51KO mouse model and found that although FKBP51 was responsive to both stress and dietary conditions, there was no interaction effect (Balsevich et al., 2014). However, this does not exclude potential interaction effects in our cell type-specific KO and OE models. Especially, our KO of FKBP51 in the PVN (Chapter 2.1) may be involved in such interaction effects, as this hypothalamic nucleus is not only considered a master regulator of the HPA axis (see 1.2.3) but is also crucial in mediating the downstream effects of POMC and AgRP activity on whole-body metabolism (see 1.7.2 and 1.7.3). Therefore, a combination of a prolonged dietary challenge and a chronic physical and psychosocial stressor, such as a CSDS, may reveal the potential of FKBP51 to exacerbate adverse effects at the interface between the stress response and whole-body metabolism.

Mechanisms

While studies in chapters 2.1, 2.2, and 2.3 provide analysis of the molecular and mechanistic role of FKBP51 underlying the observed stress- and metabolic phenotypes, this information is partially missing in chapters 2.4 and 2.5. Based on our MBH-wide manipulation study (Chapter 2.3) and the dynamics of BW progression in our KO and OE in *Sf1*-expressing neurons of the VMH (Chapter 2.4), it is suggested that autophagy signaling is the underlying mechanism of FKBP51-mediated effects on metabolism. Nevertheless, we do not investigate this further following the example of MBH-wide manipulation of FKBP51 and analyze key markers for autophagy signaling centrally and in the periphery. However, this was a deliberate decision, as the primary outcome of the VMH-specific study in chapter 2.4 was the relatively small involvement in robust FKBP51-mediated effects observed in chapter 2.3. POMC-specific KO in chapter 2.5 provides evidence for a central role of FKBP51 in this neuronal population

in steering downstream effects on BW and energy metabolism under a dietary challenge. One identified cause that may lower HFD-induced BW gain in animals with a KO is their increased activity pattern, which is already present before the dietary challenge. Therefore higher locomotion could counteract negative effects of POMC neuronal dysfunction induced by the HFD (e.g., inflammation and cell death) (Le Thuc et al., 2017; Moraes et al., 2009; Thaler et al., 2012). In line with that, inflammation in POMC neurons was shown to decrease voluntary rodent locomotion (Le Thuc et al., 2017; Zhan et al., 2013). Therefore, it is tempting to speculate that the deletion of FKBP51 in our *Pomc*$^{Fkbp5-/-}$ mice prevents inflammation-induced autophagic cell death and the associated decrease in locomotor activity, thus protecting the animals from POMC-mediated dysregulation of energy metabolism under HFD. As this study is still a work in progress, we aim to further elucidate the underlying processes that potentially mediate FKBP51 driven effects on metabolism in POMC neurons, assessing inflammatory- and apoptotic markers, autophagy signaling, and electrophysiological properties. Once we have established which direct molecular changes occur in POMC neurons lacking FKBP51, investigating the underlying circuits in which this neuronal population and second-order neurons interact will help further unravel the downstream events that lead to improved energy metabolism in our *Pomc*$^{Fkbp5-/-}$ animals. MC4R expressing neurons in the PVN are an interesting candidate in this context, as they are a target of both POMC and AgRP neurons. Interestingly, the activity of mTOR complex1 (mTORC1) has been shown to control glutatmatergic POMC inputs onto PVN parvocellular neurons, which is reduced under a HFD (Mazier et al., 2019). Therefore, in our model, FKBP51 may be directly involved in mTORC1 signaling in POMC neurons and thus reduce glutamatergic inputs onto the PVN, requiring modulation of MC4R in parvocellular PVN neurons.

3.8 Closing remarks

We elucidate cell type-specific roles of FKBP51 and its underlying mechanisms in the hormonal stress response system and energy metabolism. We show that the effects of this co-chaperone are highly dependent on its site of expression, its dosage and the age of the animals and are modulated by the dietary context. With this, we open a new avenue of research and raise awareness for developing targeted therapeutic interventions in the treatment of psychiatric- and metabolic diseases and their comorbidities.

4. Bibliography

American Psychological Association, 2022. Stress in America™ 2020 A National Mental Health Crisis. Available at https://www.apa.org/news/press/releases/stress/2020/sia-mental-health-crisis.pdf

Anand, B.K., Brobeck, J.R., 1951. Hypothalamic Control of Food Intake in Rats and Cats. Yale J. Biol. Med. 24, 123.

Aslani, S., Vieira, N., Marques, F., Costa, P.S., Sousa, N., Palha, J.A., 2015. The effect of high-fat diet on rat's mood, feeding behavior and response to stress. Transl. Psychiatry 2015 511 5, e684–e684. https://doi.org/10.1038/tp.2015.178

Azzu, V., Valencak, T.G., 2017. Energy Metabolism and Ageing in the Mouse: A Mini-Review. Gerontology 63, 327–

336. https://doi.org/10.1159/000454924

Baker, J.D., Ozsan, I., Ospina, S.R., Gulick, D., Blair, L.J., 2019. Hsp90 Heterocomplexes Regulate Steroid Hormone Receptors: From Stress Response to Psychiatric Disease. Int. J. Mol. Sci. 20. https://doi.org/10.3390/IJMS20010079

Bakula, D., Müller, A.J., Zuleger, T., Takacs, Z., Franz-Wachtel, M., Thost, A.K., Brigger, D., Tschan, M.P., Frickey, T., Robenek, H., Macek, B., Proikas-Cezanne, T., 2017. WIPI3 and WIPI4 β-propellers are scaffolds for LKB1-AMPK-TSC signalling circuits in the control of autophagy. Nat. Commun. 2017 81 8, 1–18. https://doi.org/10.1038/ncomms15637

Balsevich, G., Baumann, V., Uribe, A., Chen, A., Schmidt, M. V., 2016. Prenatal Exposure to Maternal Obesity Alters Anxiety and Stress Coping Behaviors in Aged Mice. Neuroendocrinology 103, 354–368. https://doi.org/10.1159/000439087

Balsevich, G., Häusl, A.S., Meyer, C.W., Karamihalev, S., Feng, X., Pöhlmann, M.L., Dournes, C., Uribe-Marino, A., Santarelli, S., Labermaier, C., Hafner, K., Mao, T., Breitsamer, M., Theodoropoulou, M., Namendorf, C., Uhr, M., Paez-Pereda, M., Winter, G., Hausch, F., Chen, A., Tschöp, M.H., Rein, T., Gassen, N.C., Schmidt, M. V., 2017. Stress-responsive FKBP51 regulates AKT2-AS160 signaling and metabolic function. Nat. Commun. 2017 81 8, 1–12. https://doi.org/10.1038/s41467-017-01783-y

Balsevich, G., Uribe, A., Wagner, K. V, Hartmann, J., Santarelli, S., Labermaier, C., Schmidt, M. V, 2014. Interplay between diet-induced obesity and chronic stress in mice: potential role of FKBP51. J. Endocrinol. 222, 15–26. https://doi.org/10.1530/JOE-14-0129

Balthasar, N., Dalgaard, L.T., Lee, C.E., Yu, J., Funahashi, H., Williams, T., Ferreira, M., Tang, V., McGovern, R.A., Kenny, C.D., Christiansen, L.M., Edelstein, E., Choi, B., Boss, O.,

Aschkenasi, C., Zhang, C.Y., Mountjoy, K., Kishi, T., Elmquist, J.K., Lowell, B.B., 2005. Divergence of melanocortin pathways in the control of food intake and energy expenditure. Cell 123, 493–505. https://doi.org/10.1016/J.CELL.2005.08.035

Batschauer, T., Cordeiro, J.M., Simas, B.B., Brunetta, H.S., Souza, R.M., Nunes, E.A., Reis, W.L., Moreira, E.L.G., Crestani, C.C., Santos, A.R.S., Speretta, G.F., 2020. Behavioral, cardiovascular and endocrine alterations induced by chronic stress in rats fed a high-fat diet. Physiol. Behav. 223, 113013. https://doi.org/10.1016/J.PHYSBEH.2020.113013

Baughman, G., Wiederrecht, G.J., Chang, F., Martin, M.M., Bourgeois, S., 1997. Tissue Distribution and Abundance of Human FKBP51, an FK506-Binding Protein That Can Mediate Calcineurin Inhibition. Biochem. Biophys. Res. Commun. 232, 437–443. https://doi.org/10.1006/BBRC.1997.6307

Beery, A.K., 2018. Inclusion of females does not increase variability in rodent research studies. Curr. Opin. Behav. Sci. 23, 143. https://doi.org/10.1016/J.COBEHA.2018.06.016

Bell, M.E., Bhatnagar, S., Akana, S.F., Choi, S.J., Dallman, M.F., 2000. Disruption of Arcuate/Paraventricular Nucleus Connections Changes Body Energy Balance and Response to Acute Stress. J. Neurosci. 20, 6707–6713. https://doi.org/10.1523/JNEUROSCI.20-17-06707.2000

Bellinger, L.L., Bernardis, L.L., 2002. The dorsomedial hypothalamic nucleus and its role in ingestive behavior and body weight regulation: lessons learned from lesioning studies. Physiol. Behav. 76, 431–442. https://doi.org/10.1016/S0031-9384(02)00756-4

Belvederi Murri, M., Pariante, C., Mondelli, V., Masotti, M., Atti, A.R., Mellacqua, Z., Antonioli, M., Ghio, L., Menchetti, M., Zanetidou, S., Innamorati, M., Amore, M., 2014. HPA axis and aging in depression: Systematic review and meta-analysis. Psychoneuroendocrinology. https://doi.org/10.1016/j.psyneuen.2013.12.004

Bernard, C., 1872. La constitution physico-chimique du milieu intérieur [The physicochemical constitution of the environment within]. Rev. Sci. 2, 2.

Betley, J.N., Cao, Z.F.H., Ritola, K.D., Sternson, S.M., 2013. Parallel, Redundant Circuit Organization for Homeostatic Control of Feeding Behavior. Cell 155, 1337–1350. https://doi.org/10.1016/J.CELL.2013.11.002

Biddie, S.C., Hager, G.L., 2009. Glucocorticoid receptor dynamics and gene regulation. Stress 12, 193. https://doi.org/10.1080/10253890802506409

Binder, E.B., 2009. The role of FKBP5, a co-chaperone of the glucocorticoid receptor in the pathogenesis and therapy of affective and anxiety disorders. Psychoneuroendocrinology. https://doi.org/10.1016/j.psyneuen.2009.05.021

Binder, E.B., Bradley, R.G., Liu, W., Epstein, M.P., Deveau, T.C., Mercer, K.B., Tang, Y., Gillespie,

C.F., Heim, C.M., Nemeroff, C.B., Schwartz, A.C., Cubells, J.F., Ressler, K.J., 2008. Association of FKBP5 polymorphisms and childhood abuse with risk of posttraumatic stress disorder symptoms in adults. JAMA - J. Am. Med. Assoc. 299, 1291–1305. https://doi.org/10.1001/jama.299.11.1291

Binder, E.B., Salyakina, D., Lichtner, P., Wochnik, G.M., Ising, M., Pütz, B., Papiol, S., Seaman, S., Lucae, S., Kohli, M.A., Nickel, T., Künzel, H.E., Fuchs, B., Majer, M., Pfennig, A., Kern, N., Brunner, J., Modell, S., Baghai, T., Deiml, T., Zill, P., Bondy, B., Rupprecht, R., Messer, T., Köhnlein, O., Dabitz, H., Brückl, T., Müller, N., Pfister, H., Lieb, R., Mueller, J.C., Lõhmussaar, E., Strom, T.M., Bettecken, T., Meitinger, T., Uhr, M., Rein, T., Holsboer, F., Muller-Myhsok, B., 2004. Polymorphisms in FKBP5 are associated with increased recurrence of depressive episodes and rapid response to antidepressant treatment. Nat. Genet. 36, 1319–1325. https://doi.org/10.1038/ng1479

Bjelobaba, I., Janjic, M.M., Kucka, M., Stojilkovic, S.S., 2015. Cell type-specific sexual dimorphism in rat pituitary gene expression during maturation. Biol. Reprod. 93, 1–9. https://doi.org/10.1095/BIOLREPROD.115.129320/2434219

Björntorp, P., 2001. Do stress reactions cause abdominal obesity and comorbidities? Obes. Rev. 2, 73–86. https://doi.org/10.1046/J.1467-789X.2001.00027.X

Björntorp, P., Rosmond, R., 2000. Obesity and cortisol. Nutrition 16, 924–936. https://doi.org/10.1016/S0899-9007(00)00422-6

Blair, L.J., Nordhues, B.A., Hill, S.E., Scaglione, K.M., O'Leary, J.C., Fontaine, S.N., Breydo, L., Zhang, B., Li, P., Wang, L., Cotman, C., Paulson, H.L., Muschol, M., Uversky, V.N., Klengel, T., Binder, E.B., Kayed, R., Golde, T.E., Berchtold, N., Dickey, C.A., 2013. Accelerated neurodegeneration through chaperone-mediated oligomerization of tau. J. Clin. Invest. 123, 4158. https://doi.org/10.1172/JCI69003

Bose, M., Oliván, B., Laferrère, B., 2009. Stress and obesity: the role of the hypothalamic–pituitary–adrenal axis in metabolic disease. Curr. Opin. Endocrinol. Diabetes. Obes. 16, 340. https://doi.org/10.1097/MED.0B013E32832FA137

Brix, L.M., Häusl, A.S., Toksöz, I., Bordes, J., van Doeselaar, L., Engelhardt, C., Narayan, S., Springer, M., Sterlemann, V., Deussing, J.M., Chen, A., Schmidt, M. V., 2022. The co-chaperone FKBP51 modulates HPA axis activity and age-related maladaptation of the stress system in pituitary proopiomelanocortin cells. Psychoneuroendocrinology 138, 105670. https://doi.org/10.1016/J.PSYNEUEN.2022.105670

Brobeck, J.R., 1946. Mechanism of the development of obesity in aniamsl with hypothalamic lesions. https://doi.org/10.1152/physrev.1946.26.4.541 26, 541–559. https://doi.org/10.1152/PHYSREV.1946.26.4.541

Broberger, C., 2005. Brain regulation of food intake and appetite: molecules and networks. J.

Intern. Med. 258, 301–327. https://doi.org/10.1111/J.1365-2796.2005.01553.X

Browning, K.N., Carson, K.E., 2021. Central Neurocircuits Regulating Food Intake in Response to Gut Inputs—Preclinical Evidence. Nutrients 13, 1–18. https://doi.org/10.3390/NU13030908

Cannon, W., 1915. Bodily changes in pain, hunger, fear and rage: An account of recent researches into the function of emotional excitement. D Appleton & Company. https://doi.org/10.1037/10013-000

Cheung, J., Smith, D.F., 2000. Molecular chaperone interactions with steroid receptors: an update. Mol. Endocrinol. 14, 939–946. https://doi.org/10.1210/MEND.14.7.0489

Cone, R.D., 2005. Anatomy and regulation of the central melanocortin system. Nat. Neurosci. 8, 571–578. https://doi.org/10.1038/NN1455

Cowley, M.A., Smart, J.L., Rubinstein, M., Cerdán, M.G., Diano, S., Horvath, T.L., Cone, R.D., Low, M.J., 2001. Leptin activates anorexigenic POMC neurons through a neural network in the arcuate nucleus. Nature 411, 480–484. https://doi.org/10.1038/35078085

Cowley, M.A., Smith, R.G., Diano, S., Tschöp, M., Pronchuk, N., Grove, K.L., Strasburger, C.J., Bidlingmaier, M., Esterman, M., Heiman, M.L., Garcia-Segura, L.M., Nillni, E.A., Mendez, P., Low, M.J., Sotonyi, P., Friedman, J.M., Liu, H., Pinto, S., Colmers, W.F., Cone, R.D., Horvath, T.L., 2003. The distribution and mechanism of action of ghrelin in the CNS demonstrates a novel hypothalamic circuit regulating energy homeostasis. Neuron 37, 649–661. https://doi.org/10.1016/S0896-6273(03)00063-1

De Kloet, A.D., Herman, J.P., 2018. Fat-brain connections: Adipocyte glucocorticoid control of stress and metabolism. Front. Neuroendocrinol. 48, 50–57. https://doi.org/10.1016/J.YFRNE.2017.10.005

De Kloet, E.R., de Kloet, S.F., de Kloet, C.S., de Kloet, A.D., 2019. Top-down and bottom-up control of stress-coping. J. Neuroendocrinol. 31. https://doi.org/10.1111/JNE.12675

De Kloet, E.R., Joëls, M., Holsboer, F., 2005. Stress and the brain: From adaptation to disease. Nat. Rev. Neurosci. https://doi.org/10.1038/nrn1683

Denny, W.B., Valentine, D.L., Reynolds, P.D., Smith, D.F., Scammell, J.G., 2000. Squirrel monkey immunophilin FKBP51 is a potent inhibitor of glucocorticoid receptor binding. Endocrinology 141, 4107–4113. https://doi.org/10.1210/endo.141.11.7785

Dhillon, H., Zigman, J.M., Ye, C., Lee, C.E., McGovern, R.A., Tang, V., Kenny, C.D., Christiansen, L.M., White, R.D., Edelstein, E.A., Coppari, R., Balthasar, N., Cowley, M.A., Chua, S., Elmquist, J.K., Lowell, B.B., 2006. Leptin directly activates SF1 neurons in the VMH, and this action by leptin is required for normal body-weight homeostasis. Neuron 49, 191–203. https://doi.org/10.1016/J.NEURON.2005.12.021/ATTACHMENT/61A9488A-C3F9-

4A89-BBFF-7A603A5E7DEF/MMC1.PDF

Dietrich, M.O., Zimmer, M.R., Bober, J., Horvath, T.L., 2015. Hypothalamic Agrp Neurons Drive Stereotypic Behaviors beyond Feeding. Cell 160, 1222–1232. https://doi.org/10.1016/J.CELL.2015.02.024

Dikic, I., Elazar, Z., 2018. Mechanism and medical implications of mammalian autophagy. Nat. Rev. Mol. Cell Biol. 2018 196 19, 349–364. https://doi.org/10.1038/s41580-018-0003-4

Ellacott, K.L.J., Cone, R.D., 2006. The role of the central melanocortin system in the regulation of food intake and energy homeostasis: lessons from mouse models. Philos. Trans. R. Soc. Lond. B. Biol. Sci. 361, 1265–1274. https://doi.org/10.1098/RSTB.2006.1861

Elmquist, J.K., Maratos-Flier, E., Saper, C.B., Flier, J.S., 1998. Unraveling the central nervous system pathways underlying responses to leptin. Nat. Neurosci. 1, 445–450. https://doi.org/10.1038/2164

Engelhardt, C., Tang, F., Elkhateib, R., Bordes, J., Brix, L.M., Van Doeselaar, L., Häusl, A.S., Pöhlmann, M.L., Schraut, K., Yang, H., Chen, A., Deussing, J.M., Schmidt, M. V., 2021. FKBP51 in the Oval Bed Nucleus of the Stria Terminalis Regulates Anxiety-Like Behavior. eNeuro 8. https://doi.org/10.1523/ENEURO.0425-21.2021

Farooqi, I.S., O'Rahilly, S., 2006. Genetics of obesity in humans. Endocr. Rev. 27, 710–718. https://doi.org/10.1210/ER.2006-0040

Fichna, M., Krzyśko-Pieczka, I., Żurawek, M., Skowrońska, B., Januszkiewicz-Lewandowska, D., Fichna, P., 2018. FKBP5 polymorphism is associated with insulin resistance in children and adolescents with obesity. Obes. Res. Clin. Pract. 12, 62–70. https://doi.org/10.1016/J.ORCP.2016.11.007

Fosch, A., Zagmutt, S., Casals, N., Rodríguez-Rodríguez, R., 2021. New Insights of SF1 Neurons in Hypothalamic Regulation of Obesity and Diabetes. Int. J. Mol. Sci. 2021, Vol. 22, Page 6186 22, 6186. https://doi.org/10.3390/IJMS22126186

Fries, G.R., Gassen, N.C., Rein, T., 2017. The FKBP51 Glucocorticoid Receptor Co-Chaperone: Regulation, Function, and Implications in Health and Disease. Int. J. Mol. Sci. 18. https://doi.org/10.3390/IJMS18122614

Gaali, S., Kirschner, A., Cuboni, S., Hartmann, J., Kozany, C., Balsevich, G., Namendorf, C., Fernandez-Vizarra, P., Sippel, C., Zannas, A.S., Draenert, R., Binder, E.B., Almeida, O.F.X., Rühter, G., Uhr, M., Schmidt, M. V., Touma, C., Bracher, A., Hausch, F., 2015. Selective inhibitors of the FK506-binding protein 51 by induced fit. Nat. Chem. Biol. 11, 33–37. https://doi.org/10.1038/NCHEMBIO.1699

Gassen, N.C., Hartmann, J., Schmidt, M. V., Rein, T., 2015. FKBP5/FKBP51 enhances autophagy to synergize with antidepressant action. Autophagy 11, 578.

https://doi.org/10.1080/15548627.2015.1017224

Gassen, N.C., Hartmann, J., Zschocke, J., Stepan, J., Hafner, K., Zellner, A., Kirmeier, T., Kollmannsberger, L., Wagner, K. V., Dedic, N., Balsevich, G., Deussing, J.M., Kloiber, S., Lucae, S., Holsboer, F., Eder, M., Uhr, M., Ising, M., Schmidt, M. V., Rein, T., 2014a. Association of FKBP51 with Priming of Autophagy Pathways and Mediation of Antidepressant Treatment Response: Evidence in Cells, Mice, and Humans. PLoS Med. 11. https://doi.org/10.1371/JOURNAL.PMED.1001755

Gassen, N.C., Hartmann, J., Zschocke, J., Stepan, J., Hafner, K., Zellner, A., Kirmeier, T., Kollmannsberger, L., Wagner, K. V., Dedic, N., Balsevich, G., Deussing, J.M., Kloiber, S., Lucae, S., Holsboer, F., Eder, M., Uhr, M., Ising, M., Schmidt, M. V., Rein, T., 2014b. Association of FKBP51 with Priming of Autophagy Pathways and Mediation of Antidepressant Treatment Response: Evidence in Cells, Mice, and Humans. PLOS Med. 11, e1001755. https://doi.org/10.1371/JOURNAL.PMED.1001755

Gassen, N.C., Niemeyer, D., Muth, D., Corman, V.M., Martinelli, S., Gassen, A., Hafner, K., Papies, J., Mösbauer, K., Zellner, A., Zannas, A.S., Herrmann, A., Holsboer, F., Brack-Werner, R., Boshart, M., Müller-Myhsok, B., Drosten, C., Müller, M.A., Rein, T., 2019. SKP2 attenuates autophagy through Beclin1-ubiquitination and its inhibition reduces MERS-Coronavirus infection. Nat. Commun. 2019 101 10, 1–16. https://doi.org/10.1038/s41467-019-13659-4

Gautron, L., Elmquist, J.K., Williams, K.W., 2015. Neural Control of Energy Balance: Translating Circuits to Therapies. Cell 161, 133. https://doi.org/10.1016/J.CELL.2015.02.023

Goncharova, N.D., Lapin, B.A., Khavinson, V.K., 2002. Age-associated endocrine dysfunctions and approaches to their correction. Bull. Exp. Biol. Med. https://doi.org/10.1023/A:1022614508272

Gramaglia, C., Gambaro, E., Bartolomei, G., Camera, P., Chiarelli-Serra, M., Lorenzini, L., Zeppegno, P., 2018. Increased Risk of Metabolic Syndrome in Antidepressants Users: A Mini Review. Front. Psychiatry 9, 621. https://doi.org/10.3389/FPSYT.2018.00621

Guidotti, G., Calabrese, F., Anacker, C., Racagni, G., Pariante, C.M., Riva, M.A., 2012. Glucocorticoid Receptor and FKBP5 Expression Is Altered Following Exposure to Chronic Stress: Modulation by Antidepressant Treatment. Neuropsychopharmacol. 2013 384 38, 616–627. https://doi.org/10.1038/npp.2012.225

Gupta, D., Morley, J.E., 2014. Hypothalamic-Pituitary-Adrenal (HPA) Axis and Aging, in: Comprehensive Physiology. John Wiley & Sons, Inc., Hoboken, NJ, USA, pp. 1495–1510. https://doi.org/10.1002/cphy.c130049

Hartmann, I.B., Fries, G.R., Bücker, J., Scotton, E., von Diemen, L., Kauer-Sant'Anna, M., 2016. The FKBP5 polymorphism rs1360780 is associated with lower weight loss after bariatric

surgery: 26 months of follow-up. Surg. Obes. Relat. Dis. 12, 1554–1560. https://doi.org/10.1016/J.SOARD.2016.04.016

Hartmann, J., Wagner, K., Liebl, C., Scharf, S., Wang, X., Wolf, M., Hausch, F., Rein, T., Schmidt, U., Touma, C., Cheung-Flynn, J., Cox, M., Smith, D., Holsboer, F., Müller, M., Schmidt, M., 2012. The involvement of FK506-binding protein 51 (FKBP5) in the behavioral and neuroendocrine effects of chronic social defeat stress. Neuropharmacology 62, 332–339. https://doi.org/10.1016/J.NEUROPHARM.2011.07.041

Hartmann, J., Wagner, K. V., Gaali, S., Kirschner, A., Kozany, C., Rühter, G., Dedic, N., Häusl, A.S., Hoeijmakers, L., Westerholz, S., Namendorf, C., Gerlach, T., Uhr, M., Chen, A., Deussing, J.M., Holsboer, F., Hausch, F., Schmidt, M. V., 2015. Pharmacological Inhibition of the Psychiatric Risk Factor FKBP51 Has Anxiolytic Properties. J. Neurosci. 35, 9007–9016. https://doi.org/10.1523/JNEUROSCI.4024-14.2015

Häusl, A.S., Balsevich, G., Gassen, N.C., Schmidt, M. V., 2019. Focus on FKBP51: A molecular link between stress and metabolic disorders. Mol. Metab. 29, 170–181. https://doi.org/10.1016/J.MOLMET.2019.09.003

Häusl, A.S., Brix, L.M., Hartmann, J., Pöhlmann, M.L., Lopez, J.-P., Menegaz, D., Brivio, E., Engelhardt, C., Roeh, S., Bajaj, T., Rudolph, L., Stoffel, R., Hafner, K., Goss, H.M., Reul, J.M.H.M., Deussing, J.M., Eder, M., Ressler, K.J., Gassen, N.C., Chen, A., Schmidt, M. V., 2021. The co-chaperone Fkbp5 shapes the acute stress response in the paraventricular nucleus of the hypothalamus of male mice. Mol. Psychiatry 2021 1–17. https://doi.org/10.1038/s41380-021-01044-x

Hill, J.W., Elias, C.F., Fukuda, M., Williams, K.W., Berglund, E.D., Holland, W.L., Cho, Y.R., Chuang, J.C., Xu, Y., Choi, M., Lauzon, D., Lee, C.E., Coppari, R., Richardson, J.A., Zigman, J.M., Chua, S., Scherer, P.E., Lowell, B.B., Brüning, J.C., Elmquist, J.K., 2010. Direct Insulin and Leptin Action in Pro-opiomelanocortin Neurons is Required for Normal Glucose Homeostasis and Fertility. Cell Metab. 11, 286. https://doi.org/10.1016/J.CMET.2010.03.002

Holsboer, F., 2000. The Corticosteroid Receptor Hypothesis of Depression. Neuropsychopharmacol. 2000 235 23, 477–501. https://doi.org/10.1016/s0893-133x(00)00159-7

Howes, O.D., Thase, M.E., Pillinger, T., 2021. Treatment resistance in psychiatry: state of the art and new directions. Mol. Psychiatry 2021 271 27, 58–72. https://doi.org/10.1038/s41380-021-01200-3

Huang, H., Lee, S.H., Ye, C., Lima, I.S., Oh, B.C., Lowell, B.B., Zabolotny, J.M., Kim, Y.B., 2013. ROCK1 in AgRP Neurons Regulates Energy Expenditure and Locomotor Activity in Male Mice. Endocrinology 154, 3660–3670. https://doi.org/10.1210/EN.2013-1343

Huszar, D., Lynch, C.A., Fairchild-Huntress, V., Dunmore, J.H., Fang, Q., Berkemeier, L.R., Gu,

W., Kesterson, R.A., Boston, B.A., Cone, R.D., Smith, F.J., Campfield, L.A., Burn, P., Frank, L., 1997. Targeted disruption of the melanocortin-4 receptor results in obesity in mice. Cell 88, 131–141. https://doi.org/10.1016/S0092-8674(00)81865-6

Incollingo Rodriguez, A.C., Epel, E.S., White, M.L., Standen, E.C., Seckl, J.R., Tomiyama, A.J., 2015. Hypothalamic-pituitary-adrenal axis dysregulation and cortisol activity in obesity: A systematic review. Psychoneuroendocrinology 62, 301–318. https://doi.org/10.1016/J.PSYNEUEN.2015.08.014

Jais, A., Brüning, J.C., 2017. Hypothalamic inflammation in obesity and metabolic disease. J. Clin. Invest. 127, 24. https://doi.org/10.1172/JCI88878

Jenkins, S.A., Ellestad, L.E., Mukherjee, M., Narayana, J., Cogburn, L.A., Porter, T.E., 2013. Glucocorticoid-induced changes in gene expression in embryonic anterior pituitary cells. Physiol. Genomics 45, 422–433. https://doi.org/10.1152/physiolgenomics.00154.2012

Jinwal, U.K., Koren, J., Borysov, S.I., Schmid, A.B., Abisambra, J.F., Blair, L.J., Johnson, A.G., Jones, J.R., Shults, C.L., O'Leary, J.C., Jin, Y., Buchner, J., Cox, M.B., Dickey, C.A., 2010. The Hsp90 Cochaperone, FKBP51, Increases Tau Stability and Polymerizes Microtubules. J. Neurosci. 30, 591. https://doi.org/10.1523/JNEUROSCI.4815-09.2010

Joëls, M., Baram, T.Z., 2009. The neuro-symphony of stress. Nat. Rev. Neurosci. 2009 106 10, 459–466. https://doi.org/10.1038/nrn2632

Kageyama, K., Iwasaki, Y., Watanuki, Y., Niioka, K., Daimon, M., 2021. Differential Effects of Fkbp4 and Fkbp5 on Regulation of the Proopiomelanocortin Gene in Murine AtT-20 Corticotroph Cells. Int. J. Mol. Sci. 22. https://doi.org/10.3390/IJMS22115724

Karst, H., den Boon, F.S., Vervoort, N., Adrian, M., Kapitein, L.C., Joëls, M., 2022. Non-genomic steroid signaling through the mineralocorticoid receptor: Involvement of a membrane-associated receptor? Mol. Cell. Endocrinol. 541, 111501. https://doi.org/10.1016/J.MCE.2021.111501

Kästle, M., Kistler, B., Lamla, T., Bretschneider, T., Lamb, D., Nicklin, P., Wyatt, D., 2018. FKBP51 modulates steroid sensitivity and NFκB signalling: A novel anti-inflammatory drug target. Eur. J. Immunol. 48, 1904. https://doi.org/10.1002/EJI.201847699

Kennedy, G.C., 1953. The role of depot fat in the hypothalamic control of food intake in the rat. Proc. R. Soc. London. Ser. B - Biol. Sci. 140, 578–596. https://doi.org/10.1098/RSPB.1953.0009

Kennedy, G.C., 1950. The hypothalamic control of food intake in rats. Proc. R. Soc. London. Ser. B - Biol. Sci. 137, 535–549. https://doi.org/10.1098/RSPB.1950.0065

Kim, K.W., Zhao, L., Donato, J., Kohno, D., Xu, Y., Eliasa, C.F., Lee, C., Parker, K.L., Elmquist, J.K., 2011. Steroidogenic factor 1 directs programs regulating diet-induced thermogenesis

and leptin action in the ventral medial hypothalamic nucleus. Proc. Natl. Acad. Sci. U. S. A. 108, 10673–10678. https://doi.org/10.1073/PNAS.1102364108

Kim, M.S., Pak, Y.K., Jang, P.G., Namkoong, C., Choi, Y.S., Won, J.C., Kim, K.S., Kim, S.W., Kim, H.S., Park, J.Y., Kim, Y.B., Lee, K.U., 2006. Role of hypothalamic Foxo1 in the regulation of food intake and energy homeostasis. Nat. Neurosci. 2006 97 9, 901–906. https://doi.org/10.1038/nn1731

Klöckener, T., Hess, S., Belgardt, B.F., Paeger, L., Verhagen, L.A.W., Husch, A., Sohn, J.W., Hampel, B., Dhillon, H., Zigman, J.M., Lowell, B.B., Williams, K.W., Elmquist, J.K., Horvath, T.L., Kloppenburg, P., Brüning, J.C., 2011. High-fat Feeding Promotes Obesity via Insulin Receptor/PI3k-Dependent Inhibition of SF-1 VMH Neurons. Nat. Neurosci. 14, 911. https://doi.org/10.1038/NN.2847

Krashes, M.J., Koda, S., Ye, C.P., Rogan, S.C., Adams, A.C., Cusher, D.S., Maratos-Flier, E., Roth, B.L., Lowell, B.B., 2011. Rapid, reversible activation of AgRP neurons drives feeding behavior in mice. J. Clin. Invest. 121, 1424–1428. https://doi.org/10.1172/JCI46229

Krashes, M.J., Lowell, B.B., Garfield, A.S., 2016. Melanocortin-4 receptor–regulated energy homeostasis. Nat. Neurosci. 19, 206. https://doi.org/10.1038/NN.4202

Krude, H., Biebermann, H., Luck, W., Horn, R., Brabant, G., Grüters, A., 1998. Severe early-onset obesity, adrenal insufficiency and red hair pigmentation caused by POMC mutations in humans. Nat. Genet. 19, 155–157. https://doi.org/10.1038/509

Kurrasch, D.M., Cheung, C.C., Lee, F.Y., Tran, P. V., Hata, K., Ingraham, H.A., 2007. The Neonatal Ventromedial Hypothalamus Transcriptome Reveals Novel Markers with Spatially Distinct Patterning. J. Neurosci. 27, 13624. https://doi.org/10.1523/JNEUROSCI.2858-07.2007

Le Thuc, O., Stobbe, K., Cansell, C., Nahon, J.L., Blondeau, N., Rovère, C., 2017. Hypothalamic Inflammation and Energy Balance Disruptions: Spotlight on Chemokines. Front. Endocrinol. 8, 1. https://doi.org/10.3389/FENDO.2017.00197

Lee, R.S., Tamashiro, K.L.K., Yang, X., Purcell, R.H., Harvey, A., Willour, V.L., Huo, Y., Rongione, M., Wand, G.S., Potash, J.B., 2010. Chronic corticosterone exposure increases expression and decreases deoxyribonucleic acid methylation of Fkbp5 in mice. Endocrinology 151, 4332–4343. https://doi.org/10.1210/EN.2010-0225

Lee, R.S., Tamashiro, K.L.K., Yang, X., Purcell, R.H., Huo, Y., Rongione, M., Potash, J.B., Wand, G.S., 2011. A measure of glucocorticoid load provided by DNA methylation of Fkbp5 in mice. Psychopharmacology (Berl). 218, 303. https://doi.org/10.1007/S00213-011-2307-3

Leibowitz, S.F., Hammer, N.J., Chang, K., 1981. Hypothalamic paraventricular nucleus lesions

produce overeating and obesity in the rat. Physiol. Behav. 27, 1031–1040. https://doi.org/10.1016/0031-9384(81)90366-8

Lenard, N.R., Berthoud, H.R., 2008. Central and Peripheral Regulation of Food Intake and Physical Activity: Pathways and Genes. Obesity (Silver Spring). 16, S11. https://doi.org/10.1038/OBY.2008.511

Levin, B.E., Richard, D., Michel, C., Servatius, R., 2000. Differential stress responsivity in diet-induced obese and resistant rats. Am. J. Physiol. - Regul. Integr. Comp. Physiol. 279, 1357–1364. https://doi.org/10.1152/AJPREGU.2000.279.4.R1357/ASSET/IMAGES/LARGE/H6100019 4006.JPEG

Lippi, S.L.P., 2021. Chronic Mild Unpredictable Stress and High-Fat Diet Given during Adolescence Impact Both Cognitive and Noncognitive Behaviors in Young Adult Mice. Brain Sci. 11, 1–23. https://doi.org/10.3390/BRAINSCI11020260

Luo, S.X., Huang, J., Li, Q., Mohammad, H., Lee, C.Y., Krishna, K., Kok, A.M.Y., Tan, Y.L., Lim, J.Y., Li, H., Yeow, L.Y., Sun, J., He, M., Grandjean, J., Sajikumar, S., Han, W., Fu, Y., 2018. Regulation of feeding by somatostatin neurons in the tuberal nucleus. Science (80-.). 361, 76–81. https://doi.org/10.1126/SCIENCE.AAR4983/SUPPL_FILE/AAR4983_LUO_SM.PDF

Luquet, S., Perez, F.A., Hnasko, T.S., Palmiter, R.D., 2005. NPY/AgRP neurons are essential for feeding in adult mice but can be ablated in neonates. Science 310, 683–685. https://doi.org/10.1126/SCIENCE.1115524

MacMaster, F.P., Keshavan, M., Mirza, Y., Carrey, N., Upadhyaya, A.R., El-Sheikh, R., Buhagiar, C.J., Taormina, S.P., Boyd, C., Lynch, M., Rose, M., Ivey, J., Moore, G.J., Rosenberg, D.R., 2007. Development and sexual dimorphism of the pituitary gland. Life Sci. 80, 940. https://doi.org/10.1016/J.LFS.2006.11.040

Maiarù, M., Morgan, O.B., Mao, T., Breitsamer, M., Bamber, H., Pöhlmann, M., Schmidt, M. V., Winter, G., Hausch, F., Géranton, S.M., 2018. The stress regulator FKBP51: a novel and promising druggable target for the treatment of persistent pain states across sexes. Pain 159, 1224–1234. https://doi.org/10.1097/J.PAIN.0000000000001204

Maiarù, M., Tochiki, K.K., Cox, M.B., Annan, L. V., Bell, C.G., Feng, X., Hausch, F., Géranton, S.M., 2016. The stress regulator FKBP51 drives chronic pain by modulating spinal glucocorticoid signaling. Sci. Transl. Med. 8. https://doi.org/10.1126/SCITRANSLMED.AAB3376

Matosin, N., Halldorsdottir, T., Binder, E.B., 2018. Understanding the Molecular Mechanisms Underpinning Gene by Environment Interactions in Psychiatric Disorders: The FKBP5 Model. Biol. Psychiatry. https://doi.org/10.1016/j.biopsych.2018.01.021

Mazier, W., Saucisse, N., Simon, V., Cannich, A., Marsicano, G., Massa, F., Cota, D., 2019. mTORC1 and CB1 receptor signaling regulate excitatory glutamatergic inputs onto the hypothalamic paraventricular nucleus in response to energy availability. Mol. Metab. 28, 151–159. https://doi.org/10.1016/J.MOLMET.2019.08.005

McEwen, B.S., 2003. Mood disorders and allostatic load. Biol. Psychiatry 54, 200–207. https://doi.org/10.1016/S0006-3223(03)00177-X

Meijer, O.C., Buurstede, J.C., Schaaf, M.J.M., 2018. Corticosteroid Receptors in the Brain: Transcriptional Mechanisms for Specificity and Context-Dependent Effects. Cell. Mol. Neurobiol. 2018 394 39, 539–549. https://doi.org/10.1007/S10571-018-0625-2

Milam, K.M., Stern, J.S., Storlien, L.H., Keesey, R.E., 1980. Effect of lateral hypothalamic lesions on regulation of body weight and adiposity in rats. Am. J. Physiol. 239. https://doi.org/10.1152/AJPREGU.1980.239.3.R337

Millington, G.W.M., 2007. The role of proopiomelanocortin (POMC) neurones in feeding behaviour. Nutr. Metab. 2007 41 4, 1–16. https://doi.org/10.1186/1743-7075-4-18

Moraes, J.C., Coope, A., Morari, J., Cintra, D.E., Roman, E.A., Pauli, J.R., Romanatto, T., Carvalheira, J.B., Oliveira, A.L.R., Saad, M.J., Velloso, L.A., 2009. High-Fat Diet Induces Apoptosis of Hypothalamic Neurons. PLoS One 4, e5045. https://doi.org/10.1371/JOURNAL.PONE.0005045

Moreno-Fernandez, M.E., Sharma, V., Stankiewicz, T.E., Oates, J.R., Doll, J.R., Damen, M.S.M.A., Almanan, M.A.T.A., Chougnet, C.A., Hildeman, D.A., Divanovic, S., 2021. Aging mitigates the severity of obesity-associated metabolic sequelae in a gender independent manner. Nutr. Diabetes 2021 111 11, 1–13. https://doi.org/10.1038/s41387-021-00157-0

Morton, G.J., Meek, T.H., Schwartz, M.W., 2014. Neurobiology of food intake in health and disease. Nat. Rev. Neurosci. 15, 367–378. https://doi.org/10.1038/NRN3745

Morton, G.J., Schwartz, M.W., 2001. The NPY/AgRP neuron and energy homeostasis. Int. J. Obes. Relat. Metab. Disord. 25 Suppl 5, S56–S62. https://doi.org/10.1038/SJ.IJO.0801915

Müller, T.D., Blüher, M., Tschöp, M.H., DiMarchi, R.D., 2021. Anti-obesity drug discovery: advances and challenges. Nat. Rev. Drug Discov. 2021 213 21, 201–223. https://doi.org/10.1038/s41573-021-00337-8

Myers, B., McKlveen, J.M., Herman, J.P., 2012. Neural regulation of the stress response: The many faces of feedback. Cell. Mol. Neurobiol. 32, 683–694. https://doi.org/10.1007/S10571-012-9801-Y

Myers, M.G., Olson, D.P., 2012. Central nervous system control of metabolism. Nat. 2012 4917424 491, 357–363. https://doi.org/10.1038/nature11705

Nathan, P.J., O'Neill, B. V., Napolitano, A., Bullmore, E.T., 2011. Neuropsychiatric Adverse Effects of Centrally Acting Antiobesity Drugs. CNS Neurosci. Ther. 17, 490. https://doi.org/10.1111/J.1755-5949.2010.00172.X

Noddings, C.M., Wang, R.Y.R., Johnson, J.L., Agard, D.A., 2022. Structure of Hsp90-p23-GR reveals the Hsp90 client-maturation mechanism. Nature 601, 465. https://doi.org/10.1038/S41586-021-04236-1

O'Leary, J.C., Dharia, S., Blair, L.J., Brady, S., Johnson, A.G., Peters, M., Cheung-Flynn, J., Cox, M.B., Erausquin, G. de, Weeber, E.J., Jinwal, U.K., Dickey, C.A., 2011. A New Anti-Depressive Strategy for the Elderly: Ablation of FKBP5/FKBP51. PLoS One 6, e24840. https://doi.org/10.1371/JOURNAL.PONE.0024840

Ortiz, R., Joseph, J.J., Lee, R., Wand, G.S., Golden, S.H., 2018. Type 2 diabetes and cardiometabolic risk may be associated with increase in DNA methylation of FKBP5. Clin. Epigenetics 10. https://doi.org/10.1186/S13148-018-0513-0

Ozomaro, U., Wahlestedt, C., Nemeroff, C.B., 2013. Personalized medicine in psychiatry: Problems and promises. BMC Med. 11, 1–35. https://doi.org/10.1186/1741-7015-11-132/TABLES/2

Parker, K.L., Rice, D.A., Lala, D.S., Ikeda, Y., Luo, X., Wong, M., Bakke, M., Zhao, L., Frigeri, C., Hanley, N.A., Stallings, N., Schimmer, B.P., 2002. Steroidogenic factor 1: an essential mediator of endocrine development. Recent Prog. Horm. Res. 57, 19–36. https://doi.org/10.1210/RP.57.1.19

Parvin, R., Saito-Hakoda, A., Shimada, H., Shimizu, K., Noro, E., Iwasaki, Y., Fujiwara, K., Yokoyama, A., Sugawara, A., 2017. Role of NeuroD1 on the negative regulation of Pomc expression by glucocorticoid. PLoS One 12. https://doi.org/10.1371/JOURNAL.PONE.0175435

Pei, H., Li, L., Fridley, B.L., Jenkins, G.D., Kalari, K.R., Lingle, W., Petersen, G., Lou, Z., Wang, L., 2009. FKBP51 Affects Cancer Cell Response to Chemotherapy by Negatively Regulating Akt. Cancer Cell 16, 259. https://doi.org/10.1016/J.CCR.2009.07.016

Penicaud, L., Kinebanyan, M.F., Ferre, P., Morin, J., Kande, J., Smadja, C., Marfaing-Jallat, P., Picon, L., 1989. Development of VMH obesity: in vivo insulin secretion and tissue insulin sensitivity. Am. J. Physiol. 257. https://doi.org/10.1152/AJPENDO.1989.257.2.E255

Pereira, M.J., Palming, J., Svensson, M.K., Rizell, M., Dalenbäck, J., Hammar, M., Fall, T., Sidibeh, C.O., Svensson, P.A., Eriksson, J.W., 2014. FKBP5 expression in human adipose tissue increases following dexamethasone exposure and is associated with insulin resistance. Metabolism 63, 1198–1208. https://doi.org/10.1016/J.METABOL.2014.05.015

Pöhlmann, M.L., Häusl, A.S., Harbich, D., Balsevich, G., Engelhardt, C., Feng, X., Breitsamer, M.,

Hausch, F., Winter, G., Schmidt, M. V., 2018. Pharmacological Modulation of the Psychiatric Risk Factor FKBP51 Alters Efficiency of Common Antidepressant Drugs. Front. Behav. Neurosci. 12. https://doi.org/10.3389/FNBEH.2018.00262

Qin, C., Li, J., Tang, K., 2018. The Paraventricular Nucleus of the Hypothalamus: Development, Function, and Human Diseases. Endocrinology 159, 3458–3472. https://doi.org/10.1210/EN.2018-00453

Rabasa, C., Dickson, S.L., 2016. Impact of stress on metabolism and energy balance. Curr. Opin. Behav. Sci. 9, 71–77. https://doi.org/10.1016/J.COBEHA.2016.01.011

Resmini, E., Santos, A., Aulinas, A., Webb, S.M., Vives-Gilabert, Y., Cox, O., Wand, G., Lee, R.S., 2016. Reduced DNA methylation of FKBP5 in Cushing's syndrome. Endocrine 54, 768. https://doi.org/10.1007/S12020-016-1083-6

Riecher-Rössler, A., 2017. Sex and gender differences in mental disorders. The Lancet Psychiatry 4, 8–9. https://doi.org/10.1016/S2215-0366(16)30348-0

Rotondo, F., Butz, H., Syro, L. V., Yousef, G.M., Di Ieva, A., Restrepo, L.M., Quintanar-Stephano, A., Berczi, I., Kovacs, K., 2016. Arginine vasopressin (AVP): a review of its historical perspectives, current research and multifunctional role in the hypothalamo-hypophysial system. Pituit. 2016 194 19, 345–355. https://doi.org/10.1007/S11102-015-0703-0

Russell, G., Lightman, S., 2019. The human stress response. Nat. Rev. Endocrinol. 2019 159 15, 525–534. https://doi.org/10.1038/s41574-019-0228-0

Ryan, D., Barquera, S., Barata Cavalcanti, O., Ralston, J., 2020. The Global Pandemic of Overweight and Obesity. Handb. Glob. Heal. 1–35. https://doi.org/10.1007/978-3-030-05325-3_39-1

Sabbagh, J.J., O'Leary, J.C., Blair, L.J., Klengel, T., Nordhues, B.A., Fontaine, S.N., Binder, E.B., Dickey, C.A., 2014. Age-associated epigenetic upregulation of the FKBP5 gene selectively impairs stress resiliency. PLoS One 9, 107241. https://doi.org/10.1371/journal.pone.0107241

Samuel, V.T., Shulman, G.I., 2012. Mechanisms for insulin resistance: common threads and missing links. Cell 148, 852–871. https://doi.org/10.1016/J.CELL.2012.02.017

Sanchez, E.R., 2012. Chaperoning steroidal physiology: Lessons from mouse genetic models of Hsp90 and its cochaperones. Biochim. Biophys. Acta - Mol. Cell Res. 1823, 722–729. https://doi.org/10.1016/J.BBAMCR.2011.11.006

Sapolsky, R.M., 1992. Do glucocorticoid concentrations rise with age in the rat? Neurobiol. Aging 13, 171–174. https://doi.org/10.1016/0197-4580(92)90025-S

Sapolsky, R.M., Krey, L.C., McEwen, B.S., 1986. The Neuroendocrinology of Stress and Aging:

The Glucocorticoid Cascade Hypothesis*. Endocr. Rev. 7, 284–301. https://doi.org/10.1210/edrv-7-3-284

Sapolsky, R.M., Romero, L.M., Munck, A.U., 2000. How Do Glucocorticoids Influence Stress Responses? Integrating Permissive, Suppressive, Stimulatory, and Preparative Actions*. Endocr. Rev. 21, 55–89. https://doi.org/10.1210/edrv.21.1.0389

Scammell, J.G., Denny, W.B., Valentine, D.L., Smiths, D.F., 2001. Overexpression of the FK506-binding immunophilin FKBP51 is the common cause of glucocorticoid resistance in three New World primates. Gen. Comp. Endocrinol. 124, 152–165. https://doi.org/10.1006/gcen.2001.7696

Scharf, S.H., Liebl, C., Binder, E.B., Schmidt, M. V., Müller, M.B., 2011. Expression and regulation of the Fkbp5 gene in the adult mouse brain. PLoS One 6. https://doi.org/10.1371/journal.pone.0016883

Schmidt, M. V., Levine, S., Oitzl, M.S., Van Der Mark, M., Müller, M.B., Holsboer, F., De Kloet, E.R., 2005. Glucocorticoid receptor blockade disinhibits pituitary-adrenal activity during the stress hyporesponsive period of the mouse. Endocrinology 146, 1458–1464. https://doi.org/10.1210/en.2004-1042

Schmidt, M. V., Sterlemann, V., Ganea, K., Liebl, C., Alam, S., Harbich, D., Greetfeld, M., Uhr, M., Holsboer, F., Müller, M.B., 2007. Persistent neuroendocrine and behavioral effects of a novel, etiologically relevant mouse paradigm for chronic social stress during adolescence. Psychoneuroendocrinology 32, 417–429. https://doi.org/10.1016/j.psyneuen.2007.02.011

Schmidt, M. V., Sterlemann, V., Wagner, K., Niederleitner, B., Ganea, K., Liebl, C., Deussing, J.M., Berger, S., Schütz, G., Holsboer, F., Müller, M.B., 2009. Postnatal glucocorticoid excess due to pituitary glucocorticoid receptor deficiency: Differential short- and long-term consequences. Endocrinology 150, 2709–2716. https://doi.org/10.1210/en.2008-1211

Schreiber, S.L., 1991. Chemistry and Biology of the Immunophilins and Their Immunosuppressive Ligands. Science (80-.). 251, 283–287. https://doi.org/10.1126/SCIENCE.1702904

Schwartz, M.W., Baskin, D.G., Bukowski, T.R., Kuijper, J.L., Foster, D., Lasser, G., Prunkard, D.E., Porte, D., Woods, S.C., Seeley, R.J., Weigle, D.S., 1996. Specificity of leptin action on elevated blood glucose levels and hypothalamic neuropeptide Y gene expression in ob/ob mice. Diabetes 45, 531–535. https://doi.org/10.2337/DIAB.45.4.531

Schwartz, M.W., Seeley, R.J., Tschöp, M.H., Woods, S.C., Morton, G.J., Myers, M.G., D'Alessio, D., 2013. Cooperation between brain and islet in glucose homeostasis and diabetes. Nature 503, 59. https://doi.org/10.1038/NATURE12709

Schwartz, M.W., Seeley, R.J., Woods, S.C., Weigle, D.S., Campfield, L.A., Burn, P., Baskin, D.G., 1997. Leptin increases hypothalamic pro-opiomelanocortin mRNA expression in the rostral arcuate nucleus. Diabetes 46, 2119–2123. https://doi.org/10.2337/DIAB.46.12.2119

Selye, H., 1936. A syndrome produced by diverse nocuous agents. Nature 138, 32. https://doi.org/10.1038/138032a0

Shen, W. jie, Yao, T., Kong, X., Williams, K.W., Liu, T., 2017. Melanocortin neurons: Multiple routes to regulation of metabolism. Biochim. Biophys. acta. Mol. basis Dis. 1863, 2477–2485. https://doi.org/10.1016/J.BBADIS.2017.05.007

Sheng, J.A., Bales, N.J., Myers, S.A., Bautista, A.I., Roueinfar, M., Hale, T.M., Handa, R.J., 2021. The Hypothalamic-Pituitary-Adrenal Axis: Development, Programming Actions of Hormones, and Maternal-Fetal Interactions. Front. Behav. Neurosci. 0, 256. https://doi.org/10.3389/FNBEH.2020.601939

Shi, Y.C., Lau, J., Lin, Z., Zhang, H., Zhai, L., Sperk, G., Heilbronn, R., Mietzsch, M., Weger, S., Huang, X.F., Enriquez, R.F., Baldock, P.A., Zhang, L., Sainsbury, A., Herzog, H., Lin, S., 2013. Arcuate NPY controls sympathetic output and BAT function via a relay of tyrosine hydroxylase neurons in the PVN. Cell Metab. 17, 236–248. https://doi.org/10.1016/J.CMET.2013.01.006

Sidibeh, C.O., Pereira, M.J., Abalo, X.M., J. Boersma, G., Skrtic, S., Lundkvist, P., Katsogiannos, P., Hausch, F., Castillejo-López, C., Eriksson, J.W., 2018. FKBP5 expression in human adipose tissue: potential role in glucose and lipid metabolism, adipogenesis and type 2 diabetes. Endocrine 1–13. https://doi.org/10.1007/s12020-018-1674-5

Smith, D.F., Baggenstoss, B.A., Marion, T.N., Rimerman, R.A., 1993. Two FKBP-related proteins are associated with progesterone receptor complexes. J. Biol. Chem. 268, 18365–18371. https://doi.org/10.1016/S0021-9258(17)46853-0

Sorrells, S.F., Caso, J.R., Munhoz, C.D., Sapolsky, R.M., 2009. The Stressed CNS: When Glucocorticoids Aggravate Inflammation. Neuron 64, 33. https://doi.org/10.1016/J.NEURON.2009.09.032

Soukas, A., Cohen, P., Socci, N.D., Friedman, J.M., 2000. Leptin-specific patterns of gene expression in white adipose tissue. Genes Dev. 14, 963. https://doi.org/10.1101/gad.14.8.963

Spanswick, D., Smith, M.A., Mirshamsi, S., Routh, V.H., Ashford, M.L.J., 2000. Insulin activates ATP-sensitive K+ channels in hypothalamic neurons of lean, but not obese rats. Nat. Neurosci. 3, 757–758. https://doi.org/10.1038/77660

Stechschulte, L.A., Hinds, T.D., Ghanem, S.S., Shou, W., Najjar, S.M., Sanchez, E.R., 2014a.

FKBP51 Reciprocally Regulates GRα and PPARγ Activation via the Akt-p38 Pathway. Mol. Endocrinol. 28, 1254–1264. https://doi.org/10.1210/ME.2014-1023

Stechschulte, L.A., Hinds, T.D., Khuder, S.S., Shou, W., Najjar, S.M., Sanchez, E.R., 2014b. FKBP51 Controls Cellular Adipogenesis through p38 Kinase-Mediated Phosphorylation of GRα and PPARγ. Mol. Endocrinol. 28, 1265. https://doi.org/10.1210/ME.2014-1022

Stechschulte, L.A., Qiu, B., Warrier, M., Hinds, T.D., Zhang, M., Gu, H., Xu, Y., Khuder, S.S., Russo, L., Najjar, S.M., Lecka-Czernik, B., Yong, W., Sanchez, E.R., 2016. FKBP51 Null Mice Are Resistant to Diet-Induced Obesity and the PPARγ Agonist Rosiglitazone. Endocrinology 157, 3888. https://doi.org/10.1210/EN.2015-1996

Steculorum, S.M., Ruud, J., Karakasilioti, I., Backes, H., Engström Ruud, L., Timper, K., Hess, M.E., Tsaousidou, E., Mauer, J., Vogt, M.C., Paeger, L., Bremser, S., Klein, A.C., Morgan, D.A., Frommolt, P., Brinkkötter, P.T., Hammerschmidt, P., Benzing, T., Rahmouni, K., Wunderlich, F.T., Kloppenburg, P., Brüning, J.C., 2016. AgRP Neurons Control Systemic Insulin Sensitivity via Myostatin Expression in Brown Adipose Tissue. Cell 165, 125. https://doi.org/10.1016/J.CELL.2016.02.044

Stellar, E., 1954. The physiology of motivation. Psychol. Rev. 61, 5–22. https://doi.org/10.1037/H0060347

Storer, C.L., Dickey, C.A., Galigniana, M.D., Rein, T., Cox, M.B., 2011. FKBP51 and FKBP52 in Signaling and Disease. Trends Endocrinol. Metab. 22, 481. https://doi.org/10.1016/J.TEM.2011.08.001

Thaler, J.P., Yi, C.X., Schur, E.A., Guyenet, S.J., Hwang, B.H., Dietrich, M.O., Zhao, X., Sarruf, D.A., Izgur, V., Maravilla, K.R., Nguyen, H.T., Fischer, J.D., Matsen, M.E., Wisse, B.E., Morton, G.J., Horvath, T.L., Baskin, D.G., Tschöp, M.H., Schwartz, M.W., 2012. Obesity is associated with hypothalamic injury in rodents and humans. J. Clin. Invest. 122, 153. https://doi.org/10.1172/JCI59660

Thornton, J.E., Cheung, C.C., Clifton, D.K., Steiner, R.A., 1997. Regulation of hypothalamic proopiomelanocortin mRNA by leptin in ob/ob mice. Endocrinology 138, 5063–5066. https://doi.org/10.1210/ENDO.138.11.5651

Timper, K., Brüning, J.C., 2017. Hypothalamic circuits regulating appetite and energy homeostasis: pathways to obesity. Dis. Model. Mech. 10, 679–689. https://doi.org/10.1242/DMM.026609

Tomiyama, A.J., 2019. Stress and Obesity. https://doi.org/10.1146/annurev-psych-010418-102936 70, 703–718. https://doi.org/10.1146/ANNUREV-PSYCH-010418-102936

Toneatto, J., Charó, N.L., Galigniana, N.M., Piwien-Pilipuk, G., 2015. Adipogenesis is under surveillance of Hsp90 and the high molecular weight Immunophilin FKBP51. Adipocyte

4, 239–247. https://doi.org/10.1080/21623945.2015.1049401

Toneatto, J., Guber, S., Charó, N.L., Susperreguy, S., Schwartz, J., Galigniana, M.D., Piwien-Pilipuk, G., 2013. Dynamic mitochondrial-nuclear redistribution of the immunophilin FKBP51 is regulated by the PKA signaling pathway to control gene expression during adipocyte differentiation. J. Cell Sci. 126, 5357–5368. https://doi.org/10.1242/JCS.125799/263521/AM/DYNAMIC-MITOCHONDRIAL-NUCLEAR-REDISTRIBUTION-OF

Touma, C., Gassen, N.C., Herrmann, L., Cheung-Flynn, J., Bll, D.R., Ionescu, I.A., Heinzmann, J.M., Knapman, A., Siebertz, A., Depping, A.M., Hartmann, J., Hausch, F., Schmidt, M. V., Holsboer, F., Ising, M., Cox, M.B., Schmidt, U., Rein, T., 2011. FK506 binding protein 5 shapes stress responsiveness: Modulation of neuroendocrine reactivity and coping behavior. Biol. Psychiatry 70, 928–936. https://doi.org/10.1016/j.biopsych.2011.07.023

Ullah, R., Rauf, N., Nabi, G., Yi, S., Yu-Dong, Z., Fu, J., 2021. Mechanistic insight into high-fat diet-induced metabolic inflammation in the arcuate nucleus of the hypothalamus. Biomed. Pharmacother. 142, 112012. https://doi.org/10.1016/J.BIOPHA.2021.112012

Ulrich-Lai, Y.M., Herman, J.P., 2009. Neural regulation of endocrine and autonomic stress responses. Nat. Rev. Neurosci. 2009 106 10, 397–409. https://doi.org/10.1038/nrn2647

Valentino, R.J., Van Bockstaele, E., 2008. Convergent Regulation of Locus Coeruleus Activity as an adaptive Response to Stress. Eur. J. Pharmacol. 583, 194. https://doi.org/10.1016/J.EJPHAR.2007.11.062

van der Kooij, M.A., 2020. The impact of chronic stress on energy metabolism. Mol. Cell. Neurosci. 107, 103525. https://doi.org/10.1016/J.MCN.2020.103525

Vohra, M.S., Benchoula, K., Serpell, C.J., Hwa, W.E., 2022. AgRP/NPY and POMC neurons in the arcuate nucleus and their potential role in treatment of obesity. Eur. J. Pharmacol. 915, 174611. https://doi.org/10.1016/J.EJPHAR.2021.174611

Voss-Andreae, A., Murphy, J.G., Ellacott, K.L.J., Stuart, R.C., Nillni, E.A., Cone, R.D., Fan, W., 2007. Role of the central melanocortin circuitry in adaptive thermogenesis of brown adipose tissue. Endocrinology 148, 1550–1560. https://doi.org/10.1210/EN.2006-1389

Wagner, K. V., Wang, X.D., Liebl, C., Scharf, S.H., Müller, M.B., Schmidt, M. V., 2011. Pituitary glucocorticoid receptor deletion reduces vulnerability to chronic stress. Psychoneuroendocrinology 36, 579–587. https://doi.org/10.1016/j.psyneuen.2010.09.007

Wang, R.C., Wei, Y., An, Z., Zou, Z., Xiao, G., Bhagat, G., White, M., Reichelt, J., Levine, B., 2012. Akt-mediated regulation of autophagy and tumorigenesis through Beclin 1 phosphorylation. Science 338, 956–959. https://doi.org/10.1126/SCIENCE.1225967

Wang, W., Yang, J., Xu, J., Yu, H., Liu, Y., Wang, R., Ho, R.C.M., Ho, C.S.H., Pan, F., 2022. Effects of High-fat Diet and Chronic Mild Stress on Depression-like Behaviors and Levels of Inflammatory Cytokines in the Hippocampus and Prefrontal Cortex of Rats. Neuroscience 480, 178–193. https://doi.org/10.1016/J.NEUROSCIENCE.2021.11.015

Waterson, M.J., Horvath, T.L., 2015. Neuronal Regulation of Energy Homeostasis: Beyond the Hypothalamus and Feeding. Cell Metab. 22, 962–970. https://doi.org/10.1016/J.CMET.2015.09.026

Westberry, J.M., Sadosky, P.W., Hubler, T.R., Gross, K.L., Scammell, J.G., 2006. Glucocorticoid resistance in squirrel monkeys results from a combination of a transcriptionally incompetent glucocorticoid receptor and overexpression of the glucocorticoid receptor co-chaperone FKBP51. J. Steroid Biochem. Mol. Biol. 100, 34–41. https://doi.org/10.1016/J.JSBMB.2006.03.004

Wochnik, G.M., Rüegg, J., Abel, G.A., Schmidt, U., Holsboer, F., Rein, T., 2005. FK506-binding proteins 51 and 52 differentially regulate dynein interaction and nuclear translocation of the glucocorticoid receptor in mammalian cells. J. Biol. Chem. 280, 4609–4616. https://doi.org/10.1074/jbc.M407498200

Xu, Y., Elmquist, J.K., Fukuda, M., 2011. Central nervous control of energy and glucose balance: focus on the central melanocortin system. Ann. N. Y. Acad. Sci. 1243, 1. https://doi.org/10.1111/J.1749-6632.2011.06248.X

Yang, L., Isoda, F., Yen, K., Kleopoulos, S.P., Janssen, W., Fan, X., Mastaitis, J., Dunn-Meynell, A., Levin, B., McCrimmon, R., Sherwin, R., Musatov, S., Mobbs, C. V., 2012. Hypothalamic Fkbp51 is induced by fasting, and elevated hypothalamic expression promotes obese phenotypes. Am. J. Physiol. - Endocrinol. Metab. 302, E987. https://doi.org/10.1152/AJPENDO.00474.2011

Yeh, W.C., Li, T.K., Bierer, B.E., McKnight, S.L., 1995. Identification and characterization of an immunophilin expressed during the clonal expansion phase of adipocyte differentiation. Proc. Natl. Acad. Sci. U. S. A. 92, 11081–11085. https://doi.org/10.1073/PNAS.92.24.11081

Yeo, G.S.H., Farooqi, I.S., Aminian, S., Halsall, D.J., Stanhope, R.G., O'Rahilly, S., 1998. A frameshift mutation in MC4R associated with dominantly inherited human obesity. Nat. Genet. 20, 111–112. https://doi.org/10.1038/2404

Yiallouris, A., Tsioutis, C., Agapidaki, E., Zafeiri, M., Agouridis, A.P., Ntourakis, D., Johnson, E.O., 2019. Adrenal aging and its implications on stress responsiveness in humans. Front. Endocrinol. (Lausanne). 10, 54. https://doi.org/10.3389/fendo.2019.00054

Young, E.A., Abelson, J., Lightman, S.L., 2004. Cortisol pulsatility and its role in stress regulation and health. Front. Neuroendocrinol. 25, 69–76.

https://doi.org/10.1016/J.YFRNE.2004.07.001

Zannas, A.S., Binder, E.B., 2014. Gene-environment interactions at the FKBP5 locus: Sensitive periods, mechanisms and pleiotropism. Genes, Brain Behav. 13, 25–37. https://doi.org/10.1111/gbb.12104

Zannas, A.S., Jia, M., Hafner, K., Baumert, J., Wiechmann, T., Pape, J.C., Arloth, J., Ködel, M., Martinelli, S., Roitman, M., Röh, S., Haehle, A., Emeny, R.T., Iurato, S., Carrillo-Roa, T., Lahti, J., Räikkönen, K., Eriksson, J.G., Drake, A.J., Waldenberger, M., Wahl, S., Kunze, S., Lucae, S., Bradley, B., Gieger, C., Hausch, F., Smith, A.K., Ressler, K.J., Müller-Myhsok, B., Ladwig, K.H., Rein, T., Gassen, N.C., Binder, E.B., 2019. Epigenetic upregulation of FKBP5 by aging and stress contributes to NF-κB-driven inflammation and cardiovascular risk. Proc. Natl. Acad. Sci. U. S. A. 166, 11370–11379. https://doi.org/10.1073/pnas.1816847116

Zannas, A.S., Wiechmann, T., Gassen, N.C., Binder, E.B., 2015. Gene–Stress–Epigenetic Regulation of FKBP5: Clinical and Translational Implications. Neuropsychopharmacol. 2016 411 41, 261–274. https://doi.org/10.1038/npp.2015.235

Zhan, C., Zhou, J., Feng, Q., Zhang, J. en, Lin, S., Bao, J., Wu, P., Luo, M., 2013. Acute and Long-Term Suppression of Feeding Behavior by POMC Neurons in the Brainstem and Hypothalamus, Respectively. J. Neurosci. 33, 3624–3632. https://doi.org/10.1523/JNEUROSCI.2742-12.2013

Zhang, Y., Sowers, J.R., Ren, J., 2018. Targeting autophagy in obesity: from pathophysiology to management. Nat. Rev. Endocrinol. 2018 146 14, 356–376. https://doi.org/10.1038/s41574-018-0009-1

Zheng, H., Patterson, L.M., Rhodes, C.J., Louis, G.W., Skibicka, K.P., Grill, H.J., Myers, M.G., Berthoud, H.R., 2010. A potential role for hypothalamomedullary POMC projections in leptin-induced suppression of food intake. Am. J. Physiol. Regul. Integr. Comp. Physiol. 298. https://doi.org/10.1152/AJPREGU.00619.2009

Acknowledgements

First and foremost, I would like to thank my supervisor Dr. Mathias Schmidt, who was an excellent mentor to me during my entire time in his group. Mathias, you inspire, support, and encourage us. You are a diplomat who steers his team through the ups and downs of everyday work while being like Switzerland, without taking sides or favoring anyone. You gave me the freedom to discover my strengths, and you encouraged me to pursue my professional passions. You were nothing but supportive and understanding, and most importantly: You were there, I could rely on you and I have learned that this is the key to my trust in you.

A very special thanks goes to Alex. There are no words that can describe how much I enjoyed working with you! Having you as my supervisor during my Master's opened my eyes for science and how great it can be to have someone who stands by you, supports you and with whom you make a great team! You made me stay, Alex!

Irmak, you have been an exceptional student and a great help during your almost two years here. There was a point when I couldn't imagine finishing my thesis without having you by my side. Thanks to you, I discovered my passion for teaching and learned what it means to be a supervisor. Together, we will publish two papers, that's how great a student you are! London, you are one of the most dedicated students I know. You came along at a time when I thought having a student was not the best idea. But the amount of work you took off my hands in just two months was impressive, and I am very grateful for that!

Thanks to all my friends and colleagues who made my PhD a joyful experience and supported me on my way: Max, Clara, and Karla, at the beginning of my time at the Max Planck Institute you were the heart of the AG Schmidt group! I enjoyed every single day working with you, and I loved even more that we dropped everything in the lab at 12:00 sharp to spend an hour of quality time together. That made my days back then! Joeri and Lotte, you guys were my companions: We faced the same challenges and you always supported me in my experiments (and I know it was a lot!), you gave me scientific advice and I enjoyed having you by my side throughout these challenging years. Veronika, you are brilliant! I have never seen a 'newbie' take on challenges like you did. Your commitment and the responsibility you took on right away are still overwhelming. I trusted you completely and will continue to trust you with my projects in the future. Marg, you have been my metabolism buddy and I am thankful for all the help and scientific expertise you have brought to our group! I thank the rest of the group,

Ann (you have made it this far), Sowmya (it was a pleasure sharing a bed and blanket with you!), Vera, Shila, and Fiona for all your support and I wish I could have spent more time with you guys! But I guess Corona happened...

Dani, Bianca, Andrea R., Andrea P., Caro, Lisa, Rainer, and Cornelia thank you so much for all your technical help with my animal experiments and in the lab. Your skills were the be-all and end-all for me and I couldn't have not done my PhD without you. Steffi, and Sabrina I appreciated all the work you put into our genotyping.

I would like to thank my family. My mother Gisela, who is the most loving and supportive person I have ever meet. My father, Andree, who is one of the smartest people I know, even though you are NOT in science. I wish I had your curiosity and passion for it! My brother Victor, who listens to me and is understanding of all the little problems and obstacles I have talked to you about. Without the emotional support of my family, I would have never been able to enter the profession I am in now. You never doubted me at any point and gave me the strength to pull this off! Ihr seid meine Basis im Leben, ihr erdet und unterstützt mich und ich bin unglaublich dankbar euch an meiner Seite zu haben. Ihr seid wichtig.

I would also like to thank my friends: Julia, the three years we have spent together in this institute as long-time friends have been one of my greatest supports in my PhD. Knowing that you are there, just a few steps away, and struggle with the same issues as I am, has helped me through my most difficult times. I enjoyed every little step of our friendship and collegiality. To the rest of the crew: Lara, Vanessa, Benoit, Fabi, you are my Munich family and I am so happy to have you in my life! And thanks to my friends who are not here in Munich but are my foundation in life: Kadn (you are my rock), Sarah, Sandra, Anni, and Hanna. A special thanks to Philipp, who was always by my side during the last 2.5 years of my PhD. You have been with me through my ups and downs, taking so much work off my hands when I needed it most. You were always there with open ears when I rambled about my science and gave me great input, being the incredibly intelligent and caring person you are!

Finally, I would like to thank my mice, because let's face it, without YOU my science literally would not have been possible. I have appreciated and valued every one of you! Your contribution to science could not be greater and I respect you so much for that, but I guess you had no choice. I hereby propose a toast to you, my dearest friends!

Curriculum Vitae

Name	Lea Maria Brix
Date of birth	April 27th, 1991
Nationality	German

EDUCATION

09/2018 – present	**PhD candidate** Max Planck Institute of Psychiatry, Germany Thesis: Dissecting the cell type-specific role of FKBP51 in the stress response and whole-body metabolism -The WHEN and WHERE matters-
10/2015 – 03/2018	**Master of Science** Albert-Ludwigs-University, Freiburg, (1.4)
10/2011 – 07/2014	**Bachelor of Science** Ludwig-Maximilans-University, Munich, (1.7)

AWARDS & HONORS

09/2018 – present	**Selected member** of the competitive IMPRS-TP graduate program, Munich Germany
2019 – present	**Member** of the European Brain and Behavior Society (EBBS)
2020 – present	**Member** of the Society for Neuroscience (SFN)
2021	**Recipient** of the Mifek-Kirschner-Award for excellent scientific publications: Häusl et al., 2021, The co-chaperone *Fkbp5* shapes the acute stress response in the paraventricular nucleus of the hypothalamus of male mice, *Molecular Psychiatry*
2019	**Recipient** of the EBBS travel grant and **speaker** at 'Young researchers BLITZ presentation' at the 48th EBBS
2019	**Winner** of the VLOG contest of the joint initiative: 'A healthy diet for a healthy life' (JPI HDHL)
2014	**Recipient** of a DAAD scholarship for an internship at the Charles Sturt University, Albury, Australia

Assertion/Eidesstattliche Erklärung

Hiermit versichere ich an Eides statt, dass ich die vorliegende Dissertation selbstständig und nur mit den angegebenen Quellen und Hilfsmitteln angefertigt habe. Alle Ausführungen, die wörtlich oder sinngemäß übernommen wurden, sind als solche gekennzeichnet.

Des Weiteren erkläre ich, dass ich nicht anderweitig ohne Erfolg versucht habe, eine Dissertation einzureichen oder mich der Doktorprüfung zu unterziehen. Die vorliegende Dissertation liegt weder ganz, noch in wesentlichen Teilen einer anderen Prüfungskommission vor.

München, den 01.06.2021

Lea Brix